PHTHALOCYANINES: PHOTOCHEMICAL, ELECTROCHEMICAL AND BIOMIMETIC CATALYTIC BEHAVIOUR

A thesis submitted in fulfillment of the requirements for the degree of

DOCTOR OF PHILOSOPHY

of

RHODES UNIVERSITY

by

Nthapo Sehlotho

February 2007

Dedications

To all who are interested in the study of; what things are made of,

why things happen and how they happen.

Acknowledgements

My greatest heartfelt gratitude goes to God, my creator. His presence and love have sustained me through the valleys, storms and winds of research and writing up this thesis.

I thank my supervisor Professor Tebello Nyokong for selflessly giving of her knowledge, time and guidance. Prof, working under your supervision has moulded me into a scientist I am today. I thank you for the travel opportunities you have given me; there is a saying that the world is like a book, if one does not travel, it is like reading the first page. I am not on page one, thanks to you.

To our foreign collaborators, Dr. Fethi Bedioui and Dr. Sophie Griveau at *Laboratoire de Pharmacologie Chimique et Génétique, Ecole Nationale Supérieure de Chimie de Paris, Paris, France,* I thank you for having me in your institution and sharing your expertise with me. I also thank Professor José Zagal at *Facultad de Quimica y Biologia, Universidad de Santiago de Chile, Casilla 40, Correo 33, Santiago, Chile* for his invaluable contribution to the collaboration.

I thank Rhodes University chemistry department for giving me the opportunity to study and also tutor undergraduate students. To my fellow researchers in lab S22, I thank you for being a family away from home.

A great thank you goes to my sponsors, the government of Lesotho, NRF, CCETSA and Egide (France).

Lastly, I thank my family and friends for their love and support.

Abstract

This thesis explored use of metallophthalocyanines as electrocatalysts towards thiol and thiocyanate oxidation, nitrosothiol decomposition and reduction of oxygen, as well as biomimetic and photo-catalysts of cyclohexene oxidation. 2-mercaptoethanol (2-ME), *L*-cysteine (CYS) and reduced glutathione (GSH) thiols were oxidized on cobalt tetra ethoxythiophene and cobalt tetra phenoxy pyrrole phthalocyanine modified glassy carbon electrodes, whose catalytic activity was found to depend on pH, film thickness and method of electrode modification.

Oxidation of thiocyanate (SCN^-), CYS and 2-ME was catalyzed by a self-assembled monolayer of cobalt tetraethoxythiophene Thiocyanate oxidation occurred via two electron transfer, whereas that of CYS and 2-ME required 1 electron. The oxidations of SCN^- and 2-ME were catalyzed by ring based processes, while CYS was catalyzed by both Co^{III}/Co^{II} process and ring-based processes.

Oxidation of GSH and 2-ME was conducted on screen printed graphite electrodes modified with cobalt phthalocyanine. Activity depended on method of electrode modification and CoPc % composition. Decomposition of *S*-nitrosoglutathione occurred in the presence of copper ions and $NaBH_4$. Reduced and oxidized glutathione were detected as products using cobalt phthalocyanine adsorbed on an ordinary pyrolytic graphite electrode.

Reduction of oxygen was electro-catalyzed by adsorbed manganese phthalocyanine complexes on glassy carbon electrodes. FePc, $FePc(Cl)_{16}$, CoPc

and CoPc substituted with phenoxypyrrole and ethoxythiophene ligands were also used as electro-catalysts. Oxygen reduction occurred via two electron transfer in acidic and neutral media forming hydrogen peroxide, while water was formed in basic media via four electron transfer.

Cyclohexene oxidation using *tert*-butylhydroperoxide or chloroperoxy benzoic acid as oxidants in the presence of FePc, $FePc(Cl)_{16}$ and CoPc formed cyclohexene oxide, 2-cyclohexen-1-ol, 2- cyclohexen-1-one and adipic acid. Product selectivity depended on the nature of catalyst and oxidant. The $FePc(Cl)_{16}$ catalyst was transformed into a μ-oxo dimer during the oxidation process while $M^{III}Pc$ intermediates were formed with $Co^{II}Pc$ and $Fe^{II}Pc$ catalysts.

Cyclohexene photooxidation catalyzed by zinc phthalocyanine using either red or white light formed 2-cyclohexen-1-one, 2-cyclohexen-1-ol, *trans*-cyclohexane diol, cyclohexene oxide and cyclohexene hydroperoxide via singlet oxygen and radical mechanisms. Product yields depended on the light wavelength and intensity, solvent, irradiation time and the rate of photo-degradation of the catalyst.

List of contents

Title page i

Dedications ii

Acknowledgements iii

Abstract iv

List of contents vi

List of abbreviations x

List of symbols xii

List of figures xiv

List of tables xxiii

List of schemes xxv

1. Introduction 1

1.1 Phthalocyanines 2

1.1.1 Background of phthalocyanines 2

1.1.2 Spectroscopic characterization of phthalocyanines 5

1.1.3 Electrochemistry of phthalocyanines 8

1.2 Background on electrochemical methods 10

1.2.1 Voltammetry 13

1.2.2 Mass transport 17

1.2.3 Hydrodynamic systems 18

1.2.3.1 Rotating disc electrode 19

1.2.3.2 Kinetics of electrode reactions 23

1.2.3.3 The transfer coefficient, α 24

1.2.3.4 Reaction order 26

1.3 Electro-catalysis 27

1.3.1 Use of metallophthalocyanines in electro-catalysis 27

1.3.2 Electrode modification 30

1.3.3 Characterization of modified electrodes 36

1.4 Overview of studied analytes 38

1.4.1 Electrocatalysis of thiocyanate oxidation 40

1.4.2 Electrocatalysis of thiol oxidation 43

1.4.3 Decomposition of nitrosothiols 47

1.4.4 Electrocatalysis of oxygen reduction 49

1.5 Use of metallophthalocyanines in biomimetic catalysis 55

1.6 Use of metallophthalocyanines in photo-catalysis 59

1.7 General aims of thesis 65

2. Experimental 66

2.1 Materials 67

2.2 Apparatus 68

2.3 Electrochemical methods 71

2.3.1 Electrode preparation 72

2.3.2 Electrode modification and characterization 75

2.3.2.1 Monomer adsorption 75

2.3.2.2 Electro-polymerization/deposition 76

2.3.2.3 Self-assembled monolayers 76

2.3.3 Electro-catalysis 77

2.4 Biomimetic catalysis 79

2.5 Photo catalysis 80

2.6 Syntheses 82

2.6.1 Iron (II) hexadecachlorophthalocyanine, $FePc(Cl)_{16}$ 83

2.6.2 Zinc phthalocyanine, ZnPc 83

2.6.3 Manganese tetrapentoxy pyrrole phthalocyanine 84

3. Electrocatalysis 88

3.1 Thiol oxidation 90

3.1.1 Adsorbed CoPc complexes **6b** and **6c** 90

3.1.2 Electro-deposited CoPc complexes **6b** and **6c** 106

3.1.3 Self-assembled monolayers 111

3.1.3.1 Characterization of SAM 111

3.1.3.2 *L*-cysteine oxidation on CoTEThPc-SAM 117

3.1.3.3 2-Mercaptoethanol oxidation on CoTEThPc-SAM 125

3.1.4 Screen printed carbon electrodes 128

3.2 Decomposition of *S*-nitrosoglutathione 141

3.3 Thiocyanate oxidation 146

3.4 Oxygen reduction 153

3.4.1 Characterization of new MnTPePyrPc, complex 7c 155

3.4.2 Characterization of adsorbed MnPc complexes 157

3.4.3 Oxygen reduction on MnPc complexes 163

3.4.4 Oxygen reduction on CoPc and FePc complexes 169

3.4.4.1 Characterization of adsorbed MPc complexes 170

3.4.4.2 Oxygen reduction 172

3.4.5 Mechanism of oxygen reduction 180

4. Biomimetic catalysis 193

4.1 Oxidation of cyclohexene 195

4.2 Fate of the catalysts 204

5. Photocatalysis 212

5.1. Photo-oxidation of cyclohexene 214

5.2. Solvent effects 222

5.3. Fate of the ZnPc catalyst 225

5.4. Singlet oxygen versus radical mechanisms 226

6. Conclusions 231

7. References 237

List of abbreviations

BAS	BioAnalytical systems
CE	Counter electrode
CME	Chemically modified electrodes
CPBA	Chloroperoxybenzoic acid
CV	Cyclic voltammetry
DABCO	Diazabicyclooctane
DBU	1,8-diazabicyclo[5.4.0] undec-7-ene
DCM	Dichloromethane
DMF	Dimethylformamide
DMSO	Deuterated dimethylsulfoxide
DPBF	1,3-diphenylisobenzofuran
GC	Gas chromatography
GCE	Glassy carbon electrode
GC-MS	Gas chromatography-mass spectrometry
HOMO	Highest occupied molecular orbital
HRP	Horseradish peroxidase
IR	Infrared
LMCT	Ligand-to-metal charge transfer
LOP	Lacto-peroxidase
LSV	Linear sweep voltammetry
LUMO	Lowest unoccupied molecular orbital
MLCT	Metal-to-ligand charge transfer
MPc	Metallophthalocyanine
^{3}MPc*	Excited triplet state of MPc
MPc-SAM	Metallophthalocyanine-Self-assembled monolayer
NHE	Normal hydrogen electrode
NMR	Nuclear magnetic resonance
OPGE	Ordinary pyrolytic graphite electrode
P	Porphyrin

List of symbols

α	Fraction of light absorbed/electron transfer coefficient
A	Absorbance/ ampere/ electrode area/ activity
b	Tafel slope
C	Coulomb/concentration
δ	Layer thickness
D	Diffusion coefficient
ε	Extinction coefficient
E	Potential
E^o	Standard potential
$E^{o'}$	Formal potential
E_{pa}	Anodic peak potential
E_{pc}	Cathodic peak potential
ϕ	Quantum yield
ϕ_P	Singlet oxygen quantum yield
ϕ_Δ	Photobleaching quantum yield
F	Faraday's constant
f	rotations per minute
γ	Activity coefficient
η	Overpotential
I_{pa}	Anodic peak current
I_{pc}	Cathodic peak current
k	rate constant
K	Kelvin
λ	Wavelength
m	Reaction order
m/z	Mass to charge ratio
mV	Millivolts
n	Number of electrons

n_α	Number of electrons in rate-determining step
N_A	Avogadro's number
$O_2(^3\Sigma_g)$	Triplet state oxygen
$O_2(^1\Delta_g)$	Singlet state oxygen
π	Pi-bonding
π^*	Pi anti-bonding
Q	Electrical charge
Γ	Surface coverage/concentration
Γ_{ibf}	Ion barrier factor
r	Radius of electrode
R	Gas constant
t	Time
T	Temperature
v	Scan rate/ velocity/ kinematic viscosity/ wavenumber
V	Volts
ω	Angular rotation rate
ΔE	Change in potential

List of figures

Figure 1.1: Molecular structures of 1) porphyrin (P) and 2) phthalocyanine (Pc).

Figure 1.2: Molecular orbitals involved in major absorption transitions, orbital order adapted from Gouterman.

Figure 1.3: Typical UV/Vis spectra of a) metal-free and b) metalled phthalocyanines.

Figure 1.4: Electron transfer at a metallic electrode. Potential applied to Fermi level facilitates a) reduction and b) oxidation.

Figure 1.5: Schematic representation of an electrochemical cell showing the working (WE), reference (RE) and counter electrodes (CE).

Figure 1.6: A typical cyclic voltammogram of a reduction-oxidation reaction.

Figure 1.7: Streamlines for a rotating disc electrode.

Figure 1.8: Rotating disc electrode voltammogram of an irreversible cathodic reaction.

Figure 1.9: Energy profiles for different values of charge transfer coefficients.

Figure 1.10: A schematic representation of an electro-catalytic reaction.

Figure 1.11: Structure of planes of an ordinary pyrolytic graphite.

Figure 1.12: a) Umbrella, b) octopus and c) vertical orientations of MPc-SAMs.

Figure 1.13: Electro-polymerization of NiTPhPyrPc in DMF and 0.1 M $TBABF_4$ at 200 mV/s.

Figure 1.14: Molecular structures of electro-chemically studied analytes; 2-mercaptoethanol, *L*-cysteine, *reduced*-glutathione and *S*-nitrosoglutathione.

Figure 1.15: Molecular structures of phthalocyanine complexes used in electro-catalytic oxidation of thiols and thiocyanate; CoPc, CoTPhPyrPc and CoTEThPc.

Figure 1.16: Different configurations adopted by molecular oxygen upon interaction with metal sites.

Figure 1.17: Molecular structures of phthalocyanine complexes used in electro-catalytic reduction of oxygen; MnPc, MnTAPc, MnTPePyrPc, MnTPhPyrPc, MnTMerPyPc and MnTEThPc.

Figure 1.18: Molecular structures of FePc and $FePc(Cl)_{16}$ complexes used as biomimetic catalysts for oxidation of cyclohexene.

Figure 1.19: Modified Jablonski diagram illustrating processes that occur when a phthalocyanine molecule absorbs UV/Vis light.

Figure 2.1: Photolysis setup used for zinc phthalocyanine photocatalyzed oxidation of cyclohexene.

Figure 2.2: A laser flash photolysis set up.

Figure 2.3: Photographs and schematic representations of fabricated SPCEs on alumina ceramic and Labtek platforms.

Figure 3.1: Molecular structures of phthalocyanine complexes used in electro-catalytic oxidation of thiols and thiocyanate; CoPc, CoTPhPyrPc and CoTEThPc.

Figure 3.2: Cyclic voltammograms of OPG electrodes modified by adsorption of a) CoTPhPyrPc **6b** and b) CoTEThPc **6c** in 0.5 M NaOH.

Figure 3.3: Cyclic voltammograms of oxidation of a) 2-ME, b) CYS and c) GSH on CoTEThPc **6c** and B: CoTPhPyrPc **6b** complexes adsorbed on GCE in 0.5 M NaOH solution.

Figure 3.4. Cyclic voltammograms of catalytic oxidation of 2-ME by adsorbed CoTEThPc **6c** at varying concentrations. Insert is a variation of current and concentration.

Figure 3.5. Cyclic voltammograms of oxidation of 2.5 mM 2-ME in a) 0.5 M NaOH (pH~13) and b) PBS (pH = 7.2) solution catalyzed by adsorbed CoTEThPc **6c** complex. Scan rate = 100 mV/s.

Figure 3.6. RDEs of catalytic oxidation in 0.5 M NaOH solution catalyzed by adsorbed CoTEThPc **6c**. Inserts = Koutecky-Levich plots.

Figure 3.7. Plots of, A. log I vs log C and B. $1/\omega^{1/2}$ vs 1/I for 2-ME catalytic oxidation on CoTEThPc **6c** adsorbed on GCE.

Figure 3.8. Tafel plots of thiol oxidation catalyzed by adsorbed CoTEThPc **6c**.

Figure 3.9: Electropolymerization of CoTPhPyrPc **6b** on GCE in DMF and 0.1 M $TBABF_4$ at 200 mV/s.

Figure 3.10: Cyclic voltammograms of 2.5 mM 2-ME oxidation on a) adsorbed and b) electrodeposited **6c** on GCE in 0.5 M NaOH at 100 mV/s.

Figure 3.11: Cyclic voltammograms of i) unmodified Au electrode and ii) CoTEThPc-SAM in a) 0.01 M KOH, b)1 mM $CuSO_4$ in 0.5 M H_2SO_4, c) 1 mM $Fe(NH_4)(SO_4)_2$ in 1 mM $HClO_4$ and d) 1 mM Na_2SO_4 in pH 4 solution. Scan rate = 50 mV/s.

Figure 3.12: Cyclic voltammograms of CoTEThPc-SAM in pH 4 buffer solution showing redox processes related to $Co^{III/II}$ peaks. Scan rate = 50 mV/s. Insert is variation of $Co^{III/II}$ peak current with scan rate.

Figure 3.13: Cyclic voltammograms of *L*-cysteine on i) bare Au and ii) CoTEThPc-SAM in a) pH 4 and b) pH 1, 3 and 5 solutions. Scan rate = 50 mV/s.

Figure 3.14: Pourbaix diagram for 1 mM *L*-cysteine on CoTEThPc-SAM.

Figure 3.15: UV-Vis spectral changes observed on addition of *L*-cysteine to solutions of CoTEThPc in DMF.

Figure 3.16: Plot of square root of scan rate versus peak current for 1 mM *L*-cysteine oxidation on CoTEThPc-SAM in pH 4.

Figure 3.17: Cyclic voltammograms of 2-ME in pH 4 solution on CoTEThPc-SAM.

Figure 3.18: Pourbaix diagram for 1 mM 2-mercaptoethanol on CoTEThPc-SAM.

Figure 3.19: Cyclic voltammograms of 1 mM $Fe(CN)_6^{3-}/Fe(CN)_6^{4-}$ in 0.1 M KCl on i) bare SPCE and ii) 5 % CoPc-SPCE at 100 mV/s.

Figure 3.20. Cyclic voltammograms of a) 2 mM 2-ME and b) 0.01 M GSH in 0.1 M NaOH (pH~13) on 5 % CoPc-SPCE at 50 mV/s.

Figure 3.21: Cyclic voltammograms of a) 3 mM 2-ME and b) 0.01 M GSH in PBS (pH = 7.4) on 5 % CoPc-SPCE at 50 mV/s.

Figure 3.22: a) Cyclic voltammograms of various concentrations of 2-ME in 0.1 M NaOH (pH ~ 13) on 5 % CoPc-SPCE at 50 mV/s. b) Variation of concentration and peak current for 2-ME oxidation in 0.1 M NaOH on 5 % CoPc-SPCE.

Figure 3.23: Cyclic voltammograms of 50 mM GSH at 1% CoPc-SPCE, 2.5% CoPc-SPCE and 5% CoPc-SPCE in a) PBS (pH 7.4) and b) 0.1 M NaOH aqueous solution.

Figure 3.24: Cyclic voltammograms of a) 10 mM GSH and b) 1 mM $K_4Fe(CN)_6$ in PBS (pH 7.4) at different 1% and 2.5% CoPc-SPCEs.

Figure 3.25: Cyclic voltammograms of a) 3 mM 2-ME and b) 1 mM $K_4Fe(CN)_6$ in PBS (pH 7.4) at different 1% and 2.5% CoPc-SPCEs.

Figure 3.26: Cyclic voltammograms of CoPc adsorbed on OPG in PBS (pH 7.4) at 50 mV/s.

Figure 3.27: Cyclic voltammograms of CoPc adsorbed on OPG in a) commercial Dulbecco phosphate buffer saline (pH 7.4), in the presence of b) 5 mM glucose, c) 5 mM glucose + 10 µM $Cu(NO_3)_2$ and d) 5 mM glucose + 10 µM $Cu(NO_3)_2$ + 1 mM GSH at 50 mV/s.

Figure 3.28: Cyclic voltammograms of CoPc adsorbed on OPG in a) aerobic phosphate buffer (pH 7.4), in the presence of b)1 mM GSNO, c) 1 mM GSNO + 0.025 mM $Cu(NO_3)_2$ and d) after immediate addition of 1 mM $NaBH_4$ and e) 1 minute later curve at 50 mV/s.

Figure 3.29: Cyclic voltammograms of 1 mM thiocyanate in pH 4 solution on a) bare Au and b) CoTEThPc-SAM. Scan rate = 50 mV/s.

Figure 3.30: Pourbaix diagram of 1 mM thiocyanate on CoTEThPc-SAM.

Figure 3.31: Plots of a) E_p versus log υ and b) log i_p vs log $[SCN^-]$ for oxidation of thiocyanate on CoTEThPc-SAM in pH 4.

Figure 3.32: UV-Vis spectral changes observed on addition of SCN^- to solutions of CoTEThPc in DMF.

Figure 3.33: Molecular structures of phthalocyanine complexes used in electro-catalytic reduction of oxygen; MnPc, MnTAPc, MnTPePyrPc, MnTPhPyrPc, MnTMerPyPc and MnTEThPc.

Figure 3.34: UV/Visible spectrum of MnTPePyrPc **7c** in DMF.

Figure 3.35: Cyclic voltammograms in i) nitrogen-purged and ii) oxygen saturated pH 5 buffer solutions of complexes **7a** to **7f**. Scan rate = 50 mV/s.

Figure 3.36: Pourbaix diagram for $Mn^{III/II}$ couple of complex **7c**.

Figure 3.37: Cyclic voltammogram of **7c** showing $Mn^{III/II}$ couple in pH 12 at scan rates of 100 - 400 mV/s. Insert is a plot of peak current versus scan rate.

Figure 3.38: Cyclic voltammograms of oxygen reduction in pH 12 for adsorbed MnPc complexes a) **7a**, **7b** and **7e**, b) **7c**, **7d** and **7f** at 50 mV/s.

Figure 3.39: Plot of square root of scan rate versus peak current for oxygen reduction on MnPc in pH 12.

Figure 3.40: Rotating disk electrode voltammograms of adsorbed MnPc complexes in pH a) 5 and b) 12 oxygen saturated solutions.

Figure 3.41: Cyclic voltammograms in pH 7 buffer solution of glassy carbon electrodes modified by adsorption of a) **6a** and b) **8** at 50 mV/s.

Figure 3.42: Plots of I_p versus ν for $M^{III/II}$ peak of a) CoPc and b) FePc adsorbed on GCE in pH 7 buffer solution.

Figure 3.43: Cyclic voltammograms of oxygen reduction reaction in oxygen saturated pH 7 buffer solutions on unmodified GCE, **6a**, **6b**, **6c**, **8** and **9** modified electrodes at 50 mV/s.

Figure 3.44: Pourbaix diagram of oxygen reduction reaction electro-catalyzed by complexes **6a, 6b, 6c, 8 and 9.**

Figure 3.45: Rotating disk electrode (RDE) voltammograms of oxygen reduction in pH 12 on adsorbed MPc complexes.

Figure 3.46: Tafel slopes of oxygen reduction reaction electro-catalyzed by complexes **6a, 6b, 6c, 8 and 9** in pH 12 buffer solutions.

Figure 3.47: UV/Visible spectra of complexes **7a**, **7c** to **7f** in DMF.

Figure 3.48: UV/Visible spectra of complexes **6a, 6b, 6c** and **9** in DMF.

Figure 4.1: Gas chromatograms for biomimetic oxidation of cyclohexene using TBHP as an oxidant and $FePc(Cl)_{16}$ as the catalyst.

Figure 4.2: Variation of product yield with time for i) 2-cyclohexen-1-one, ii) 2 cyclohexen-1-ol and iii) cyclohexene oxide.

Figure 4.3: Variation of product yield with substrate to oxidant molar ratios for i) 2-cyclohexen-1-one ii) 2-cyclohexen-1-ol and iii) cyclohexene oxide.

Figure 4.4: Variation of product yield with the amount of catalyst for i) 2-cyclohexen-1-one ii) 2-cyclohexen-1-ol and iii) cyclohexene oxide.

Figure 4.5: Effect of the nature of catalyst on the 2-cyclohexen-1-one product yield for i) $FePc(Cl)_{16}$ ii) FePc and iii) CoPc catalysts.

Figure 4.6: Absorption spectral changes observed on addition of 0.5 mol dm^{-3} TBHP oxidant to a reaction mixture of $FePc(Cl)_{16}$ catalyst and cyclohexene.

Figure 4.7: Absorption spectral changes observed on addition of 0.5 mol dm^{-3} CPBA oxidant to a reaction mixture of $FePc(Cl)_{16}$ catalyst and cyclohexene.

Figure 4.8: Absorption spectral changes observed on addition of 0.5 $moldm^{-3}$ TBHP oxidant to a reaction mixture of a) FePc and b) CoPc catalysts and cyclohexene.

Figure 5.1: Gas chromatogram of cyclohexene oxidation photo-catalyzed by ZnPc in 1,4-dioxane under white light irradiation.

Figure 5.2: Variation of 2-cyclohexen-1-one with time on photolysis with i) white or ii) red light and in the presence of ZnPc photocatalyst.

Figure 5.3: Variation of product yield with time for i) 2-cyclohexen-1-one ii) 2-cyclohexen-1-ol iii) *trans*-cyclohexanediol and iv) cyclohexene oxide under white light irradiation.

Figure 5.4: Photodegradation of ZnPc in 1,4-dioxane with visible light.

Figure 5.5: A triplet absorption curve of ZnPc in THF.

Figure 5.6: Variation of absorbance of ZnPc catalyst with time upon white light photolysis at various light intensities.

Figure 5.7: Kinetic curves for product formation from the ZnPc-photocatalyzed oxidation of cyclohexene in 1,4-dioxane under white light irradiation conditions in the presence of i) air, ii) nitrogen, iii) bubbled oxygen, iv) DPBF and v) DABCO.

List of tables

Table 1.1: Electrochemical data for electro-catalytic oxidation of thiocyanate by self-assembled monolayers of metallophthalocyanines on gold electrodes in pH 4 solutions.

Table 1.2: Electrochemical data for 2-mercaptoethanol, *L*-cysteine and *reduced* glutathione oxidation.

Table 1.3: Electrochemical data for oxygen reduction catalyzed by MPcs.

Table 1.4: Data for cyclohexene epoxidation catalyzed by MPs and MPcs.

Table 1.5: Data for photocatalyzed oxidation of cyclohexene by metallo-porphyrins.

Table 2.1: Electrodes and modifiers used for electrocatalysis of thiol & thiocyanate oxidation and oxygen reduction.

Table 3.1: Catalytic efficiency of adsorbed CoTEThPc **6c** and CoTPhPyrPc **6b** in terms of peak potentials E_p and currents I_p in 0.5 M NaOH.

Table 3.2: Electrochemical data for thiol oxidation in 0.5 M NaOH catalyzed by complexes **6b** and **6c**.

Table 3.3: Catalytic current intensities of electrodeposited CoTEThPc **6c** and electro-polymerized CoTPhPyrPc **6b** on glassy carbon electrode for the electro-oxidation of 2-ME.

Table 3.4: Electrochemical data of thiol and thiocyanate oxidation on electrodes modified by CoPc complexes.

Table 3.5: Catalytic factor (f) calculated for the oxidation of GSH and 2-ME in neutral aqueous solution for different CoPc-SPCEs.

Table 3.6: Oxygen reduction data in pH 5 for complexes **7a - 7f** adsorbed on GCE.

Table 3.7: Oxygen reduction data for complexes **6a**, **6b**, **6c**, **8** and **9** in pHs 2, 7 and 12.

Table 4.1. Product yields, selectivities and turnover numbers for the oxidation of cyclohexene using TBHP oxidant and $FePc(Cl)_{16}$ catalyst in a 3:7 DMF-CH_2Cl_2 solvent mixture.

Table 4.2: Product selectivities for cyclohexene oxidation using $FePc(Cl)_{16}$ **9**, FePc **8** and CoPc **6a** catalysts and TBHP oxidant.

Table 5.1: Comparison of cyclohexene ZnPc-photocatalyzed oxidation product yields in the various solvents at various light intensities with white light irradiation.

List of schemes

Scheme 1.1: Examples of phthalocyanine synthetic routes.

Scheme 1.2: Type II mechanism of photo-catalysis.

Scheme 1.3: Type I mechanism of photo-catalysis.

Scheme 3.1: Thiol oxidation mechanism in alkaline media.

Scheme 3.2: Mechanism of *L*-cysteine oxidation in acidic media catalyzed by $Co^{III}Pc/Co^{II}Pc$ redox couple.

Scheme 3.3: Mechanism of *L*-cysteine oxidation in acidic media catalyzed by $Co^{III}Pc^{-1}$ /$Co^{III}Pc^{-2}$ redox couple.

Scheme 3.4: Thiocyanate oxidation mechanism in acidic media catalyzed by $Co^{III}Pc^{-1}$ /$Co^{III}Pc^{-2}$ redox couple.

Scheme 3.5: Synthesis of MnTPePyrPc **7c**.

Scheme 3.6: Oxygen adsorption onto an electrode.

Scheme 3.7: Mechanism of oxygen reduction catalyzed by MnPc complexes.

Scheme 3.8: Mechanism of oxygen reduction catalyzed by CoPc and FePc complexes.

Scheme 4.1. The mechanism for $Fe^{II}Pc(Cl)_{16}$ transformation during the catalytic oxidation of cyclohexene.

Scheme 4.2. Products formed from oxidation of cyclohexene by TBHP or CPBA oxidants in the presence of $FePc(Cl)_{16}$, CoPc or FePc catalysts.

Scheme 5.1: Type I mechanism of photo-catalysis.

Scheme 5.2. Hydrogen abstraction and formation of MPc radicals.

Scheme 5.3. Quenching of excited states by chlorinated solvents.

Scheme 5.4: Type II mechanism of photolysis.

Scheme 5.5: Degradation of MPc by singlet oxygen.

Scheme 5.6: Suggested mechanism for the formation of photolysis products.

Chapter 1

Introduction

1.1 Phthalocyanines

The main aim of the project is to use phthalocyanines (Pcs) as catalysts, hence their properties will be discussed first.

1.1.1 Background of phthalocyanines

Phthalocyanines are conjugated, aromatic, symmetrical, macrocyclic complexes with an 18 π electron system[1]. They contain four isoindole groups which are linked by four nitrogen atoms. Unmetallated Pcs (**2**, Fig. 1.1) are planar exhibiting D_{2h} symmetry whereas their metallated counterparts exhibit D_{4h} symmetry. They are similar to naturally occurring porphyrins (**1**, Fig. 1.1); but have extended conjugation engendered by benzene rings, hence have improved chemical and thermal stability. Another set consisting of four benzene rings can be fused onto the Pc ring yielding naphthalocyanines, then subsequently anthralocyanines.

Phthalocyanines were discovered in the 1930's and were used as blue and blue-green pigments and dyes[2]. Over time, their properties have been developed, these include semi-conductivity in the 1940's[3] and synthetic modifications in the 1970's[4]. Amongst their numerous applications, they are now currently employed as photo-sensitizers in photodynamic therapy of cancer (PDT)[5,6], involved in linear[7] and non-linear optics[8], used as electro[9,10] and biomimetic[11,12] catalysts and as fluorescent agents[13]. They are also used as thin, light-absorbing films to coat compact discs (CDs)[14].

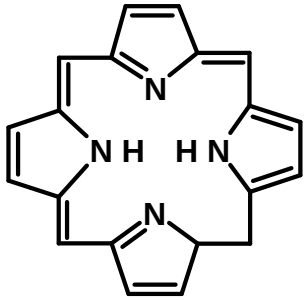

Porphyrin 1

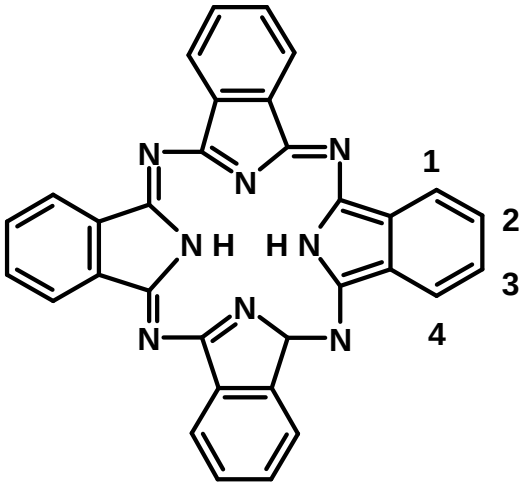

Phthalocyanine 2

Figure 1.1: Molecular structures of 1) porphyrin (P) and 2) phthalocyanine (Pc).

Pcs are synthesized by various methods (Scheme 1.1) and these include cyclotetramerization of a) phthalonitriles **3**[15], b) phthalic anhydrides **4**[16] and c) phthalimides **5**[17]. Formation of Pcs from condensation of phthalonitriles occurs upon heating in an appropriate high boiling solvent such as 1-pentanol in the presence of an organic base such as 1,8-diazabicyclo[5.4.0]undec-7-ene (DBU)[18]. Condensation of phthalic anhydrides **4** and phthalimides **5** to form Pcs occurs in the presence of a nitrogen source such as urea and a catalyst such as ammonium molybdate[19]. Unsubstituted Pcs have 16 hydrogen atoms on the ring which are ideal substitution sites. Substituents can be introduced onto the precursors to afford ring substituted Pcs[20]. Ring substitution occurs on peripheral (2 and 3) or non-peripheral positions (1 and 4) (see 2, Fig. 1.1 for numbering), depending on the initial substitution position on the precursors.

Metallation in Pcs is afforded by performing precursor condensation reactions in the presence of metal salts[21]. It can also be achieved by refluxing

the metal-free H_2Pc in the presence of a metal salt forming metallophthalocyanines (MPc)[22]. This makes a way for axial ligation occurrence on the central metal, depending on its oxidation state. Metallation of Pcs with metals that fit in the cavity of the ring such as zinc[23] leads to symmetry change from D_{2h} (H_2Pc) to D_{4h}. Other metals such as tin[24] lie out of plane of the Pc ring hence have a symmetry of C_{4v}. Generally, symmetry change is governed by central metal size, axial and ring substituents, as well as the nature of solvents[25].

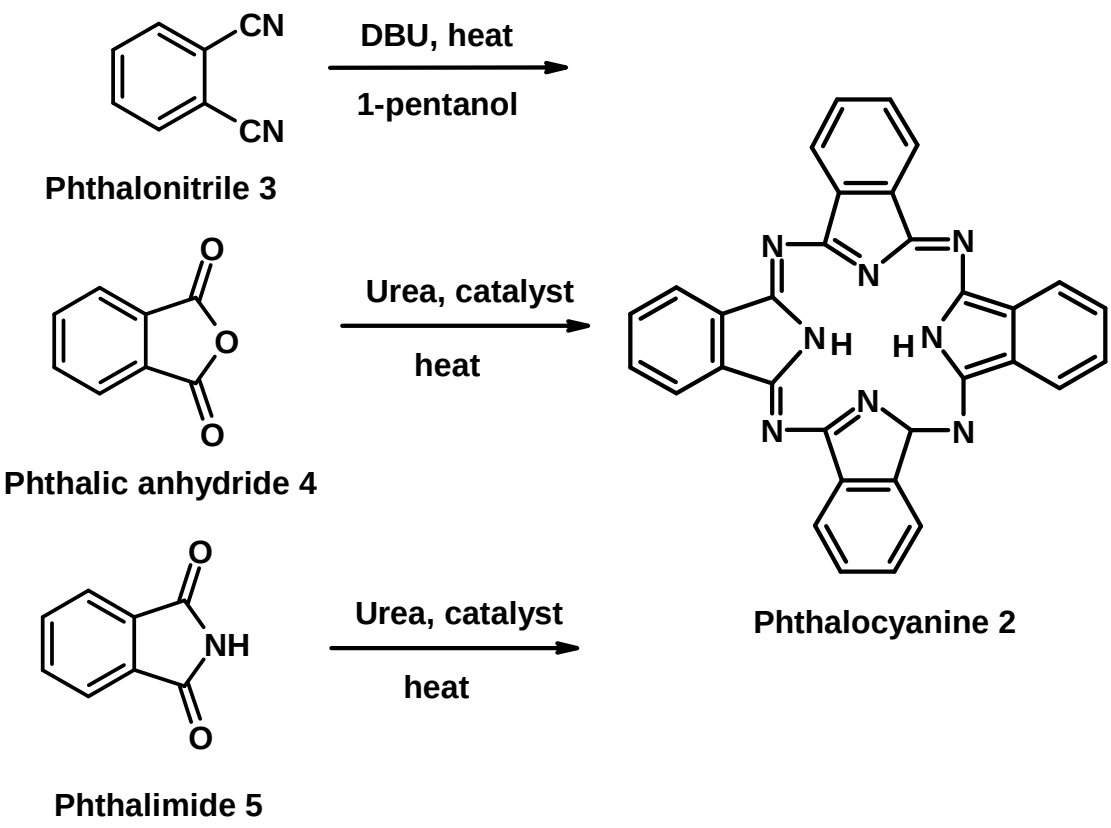

Scheme 1.1: Examples of phthalocyanine synthetic routes.

Properties of Pcs can be changed or fine-tuned by substitution[25,26]. For instance, amphiphilicity[27] can be endowed by ring substitution with hydrophilic

and hydrophobic groups. In addition, substitution eliminates aggregation[28], which is basically Pc-Pc stacking. Axial and ring substituents create steric hinderance hence the bulkier the ligands, the more pronounced the effect. Substitution also makes way for making complex structures such as porphyrin-phthalocyanine conjugates[29]. Substituents can also coordinate to form μ-oxo dimers[30], sandwich-type dimers[31], polymers[32] or long chain Pc complexes[33]. Moreover, substitution facilitates chromatographic analysis because of varying polarity[34]. Symmetry of the Pc may be altered by substitution due to geometric perturbations[35].

1.1.2 Spectroscopic characterization of phthalocyanines

Pcs make colourful solutions, depending on the solvent, central metal and substituents on the ring. They exhibit strong absorption in the red region of the electromagnetic spectrum with extinction coefficients[36,37] greater than 10^5 L mol^{-1} cm^{-1}. The peak positions vary depending on the nature of the Pc. The main absorption peak at around 670 nm is called the Q-band[38] and it stems from π-π* transitions ($a_{1u} \rightarrow e_g$, Fig. 1.2). Vibronic bands are observed in the proximity of Q-bands due to vibrational transitions[39]. There are also π-π* transitions in the blue giving rise to B-bands[40], also known as Soret bands ($a_{2u}/b_{1u} \rightarrow e_g$, Fig. 1.2). A single B band is observed around 350 nm due to superimposition of B_1 and B_2 bands. There is also a band observed around 500 nm for some transition metal MPcs[41]. It is attributed to charge transfer transitions from metal to ligand (MLCT) or from ligand to metal (LMCT)[42]. Moreover, additional N and L bands are observed in transparent solvents

such as dichloromethane at high energy (higher than the B band) for Pcs metallated with non-transition metals[36].

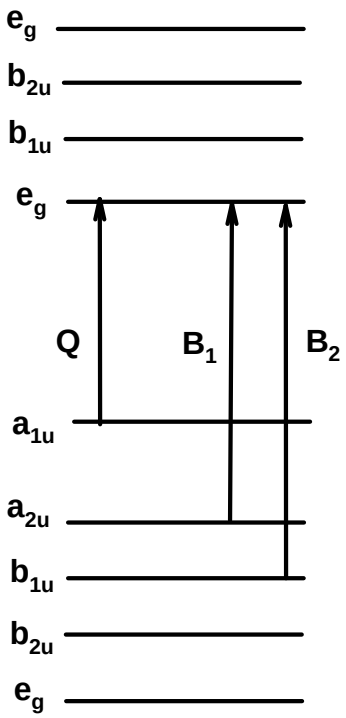

Figure 1.2: Molecular orbitals involved in major absorption transitions, orbital order adapted from Gouterman.

Metal and ring substitution alter positions of the highest occupied molecular orbital (HOMO) or lowest unoccupied molecular orbital (LUMO) energy levels resulting in different colours and absorption peak positions[43,44]. Metal-free Pcs exhibit a split Q-band whereas their metallated counterparts have a single distinct peak (Fig. 1.3). This is due to the fact that the e_g (LUMO) energy level of metal-free Pcs is non-degenerate[45]. Metallation makes the e_g energy level degenerate, thus only one electronic transition from the a_{1u} level occurs[46], resulting in an increase of symmetry from D_{2h} to D_{4h}. It has also been reported that the Q-band shifts to the red as size of central metal increases[47]. Ring[48] or axial[49] substitution with electron withdrawing

groups increase the HOMO-LUMO energy gap and cause bathochromic shifts whereas their electron donating counterparts reduce it leading to hypsochromic shifts. Non-peripheral substitution results in a larger red shift of the Q-band compared to peripheral substitution[50]. This is due to perturbation of the HOMO, raising its energy, resulting in shifts to longer wavelengths.

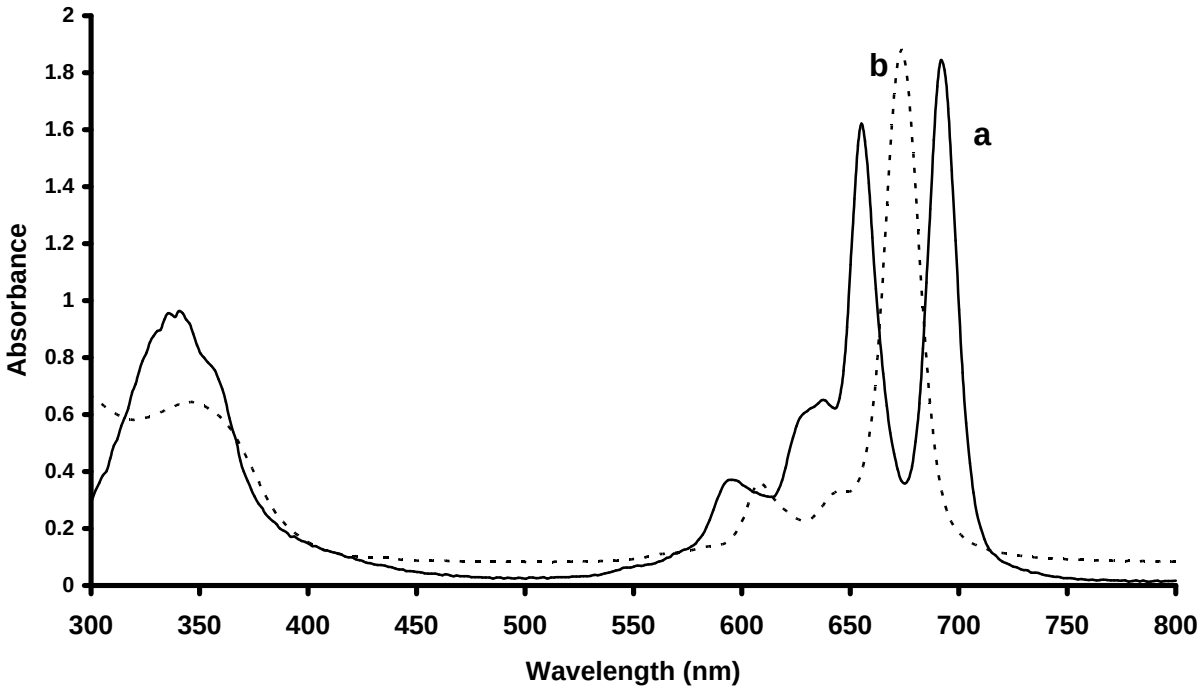

Figure 1.3: Typical UV/Vis spectra of a) metal-free and b) metalled phthalocyanines.

Protonation of aza-methine nitrogens of the Pc has been reported by Ogunsipe et al.[51] to result in symmetry loss. Odd-numbered protonation results in D_{2h} symmetry, hence a split Q-band. Even-numbered protonation exhibits D_{4h} symmetry, hence a single Q-band peak. When only two nitrogens have been protonated, D_{4h} symmetry is obtained when hydrogen atoms have adopted a *–cis* configuration. If protonation is unsymmetrical, i.e. *–trans,* the symmetry is C_{4v}, hence the Q-band is split. As a matter of fact, lack of symmetry shifts the Q-band to longer wavelengths[52].

The nature of solvent affects UV/Vis spectra of Pcs[53]. Conjugated and aromatic solvents shift Q-bands to the red[54]. Solvents such as chloroform oxidize the Pc ring leading to a decrease of Q-band intensity, appearance of a broad charge-transfer peak around 500 nm and colour change to purple[39]. Decomposition of solvents such as DMSO[55] forms various ligating substances which coordinate with the Pc yielding multiple Q-bands. Peaks associated with n-π^* transitions shift to the blue with increasing solvent polarity whereas π-π^* transitions shift to the red[56]. Furthermore, solvents with high refractive indices such as 1-chloronaphthalene reduce the HOMO-LUMO energy gap, hence cause a red shift[57].

Phthalocyanines maybe characterized by other techniques such as infra-red (IR) and nuclear magnetic resonance (NMR) spectroscopies, as well as mass spectrometry and elemental analysis.

1.1.3 Electrochemistry of phthalocyanines

The electrochemical activity of unmetallated Pcs is related to processes occurring on the ring. Oxidation is removal of electron(s) from the HOMO while reduction is the addition of electron(s) to the LUMO, in H_2Pc derivatives. The Pc skeleton exists as a dianion, Pc(-2), successive removal of up to two electrons from the HOMO (a_{1u}) results in the formation of Pc(-1) and Pc(0) π-cation radicals, respectively[58]. Similarly, successive addition of up to four electrons to the LUMO (e_g) results in the formation of Pc(-3), Pc(-4), Pc(-5) and Pc(-6) π-anion radicals respectively[59]. These processes can be monitored with electrochemical methods such as amperometry. Peak

separation between the first oxidation and reduction processes is equal to ~1.6 V for H_2Pc[60].

Metallophthalocyanines (MPcs) containing electroactive central metals exhibit electroactivity associated with the central metals, in addition to ring processes[61]. Examples of electroactive metals include cobalt, iron and manganese while electrochemically inactive metals include zinc and magnesium. Peaks or couples linked to oxidation or reduction of the central metal usually lie between those for ring oxidation or reduction processes[62]. Moreover, electroactive ligands substituted on the Pc also exhibit their own characteristic redox peaks or couples[63]. Potentials at which redox couples are observed depend on the nature of the molecule and solvent[64]. Redox processes of MPc complexes are assigned successfully using spectro-electrochemistry[65,66]. This technique involves recording UV/Vis spectra as potential is applied. It therefore requires unique electrodes such as indium tin oxide (ITO)[67,68], which are optically transparent, conductive, mechanically strong, resistant to corrosion and exhibit low background currents.

Central metal or phthalocyanine ring oxidation and reduction can be afforded by other non-electrochemical methods. Oxidation is afforded by use of oxidizing agents such as bromine, and photochemically by irradiation with light of suitable wavelength in the presence of an appropriate electron acceptor. On the other hand, reduction is achieved by use of reducing agents such as sodium borohydride and by photochemical irradiation in the presence of an appropriate electron donor. Ring oxidation to π cation radical is accompanied by loss of intensity of the Q band[39], formation of new bands[36]

near 500 nm (charge transfer), 830 nm (Pc^{-1} monomer), 720 nm and 1040 nm due to $(Pc^{-1})_2$ dimer and solution colour change to purple[1].

Ring reduction involves addition of electrons to the e_g LUMO energy level resulting in the collapse of the Q-band[69] and formation of two bands in the 500 - 600 nm region[70]. Additional bands are observed near 780 and 860 nm. Ring reduction is accompanied by colour change[71] to bluish purple, purple, blue and blue-green for Pc^{-3} anion, Pc^{-4} dianion, Pc^{-5} trianion and Pc^{-6} tetraanions respectively. Furthermore, oxidation or reduction processes occurring at the central metal of MPcs are characterized by a shift of the Q-band without a drastic decrease of peak intensity[1]. Intensities of B and Q bands are not affected since they are due to π-π transitions. However, charge transfer bands near 500 nm due to metal to ligand (MLCT) or ligand to metal (LMCT) transitions may be lost or formed.

1.2 Background on electrochemical methods

Electrochemical methods play an important part in this thesis hence the background on electrochemistry is provided in this section. Electrochemistry is a branch of chemistry that deals with reactions that occur on the interface of an electronic conductor and an ionic conductor. In metallic electrodes, electrons are removed or transferred to the highest occupied orbital, the Fermi level E_f (Fig. 1.4). Consider a typical reduction reaction; $O + ne^- \rightarrow R$, where O and R are soluble. For a reduction, there is a minimum energy that the transferable electrons from the electrode must have before electron transfer can occur, corresponding to a negative E (V). The inverse is true for oxidation;

there is a maximum energy that the lowest unoccupied level in the electrode can have to receive electrons from species in solution, corresponding to a positive E(V). Different potentials applied to the electrode can change the direction of electron transfer.

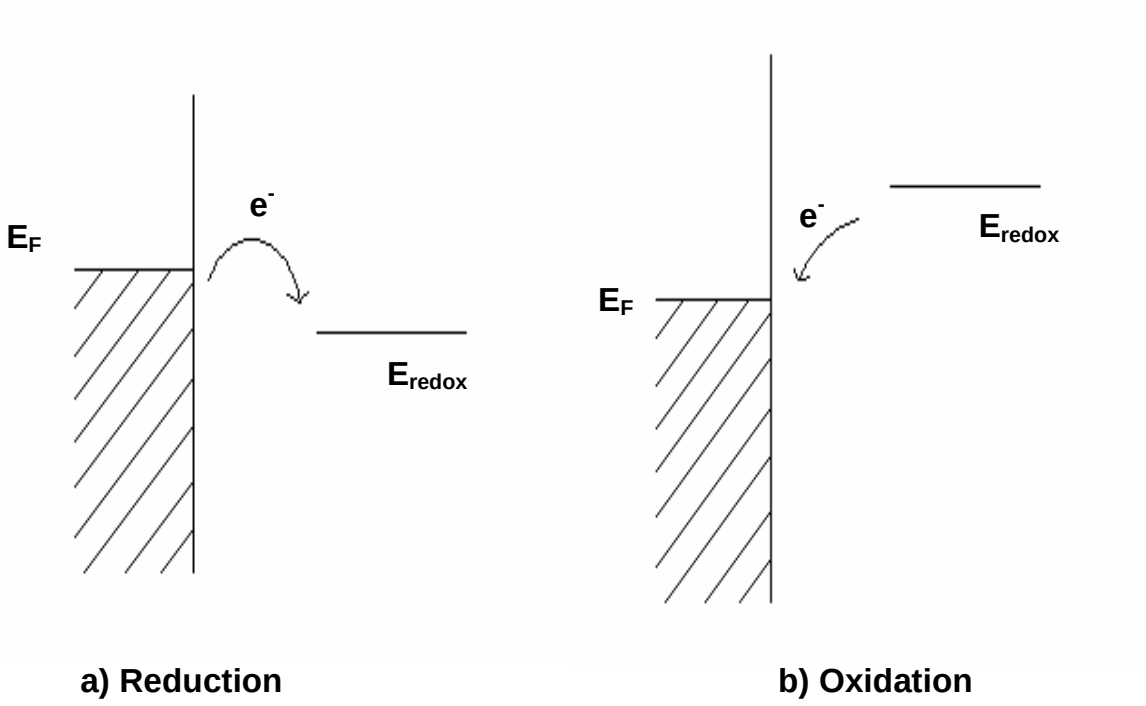

Figure 1.4: Electron transfer at a metallic electrode. Potential applied to Fermi level facilitates a) reduction and b) oxidation.

Electrochemical reactions are studied by various techniques such as voltammetry. Voltammetry is based on measurement of current as a function of potential applied to the working electrode (WE)[72]. An experimental set-up usually used for voltammetry is shown in Fig. 1.5.

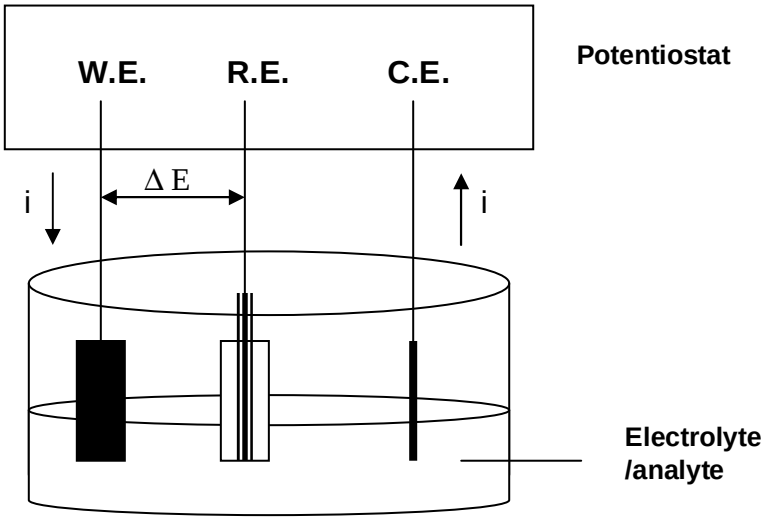

Figure 1.5: Schematic representation of an electrochemical cell showing the working (WE), reference (RE) and counter electrodes (CE).

Electrochemical reactions[73] occur on the working electrode (WE) and potential is measured relative to a reference electrode (RE) of known potential. The WE acts as a source or sink of electrons for exchange with the interfacial region. This region consists of electrolyte solution adjacent to the electrode surface where charge distribution differs from that in the solution bulk. The WE must be an electronic conductor and must be electrochemically inert, i.e. does not generate current when potential is applied. There is a wide variety of materials used as WE, choice of material depends on the potential window required.

The RE must be chemically and electrochemically reversible, i.e. its potential must be governed by Nernst equation and should not change with time. It must also be non-polarizable meaning its potential must remain constant when a small current passes through, otherwise it should regain its

original value after such current flow. Lastly, it must have a small potential thermal coefficient, i.e. its potential must be temperature independent. The counter electrode (CE) has to be more conducting than the RE, otherwise current flow might alter potential of the reference electrode. CE should have a much larger surface area than the WE (at least 5 times). Since electrode reaction rate is strongly dependent on surface area, it is recommended that a CE of much larger surface area compared to the WE must be used to obtain a much faster reaction rate for the reaction occurring at the CE than those occurring at the WE. Thus the reactions occurring at the WE are the slowest, they determine the overall reaction rate and the data obtained through the potentiostat reflect the behaviour and properties of reactions occurring at the WE.

1.2.1 Voltammetry

Voltammetry is a potential sweep technique that is widely used to study electrode processes as mentioned earlier. It consists of application of a continuously time-varying potential to the WE at any measured rate. In linear sweep voltammetry (LSV), potential is scanned from the initial potential E_i in one direction stopping at the final potential E_f, whereas in cyclic voltammetry (CV), the sweep direction is reversed at E_f to the initial potential (E_i). The scan direction can be either positive or negative depending on the reaction studied. Application of potential results in the occurrence of oxidation or reduction reactions of electroactive species in solution. In addition, adsorption,

deposition or polymerization may occur. A typical cyclic voltammogram (CV) of a general reduction-oxidation reaction $R \leftrightarrow O + ne^-$ is shown in Fig. 1.6.

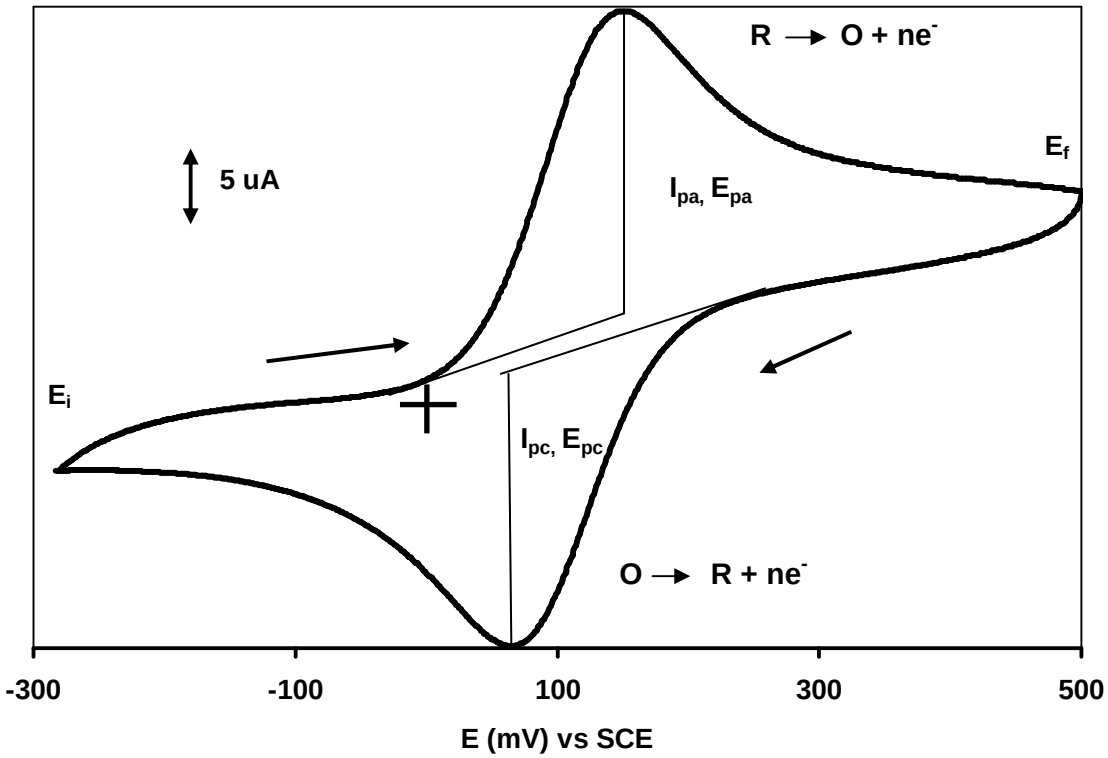

Figure 1.6: A typical cyclic voltammogram of a reduction-oxidation reaction.

At the beginning of potential sweep, nothing happens thus background current is detected. At a potential close to E_{pa}, R gets oxidized to O and the current increases because of electron transfer. At potential E_{pa}, the current reaches its maximum since equilibrium is reached between surface concentrations of O and R. Generally, there is an on-going competition between electron transfer at the electrode surface and diffusion of fresh solution towards the electrode surface. As potential application continues, the diffusion layer increases, decreasing the driving force for diffusion. Therefore less compound (R) arrives at the surface of the electrode per unit time, thus current signal becomes smaller; decaying exponentially following a profile

proportional to $t^{-1/2}$. When potential E_{pc} is reached, O gets reduced back to R and the formed R subsequently moves into the bulk of the solution. If potential sweep continues, the cycle recurs. The potential of the half reactions is given by Nernst equation (eq. 1.1):

$$E = E^0 - \frac{RT}{nF} \ln \frac{[R]}{[O]} \qquad 1.1$$

where E^o is standard electrode potential (potential when all reactants and products are at unit activity), R is the gas constant, n is number of moles of electrons, F is Faraday's constant, T is temperature in Kelvin, [R] and [O] are activities of reduced and oxidized species respectively.

Substituting numerical values for the constants and converting to base 10 logarithms at 25ºC, eq. 1.1 becomes eq.1.2,

$$E = E^0 - \frac{0.0592}{n} \log \frac{[R]}{[O]} \qquad 1.2$$

Activity of a species a_x is related to its molar concentration [X] by equation 1.3:

$$A_x = \gamma_x [X] \qquad 1.3$$

where γ_x is activity coefficient of X, a parameter that depends on ionic strength of the solution. It is usually approximated to be unity because of high concentrations of electrolytes added in solution hence activity is equal to molar concentration.

Reversible systems

When surface concentrations of O and R are maintained at values required by the Nernst equation, the system is in equilibrium throughout the potential scan. Species formed in the forward reaction is regenerated in the

reverse reaction, i.e. $O + ne^- \leftrightarrow R$. The reaction is termed reversible and it has the following characteristics:

1. Peak current, i_P (A) is given by the Randles-Sevcik equation at 25ºC, (eq. 1.4):

$$i_p = 2.69x10^5 n^{3/2} ACD^{1/2} v^{1/2} \qquad 1.4$$

where n is number of moles of electrons transferred, A is electrode area (cm^2), C is molar concentration (mol/L), D is diffusion coefficient (cm^2/s) and v is the scan rate (V/s).

2. Peak separation, ΔE ($E_{pc} - E_{pa}$) = 59/n mV at all scan rates at 25ºC.
3. Peak current ratio, $I_{pa}/ I_{pc} = 1$ at all scan rates.
4. Peak current function, $i_p/v^{1/2}$ is independent of scan rate.
5. The formal potential Eº' is given by mean of peak potentials. Eº' is potential when the ratio of analytical concentrations of reactants and products are exactly unity, for the reaction stoichiometry of 1.
6. The electrode reaction kinetics are fast to maintain Nernstian concentrations.
7. Oxidized and reduced species are stable.
8. Peaks are sharp and intense.

Irreversible systems

On the other hand, when the system is not in equilibrium and surface concentrations of O and R are not maintained at values required by the Nernst equation, it is said to be irreversible. The most common irreversible system has no return peak. Irreversible processes have the following features:

1. Peak current is given by the Randles-Sevcik equation at 25ºC (eq. 1.5):

$$i_p = 2.99x10^5 n^{3/2}(\alpha n_\alpha)^{1/2} A C D^{1/2} v^{1/2} \qquad 1.5$$

   where the symbols have their usual meaning, α is a transfer coefficient and n_α is number of electrons involved in a charge transfer step.
2. Peak current function, $i_p/v^{1/2}$ is dependent on scan rate.
3. Slow electrode reaction kinetics.
4. Peaks are broad and small.

Some processes are intermediate between reversible and irreversible; they are said to be quasi-reversible. There is a return peak but peak separation ΔE is greater than 59/n mV. Peak separation increases with increasing scan rate since to maintain Nernstian surface concentrations of O and R, electron transfer kinetics should be fast and this depends on the relative values of standard electron transfer rate constant k_0 and the scan rate. Reversibility can be restored by increasing the scan rate; this eliminates the effect of the reaction ($R \rightarrow P$) that follows the electron transfer.

1.2.2 Mass transport

Analyte movement from the bulk solution, through the interfacial region, onto the electrode can occur via diffusion, migration or convection. Diffusion is species movement driven by a concentration gradient. Convection is forced movement and can be achieved by agitation or stirring. Migration occurs against a charge gradient under the influence of the electric field and is therefore for charged species only. To relate analytical signal to the concentration of analyte in solution in amperometric experiments, the mode of

ion transport must be solely diffusion. Migration is eliminated by addition of high concentrations of an inert electrolyte so that it carries all the charge. Convection is eliminated by carrying out experiments in steady conditions, avoiding any physical movement. A number of electrochemical reaction parameters can be obtained from the voltammograms, but there are limitations which include the following;

1. The effects of slow heterogeneous electron transfer and chemical reactions cannot be separated. If they are both present, then rate constants for these processes can be calculated only by simulation methods.
2. There is a background charging current throughout the experiment which restricts the detection limit to about 10^{-5} M. In addition, the ratio of the peak faradaic current to the charging current decreases with increasing scan rate v (since peak current i_p is proportional to $v^{1/2}$), and this places an upper limit on the value of v that can be used.

1.2.3 Hydrodynamic systems

Electrode reactions are studied in reproducible experimental conditions so comparisons can be made and authentic conclusions drawn. To obtain both kinetic and thermodynamic parameters, conditions where the system is not reversible are used. Reversible reactions kinetics are faster than mass transport, hence k_o (standard rate constant) is much greater than k_d (mass transfer coefficient). k_o cannot be changed so k_d has to be increased until the reaction becomes at least quasi-reversible. This is done by various methods:

1. Hydrodynamic = increasing convection
2. Microelectrodes = decreasing size
3. Linear sweep = increasing sweep rate
4. Step and pulse techniques = increasing amplitude and/or frequency
5. Impedance = increasing perturbation frequency and registering higher harmonics.

These methods basically facilitate mass transport hence more analyte reaches the electrode. This enhances measured currents, leading to greater sensitivity and reproducibility.

1.2.3.1 Rotating disc electrode

In hydrodynamic systems, convection is increased by rotating the working electrode. This makes rotating disc electrode (RDE) systems ideal for studying electrode reactions. The following apply for RDE systems:

1. Rate of reaction is varied by altering rotation speed. The higher the rotation speed, the faster the reaction.
2. Analyte flow near electrode is laminar instead of turbulent as in solution bulk, and this enables velocity calculations.
3. The system does not depend significantly on physical properties of electrolytes.
4. Natural convection is suppressed.
5. Peak and limiting currents (I_p and I_L) are obtained from one experiment.
6. Interfacial region is confined close to the electrode surface. When the thickness of the stagnant layer remains constant throughout the

duration of the experiment, the electrode surface becomes uniformly accessible to electroactive species that arrive from solution bulk.

7. Derived equations agree well with theory and experiment.

Hydrodynamic systems have the same set-up as an ordinary electrochemical cell and they are usually monitored with LSV[74]. The only difference is the working electrode rotates hence mass transport is governed by both convection and diffusion. A rotating disc electrode consists of a disc electrode embedded in the middle of a plane surface that rotates around its axis in a fluid, the disc being centered on the axis. The electrode body is usually cylindrical with a sheath around the disc; the sheath is significantly larger than the disc so as to approximate a surface of infinite dimension. It is assumed that there are no edge effects, which are convection effects caused by walls of the cell, electrode body, etc. As a result of rotation, the solution is sucked towards the disc and spread out sideways, Fig.1.7.

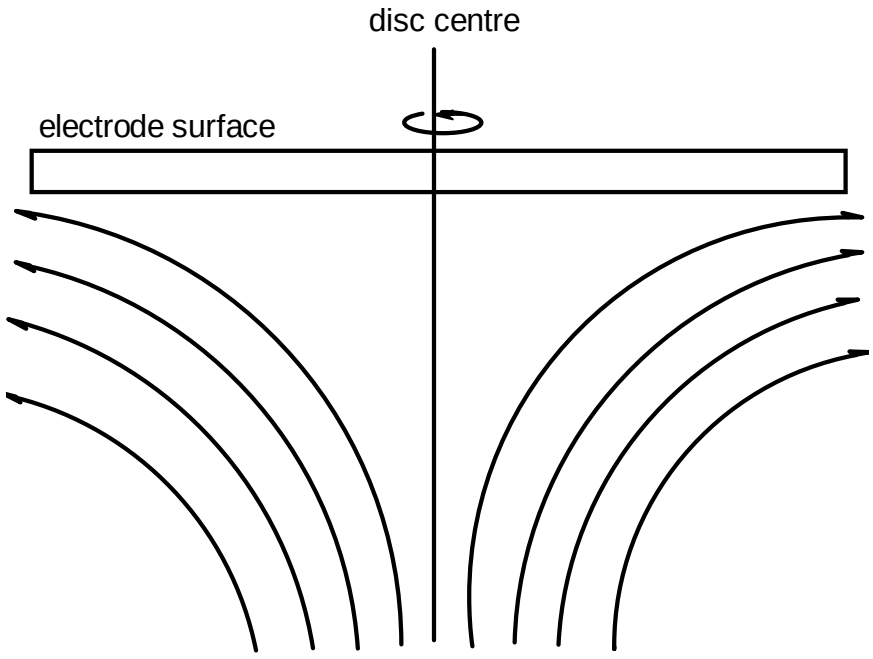

Figure 1.7: Streamlines for a rotating disc electrode.

There are different regions of solution flow in RDE systems. In the bulk of the solution, the flow is turbulent due to electrode rotation. The extent of turbulence depends on the speed of rotation. The flow becomes less turbulent closer to the electrode surface. Adjacent to the electrode surface, the flow then becomes laminar i.e. parallel layers of solution slide by each other parallel to the electrode. Velocity gradients occur within this layer of thickness δ_H. Very close to the electrode surface, there is a thin layer, almost stuck to it called the stagnant layer. It has thickness δ and the assumption is there is no convection within that diffusion layer. It has been demonstrated that:

$$\delta = \left(\frac{D}{v}\right)^{1/3} \delta_H \qquad 1.7$$

where D is the diffusion coefficient and v is the velocity. In aqueous solution, D ~10^{-5} cm^2/s and v ~10^{-2} cm^2/s, therefore $\delta \sim 0.1\ \delta_H$. This shows how thin and compact the stagnant layer is relative to the solution bulk hence the assumption that convection does not occur within it.

In the bulk of the solution, concentrations are maintained homogeneous by the stirring action. As long as the electrode area is small and the experiment is not prolonged, the bulk concentrations will not be altered appreciably by the electrolytic conversion of O to R at the surface. The removal of O at the electrode surface sets up a concentration gradient across the stagnant solution layer. O diffuses across this layer to the electrode surface where it is electrolyzed to R, which then diffuses back across the layer into the bulk solution.

As the rotation speed is increased the distance that the material can diffuse from the surface before being removed by convection is decreased.

This results in a higher flux of material to the surface at higher rotation speeds. It is for this reason that upper limit of rotation speed is set at 10 000 rotations per minute (r.p.m.) to inhibit electrode passivation and fouling. It also ensures conformity to equations that describe analyte movement in RDE experiments. The mass transport limited current arises from the fact that the system reaches a steady state and so the current reaches a plateau once the equilibrium at the surface is driven to the products side. A typical rotating disc electrode voltammogram (Fig.1.8) exhibits a sigmoidal shaped wave, the height of which provides the analytical signal.

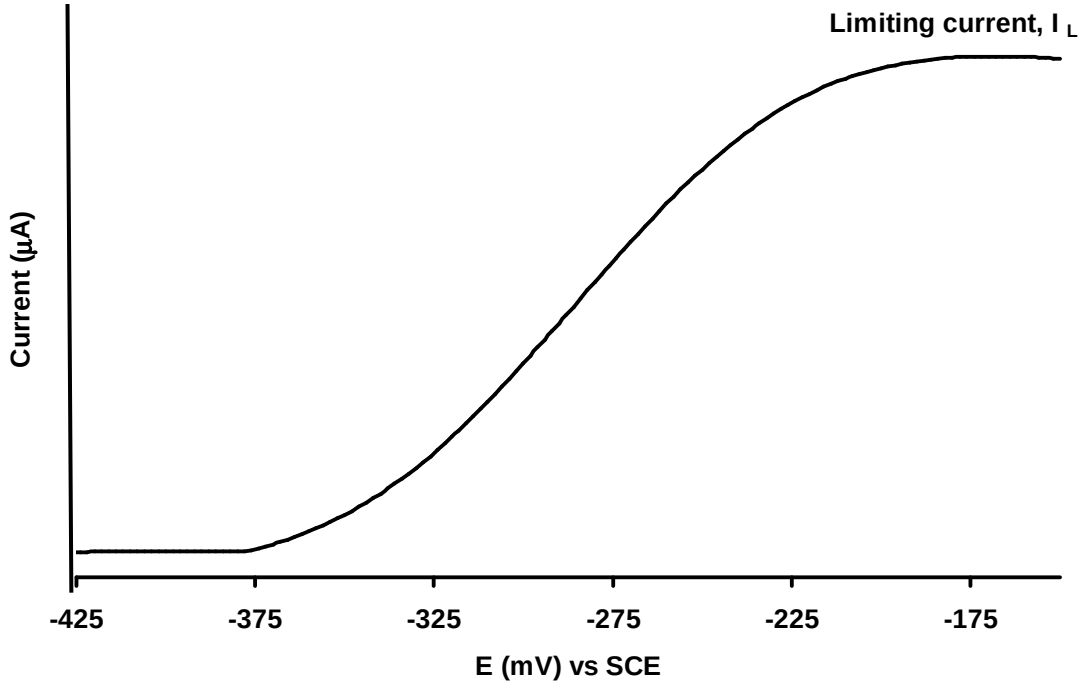

Figure 1.8: Rotating disc electrode voltammogram of an irreversible cathodic reaction.

At the start of the wave, mass transport is controlled by convection and the currents are termed kinetic currents (I_K)[75]. As potential sweep continues and approaches the value at which the reaction $O + ne^- \leftrightarrow R$ occurs, current signal rises. At this point, mass transport is governed by diffusion. The rate of

transport of electroactive species is equal to the rate of their reaction on the electrode surface under steady state conditions. A plateau is reached when all O or R that reaches the electrode is reduced or oxidized, and this is termed the limiting current I_L. It is predicted by Levich equation (eq. 1.8);

$$I_L = 0.62nFAD^{2/3}\omega^{1/2}v^{-1/6}C \qquad 1.8$$

where A is electrode area, v is kinematic viscosity (cm^2/s), which is a ratio of solution's viscosity to its density. ω is angular rotation rate of the electrode (radians/second); calculated from rotations per minute (f) using the relationship, $\omega = 2\pi f/60$. At a uniformly accessible electrode, I_L is directly proportional to the electrode area. When the electrode area is large, there will be more room for high concentrations of analyte to reach the electrode and undergo the chemical reaction, hence the limiting current will be higher.

The Levich equation can be used to give valuable information. When all constants are known, the total number of electrons involved in an electrode reaction can be determined. A linear variation of limiting current and square root of angular rotation rate indicates a diffusion-controlled process.

1.2.3.2 Kinetics of electrode reactions

Electrode reaction kinetics are measured as current is passed in hydrodynamic systems[76,77]. The mass transfer coefficient k_d describes the rate of diffusion within diffusion layer of thickness $\delta + \delta_H$ (see above); k_a and k_c are rate constants of the electrode reactions for oxidation and reduction respectively. For a simple electrode reduction reaction $O + ne^- \rightarrow R$, the rate constant is;

$$k_c = k_0 \exp\left[\frac{-\alpha_c nF(E - E^{0'})}{RT}\right] \qquad 1.9$$

For oxidation, it is;

$$k_a = k_0 \exp\left[\frac{-\alpha_a nF(E - E^{0'})}{RT}\right] \qquad 1.10$$

where k_o is the standard rate constant. α_a and α_c are charge transfer coefficients for anodic and cathodic processes respectively. k_a and k_c maybe determined from kinetic currents (I_K) as shown by eqn. 1.11 for k_c,

$$I_K = nFCAk_c \qquad 1.11$$

where symbols are as described above.

1.2.3.3 The transfer coefficient, α

The transfer coefficient is a measure of symmetry of the activated barrier and it varies between 0 and 1. α is equal to 0.5 for a metallic electrode and a simple electron transfer process, indicating that the activated complex is exactly halfway between products and reactants on the reaction coordinate; the structure of the activated complex reflecting reagent and product equally (Fig. 1.9b). For a simple one step electron transfer, $\alpha_a + \alpha_c = 1$. α valued at 0 or 1 indicates that the activated complex has predominantly the structure of oxidized or reduced species respectively (Fig. 1.9 a and c).

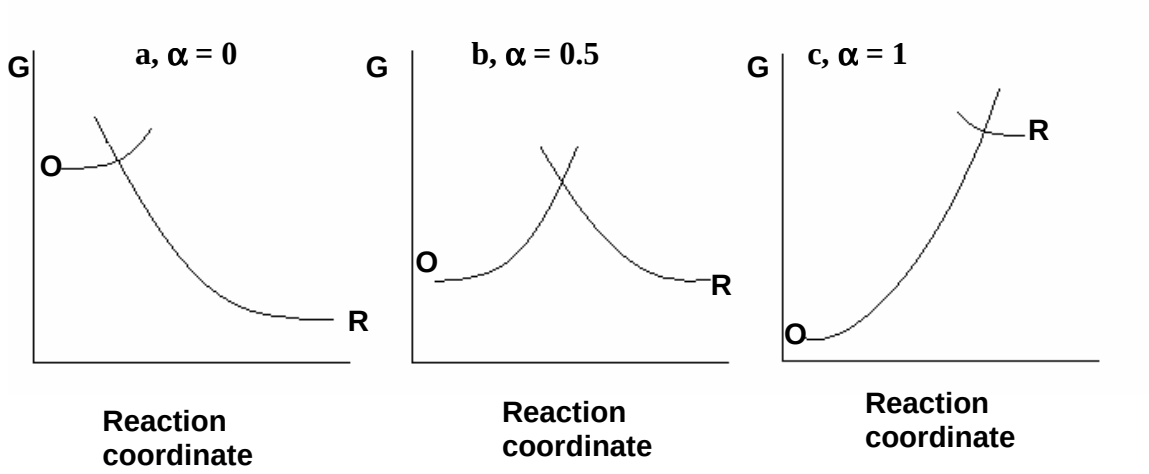

Figure 1.9: Energy profiles for different values of charge transfer coefficients. O is oxidized and R is reduced species. G is standard free energy.

The transfer coefficient maybe determined from a Tafel plot; a plot of logarithm of background corrected (I) current versus overpotential (η). Data is taken from a rotating disc electrode voltammogram shown in Fig. 1.8. Tafel equation is expressed as[78]:

$$\eta = a + b \log I \qquad 1.12$$

where η is the overpotential, a is the exchange current density (I_o). Tafel slope is given by b, which is equal to $-2.3RT/\alpha_c nF$ and $2.3RT/nF(1 - \alpha_a)$ for cathodic and anodic reactions respectively. The useful part of the Tafel plot for kinetics is at low overpotentials; the foot of the wave in Fig. 1.8. A linear Tafel plot is obtained when kinetic currents are used in eq. 1.12. When one electron is involved in the rate-determining step and the transfer coefficient is 0.5, the Tafel slope becomes 0.118 V/decade[79]. The Tafel slope of 0.059 V/decade is obtained when $\alpha = 1$, and one electron is transferred during the rate-determining step. However, in electrocatalysis, higher Tafel slopes have been reported for one electron rate-determining processes and this has been

attributed to high transfer coefficients or strong binding between analytes and catalysts[80]. Furthermore, it has been postulated that Tafel slopes close to 0.118 V/decade involve Temkin kinetics whereas those close to 0.059 V/decade involve Langmuir kinetics[81]. These are related to adsorption conditions of catalysts on electrodes.

1.2.3.4 Reaction order

Reaction order can be determined from plots of 1/I versus $\omega^{-1/2}$ based on Koutecky-Levich equation[75] (eq. 1.13):

$$\frac{1}{I} = \frac{1}{nFCAk_c} + \frac{1}{0.62nFAD^{2/3}\omega^{1/2}v^{-1/6}C} \qquad 1.13$$

where symbols have their usual meaning. Current variables (I) are taken at different potentials along the rising part of the wave, at different rotation speeds. Parallel linear plots of 1/I versus $\omega^{-1/2}$ at different potentials indicate first order reaction[82]. Note that the y-intercept of the 1/I versus $\omega^{-1/2}$ plots give rate constants of electrode reactions.

The reaction order m, can also be determined from the following equation[83], eq. 1.14:

$$\log I = \log I_K + m \log\left(1 - \frac{I}{I_L}\right) \qquad 1.14$$

where symbols have their usual meaning. I values are taken at the reaction peak potential (E_{pa} or E_{pc}) determined from cyclic voltammetry or peak at half-height in RDE voltammograms. The value of I at this potential and different rotation speeds is then employed in eq. 1.14.

1.3 Electrocatalysis

It has already been mentioned that the principal aim of the project is to use phthalocyanines as catalysts. Electrocatalysis is one type of catalysis where these complexes have been extensively used, hence this is discussed in this section. Electrocatalysis is defined as the increase of electron transfer rate of electrochemical reactions by using a catalyst. The catalyst acts as a mediator, thus it takes an active part in the reaction but is not consumed.

1.3.1 Use of metallophthalocyanines in electrocatalysis

Electrochemical reactions are monitored successfully on conventional working electrodes such as glassy carbon electrodes. However, some reactions occur slowly and with difficulty. This has brought about the use of electrocatalysts to counteract these problems. Phthalocyanine complexes have been used as electrocatalysts in various reactions such as thiol oxidation[10] and oxygen reduction[84]. This is because these complexes have various oxidation states. They can also be metallated with electroactive central metals such as cobalt, iron and manganese, which greatly enhance their electrocatalytic behaviour. Ligands substituted on the Pc ring can be electroactive, contributing to the overall electrocatalytic efficiency of the Pc. Electroactive phthalocyanines interact with reagents while undergoing electrochemical reactions thereby facilitating electron transfer processes[85]. This leads to reactions occurring at reduced overpotentials[86] and increased

current densities[87] rendering phthalocyanine complexes as good electrocatalysts.

The redox (O/R) couple of the electrocatalyst basically mediates and therefore hastens electron transfer process between the electrode and the substrate, (Fig. 1.10). The electrochemical reaction undergone by the substrate, oxidation in this case, will occur at a potential close to the O/R formal potential, $E^{o'}$ of the electrocatalyst. The return peak of the O/R couple (O $\rightarrow$ R), will not be observed since the oxidized species would have interacted with the substrate.

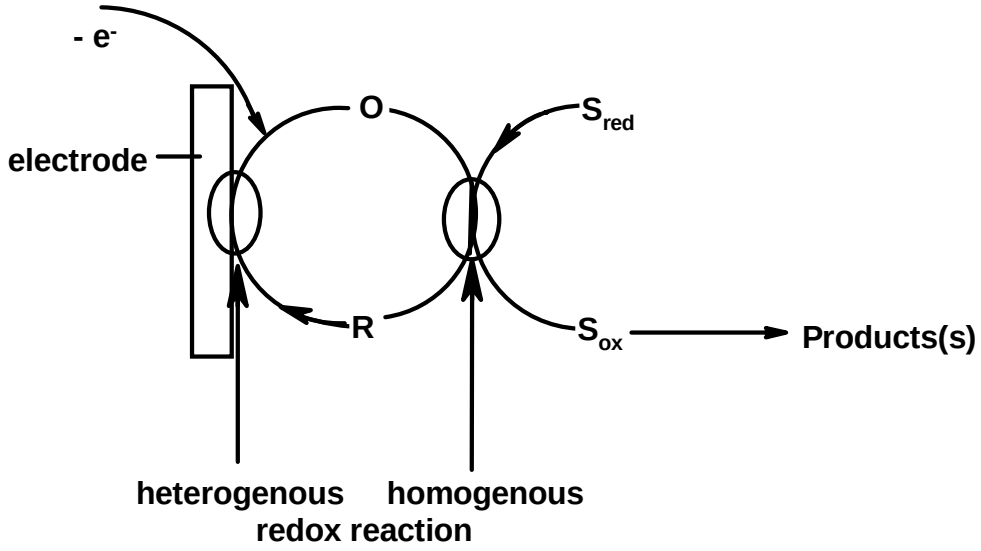

Figure 1.10: A schematic representation of an electrocatalytic reaction. S is the substrate.

Examples of reaction mechanisms electrocatalyzed by metallo-phthalocyanines include oxygen reduction whereby oxidation of the central metal forming superoxide anion occurs first[88]. This is followed by reduction of the formed adduct, during which oxygen gets reduced. This is represented by the following reaction sequence,

$$M^{II}Pc^{-2} + O_2 \rightarrow [PcM^{III\cdots\cdots}O_2^{-}] \quad 1.15$$

$$[PcM^{III\cdots\cdots}O_2^{-}] + e^{-} \xrightarrow{r.d.s} PcM^{II} + O_2^{-} \quad 1.16$$

$$O_2^{-} + H_2O + e^{-} \xrightarrow{fast} HO_2^{-} + OH^{-} \quad 1.17$$

where r.d.s is the rate-determining step.

Another example showing a metal oxidation-mediated catalytic reaction has been reported to hold for *L*-cysteine oxidation in acidic media. The process is initiated by oxidation of $Co^{II}Pc$ to $Co^{III}Pc$ and subsequent cysteine oxidation by $Co^{III}Pc$ while regenerating the initial $Co^{II}Pc$ catalyst[89].

$$M^{II}Pc^{-2} \rightarrow [M^{III}Pc^{-2}]^{+} + e^{-} \quad 1.18$$

$$[M^{III}Pc^{-2}]^{+} + RSH \rightarrow M^{II}Pc^{-2} + RS^{\bullet} + H^{+} \quad 1.19$$

$$2RS^{\bullet} \rightarrow RSSR \quad 1.20$$

where RSH denotes a thiol and RSSR a disulphide.

Moreover, electrooxidation of *L*-cysteine mediated by ring-based processes of phthalocyanine complexes metallated with platinum group metals, namely ($(CN)_2RhPc^{-}$), (DMSO)(Cl)RhPc, $(DMSO)_2RuPc$ and $(DMSO)_2OsPc$ has been reported to occur according to equations 1.21 - 1.23[90],

$$MPc^{-2} \rightarrow [MPc^{-1}]^{+\cdot} + e^{-} \quad 1.21$$

$$2[MPc^{-1}]^{+\cdot} \rightarrow ([MPc^{-1}]^{+\cdot})_2 \quad 1.22$$

$$([MPc^{-1}]^{+\cdot})_2 + RSH \rightarrow MPc^{-2} + RSSR \quad 1.23$$

where RSH and RSSR are thiol and disulphide respectively.

1.3.2 Electrode modification

Conventional surfaces that are used as working electrodes are made of various materials; criterion of choice is governed mainly by the useful potential range in a particular solvent and electrolyte for reactions studied. Electrode's potential window is limited by solvent and electrolyte decomposition, electrode dissolution and passivation. Factors such as microstructure and roughness of the electrode surface, blocking of active sites by adsorbed species and nature of functional groups on the electrode surface are also taken into consideration as they affect kinetics of electrode reactions. In this work, the following electrode materials have been used; glassy carbon (GCE), ordinary pyrolytic graphite (OPG), gold and screen printed carbon (SPCE).

GCE is the most commonly used carbon electrode. It is made up of an amorphous form of carbon. It is denser than natural graphite, isotropic, non-homogenous and with unknown composition. GCE can be polished to a mirror finish and does not show any memory effects, hence can be used in ultratrace analysis. It has surface functionalities such as OH and COOH groups. Its surface characteristics and area are inconsistent but a new layer is exposed after polishing. GCE is hard and resistant to chemical attack and thus more mechanically durable. Chemical resistance is a consequence of the disordered structure and therefore the inability to form intercalation compounds. It is also highly resistant to corrosion by acid and alkaline agents. It is a good thermal conductor with a high level of resistance to thermal shock, thus it can be employed in various temperatures.

OPG is made of ordered sheets of hexagonally bonded carbon atoms arranged in the same direction (Fig. 1.11). It has distinct planes, the basal and the edge; of varying population of chemical functionalities. The plane exposed on the surface is dependant on pre-treatment method. The basal plane surface is non-ionic, hydrophobic and rich in π-electron density. The high π-electron density permits strong chemisorptive interactions, especially with unsaturated compounds. The edge plane has carboxylic acid and hydroxyl groups which makes it more conducting than the basal plane. These groups can be enhanced by chemical pre-treatment procedures such as heating in air at elevated temperatures (400 - 500 ^{o}C), leaving the surface oxidized. Electroactive species can then be attached onto the electrode after activation, leading to formation of chemically modified electrodes. Pyrolytic graphite is anisotropic, very reproducible and slightly denser than natural graphite. It is more porous than glassy carbon, thus allows easy adsorption of electrode modifiers.

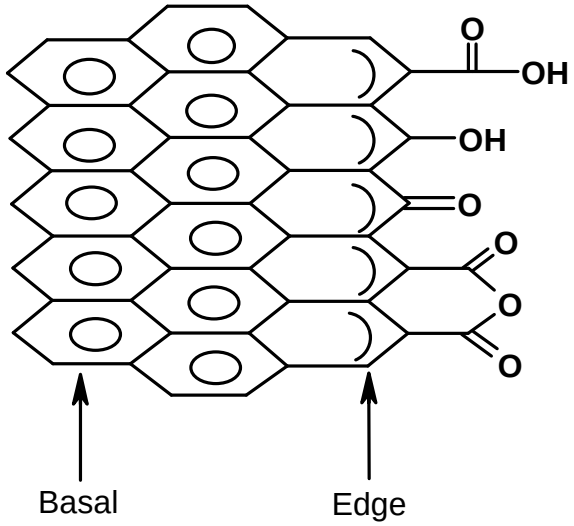

Figure 1.11: Structure of planes of an ordinary pyrolytic graphite.

SPCEs are made of carbon black. These electrodes are made by printing a mixture of graphite powder in an appropriate solvent onto ceramic tiles[91]. They are highly miniaturized compared to their conventional, orthodox counterparts. They are thus more applicable in biological systems where their small size enables facile manoeuvring[92]. SPCEs offer advantages of use of small sample volumes and avoidance of electrolyte leakage problems[93]. Their methods of preparation are amendable to mass production hence they are made at low cost and reproducibly. The electrodes are disposable hence eliminate the extra, tiresome duty of cleaning and polishing.

Gold is a noble metal; as an electrode it is highly conductive exhibiting negligible background currents, high sensitivity and reproducibility. It is however prone to corrosion and passivation.

The aforementioned electrodes namely GCE, OPG, Au and SPCEs can be chemically modified with Pcs to enhance their electrocatalytic character. There are various methods of electrode modification depending on the electrode material, properties of the Pc and analytes as well as the type of reaction studied. These include composite carbon cements[94], spin coating[95], vapour deposition[96], Langmuir-Blodgett films[97], (drop-dry) adsorption[98], self assembly[99], electrodeposition[100] and electropolymerization[101]. Electrode modification methods used in this work include adsorption (drop-dry) whereby a known volume of Pc solution is spread onto the electrode surface and rinsed off after a known time interval. The Pc adheres onto the electrode material and the bulk of the Pc film is held together by simple π-π interactions between the N_4 macrocycles[102]. There is also a likelihood of forming rough

MPc films[103] upon solvent evaporation. This can be prevented by shortening adsorption time hence allowing only partial evaporation.

Self-assembly method[104] was also used in this work whereby the Pc molecule self-organizes onto electrodes during immersion in Pc solution leading to formation of self-assembled monolayers (SAMs). These are usually formed on gold or silver electrodes via the strong covalent silver/gold-sulphur bond by sulphur-containing Pcs[105]. The sulphur moiety of the Pc can be either axially or ring substituted. MPc-SAMs have been reported to be dense and highly ordered exhibiting regular and packed orientation on the electrodes. Generally, SAM orientation on the electrode is determined by the number, position and size of ring substituents on the Pc. They adopt an umbrella-like[106] orientation on the electrode when the MPc bonds to the electrode by an axially bound sulphur ligand (Fig. 1.12 a). An octopus[107] orientation is adopted when the MPc lies flat on the electrode via sulphur-containing ring substituents (Fig. 1.12 b).

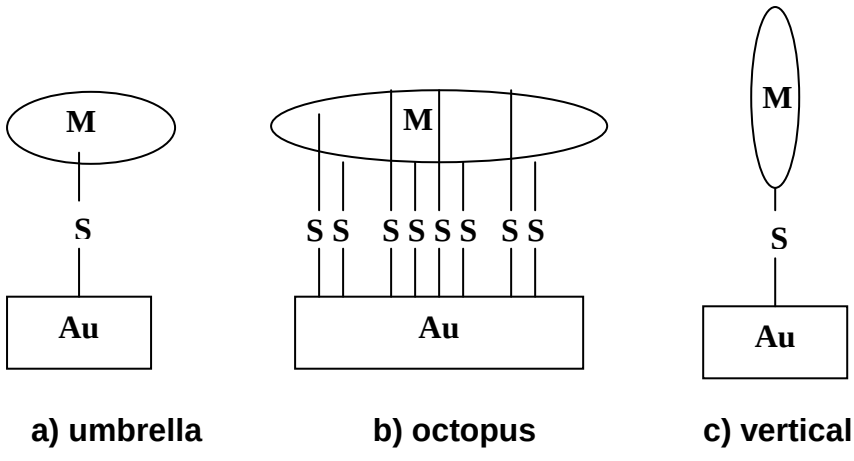

Figure 1.12: a) Umbrella, b) octopus and c) vertical orientations of MPc-SAMs.

Another method of forming MPc-SAMs on gold electrodes involves pre-forming SAM with an appropriate ligand which will then coordinate with the MPc, adopting a vertical orientation on the electrode (Fig. 1.12 c). This method eliminates the tedious, time-consuming duty of synthesizing sulphur-containing MPcs. Ozoemena et al.[108] formed SAM with 4-mercaptopyrimidine on gold and then axially ligated FePc via the Fe-N bond onto the SAM. Mixed SAMs have also been formed by electrode immersion into a mixture of different thiols[109]. The solvent in which the Pc is dissolved affects the composition of the monolayer. Ethanol is the preferred solvent because it does not have a 'memory effect'; it does not get incorporated into the SAM[109]. Desirable solvents evaporate easily and also reduce gold oxide that is readily formed on gold electrodes upon air exposure. Moreover, long adsorption times of at least 12 hours afford formation of defect-free and well-ordered SAMs[110]. Self-assembled monolayers are exploited as electrocatalysts because they are stable and reproducible.

Electrodes were also modified by electrodeposition and electro polymerization in this work. These methods involve repetitive oxidative or reductive cycling around appropriate MPc redox processes resulting in the coating of the MPc film onto the electrode. With electrodeposition, simple MPc layer stacking occurs[111] whereas with electropolymerization, polymeric films are formed[112]. Electropolymerization is initiated with difficulty because it strongly depends on electrode material, polishing and MPc monomer solution[113]. Polymer radical ions must be capable of instigating oxidation or reduction of fresh monomer to sustain polymer growth, otherwise electrode passivation soon occurs and film growth is prevented.

Formation of electrodeposited and electropolymerized MPc films is accompanied by peak current increase of appropriate redox peaks as repetitive cycling occurs, due to increased MPc mass density on the electrode. In addition, new peaks are formed ascribed to the polymer during electropolymerization. Electropolymerization of nickel tetraphenoxy pyrrole phthalocyanine (NiTPhPyrPc) is illustrated in Fig. 1.13 showing peak current increase of MPc redox couples[114]. Film thickness is related to number of scans assuming one cycle deposits a layer of film. Polymeric films are thin, sleek, compact, reproducible and definite. They are used in electrocatalysis where they offer electron transfer mediation, stability and long lifetimes.

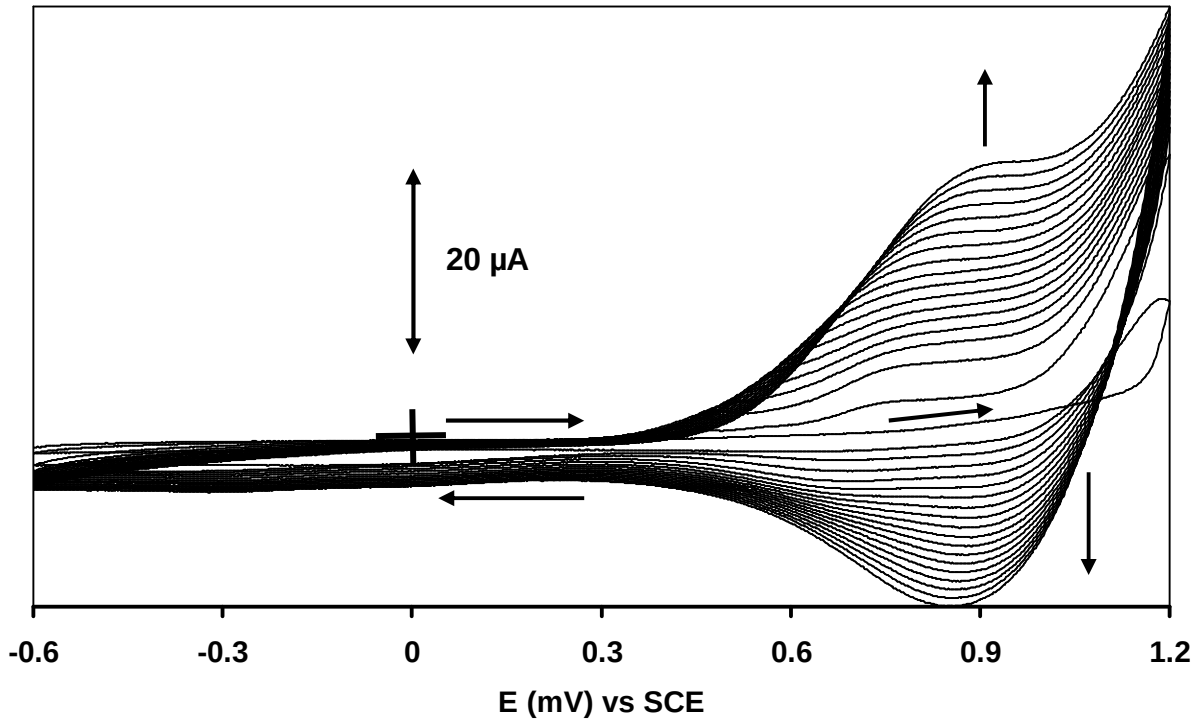

Figure 1.13: Electropolymerization of NiTPhPyrPc in DCM and 0.1M $TBABF_4$ at 200 mV/s.

Non-conventional screen printed carbon electrodes (SPCEs) were also employed in this work. They are modified by incorporating well-chosen metallo- phthalocyanine catalysts in the graphite ink during fabrication to fine-

tune their catalytic behaviour towards specific analytes[115], as was the case in this work. These electrodes can also be modified by already-discussed methods such as electrodeposition[116] and electropolymerization[117].

1.3.3 Characterization of modified electrodes

There are various methods that are employed to confirm chemical modification of electrodes such as FT-Raman[118] and IR spectroscopy[119], scanning-probe measurements[120], electrochemistry[121] and x-ray photo electron spectroscopy[122]. In cyclic voltammetry, peaks due to the MPc electrode modifiers are prominent if film formation on the electrode surface is successful. Moreover, polymer peaks should also be eminent, in the case of electropolymerization.

The amount of electroactive species (Γ_{MPc}) on the electrode surface is determined by integration of MPc peak area using the following relationship (eq. 1.24),

$$Q = nFA\Gamma_{MPc} \qquad 1.24$$

where Q is charge under oxidative or reductive MPc peak, n is number of moles of electrons transferred, F is Faraday's constant and A is electrode area. Surface coverage can also be determined by recording CVs of the surface-confined MPc redox process at various scan rates using the relationship (eq. 1.25),

$$I_P = \frac{n^2F^2Av\Gamma_{MPc}}{4RT} \qquad 1.25$$

where I_p is peak current, v is the scan rate, R is the gas constant, T is the temperature and the rest of the constants have their usual meaning. This equation can only be used if the I_p versus v plot is linear and passes through the origin. Surface coverage in the 10^{-10} mol/cm^2 indicates that there is a monolayer of MPc on the electrode[123].

Formation of SAMs on electrodes is probed by exploring their barrier propensity towards occurrence of electrode reactions. Electrochemical methods used for establishing SAM formation include blockage of gold oxide formation[124,125], under-potential deposition (UPD) of metals such as copper[126] and prevention of electron transfer in redox reactions[127,128] such as $[Fe(H_2O)_6]^{3+}/[Fe(H_2O_6)]^{2+}$. When SAM has been formed, lower currents if any, are observed for these processes. Factors used to qualitatively characterize SAMs include ion barrier factor (Γ_{ibf})[129] which is calculated using eq. 1.26[130],

$$\Gamma_{ibf} = 1 - \frac{Q_{SAM}}{Q_{Bare}} \qquad 1.26$$

where Q_{SAM} and Q_{BARE} is charge under peaks of MPc-SAM and bare gold electrodes, respectively. This factor is a measure of how well SAMs have isolated Au electrode surface from the electrolyte. The disappearance of the gold oxide or UDP peaks of Cu is used to establish SAM formation as well as to calculate ion barrier factor. Γ_{ibf} should be equal to unity for complete isolation of Au from the aqueous solution.

Another factor that is used to characterize SAMs is interfacial capacitance, C_s. It is a measure of ion permeability through SAM, it tells us how densely packed and defect free the SAM is[131]. The closer the calculated C_s value is to zero, the fewer the defects and pinholes of the SAM. This

indicates that the SAM is less permeable to the electrolyte ions which would otherwise traverse to the electrode surface. A decrease in charging current observed with MPc-SAMs, is attributed to the presence of a layer of low dielectric constant between the electrode and the electrolyte. C_s is calculated using eq. 1.27[132],

$$C_s = \frac{i_{ch}}{vA} \qquad 1.27$$

where i_{ch} is the background charging current (μA), v is the scan rate (V s^{-1}) and A is the electrode area.

1.4 Overview of studied analytes

A range of analytes that has been studied electrochemically in this work and catalyzed by metallophthalocyanines is shown in Fig. 1.14. They are 2-mercaptoethanol (2-ME), *L*-cysteine (CYS), reduced-glutathione (GSH), thiocyanate (SCN^-), *S*-nitrosoglutathione (GSNO) and oxygen. 2-ME is a thiol that is involved in cleaving protein disulfide bonds in humans[133]. This disulfide bond intermolecular cleavage allows protein subunits to separate facilitating migration. CYS is a non-essential thiolic amino acid that maintains the structure of proteins in our bodies amongst its numerous biological roles[134]. GSH is an endogenous antioxidant that plays a major role in reducing reactive oxygen species formed during cellular metabolism and the respiratory burst[135]. It also forms disulfide bonds with cysteine residues in proteins. The above-mentioned thiols namely 2-ME, CYS and GSH are involved in industrial processes as well; such as oil-sweetening[136] and food deterioration marking[137]. Consequently, they end up being pollutants.

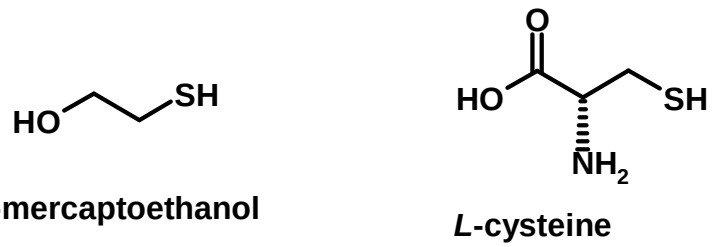

2-mercaptoethanol

***L*-cysteine**

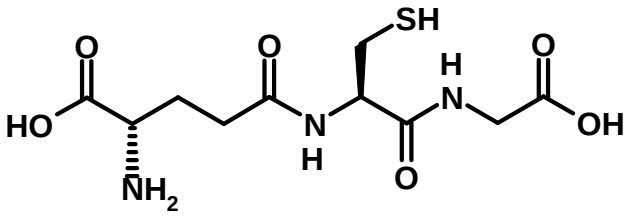

reduced-glutathione

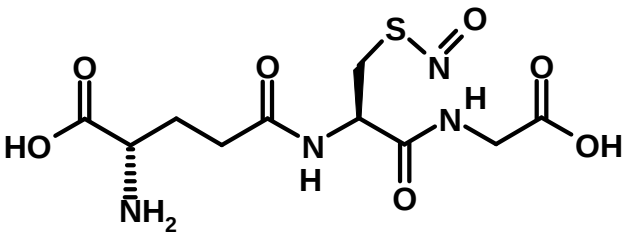

***S*-nitrosoglutathione**

Figure 1.14: Molecular structures of electrochemically studied analytes; 2-mercapto-ethanol, *L*-cysteine, *reduced*-glutathione and *S*-nitrosoglutathione.

S-nitrosoglutathione (GSNO) is a nitrosothiol, a biologically important molecule that plays a crucial role in storage, transport and release of nitric oxide (NO)[138], which is in turn involved in smooth muscle relaxation[139] and vasodilation[140], among its various physiological roles. GSNO has been used clinically to inhibit platelet aggregation[141] and to treat high blood pressure in pregnant women[142]. Thiocyanate is a pseudo-halide oxidized by mammalian peroxidases forming products which exhibit powerful anti-bacterial activities[143]. Clinical studies show that the amount of SCN^- found in biological matrices such as saliva and urine are indicative of cigarette smoking[144]. Concentrations in the range of 10^{-5} - 10^{-3} mol/dm^3 indicate heavy smoking[145].

Oxygen is a source of life; it generates energy in our bodies. The same capacity is exploited industrially in fuel cells[146].

The above analytes need to be studied, detected and quantified. This will provide invaluable insight into their biological and industrial properties, their levels in the environment and bodies, as well as ways of eliminating or reducing their pollutant capacity. In this work, they will be studied by electrochemical techniques where electrochemical sensors will be employed. These methods are so chosen because of their inherent sensitivity, selectivity, simplicity, facileness and low detection limits.

1.4.1 Electrocatalysis of thiocyanate oxidation

Oxidation of thiocyanate occurs at high overpotentials on conventional electrodes, hence the need for catalysis. Analysis and detection of thiocyanate anion involves oxidation to dirhodane/thiocyanogen ($(SCN)_2$) intermediate which subsequently hydrolyzes to form cyanide and sulphate ions[147]. This mechanism has been observed for SCN^- oxidation by horseradish peroxidase (HRP) as follows[148],

$$SCN^- \xrightarrow{HRP} SCN^\bullet \qquad 1.28$$

$$SCN^\bullet + SCN^\bullet \rightarrow (SCN)_2 \qquad 1.29$$

$$3(SCN)_2 + 4H_2O \rightarrow CN^- + 5SCN^- + 8H^+ + SO_4^{2-} \qquad 1.30$$

When catalyzed by lacto-peroxidase (LPO), thiocyanate oxidation occurs at less positive potentials and greater turnover values via two electron transfer steps[149]. The formed thiocyanogen ($(SCN)_2$) intermediate hydrolyzes forming

the most stable oxidation product HOSCN which subsequently dissociates at pH > 5.3[150] as follows,

$$H_2O_2 + 2SCN^- + 2H^+ \xrightarrow{LPO} (SCN)_2 + 2H_2O \quad 1.31$$

$$(SCN)_2 + H_2O \rightarrow HOSCN + SCN^- + H^+ \quad 1.32$$

$$HOSCN \Leftrightarrow H^+ + OSCN^- \quad 1.33$$

HOSCN is obtained at equimolar concentrations of H_2O_2 and SCN^-, CN^- may be formed when the ratio of $[H_2O_2]$ to $[SCN^-]$ exceeds one. Higher turnovers are obtained with LPO catalysis than HRP because the formed CN^- in the latter binds with the heme Fe deactivating the enzyme. SCN^- oxidation products vary with the type of enzyme used depending on initial binding sites of SCN^- with the enzyme[151,152].

Catalysts containing Fe are the most efficient because Fe is the catalytic moiety of biological enzymes such as Cytochrome P450s which catalyze SCN^- oxidation reactions. Direct one step two-electron oxidation of SCN^- in the presence of Fe(V) or Fe(III) has been reported[153]. The lowest overpotential has been observed in acidic conditions, pH 4 being the optimum[154]. Literature is scanty on SCN^- oxidation catalyzed by MPcs. The reaction occurs in pH 4 buffer solutions at about 0.72 V versus the saturated calomel electrode (SCE) on bare gold and on MPc-SAMs as tabulated in Table 1.1[155]. The most promising electrocatalysis was by a self-assembled monolayer of FePc axially ligated to mercaptopyridine on gold electrodes where SCN^- oxidation occurred at 0.6 V/(SCE) in pH 4 buffer solution[106]. The proposed mechanism involved axial ligation of SCN^- to the central metal of the MPc, followed by oxidation to HSCN as follows[156];

$$M^{II}Pc^{-2} + nSCN^{-} \leftrightarrow (SCN)_n - M^{II}Pc^{-2} \quad 1.34$$

$$(SCN)_n - M^{II}Pc^{-2} + nH^{+} \leftrightarrow M^{II}Pc^{-2} + nHSCN \quad 1.35$$

where n = 1 or 2.

Table 1.1: Electrochemical data[155] for electrocatalytic oxidation of thiocyanate by self-assembled monolayers of metallophthalocyanines on gold electrodes in pH 4.

MPc complex[a]	**E (V) / (SCE)[b]**
CoOBTPc	0.74
CoOHETPc	0.71
FeOBTPc	0.72
FeOHETPc	0.70

[a] OBT is octabutylthio $(SC_4H_9)_8$ and OHET is octahydroxyethylthio$(SC_2H_4OH)_8$.

[b] A correction factor of -0.045 V was used to convert potentials from V/(Ag|AgCl) to V/(SCE)[155].

Aims of thesis

This work attempts to oxidize thiocyanate at lower potential values, increased current densities, improved catalyst stability and reproducibility by self assembled monolayer of a new metallophthalocyanine complex, namely cobalt tetraethoxy thiophene phthalocyanine (CoTEThPc, **6c**) shown in Fig. 1.15. This complex is peripherally substituted with electron donating groups which are expected to enhance oxidation. Moreover, the substituents have a sulphur moiety for formation of MPc-SAM on the gold electrode.

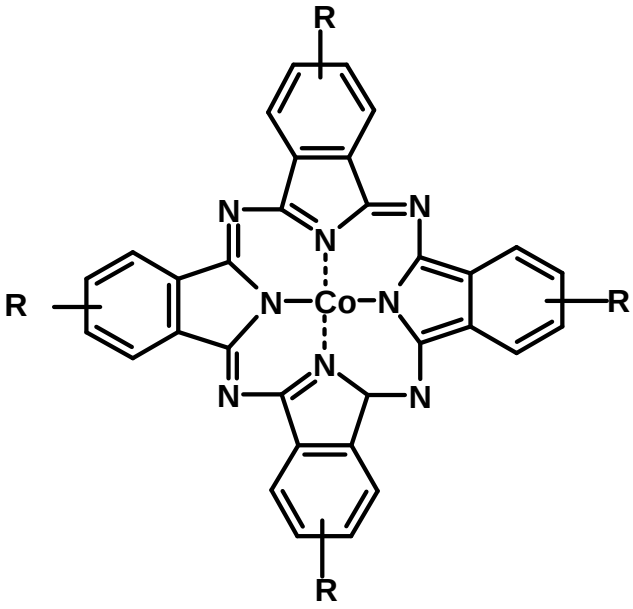

R = H (6a, CoPc)

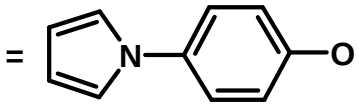

(6b, CoTPhPyrPc)

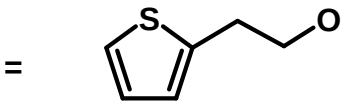

(6c, CoTEThPc)

Figure 1.15: Molecular structures of phthalocyanine complexes used in electrocatalytic oxidation of thiols and thiocyanate; CoPc, CoTPhPyrPc (cobalt tetraphenoxy pyrrole phthalocyanine) and CoTEThPc (cobalt tetraethoxythiophene phthalocyanine).

1.4.2 Electrocatalysis of thiol oxidation

Analysis and detection of thiols (RSH) involves oxidation to their corresponding disulphides (RSSR). However, thiol oxidation occurs at over-potentials exceeding 1V on conventional carbon electrodes. The reaction has been electrocatalyzed successfully with MPcs, thus occurring at less positive

overpotentials. MPcs with cobalt as the central metal exhibited the best catalytic behaviour for thiol oxidation amongst other transition metals[157], and this was attributed to good orbital overlap between its d-orbitals (d_{xz} and d_z^2) and the thiol sp-orbitals as predicted by perturbation theory. It has also been reported that thiol oxidation occurs at lower potentials in alkaline media because of predominance of thiolate ions; pK_as of 2-ME, CYS and GSH lie between 8 and 10[158]. At pH greater than 8, thiolate anions are prevalent, readily available to interact with catalysts and subsequently get oxidized.

Shortcomings encountered with use of MPcs in thiol oxidation reactions include short catalyst lifetime, irreproducibility and instability[9]. Electrodes modified by adsorbed MPcs are short-lived because of weak interactive forces between the electrode and the MPc. Their electropolymerized counterparts have compact films hence are more thermally and chemically long-lasting[159]. The only great challenge with the latter is initiating polymerization and obtaining reproducible films since it depends strongly on electrode material, polishing and the MPc monomer solution.

Thiol oxidation occurs via various mechanisms depending on the reaction conditions and the catalytic site. *L*-cysteine oxidation in pH 4 catalyzed by ring processes of some platinum group metal phthalocyanines was discussed above, equations 1.19 – 1.21. Catalysis mediated by metal oxidized MPcs was also described above in equations 1.16 – 1.18. Moreover, thiols can reduce central metals of MPcs to form coordinate adducts. These intermediates subsequently get oxidized, disintegrate and release thiolate radicals that dimerize to form disulphides by eqs. 1.36 – 1.40[160];

$$R\text{-}SH \rightarrow RS^- + H^+ \quad 1.36$$

$$RS^- + PcM^{II} \rightarrow [PcM^{I} - (SR)]^- \quad 1.37$$

$$[PcM^{I} - (SR)]^- \xrightarrow{r.d.s} [PcM^{II} - (SR)] + e^- \quad 1.38$$

$$[PcM^{II} - (SR)] \rightarrow PcM^{II} + RS^{\bullet} \quad 1.39$$

$$RS^{\bullet} + RS^{\bullet} \xrightarrow{fast} RS\text{-}RS \quad 1.40$$

where r.d.s is the rate-determining step. Other abbreviations are as defined earlier.

There are numerous reports on electrocatalytic thiol oxidation mediated by MPcs. These were conducted on different electrode materials, electrolytes, pH media, catalysts as well as different mode of electrode modification. 2-ME, CYS and GSH oxidations data is tabulated in Table 1.2. Thiol oxidation occurs easily in alkaline media because thiols readily dissociate in such media, thereby interacting with catalysts, and consequently getting oxidized. This is recapitulated in Table 1.2 whereby 2-ME oxidation is reported only in alkaline solutions. This work therefore aims to carry out thiol oxidation in acidic conditions and at lower potentials than already reported. This will enable eradication of thiols in industrial waste regardless of pH of the effluents.

Table 1.2: Electrochemical data[155] for 2-mercaptoethanol, l-cysteine and *reduced* glutathione oxidation.

Complex[a]	Electrode	Method of Modification	Analyte	E (V) / (SCE)[b]	Medium
CoTAPc	GCE	Polymer	2-ME	-0.29	0.5 M NaOH
CoTAPc	GCE	Drop-dry	2-ME	-0.32	0.5 M NaOH
CoOBTPc	Au	SAM	CYS	0.38	pH 4
CoOHETPc	Au	SAM	CYS	0.46	pH 4
CoPc	GCE	Deposition	CYS	0.63	pH 3.5
CoPc	GCE	Deposition	CYS	-0.03	pH 9
CoTSPc	OPGE	Dip-dry	CYS	0.2	0.2 M NaOH
CoPc[c]	OPGE	Drop-dry	GSH	0.0	pH 7.4

[a]TA is tetraamino, TS is tetrasulphonato, OBT and OHET are as defined above.

[b] A correction factor of -0.045 V was used to convert potentials from V/(Ag|AgCl) to V/(SCE)[155].

[c]reference[161]

Aims of thesis

To oxidize 2-mercaptoethanol, *L*-cysteine and *reduced*-glutathione at reduced overpotentials, increased current intensities, faster electron transfer rates in a wide pH range and increased detection limits using the following new metallo-phthalocyanine complexes (Fig. 1.15): Cobalt tetraphenoxy pyrrole phthalocyanine (CoTPhPyrPc, **6b**) and cobalt tetraethoxy thiophene phthalocyanine (CoTEThPc, **6c**). These complexes have cobalt as the central metal because it has been reported to exhibit excellent electrocatalytic behaviour towards thiol oxidation. Phenoxy pyrrole ligand is used as a

substituent because it can polymerize via the pyrrole group[101]. The ethoxy thiophene ligand induces self-assembly capability to the MPc via the sulphur group. Moreover, phenoxy pyrrole and ethoxy thiophene substituents are electron donating, making cobalt easy to oxidize[93], thus enhancing thiol oxidation.

1.4.3 Decomposition of nitrosothiols

Nitrosothiols (RSNO) decompose in human bodies via homolytic cleavage of the S-N bond yielding nitric oxide (NO) and the corresponding disulphide (RSSR)[162]. Copper and selenium containing proteins have been reported to catalyze this reaction in biological systems[163]. Furthermore, homolytic cleavage of RSNOs can be triggered by light[164] or reduced metal catalysis[165] such as Cu^{+}. Small molecular weight thiols such as glutathione and cysteine mediate nitrosothiol decomposition by reduced metal ion catalysis. Chemically synthesized reducing agents such as sodium borohydride ($NaBH_4$) and sodium dithionite ($Na_2S_2O_4$) still perform the same function[166]. GSNO decomposition catalyzed by cupric ions occurs via the following sequence,

$$GSNO \xrightarrow{Cu^{+}} GS^{\bullet} + NO \qquad 1.41$$

$$GS^{\bullet} + GS^{\bullet} \rightarrow GSSG \qquad 1.42$$

It has been reported that reduced metal ions are more efficient catalysts than their oxidized counterparts. However, metal salts in the reduced oxidation state (eg. Cu^{+}) are unstable. Their higher valency counterparts are

used instead, reduced in situ and dissipated in nitrosothiol decomposition before reoxidation; hence the use of reducing agents. The catalytic redox state of copper was investigated by comparison of degree of a decline in amount of nitric oxide detected in the presence of chelating agents[167]. The amount of nitric oxide detected was lower in the presence of copper (I) chelator (neocuproine) showing that free copper (I) is needed, thus the catalytic redox state is +1.

Nitric oxide can be detected by various methods such as use of Clark-type electrodes[168]. Detection of nitric oxide is difficult because of its low concentration, high activity and fleeting presence. NO is an extremely powerful ligand, it reacts with hemeproteins, metalloenzymes, non-heme metal complexes to form various adducts[169]. On the other hand, disulphides can be detected electrochemically using cobalt phthalocyanine modified carbon electrodes[161,170]. Concentrations in the micromolar range can be detected with high sensitivity; ideal for biological applications.

S-nitrosoglutathione decomposition reaction has been studied extensively in physiological conditions by detecting NO release[166,167], whose challenges have been mentioned above. It is therefore important to study this reaction by detecting GSSG, so as to have a complete sketch of the overall GSNO decomposition process.

This work explores for the first time GSH/GSSG detection from Cu^{+}-catalyzed GSNO decomposition using an ordinary pyrolytic graphite (OPG) electrode modified by adsorption of cobalt phthalocyanine, complex **6a**; the reaction being monitored by cyclic voltammetry. Detection limits are aimed at

micromolar range or less for application in biological systems where GSNO decomposition takes place.

1.4.4 Electrocatalysis of oxygen reduction

Oxygen reduction is a very important biological and industrial reaction. It is a cathode reaction in fuel cells, potentially efficient, emission free energy source[171]. The reaction should occur at the least negative potential for efficient energy production. It is desirable that the reaction goes to completion and forms water via a four electron transfer mechanism. However, oxygen gets reduced to hydrogen peroxide via a two electron process but the peroxide can still get reduced further via another two electron process to form water.

Platinum electrocatalyzes oxygen reduction to water in fuel cells[172], hence yielding high power output. However, in direct methanol fuel cells, Pt is not methanol tolerant[173]. Also, Pt is a noble and expensive metal hence substitutes have to be found. Generally, fuel cell catalysts should catalyze four-electron oxygen reduction, be thermally and chemically stable, have a long lifetime and tolerate the fuel used. Moreover, the reaction product water should be easily managed[146].

N_4 metal chelates such as metallophthalocyanines (MPcs), metalloporphyrins (MPs) and metallotetraaza-annulenes (MTAA) have been studied as precious metal fuel cell alternative electrocatalysts[174]. Porphyrins interact with oxygen in nature so oxygen reduction is not alien to them[175]. However, porphyrins are not thermally and chemically stable. They cannot

withstand harsh fuel cell environments hence are short-lived. Furthermore, they mostly catalyze two electron transfer which subsequently yields low energy output[176]. Stability can be improved by pyrolysis at high temperatures (300 - 900ºC)[177], but this entails alteration of integrity of the macrocycles and it becomes difficult to identify the nature of the catalytic site. Also, some porphyrin complexes sublime at such elevated temperatures. Oxygen reduction catalysis via four electron transfer can be improved by using thick films and this is achieved by polymerization[178]. Pyrolysis also promotes four electron oxygen reduction[177].

MPcs have improved chemical and thermal stability compared to MPs, hence are the most promising candidates. MPcs have good tolerance of fuel electrolytes such as acids[171], polymers[172] and methanol[173]. Generally, MPcs are efficient in alkaline solutions even though this medium poses difficulty of electrolyte decarbonation[179]. Performance of MPcs depends on the central metal, ligands and support[180]. Their activity towards oxygen reduction is better with dimeric species than their monomeric counterparts. This was observed with μ-oxo-bridged dimer of iron (III) pyridine Pc[181]. The geometry is cofacial on electrodes facilitating coordination and splitting of oxygen. It has been reported that metals with half-filled d-orbitals such as Fe and Mn are better oxygen reduction catalysts[182]. The net MPc catalytic activity is linked to the redox potential of the $M^{III/II}$ process; the more positive the redox potential, the higher the activity[183]. The redox potential is affected by substituents as well; electron donating ligands shift it to the negative while electron withdrawing ones shift it to the positive[184].

The extent of completion of oxygen reduction depends on the interaction of oxygen with the catalytic site on the electrode surface. Zagal et al.[185] postulated that the rupture of O-O bond leads to formation of water when oxygen interacts simultaneously with two active sites on the electrode surface. This favourable adopted oxygen-catalyst interaction is called 'bridge-*cis*' illustrated in Fig. 1.16. Other single site interactions lead to two electron transfer resulting in formation of hydrogen peroxide and they are 'end-on, side-on and bridge-*trans*' (Fig. 1.16). Since degree of oxygen reduction completeness depends on the interaction of oxygen with the catalytic site, it is therefore expected that an adduct formed upon such an interaction should be long-lived. It follows also that the interaction is more likely to be successful when there is a high concentration of catalyst on the electrode surface.

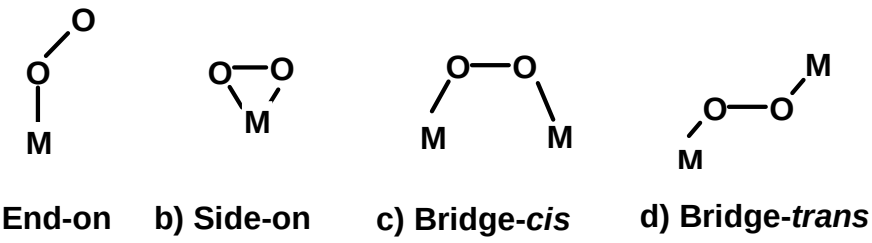

a) End-on **b) Side-on** **c) Bridge-*cis*** **d) Bridge-*trans***

Figure 1.16: Different configurations adopted by molecular oxygen upon interaction with metal sites.

Metallophthalocyanines do catalyze oxygen reduction reaction; electroactivity depends on the central metal, substituents, pH, electrode type and mode of electrode modification[186,187]. Their setbacks include promotion of two electron transfer process yielding hydrogen peroxide hence low energy output[188], and instability. Table 1.3 shows data obtained for MPc-catalyzed oxygen reduction, where electrodes were modified by drop-dry method.

Oxygen reduction to hydrogen peroxide is the most common as shwon in Table 1.3, the most positive potential being -0.13V/(SCE) in acidic media. Complete reduction to water occurs at more negative potentials, which is undesirable. The aim of this work therefore is to develop a catalytic system that will promote oxygen reduction via four electron transfer to water at the lowest potential and at a wide pH range. Manganese phthalocyanine complexes have the potential since manganese has up to four oxidation states (I to IV), hence are employed in this study.

Table 1.3: Electrochemical data for oxygen reduction catalyzed by MPcs.

Complex[a]	**Electrode**	**E(V)/(SCE) (O_2/H_2O_2)[b]**	**E(V)/(SCE) (H_2O_2/H_20)[b]**	**Medium**	**Ref.**
FeTSPc	OPG	-	-0.78	0.1M NaOH	182
MnTSPc	OPG	-	-0.82	0.1 M NaOH	183
CoTSPc	OPG	-0.74	-	0.1 M NaOH	183
CoTAPc	GC[b]	-0.62	-	0.1 M NaOH	188
CoTAPc	GC	-0.60	-	0.1 M NaOH	187
CoTAPc	GC[b]	-0.34	-0.52	0.05 M H_2SO_4	187
CoTAPc	GC	-0.24	-	0.05 M H_2SO_4	187
CoTAPc	HOPG	-0.60	-	pH 1.65	178
CoTAPc	GC[c]	-0.13	-0.58	pH 4	179
CoTAPc	GC[c]	-0.25	-0.83	pH 13	179
CoCRPc	HOPG	-0.38	-1.06	pH 4	186
CoTNPc	HOPG	-0.48	-0.87	pH 4	187

[a] CR denotes crown ether, TN tetranitro, TS and TA have been defined above.

[b] A correction factor of -0.045 V was used to convert potentials from V/(Ag|AgCl) to V/(SCE)[155].

[c] Electrodes were modified by electropolymerization.

Aims of thesis

To conduct oxygen reduction on glassy carbon electrode modified by adsorption of manganese phthalocyanine complexes. The reaction is expected to occur at positive potentials in a wide pH range, via four electron transfer process on stable, long-lived catalysts. Manganese is used as a central metal because it has been reported to exhibit the best electrocatalytic behavior towards oxygen reduction. This is because its d-orbitals are half filled and of energy that allows constructive overlap and energy transfer with the p-orbitals of oxygen[189]. Complexes employed are (Fig. 1.17): a) manganese phthalocyanine (MnPc, **7a**), b) manganese tetraamino phthalocyanine (MnTAPc, **7b**), c) manganese tetrapentoxy pyrrole phthalocyanine (MnTPePyrPc, **7c**), d) manganese tetraphenoxy pyrrole phthalocyanine (MnTPhPyrPc, **7d**), e) manganese tetramercapto pyrimidine phthalocyanine (MnTMerPyPc, **7e**) and f) manganese tetraethoxy thiophene phthalocyanine (MnTEThPc, **7f**). All complexes are new except MnPc and MnTAPc, allowing investigation of substituents effect on electrocatalytic activity.

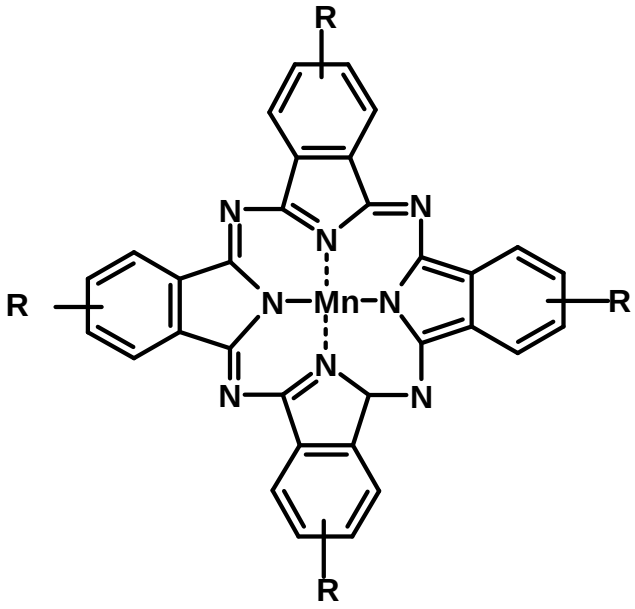

Complex	R	Abbreviation
7a	H	MnPc
7b	NH_2	MnTAPc
7c	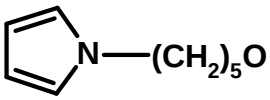	MnTPePyrPc
7d	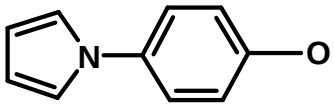	MnTPhPyrPc
7e	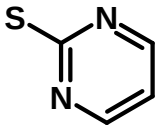	MnTMerPyPc
7f	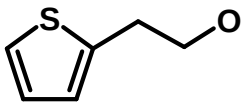	MnTEThPc

Figure 1.17: Molecular structures of phthalocyanine complexes used in electrocatalytic reduction of oxygen; MnPc (manganese phthalocyanine), MnTAPc (manganese tetraamino phthalocyanine), MnTPePyrPc (manganese tetra pentoxy pyrrole phthalocyanine), MnTPhPyrPc (manganese tetraphenoxypyrrole phthalocyanine), MnTMerPyPc (manganese tetramercaptopyrimidine phthalocyanine) and MnTEThPc (manganese tetraethoxythiophene phthalocyanine).

1.5 Use of metallophthalocyanines in biomimetic catalysis

This section describes the use of MPcs as biomimetic catalysts in addition to electrocatalysis described above. Experiments were undertaken to explore biomimetic catalytic activity of MPcs for oxidation of a selected substrate cyclohexene. Cyclohexene is produced in large quantities by petroleum industrial companies as waste or bi-products. It is therefore imperative to re-use such compounds for other purposes as a way of conserving our already-scarce and depleted natural resources. Alkenes can be partially oxidized to fine chemicals such as alcohols, ketones and aldehydes; which can then be used for other beneficial purposes. Alkene oxidation reactions have been conducted by use of oxidizing agents but these reactions are very slow and yield minute products. There is a need to speed up the reactions, to keep up with the rate of alkene production from petroleum industries as well as increase oxidation product yields.

Biomimetic catalysis stems from catalytic activity of a family of enzymes called Cytochrome P450 which catalyzes numerous oxidation reactions that occur in human bodies. These enzymes have a -*haem* group (porphyrin) and they use the Fe moiety as a catalyst. Porphyrins have been synthesized and used to mimic the behaviour of Cytochrome P450 enzymes[190]. Porphyrins have been used as catalysts in oxidation of alkanes and alkenes with great success[191]. The only setback is chemical and thermal instability[192]. This was however circumvented by ring substitution with electron withdrawing ligands[193].

Phthalocyanines have been used as catalysts for alkane and alkene oxidation reactions to mimic Cytochrome P450s[194]. Phthalocyanines have improved thermal and chemical stability; they are cheaper and more readily available than porphyrins. Their resistance towards oxidative degradation and catalytic capability are also improved by ring substitution with electron withdrawing groups such as halogens[195]. Metallophthalocyanines oxidize the relatively inert carbon-hydrogen bonds in the presence of oxidants (ROOH) according to the overall mechanism, eq. 1.43 – 1.44[196],

$$M^{n}Pc + 2ROOH \rightarrow [M^{n+1}Pc]^{+} + ROO^{\bullet} + RO^{\bullet} + H_2O \qquad 1.43$$

$$ROO^{\bullet}, RO^{\bullet} + C{=}C \rightarrow \text{epoxide, alcohol, ketone} \qquad 1.44$$

where $ROO^{\bullet}$ + $RO^{\bullet}$ are oxidant radicals. The reaction involves interaction of MPcs with oxidants forming high valent intermediates and oxidant radicals. The latter yield epoxides by addition to the olefin double bond or allylic oxidation products such as alcohols and ketones by abstracting an allylic hydrogen atom[197]. No oxidation products are detected when oxidation reactions occur in the presence of radical scavengers showing involvement of radicals[198].

Oxidation of alkanes and alkenes by MPcs allows control of the active form of oxygen, hence results in selectivity of formed products. Product selectivity has been reported to depend also on the nature of oxidant used[199]; cyclohexene epoxidation occurred only when hydrogen peroxide was used as an oxidant instead of *tert*-butyl hydroperoxide (TBHP)[200]. Selectivity can also be fine-tuned by the type and oxidation state of central metal of the MPc[194], and the ability of the central metal to form μ-oxo or peroxo-bridged intermediate compounds. CoPc-catalyzed cyclohexene oxidation yields more

cyclohexenol than cyclohexenone whereas the inverse holds for FePc catalyst[201]. Furthermore, catalytic activity depends on the central metal; higher cyclohexene oxidation product yields were obtained when Fe was the central metal, followed by Mn, then Co[201].

The solvent in which the reaction occurs affects product selectivity[202]. Basic solvents stabilize catalysts against oxidative degradation by their electron donating ability. Coordinating solvents shield the catalysts from attack by oxidants. Radicals are stabilized in basic solvents[203], hence prolonging substrate interaction with the catalytic species. Generally, MPc-catalyzed hydrocarbon oxidations result in high turnover rates, wide product range and product yields of ~100 %[204]. Table 1.4 shows data for cyclohexene oxidation catalyzed by MPs and MPcs yielding cyclohexene epoxide.

Substituted manganese porphyrins were good catalysts[205]; their epoxide yields were comparable to those obtained with iron phthalocyanine complexes. However, they were short-lived since they complexed with the oxidant forming a very unstable oxo-Mn(V) intermediate. This high valent intermediate however leads to formation of allylic products (alcohols and ketones). Amongst the phthalocyanine catalysts, those with iron as the central metal exhibited highest epoxide yields. This was even more pronounced with axial[206] or ring substitution[207], which has been reported to stabilize Pc complexes against oxidative degradation.

Table 1.4: Data for cyclohexene epoxidation catalyzed by MPs and MPcs.

Catalyst[a]	Solvent	Oxidant	% Yield	Ref.
$MnM_{2\text{-}OH}$ PTTP(Ac)	CH_2Cl_2	O_2, (Iodosylbenzene)	49	205
$MnM_{2\text{-}Br}$ PTTP(Ac)	CH_2Cl_2	O_2, (Iodosylbenzene)	55	205
ClFePc	CH_2Cl_2:MeOH: H_2O 80:18:2	Iodosylbenzene, (Imidazole)	56	206
MnPc	CH_2Cl_2	O_2, (isobutyraldehyde)	25	201
FePc	CH_2Cl_2	O_2, (isobutyraldehyde)	32	201
CoPc	CH_2Cl_2	O_2, (isobutyraldehyde)	13	201
FeTTBPc	CH_2Cl_2	O_2, (isobutyraldehyde)	57	207
MnTTBPc	CH_2Cl_2	O_2, (isobutyraldehyde)	38	207
CoTTBPc	CH_2Cl_2	O_2, (isobutyraldehyde)	21	207

[a] $MnM_{2\text{-}OH}$PTTP(Ac) is (5-(2-hydroxyphenyl)-10,15,20)-tritolylporphyrinmanganese(III) acetate, $MnM_{2\text{-}Br}$PTTP(Ac) is (5-(2-(3-bromo-1-propoxy)phenyl)-10,15,20)-tritolylporphyrin manganese(III) acetate and TTBPc is tetra-tert-butylphthalocyanine.

Aims of thesis

To catalyze oxidation of cyclohexene by Cytochrome P450 mimics - iron poly-chloro phthalocyanine complex ($FePc(Cl)_{16}$ **9**, Fig. 1.18) in the presence of chemical oxidants. Fe is chosen as the central metal because it is the catalytic moiety in Cytochrome P450 enzymes and FePc complexes gave highest yields towards cyclohexene oxidation as shown in Table 1.4. The complex is halogenated on the ring to improve stability against oxidative degradation. Cyclohexene oxidation has been studied extensively with

porphyrins as catalysts and not phthalocyanines, hence the study of FePc derivatives in this work. The principal aim is to improve product selectivity and range. The reaction is conducted in a solvent mixture that has a coordinating ability that will protect the catalyst against oxidative degradation. The catalytic activity of $FePc(Cl)_{16}$ **9** is compared to that of unsubstituted FePc **8** and CoPc **6a**.

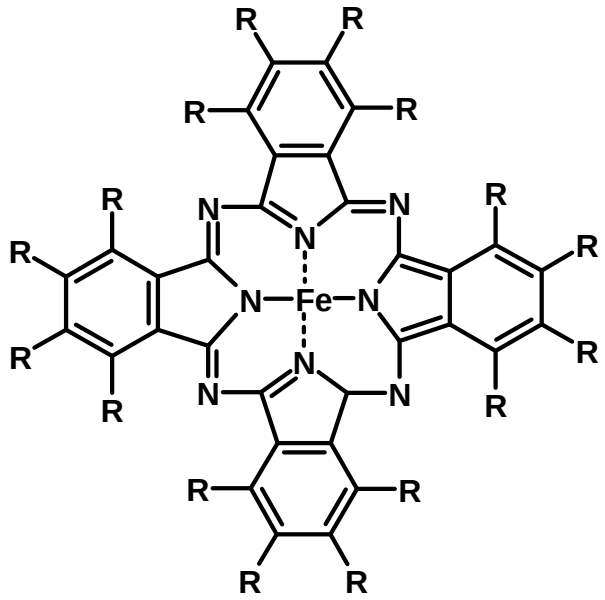

R = H; (FePc, 8) and R = Cl; ($FePc(Cl)_{16}$, 9)

Figure 1.18: Molecular structures of FePc and $FePc(Cl)_{16}$ complexes used as biomimetic catalysts for oxidation of cyclohexene.

1.6 Use of metallophthalocyanines in photo-catalysis

This section explores the use of metallophthalocyanines as photo catalysts for oxidation of cyclohexene. It compares product type and selectivity for cyclohexene oxidation achieved by biomimetic and photo-catalysis by MPcs. MPcs can be employed in photo-catalyzed reactions because of their light-

absorbing capability. As mentioned earlier, these complexes absorb strongly in the UV/Vis region of the electromagnetic spectrum. Their most intense absorption peak is called the Q-band, observed at around 670 nm. A series of changes occurs when these molecules absorb light described by Jablonski[208,209]; and are represented by the modified Jablonski diagram (Fig. 1.19). UV/Vis light absorption (Abs) excites molecules from the ground state (S_0) to the excited singlet state (S_n). The molecules then lose the acquired energy through several processes to regain equilibrium according to the LeChatelier principle.

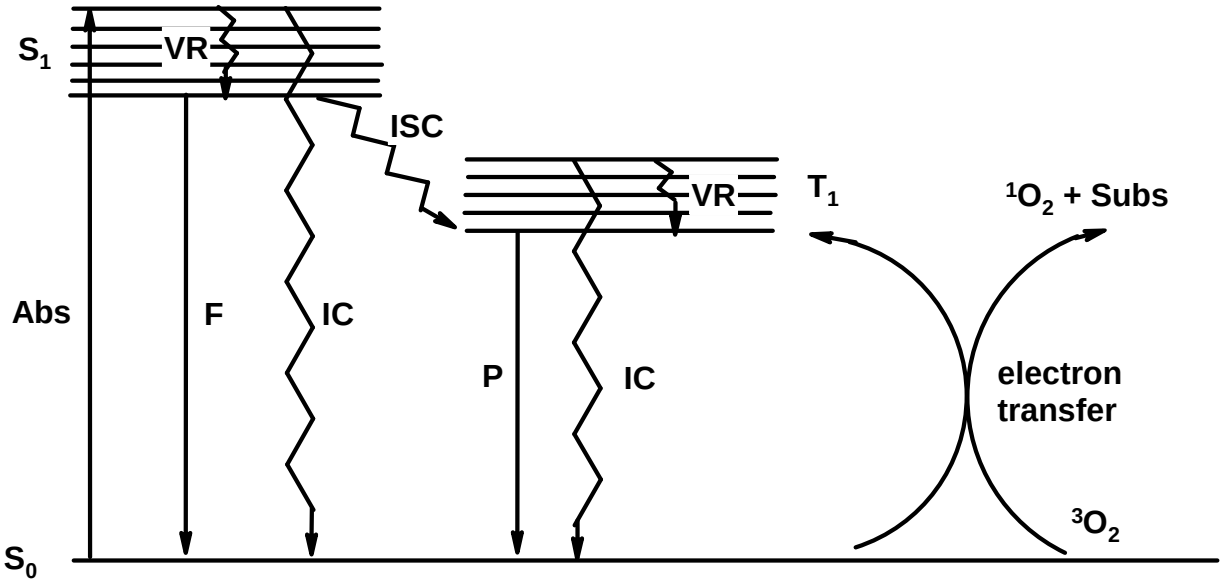

Figure 1.19: Modified Jablonski diagram illustrating processes that occur when a phthalocyanine molecule absorbs UV/Vis light. *Key;* wavy arrows indicate radiationless transitions whereas straight lines indicate radiative transitions.

Energy can be lost by radiationless vibrational relaxation (VR) from higher vibrational energy states to the first energy level of S_1; from which relaxation to the ground state occurs via fluorescence (F). Energy loss can also occur via non-radiative internal conversion (IC) from S_1 to S_0. The third

way is via intersystem crossing (ISC), which is transfer from the excited singlet (S_1) to the excited triplet state (T_1). Subsequently relaxation to the ground state occurs via phosphorescence (P) or non-radiative internal conversion. Alternatively, the first excited triplet state (T_1) can interact with substrates (subs) and induce a series of chemical reactions. In this work, oxygen is the substrate that absorbs energy getting excited from the triplet to the singlet state, hence triggering a series of photo-catalyzed reactions.

Cyclohexene is a substrate whose oxidation is photo-catalyzed by zinc phthalocyanine (ZnPc **10**) in this work. The aim is to conduct the reaction while avoiding catalyst destruction by harsh oxidizing agents as employed in biomimetic catalysis. Phthalocyanine complexes need to have a diamagnetic central metal for generation of sufficient singlet oxygen. $FePc(Cl)_{16}$ employed in biomimetic catalysis is paramagnetic and cannot be employed in photocatalysis. Zinc phthalocyanine is used as a photo-catalyst because its central metal zinc is a diamagnetic metal whose excited singlet state ($^1MPc^*$) is known to undergo intersystem crossing (ISC) to the excited triplet state ($^3MPc^*$) readily. Since the excited triplet state will be highly populated, it is expected that it will interact constructively with ground triplet state molecular oxygen ($^3O_2$) generating excited singlet state oxygen ($^1O_2$). Singlet oxygen is very reactive and will therefore consequently catalyze the substrate cyclohexene. This is known as Type II mechanism of photo-catalysis described by Scheme 1.2[210]:

$$MPc \xrightarrow{h\nu} {}^1MPc^* \xrightarrow{ISC} {}^3MPc^* \quad 1.45$$

$${}^3MPc^* + {}^3O_2 \rightarrow {}^1O_2 + MPc \quad 1.46$$

$${}^1O_2 + \text{substrate} \rightarrow \text{Oxidation products} \quad 1.47$$

Scheme 1.2: Type II mechanism of photo-catalysis.

However, the excited triplet state of the MPc not only generates singlet state oxygen upon interaction with triplet state oxygen, but also radicals[211]. It also interacts with cyclohexene substrate generating radical ions, which propagate further radical ion formation and subsequently afford catalyzed substrate oxidation[212]. This is known as Type I mechanism and it is represented by Scheme 1.3[213]:

$${}^3MPc^* + {}^3O_2 \rightarrow O_2^{-\bullet} + MPc^{+\bullet} \quad 1.48$$

$${}^3MPc^* + Subs \rightarrow MPc^{-\bullet} + Subs^{+\bullet} \quad 1.49$$

$$MPc^{-\bullet} + {}^3O_2 \rightarrow O_2^{-\bullet} + MPc \quad 1.50$$

$$O_2^{-\bullet} \xrightarrow{H^+} HO_2^{\bullet} \quad 1.51$$

$$HO_2^{\bullet} + Subs \rightarrow H_2O_2 + Subs^{\bullet} \quad 1.52$$

$$Subs^{+\bullet}, Subs^{\bullet}, H_2O_2 \rightarrow \text{Oxidation products} \quad 1.53$$

Scheme 1.3: Type I mechanism of photo-catalysis. Subs is substrate, cyclohexene in this case.

It has been reported that Type II mechanism is more prevalent in photo-initiated oxidation reactions[214], thus the magnitude of singlet oxygen quantum yields (ϕ_Δ) which express the amount of singlet oxygen generated per quanta of light is often employed as a main criteria in choosing photosensitizers used in photocatalytic reactions. It is for this reason that ZnPc is used in this work, since it has been reported to have high ϕ_Δ of ~ 0.6

in different organic solvents[215,216]. Triplet lifetime (τ_T) of the photosensitizer in a particular reaction medium should also be considered so as to maximize efficiency of the reaction. The triplet lifetime should be long enough to interact constructively with triplet state oxygen. Lifetime of formed radicals should also be long enough to effect catalysis.

Literature is very scanty on the use of MPcs as alkene photocatalysts. Cyclohexene oxidation has been performed by metallo-porphyrins successfully and the results are shown in Table 1.5. Product selectivity has been observed to vary with ring substituents for the porphyrin of the same metal[217,218]. Electron withdrawing substituents increased catalyst stability and hence improved product yields[219], the higher their number, the more prominent the effect. In most cases, cyclohexene photocatalysis yields mainly cyclohexene hydroperoxide which disintegrates into cyclohexenol and cyclohexenone with time[220]. Generally photocatalyzed cyclohexene oxidation involves radical mechanism but formed products vary according to the central metal, substituents and reaction medium.

Table 1.5: Data for photocatalyzed oxidation of cyclohexene by metalloporphyrins.

Catalyst[a]	Solvent	Oxidant	Products	Reference
$Sb^{V}TPP(OCH_3)_2$	33% aq. acetonitrile	H_2O	2-cyclohexenol 3,3'-bicyclohexenyl	217
$Sb^{V}TPP$	5 % aq. acetonitrile	H_2O	2-cyclohexenone 3-cyclohexenone	218
$Ti(O)TPPCl_8$	CH_2Cl_2	O_2	Cyclohexene hydroperoxide	219
$Ti(O)TPPCl_4$	CH_2Cl_2	O_2	Cyclohexene hydroperoxide	219
PdTMPyP	ethanol	O_2	Cyclohexene hydroperoxide	220
FeTBCPP	ethanol	O_2	Cyclohexene hydroperoxide	220

[a] $Sb^{V}TPP(OCH_3)_2$ is dimethoxy coordinated tetraphenyl porphyrinato antimony (V), $Sb^{V}TPP$ is tetraphenyl porphyrinato antimony (V), $Ti(O)TPPCl_8$ is meso-tetrakis (2,6-dichlorophenyl) porphyrinato titanium, $Ti(O)TPPCl_4$ is meso-tetrakis (4-chlorophenyl) porphyrinato titanium, PdTMPyP is meso-tetrakis (N-methyl-4-pyridyl) porphyrinato palladium (II) and FeTBCPP is meso-tetrakis (2,6-dichlorophenyl) porphyrinato iron (III).

Aims of thesis

This work aims to catalyze oxidation of cyclohexene by radicals or singlet oxygen generated upon irradiation of zinc phthalocyanine; only porphyrins have been used as photo-catalysts. The reaction sequence and mechanism will be probed as well as factors affecting the extent of reaction and product selectivity. Type of oxidation products formed will be compared with those formed via biomimetic catalysis by iron phthalocyanines. Lastly, catalyst lifetime will be improved by eliminating use of oxidizing agents and

thereby investigate the effect of prolonged catalyst presence on product formation.

1.7 General aims of thesis

Goals of this thesis are summarized as follows:

a) To modify electrodes by adsorption, self-assembly, electrodeposition and electropolymerization of appropriate metallophthalocyanines (MPcs, Figs. 1.15 and 1.17) and use them as electrocatalysts for reduction of molecular oxygen, oxidation of thiocyanate (SCN^-), as well as oxidation of thiols, namely 2-mercaptoethanol (2-ME), *L*-cysteine (CYS) and *reduced*-glutathione (GSH).

b) Use hexadecachloro iron phthalocyanine ($FePc(Cl)_{16}$) complex as a biomimetic catalyst for cyclohexene oxidation using *tert*-butylhydroperoxide (TBHP) and chloroperoxybenzoic acid (CPBA) as oxidants. To compare its catalytic activity to that of unsubstituted FePc and CoPc: To determine the effects of ring substitution with electron withdrawing chloride anions, nature of central metal and oxidant on product selectivity, turnovers and yields.

c) Use zinc phthalocyanine (ZnPc) complex as a photocatalyst for cyclohexene oxidation using singlet oxygen and radicals generated upon the Pc's excitation with UV/Vis light. To compare product yields, selectivity and turnovers with those obtained from biomimetic catalyzed oxidation reaction.

Chapter 2

Experimental

This section describes experimental procedures carried out in this work.

2.1 Materials

Dimethylformamide (DMF), tetrahydrofuran (THF), dichloromethane (DCM), dimethyl sulphoxide (DMSO), DMSO-d_6, methanol, ethanol and acetone were purchased from SAARCHEM, Johannesburg, South Africa. They were of HPLC/GC grade and used as received. *L*-cysteine (CYS), 2-mercaptoethanol (2-ME), reduced glutathione (GSH), *S*-nitrosoglutathione (GSNO), urea, cyclohexanone, tetrabutyl-ammonium tetrafluoroborate ($TBABF_4$), 1-pentanol, zinc acetate, 5-amino pentanol, 2,5-dimethoxytetrahydrofuran, cyclohexene, *tert*-butylhydroperoxide (TBHP, 70% in water), chloro-peroxybenzoic acid (CPBA), diazabicyclooctane (DABCO), cyclohexene oxide, 2-cyclohexen-1-ol, 2-cyclohexen-1-one, 1,3-diphenylbenzofuran (DPBF), 3,4-dichloroanhydride, phthalonitrile, *trans*-1,2-cyclohexanediol and adipic acid were purchased from Aldrich, Steinheim, Germany. They were of analytical reagent grade and used without any further purification.

Potassium thiocyanate, iodine and bromine were purchased from Riedel-de Haen, Steinheim, Germany; 2-thienyl-2-ethanol was from Fluka, Steinheim, Germany; tert-butanol and nitrobenzene were purchased from Merck, Steinheim, Germany; and they were used as received. Hydrogen peroxide (H_2O_2), KH_2PO_4, K_2HPO_4, $NaBH_4$, NaOH, $Fe(CN)_6$, Na_2HPO_4, NaH_2PO_4, KOH, Na_2SO_4, NaCl, KBr, $CaCl_2$, $MnCl_2$, K_2CO_3, HCl, KCl, $HClO_4$, $Fe(NH_4)(SO_4)_2$, $CuSO_4$, H_2O_2, H_2SO_4, lithium, potassium iodide, ammonium molybdate, iron chloride tetrahydrate ($FeCl_2.4H_2O$), 2-propanol, glacial acetic acid, 1,4-dioxane, potassium and sodium thiosulphate, pH 4 and pH 7

phosphate buffer tablets were purchased from SAARCHEM, Johannesburg, South Africa. They were of reagent grade and used as received.

Cellulose acetate was purchased from Sigma Chemical (Paris, France), whereas graphite powder was from Fluka (Paris, France). Alumina ceramic plates were purchased from The Laser Cutting Company Ltd. (Sheffield, UK) while silver-silver chloride ink was from GEM-Gwent (Pontypool, UK). These reagents were used as received. Iron (II) phthalocyanine (FePc) and cobalt phthalocyanine (CoPc) were purchased from Aldrich (Steinheim, Germany) while MnPc was from EASTMAN (Miami, USA). They were of analytical reagent grade and used without any purification. Zinc phthalocyanine and iron hexadecachloro phthalocyanine ($FePc(Cl)_{16}$) were synthesized; the procedure is outlined below.

Cobalt tetra phenoxypyrrole phthalocyanine (CoTPhPyrPc **6b**)[101] and cobalt tetra ethoxythiophene phthalocyanine (CoTEThPc **6c**)[221] were synthesized and characterized as reported by our research group, as well as manganese complexes tetra substituted with amino (MnTAPc **7b**)[112], phenoxy pyrrole (MnTPhPyrPc **7d**)[101], mercaptopyrimidine (MnTMerPyPc **7e**)[222] and ethoxy thiophene (MnTEThPc **7f**)[221]. The synthesis of pentoxy pyrrole substituted MnPc (MnTPePyrPc **7c**) will be discussed below.

2.2 Apparatus

Electrochemical experiments were carried out using the conventional three-electrode cell system and a Princeton Applied Research Inc. potentiostat/galvanostat model 263A (USA) or a BioAnalytical Systems (BAS)

100 B/W Electrochemical Workstation. pH values were measured using a pH meter (WTW, Germany).

IR spectra (KBr pellets) were recorded on a Perkin-Elmer spectrum 2000 Fourier Transform Infrared (FTIR) spectrometer. ^{1}H-nuclear magnetic resonance (^{1}H-NMR, 400 MHz) spectra were obtained in DMSO-d_6 using Bruker EMX 400 NMR spectrometer. Adsorption column chromatography was performed using silica gel 60 (0.040 - 0.063 mm) obtained from Merck. Elemental analyses were performed with a Carlo Erba NA 1500 Nitrogen analyzer at the University of the Western Cape, Cape Town, South Africa.

The GC traces were recorded with a Hewlett-Packard HP 5890 Gas Chromatograph fitted with an FID detector, using a cross-linked methyl siloxane capillary column (30 m length, 0.32 mm internal diameter and 0.25 μm film thickness). The parameters for analysis were: carrier gas N_2 at 30.7 cm s^{-1}, injector temperature = 200 °C, detector temperature = 250 °C. Mass spectra were recorded with Finnnigan LCQ-MS coupled with J & W Scientific column of 30 m length, 0.32 mm internal diameter and 0.25 μm film thickness. UV/Visible spectra were recorded with the Cary 500 UV/Visible/NIR spectrophotometer.

Irradiation in the visible region was carried out with a General Electric Quartz line lamp (300 W), with a 600 nm glass cut off filter (Schott) being used to filter off ultraviolet light, leaving the Pc's Q-band; the excitation area of interest. The photolysis set-up is shown in Fig. 2.1. For irradiation using white light, the 600 nm glass filter was left out. The light intensity was measured with a power meter (POWER MAX5100-with incorporated Molectron detector)

and unless otherwise stated the white light intensity used was 5.2 x 10^{16} photons s^{-1} cm^{-2}.

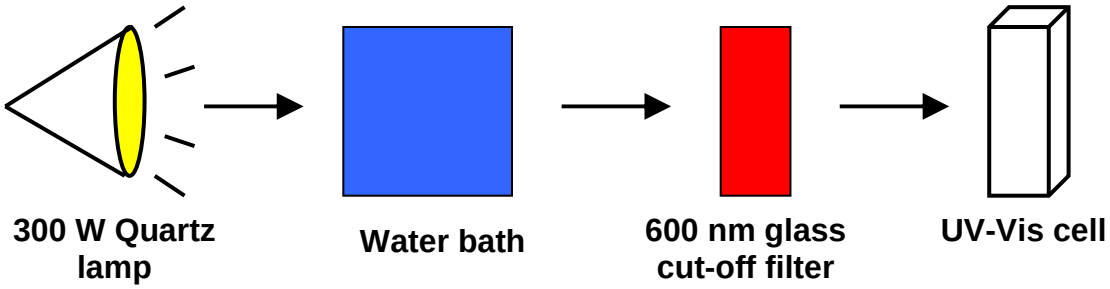

Figure 2.1: Photolysis setup used for zinc phthalocyanine photocatalyzed oxidation of cyclohexene.

The already mentioned GC and GC-MS were used for analysis of photocatalytic reactions. Absorbance measurements for detection of hydroperoxides iodometrically were done with a Pharmacia Biotech Novaspec II spectrophotometer.

Triplet life times (τ_T) were recorded with a laser flash photolysis system (Fig. 2.2). The excitation pulse was provided by a Nd-Yag laser, providing 400 mJ, 90 ns pulses of laser light at 10 Hz, pumping Lambda -Physik FL3002 dye laser. Single pulse energy was 7 mJ. A 300 W xenon arc lamp (Thermo Oriel) provided the analyzing light. The kinetic curves were averaged over 256 laser pulses using a Tektronix TDS 360 Digital Oscilloscope. The triplet life time values were determined by exponential fitting of the kinetic curves using the program ORIGINPro 7.5. The solutions for triplet state life times were introduced into a 0.2 mm path length UV/Visible spectrophotometric cell, deaerated using nitrogen and photolysed at the Q band maxima.

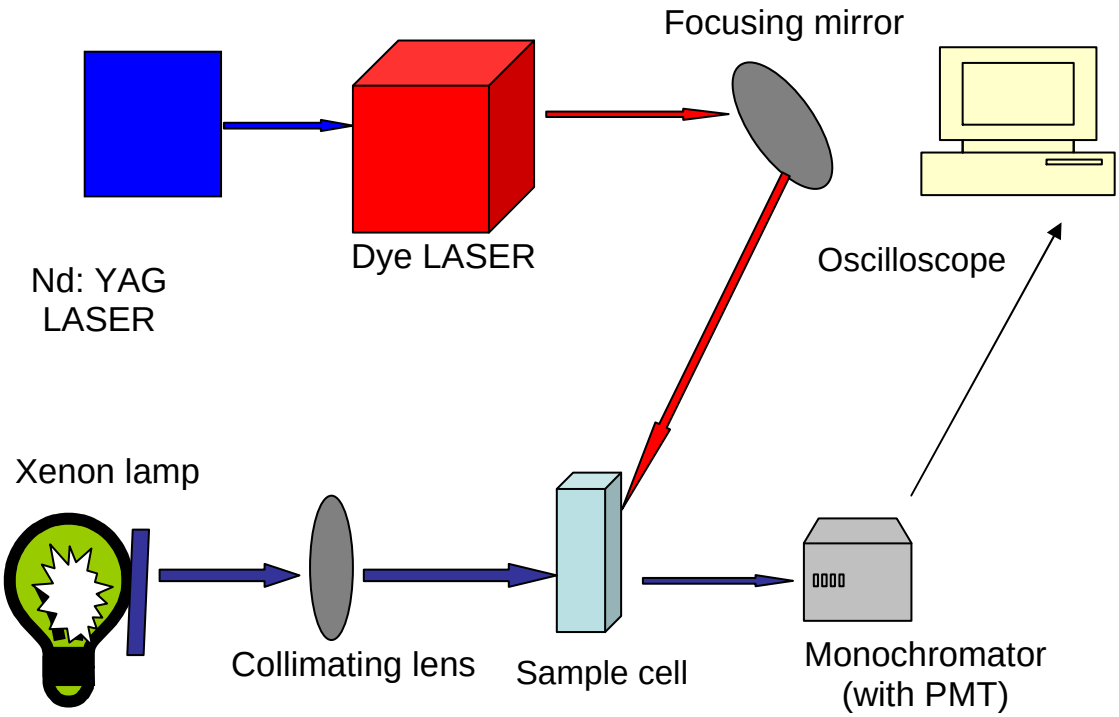

Figure 2.2: A laser flash photolysis set up.

2.3 Electrochemical methods

Ordinary pyrolytic graphite (OPG), gold (Au), screen printed carbon (SPC) and glassy carbon (GC) electrodes were used as working electrodes. A spiral platinum wire was used as a counter electrode and a saturated calomel electrode (SCE) or silver|silver chloride (Ag|AgCl) wire were used as reference electrodes. AgCl was deposited chronoamperometrically onto a Ag wire at 1.5 V for 40 minutes in a saturated KCl solution where a Pt wire was used as both the reference and counter electrodes. To convert potentials expressed versus Ag|AgCl to SCE, a correction factor of -0.011 V was determined and used.

2.3.1 Electrode preparation

A glassy carbon (GC) disk electrode from Radiometer-Tacussel (France) was mounted on Teflon and had a geometrical area of 0.071 cm^2. It was cleaned before each experiment by polishing on 1 and 0.25 μm diamond pastes, followed by extensive rinsing with ultra-pure Millipore water. Another GC electrode of 0.071 cm^2 was purchased from BAS and cleaned by polishing on alumina (<10 μM) slurries on a BAS feltpad. An ordinary pyrolytic graphite (OPG) electrode of 0.44 cm^2 was obtained from Pine Instruments (USA). It was cleaned by polishing on 800 and 1200 grit emery paper and 1 μm alumina, followed by rinsing with ultra-pure Millipore water. Au electrode of 0.020 cm^2 was purchased from BAS and cleaned on alumina slurries on a diamond pad, then on a smoother Buehler pad. The electrode was rinsed with Millipore water and sonicated in ethanol to remove residual alumina particles. The electrode was then immersed in a strong oxidizing piranha solution (1:3 (v/v) 30% H_2O_2 and concentrated H_2SO_4) to remove any organic particles that could still be on the electrode. All electrodes were rinsed with Millipore water after polishing, followed by respective solvents in which experiments were to be conducted.

Screen printed carbon electrodes (SPCEs) were fabricated by printing graphite ink (Fluka, France) mixture in cyclohexanone onto alumina ceramic plates obtained from The Laser Cutting Company Ltd. (Sheffield, UK). The counter and working electrodes as well as the conducting tracks were prepared using a graphite ink. The ink was prepared by mixing 1.4 g graphite powder with 3.4 g of cyclohexanone mixture containing 7 % w/w cellulose

acetate binder. Another batch was incorporated with cobalt phthalocyanine (CoPc) complex. Two procedures were used. In the first one, 0.7 g of graphite powder was mixed with 2 g of cellulose acetate solution in cyclohexanone. CoPc (37 mg) was then added and mixed for 30 minutes using Roll-mill, affording 5 % CoPc-SPCE. The viscosity of the resulting ink modified with CoPc was adjusted by adding a few droplets of cyclohexanone. The obtained electrodes are denoted as 5 % CoPc-SPCE.

In the second procedure, 100 mg of CoPc was dissolved in 20 mL of chloroform. Different volumes of this solution were mixed with 1 g graphite powder, made up to 11 g with cyclohexanone and homogenized. Mixing 2, 5 or 10 mL of CoPc chloroform solution with 1 g graphite powder afforded % CoPc composition of 1.0, 2.5 or 5.0 %, respectively. Then 0.7 g of this mixture was mixed with 2 g of cellulose acetate binder (7 % in cyclohexanone) to make the ink which was then homogenized with a Roll-mill. The obtained electrodes are denoted 1 % CoPc-SPCE, 2.5 % CoPc-SPCE, and 5 % CoPc-SPCE, respectively. Finally, silver-silver chloride ink (GEM-Gwent ,Pontypool, UK) was printed onto the ceramic plates and used as a reference electrode.

SPCEs were made by printing onto alumina ceramic tiles (The Laser Cutting Company Ltd., Sheffield, UK) and permanox-recovered plastic substrate (InterMed, Nunc, USA). Two electrode configurations (Fig. 2.3a and b) were designed; a) is a three-electrode configuration that was initially designed by Ledru et al.[91] for amperometric biosensing in flow injection analysis. A five electrode set-up (Fig. 2.3b) was designed to obtain an optimal number of electrodes for use in multidetection of one or several analytes, or

for mapping production of a target species released from a chosen cell culture as used by Miserere et al.[117].

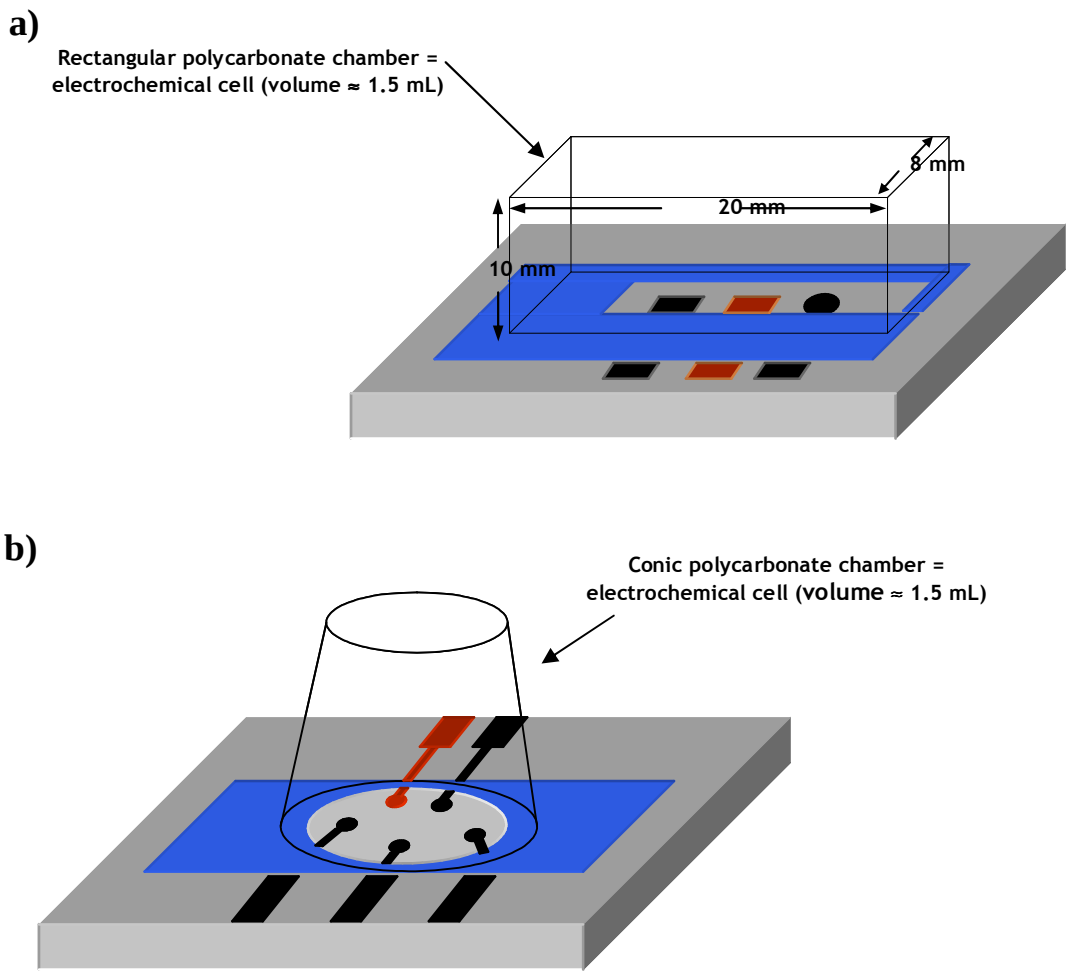

Figure 2.3: Photographs and schematic representations of fabricated SPCEs on alumina ceramic and Labtek platforms. Electrochemical cells constructed by mounting hollow plastic tubes and covering with parafilm.

Ink printing was performed using a DEK Albany model 245 semi-automatic machine (Granby-UK). Stainless screens with a 200 mesh and variable thickness were used in electrode preparation. Ag|AgCl ink obtained from GEM-Gwent was printed and used as a reference electrode (13 μm thickness) presenting a stable half-cell potential 0.276 V vs normal hydrogen

electrode (NHE). Counter and working electrodes (23 μm thickness), as well as conducting tracks were also printed using graphite-cellulose acetate ink described above. Finally the non-conductive dielectric layer of 36 μm thickness was printed to define the working area surface. Note that in the case of the five-electrode configuration (Fig. 2.3b), there is a difference in the real active area from one electrode to another due to the uncoated section of the tracks left after the non-conductive dielectric layer was printed. All printed layers were cured at room temperature for 6 hours.

2.3.2 Electrode modification and characterization

2.3.2.1 Monomer adsorption

Glassy carbon and ordinary pyrolytic graphite working electrodes were modified with monomers of CoTPhPyrPc **6b** and CoTEThPc **6c** complexes by placing 10 μL of 1 mM solution of the complexes in THF and DCM, respectively, on the electrode surface for 30 minutes. Unabsorbed complexes were removed by rinsing with their respective solvents, followed by rinsing with ethanol. Adsorption of CoPc **6a** onto OPG electrode as well as of MnPc complexes **7a** - **7f** onto glassy carbon electrodes was afforded by spreading out 10 μL of 1 mM solution of the complexes in DMF for 30 minutes. Similarly, residual solution was rinsed off with DMF, then ethanol before further use in experiments.

2.3.2.2 Electropolymerization/electrodeposition

Electropolymerization of CoTPhPyrPc **6b** onto a glassy carbon electrode was achieved by repetitive cycling of the electrode between -0.6 and 1.6 V/(SCE) at 0.2 Vs^{-1} in a 1 mM DCM solution of the complex containing 0.1 M $TBABF_4$. The growth of the film was observed by monitoring the increase in the charge attributed to the reversible redox couple of the metal centre $Co^{III/II}$ located at ~0.85 V/(SCE). Electrodeposition of CoTEThPc **6c** onto the GCE was achieved in the range 0.2 to 1.6 V/(SCE) at 0.2 Vs^{-1} in a 1 mM THF solution of the complex containing 0.1 M $TBABF_4$ electrolyte. Electrodeposition of the complex on the electrode was observed by charge increase of the signal attributed to the $Co^{III/II}$ couple at ~0.90 V/(SCE), and also with the signal at ~1.6 V/(SCE) due to the oxidation of the thiophene group.

2.3.2.3 Self-assembled monolayers

A self-assembled monolayer of CoTEThPc **6c** was formed by immersing a clean Au electrode in a nitrogen-purged 1 mM CoTEThPc **6c** solution in DMF for 72 hours at room temperature. The longer the immersion time period, the better the MPc arrangement on the electrode. The CoTEThPc-SAM electrode was then rinsed with DMF and Millipore water. CVs of CoTEThPc-SAM were scanned in 0.01 M KOH, 1 mM $CuSO_4$ in 0.5 M H_2SO_4, 1 mM $Fe(NH_4)(SO_4)_2$ in 1 mM $HClO_4$ solutions to check blockage of

anodic gold oxide formation, under-potential deposition (UDP) of Cu and the $[Fe(H_2O)_6]^{3+}/[Fe(H_2O)_6]^{2+}$ redox couple, respectively.

For all modified electrodes, CVs were recorded in oxygen-free buffer solutions to check redox couples of MPc films on the electrode surfaces. Buffer solutions were prepared from commercial phosphate buffer tablets and the pH adjusted to the required value by addition of 0.5 M NaOH or 0.5 M H_2SO_4 accordingly. In other cases, buffer solutions composed of NaH_2PO_4 or KH_2PO_4, Na_2HPO_4 or K_2HPO_4 and NaOH salts. Electrolytic solutions were routinely deoxygenated by bubbling with argon or nitrogen. An oxygen-free atmosphere was maintained during voltammetric scans, except for oxygen reduction reactions.

2.3.3 Electrocatalysis

Electrodes modified with metallophthalocyanines were employed in electrocatalysis of analyte reactions, details of which are summarized in Table 2.1. Glassy carbon electrodes modified by adsorption, electropolymerization and electrodeposition of CoTPhPyrPc **6b** and CoTEThPc **6c** were used to electrocatalyze oxidation of 2-mercaptoethanol (2-ME), *L*-cysteine (CYS) and *reduced*-glutathione (GSH). In another set of experiments, GSH was catalyzed by CoPc **6a** adsorbed on an ordinary pyrolytic graphite (OPG) electrode. GSH and 2-ME were also electrocatalyzed by CoPc **6a** incorporated into screen printed carbon electrodes (SPCEs). Reactions were conducted in pH 13 (0.5 M NaOH) and pH 7 buffer solutions, the latter composed of KH_2PO_4 and NaOH salts. *S*-nitrosoglutathione (GSNO)

decomposition reaction was conducted in pH 7 buffer solution on CoPc adsorbed on OPG electrode.

Table 2.1: Electrodes and modifiers used for electrocatalysis of thiol & thiocyanate oxidation and oxygen reduction.

Analyte	Electrode	Modifier	Method
2-ME	GCE	**6b, 6c**	Adsorption, polymerization, electrodeposition
	RDE	**6b, 6c**	Adsorption
	Au	**6c**	SAM
	SPCE	**6a**	Composite paste
CYS	GCE	**6b, 6c**	Adsorption, polymerization, electrodeposition
	RDE	**6b, 6c**	Adsorption
	Au	**6c**	SAM
GSH	GCE	**6b, 6c**	Adsorption, polymerization, electrodeposition
	RDE	**6b, 6c**	Adsorption
	SPCE	**6a**	Composite paste
	OPG	**6a**	Adsorption
SCN^-	Au	**6c**	SAM
O_2	GCE & RDE	**6a - 6c, 7a - 7f, 8, 9**	Adsorption

CoTEThPc **6c**-SAM was used to electrocatalyze the oxidation of thiocyanate (SCN^-), *L*-cysteine and 2-mercaptoethanol. Reactions were conducted in buffer solutions of pH range 1 - 7 since SAMs desorb from electrode surfaces in alkaline media, after the first scan. pH 4 and pH 7 solutions were prepared using commercial phosphate buffer tablets; the rest of the pH range was obtained by adjusting the pH with addition of acid (0.5 M H_2SO_4) or alkali (0.5 M NaOH) as required. Oxygen reduction studies were conducted on manganese phthalocyanine complexes adsorbed on glassy

carbon electrodes in buffer solutions of pH 1 - 13. Oxygen gas was then bubbled into the buffer solutions to attain saturation.

Thiocyanate and thiol oxidation as well as oxygen reduction reactions were studied using cyclic voltammetry (CV) and rotating disc electrode (RDE) voltammetry.

2.4 Biomimetic reactions

These reactions were employed for transformation of cyclohexene. The solvent mixture containing DMF and DCM (3:7) was employed for the catalysis, since all the reagents dissolved and this ratio has been reported to give highest product yields for cyclohexane oxidation catalyzed by the $FePc(Cl)_{16}$ complex[196]. Cyclohexene (1.5 M) oxidation was attempted at room temperature in the DMF/DCM solvent mixture for 8 hours. The same reaction was attempted in the presence of either 0.5 M oxidants (TBHP or CPBA) or 1.5 mg/mL of catalyst ($FePc(Cl)_{16}$ **9**, CoPc **6a** or FePc **8**), and when oxidant and catalyst were both present.

The reaction was monitored by recording GC traces as the oxidation reaction progressed. Integrity of the catalysts during the course of the reactions was probed by recording UV/Visible absorption spectra. The oxidation products were identified by spiking using standards and by comparison of retention times of standards with those of product peaks in gas chromatography. The nature of the products was also determined by a gas chromatograph connected to a mass spectrometer (GC-MS). Reactions were run at least in triplicates and not always using the same batches of the

catalysts, oxidant or substrate. Product yields were calculated based on the substrate using equation 2.1;

$$\% \text{ yield} = \frac{[\text{product}]}{[\text{cyclohexene}]} \text{ x } 100\% \qquad 2.1$$

Turnover numbers were calculated using the ratio of moles of product to initial moles of catalyst, eq. 2.2;

$$\frac{\text{product moles}}{\text{initial catalyst moles}} \qquad 2.2$$

Product selectivity was determined as the relative distribution of formed products.

2.5 Photocatalytic reactions

Photocatalytic reactions for phototransformation of cyclohexene were conducted in a number of solvents, namely THF, 3:7 DMF-CH_2Cl_2 and 1,4-dioxane. However, catalytic reactions were studied mainly in the latter since both cyclohexene and ZnPc dissolved completely and oxidation products were obtained in the highest yields compared to the other two solvents. The reaction mixtures consisting of known amounts of the catalyst (ZnPc **10**) and the substrate (cyclohexene) were prepared in 5 mL glass sample vials and their gas chromatograph (GC) traces recorded. This was followed by irradiation of the reaction mixtures with either red or white light for a noted time period, while stirring. Reactions were run at least in triplicates and with varying amounts of reagents used and irradiation periods.

GC traces were recorded periodically during the course of the reaction. Similarly, UV/Visible absorption spectra were recorded periodically but the solutions had to be diluted before recording the spectra. For monitoring the fate of the catalyst, experiments were conducted in a 1 cm path-length spectrophotometric cell fitted with a tight fitting stopper. Concentrations of the catalyst were determined using its molar extinction coefficient. This was determined spectrophotometrically and was found to be 1.8 x 10^5 dm^3 mol^{-1} cm^{-1} in 1,4-dioxane at 665 nm.

In order to determine the catalytic effect of ZnPc under white light, GC traces for the photolysis of cyclohexene in the absence of ZnPc were subtracted from those in the presence of the catalyst, since cyclohexene degrades to some small degree in the absence of a catalyst, under white light conditions.

The oxidation products were identified by spiking using standards and by measurements of retention times in gas chromatography. The nature of the products were further confirmed by mass to charge ratios of molecular ion peaks and fragmentation patterns as obtained from a gas chromatograph connected to a mass spectrometer (GC-MS). Cyclohexene hydroperoxide was identified using iodine liberation methods, followed by titration of iodine with sodium thiosulphate or recording of the ultra violet spectra of iodine at 351 nm[223,224].

Singlet oxygen is the reactive species in photocatalysis reactions and its quantum yield is important. Singlet oxygen quantum yields (ϕ_Δ) which express the amount of singlet oxygen generated by phthalocyanine complex per quanta of light could not be determined in this work. This is because there

is no reference in solvents which were employed for photocatalysis, namely THF, 3:7 DMF-CH_2Cl_2 and 1,4-dioxane. However relative singlet oxygen quantum yields were determined by monitoring the rate of degradation of 1,3-diphenyl isobenzofuran (DPBF) a radical scavenger upon interaction with singlet oxygen generated from irradiation of MPc in the presence of oxygen, using the set-up shown in Fig. 2.1.

Photobleaching quantum yields (ϕ_P) which express photodegradation of MPcs per quanta of light irradiated were also determined using the set-up shown in Fig. 2.1. ϕ_P gives a measure of stability of the MPc towards light. This is important because the amount of light employed in photocatalytic reactions should not be too high so not to degrade the catalyst in the process. Equation 2.3 was employed in the calculations,

$$\phi_P = \frac{(C_0 - C_t)V}{I_{abs}t} \qquad 2.3$$

where C_o and C_t in mol L^{-1} are the Pc concentrations before and after irradiation respectively. V is the reaction volume, t is the irradiation time, and I_{abs} is absorbed light intensity; the overlap integral of the radiation source intensity and the absorption of the Pc (the action spectrum)[26]. $I_{abs} = \alpha SI/N_a$ where α is a fraction of light absorbed by the MPc, S the irradiated sample vial area, I is light intensity and N_a is the Avogadro's number.

2.6 Syntheses

This section deals with the syntheses of MPc complexes ($FePc(Cl_{16})$ and ZnPc) which were not readily available in the laboratory and had to be

synthesized even though their synthesis is known. Of the MnPc complexes, MnTPePyrPc **7c** was the only one whose synthesis had not been reported before and its synthesis is therefore reported below.

2.6.1 Iron (II) hexadecachlorophthalocyanine, $FePc(Cl)_{16}$, 9

$FePc(Cl)_{16}$ was synthesized, purified and characterized according to literature methods[225]. 3,4-Dichloroanhydride (0.01 mol), 0.0025 mol iron (II) chloride tetrahydrate, (0.4 mmol) ammonium molybdate and excess urea (~0.05 mol) were finely ground together and added to 10 mL nitrobenzene. The mixture was heated under reflux for 5 hours between 180 - 190 ^{o}C. The solid products were filtered and washed with methanol. The products were then Soxhlet extracted overnight using methanol to remove the remaining nitrobenzene. The resulting deep green solid was boiled for 5 minutes in 1 M HCl (30 mL) saturated with sodium chloride. The solid product was isolated by centrifuge and heated at 90 ^{o}C for 30 minutes in 1 M NaOH saturated with NaCl. The product was again isolated by centrifuge and treated with 1.0 M HCl and NaOH. Finally, the dark green solid was washed with water until free from NaOH and dried at 100 ^{o}C overnight.

$FePc(Cl)_{16}$: IR (KBr disk) v/cm^{-1}: 1709, 1645, 1392, 1318, 1273, 1214, 1195, 1158, 1089, 753, 715.

UV-Visible (DMF): λ_{max}/nm (log ε) : 677 (4.87), 335 (3.34).

2.6.2 Zinc phthalocyanine, ZnPc, 10

ZnPc was synthesized, purified and characterized using literature methods[226]. A solution of 0.6 mmol of phthalonitrile and zinc acetate (0.023 mmol) in 5 mL dry 1-pentanol was refluxed for 20 minutes in the presence of nitrogen. Refluxing was continued until the UV-Visible spectrum of the solution had a distinct Q-band - characteristic of a phthalocyanine. This occurred within an hour. Pentanol was removed by blowing out with nitrogen while heating continued. The product was transferred into 10 mL of water and the pH adjusted to 5 using dilute HCl. The product was then filtered and the unreacted phthalonitrile was removed by Soxhlet extraction with methanol.

ZnPc: IR (KBr) v/cm^{-1}: 1612, 1513, 1467, 1328, 1093, 725.

UV-Visible (DMF): λ_{max}/nm (log ε) : 672 (5.2), 344 (3.7).

^{1}H NMR DMSO-d_6; δ (ppm): 9.44 (d, 4H), 8.26 (d, 4H), 7.70 (m, 8H)

2.6.3 Manganese tetrapentoxy pyrrole phthalocyanine (MnTPePyrPc, 7c)

Manganese tetrapentoxy pyrrole phthalocyanine (MnTPePyrPc, **7c**) was synthesized by adopting a procedure reported before for the synthesis of tetra propoxy pyrrole substituted metal phthalocyanines as follows, (Scheme 3.5)[227].

N-pyrrole substituted pentan-1-ol, 12. Compound **12** was synthesized according to the procedure reported for the synthesis of the ethanol analogue[227] . 5-Aminopentanol (50 g, 0.817 mol) was added to 100 mL of glacial acetic acid with continuous stirring. The mixture was cooled in an ice bath containing sodium chloride (NaCl), keeping the temperature below 20 ^{o}C

since the reaction is exothermic. One portion of 25 g (0.19 mol) of 2,5-dimethoxytetrahydrofuran **11** was then added to the solution while stirring and left to stand for 10 minutes. The acetic acid was distilled off under reduced pressure and the residue was treated with 200 mL of water. The product was extracted five times from water with dichloromethane (DCM). The extracted organic solution was treated, three times, with a saturated aqueous solution of sodium sulphate followed by distilling off DCM. The residue was stirred overnight with a mixture of 30 mL methanol and 30 mL 20% aqueous solution of NaCl. Then the mixture was saturated with NaCl while stirring and left to stand for 30 minutes. The mixture was then transferred into a separating funnel and the organic product was extracted with DCM. Since there were traces of water in the DCM extract, the product was dried with calcium chloride. Finally, DCM was distilled off under reduced pressure. Yield: 30%.

IR (KBr) v/cm^{-1}: 3097, 2939, 1655, 1503, 1430, 1280, 1087, 1070, 982, 866, 730.

^{1}H NMR DMSO-d_6: δ (ppm): 3.2 (d, 1H, pyrrole), 4.0 - 3.6 (m, 10H, pentyl), 6.30 (t, 2H, pyrolle), 6.91 (t, 2H, pyrrole).

5-(Pyrrol-1-yl)pentoxy phthalonitrile, 13. Compound **13** was synthesized by following literature reports for similar complexes[227]: 5-(pyrrol-1-yl) pentan-1-ol **12** (0.3 g, 1.9 mmol) and 0.27 g (1.56 mmol) of 4-nitrophthalonitrile (synthesized according to reported method[228]) were added to 0.6 g dry K_2CO_3 in 15 mL dry DMSO. The mixture was stirred under nitrogen for 48 hours at room temperature. The product was poured into 100 mL of 0.1 M HCl solution to afford a yellowish-brown precipitate. The precipitated product was washed

with cold water (four times) and finally with methanol (two times). The resulting solid was dried in the oven at 50 ^{o}C.

IR (KBr) v/cm^{-1}: 3442, 3106, 3063, 2229 (C≡N), 1598, 1516, 1486, 1244 (C-O-C), 1205, 1076, 840, 727.

^{1}H NMR DMSO-d_6: δ (ppm): 6.29 (s, 2H), 7.30 (d, 2H), 7.38 (d, 2H), 7.44 (m, 1H), 7.50 (d, 2H), 7.85 (d, 1H), 8.10 (d, 1H).

Manganese tetrapentoxy pyrrole phthalocyanine (MnTPePyrPc, 7c). The first step was the synthesis of unmetallated tetrapentoxy pyrrole phthalocyanine (H_2TPePyrPc, **14**) which was achieved by dissolving 1.2 g (4.30 mmol) of 5-(pyrrol-1-yl)-pentoxyphthalonitrile, **13** in 15 mL dry pentanol and stirring under reflux for 15 minutes. Following this, 10 mg lithium was added to the mixture while stirring and the solution turned green immediately. UV-Visible spectra of the product were used to monitor the formation of the Pc. After one hour, the product was allowed to cool to room temperature and methanol was added to the solution to precipitate out the product. The product was Soxhlet extracted with methanol for 24 hours, to remove unreacted phthalonitrile. After this treatment, the product was found to be predominantly metal free Pc. No further purification was done. Complex **14** was used for synthesis of the manganese derivative **7c**, by reaction of 0.4 g (0.36 mmol) of **14** with 0.027 g (0.023 mmol) of manganese chloride in dry pentanol under reflux for 1 hour. The solution was transferred into distilled methanol to precipitate out the solid. Finally, the product was purified by column chromatography using dichloromethane as eluting solvent and its purity was confirmed by thin layer chromatography. Characterization of the products gave satisfactory results.

H_2TPePyrPc, 14: Yield: 60%. IR (KBr) v/cm^{-1}: 3280, 3097, 2930, 2865, 1615, 1487, 1235 (C-O-C), 1090, 940, 826, 721.

UV-Visible (DMF): λ_{max}/nm, (log ε): 330 (4.48), 635 (4.01), 670 (4.65), 700 (4.65).

^{1}H NMR DMSO-d_6: δ (ppm): 6.19 (d, 8H, pyrolle), 7.32 (d, 8H, pyrrole), 8.41 (s, 4H, Pc), 9.00 (s, 8H, Pc).

MnTPePyrPc, 7c: Yield: 92%. IR (KBr) v/cm^{-1}: 2930, 2856, 2370, 1638, 1509, 1341, 1244 (C-O-C), 1137, 1082, 823, 710, 630, 285 (Mn-Cl).

UV-Visible (DMF): λ_{max}/nm, (log ε): 641 (4.4).

Elemental analysis: $C_{68}H_{68}MnN_{12}O_4$ (1171 $gmol^{-1}$). Analytically calculated: C, 69.63%; H, 5.83%; N, 14.29%. Found: C, 68.7%; H, 5.64%; N, 13.56%.

Chapter 3

Electrocatalysis

Metallophthalocyanines are applied principally in electrocatalysis of oxidation of thiols and thiocyanates as well as reduction of oxygen in this thesis. This section lays out the results obtained from these studies.

This work has been published in the following journals as;

1. Nthapo Sehlotho, Sophie Griveau, Nadine Ruillé, Mohammed Boutjita, Tebello Nyokong and Fethi Bedioui.
   Electrocatalyzed oxidation of reduced glutathione and 2-mercaptoethanol by cobalt phthalocyanine-containing screen printed graphite electrodes.
   Mater. Sci. Eng., (2006) Article in press.
2. Nthapo Sehlotho, Sophie Griveau, Tebello Nyokong and Fethi Bedioui.
   Cobalt phthalocyanine molecular electrode for the electrochemical investigation of the release of glutathione upon copper-catalyzed decomposition of S-nitrosoglutathione.
   Electroanalysis, (2006) Article in press.
3. Nthapo Sehlotho and Tebello Nyokong.
   Effects of ring substituents on electrocatalytic activity of manganese phthalocyanines towards the reduction of oxygen.
   J. Electroanal. Chem., 595 (2006)161-167.
4. Nthapo Sehlotho and Tebello Nyokong.
   Electrocatalytic oxidation of thiocyanate, *L*-cysteine and 2-mercaptoethanol by self-assembled monolayer of cobalt tetraethoxy thiophene phthalocyanine.
   Electrochim. Acta, 55 (2006) 4463-4470.
5. Nthapo Sehlotho, Tebello Nyokong, José H. Zagal and Fethi Bedioui.
   Electrocatalysis of oxidation of 2-mercaptoethanol, *L*-cysteine and reduced glutathione by adsorbed and electrodeposited cobalt tetra phenoxypyrrole and tetra ethoxythiophene substituted phthalocyanines.
   Electrochim. Acta, 51 (2006) 5125-5130.

For publications 1, 2 and 5, experiments were conducted in Laboratoire de Pharmacologie Chimique et génétique, Ecole Nationale Supérieure de Chimie de Paris, FRANCE, Aug – Dec 2004 and Feb – May 2006 as a collaboration between governments of France and South Africa.

3.1 Thiol oxidation

3.1.1 Adsorbed CoPc complexes, 6b and 6c

Phthalocyanines metallated with cobalt compared to other transition metals such as Fe and Mn have been reported to exhibit excellent catalytic activity towards thiol oxidation; this is attributed to good orbital overlap between cobalt's d-orbitals and sp-orbitals of the thiols. On this basis, cobalt phthalocyanine complexes **6b** and **6c**, Fig. 3.1 are employed as electro catalysts towards thiol oxidation in this work. These complexes are ring-substituted with phenoxy pyrrole and ethoxy thiophene ligands respectively, allowing the study of substituent effect on the catalytic oxidation of thiols. Moreover, pyrrole ligand forms stable polymers hence it was connected by a phenoxy spacer to enhance polymerization while the thiophene ligand forms stable self-assembled monolayers via the sulphur moiety. Different methods of electrode modification, namely adsorption, electropolymerization and self-assembly will therefore be employed and compared in terms of efficiency towards thiol oxidation.

Electrochemical properties and thiol catalytic activity of CoPc **6a** has been studied extensively[157]: Adsorption of **6b** and **6c** was confirmed by recording cyclic voltammograms of modified glassy carbon (GC) electrodes in 0.5 M NaOH solutions (pH ~ 13). Thiol oxidation was to be conducted in such alkaline media based on the fact that it has been reported to occur at much less negative potentials at pHs greater than dissociation constants of thiols[158], hence electrode characterization was done in alkaline media. For thiols that

were studied in this work namely, 2-mercaptoethanol (2-ME), *L*-cysteine (CYS) and *reduced*-glutathione (GSH), their pK_as lie between 8 and 10[82,158].

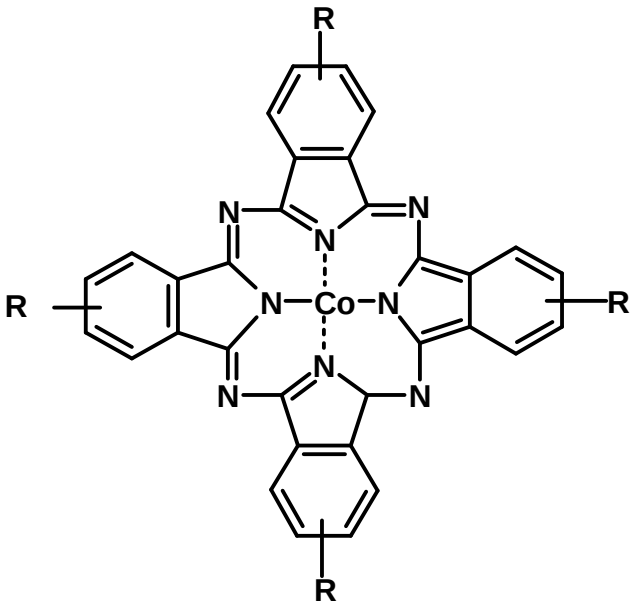

R = H (6a, CoPc)

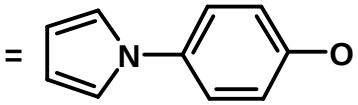

(6b, CoTPhPyrPc)

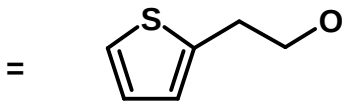

(6c, CoTEThPc)

Figure 3.1: Molecular structures of phthalocyanine complexes used in electrocatalytic oxidation of thiols and thiocyanate; CoPc, CoTPhPyrPc (cobalt tetraphenoxy pyrrole phthalocyanine) and CoTEThPc (cobalt tetraethoxythiophene phthalocyanine).

Fig. 3.2 shows the cyclic voltammograms of adsorbed CoTPhPyrPc **6b** and CoTEThPc **6c** complexes on ordinary pyrolytic graphite (OPG) electrode. In both cases a pair of quasi-reversible peaks which can be related to $Co^{II/I}$ redox process was observed at ~ -0.66 V and -0.68 V/(SCE) for **6b** and **6c**,

respectively. Surface coverage was determined by integration of charge under the peaks and was found to be 9.85 and 1.23 x 10^{-10} mol/cm^2 for **6b** and **6c** respectively. The surface coverage values of ~ 1 x 10^{-10} mol/cm^2 indicate that adsorbed films are lying flat and are composed of one layer of MPc[108,123], though there is a higher concentration of **6b** (9.85 x 10^{-10}) than of **6c** (1.23 x 10^{-10}) on the electrode surface.

A different electrode OPG was employed for characterization other than glassy carbon electrodes on which thiol oxidation was to be conducted because OPG offers excellent MPc adsorption by virtue of being more porous compared to GC electrodes. It is rich in π-electron density permitting strong chemisorptive interactions hence forms more intact films. However OPG electrodes show 'memory effects' thus desorption of MPc complexes or any other material by polishing and sonication is tedious and difficult leading to the electrode surface wearing off in the process, rendering OPG electrodes less user-friendly and expensive in terms of re-use. OPG electrodes were therefore used only for characterization purposes whereas GC electrodes were used for routine analyses, as the latter are easy to clean, modify and re-use.

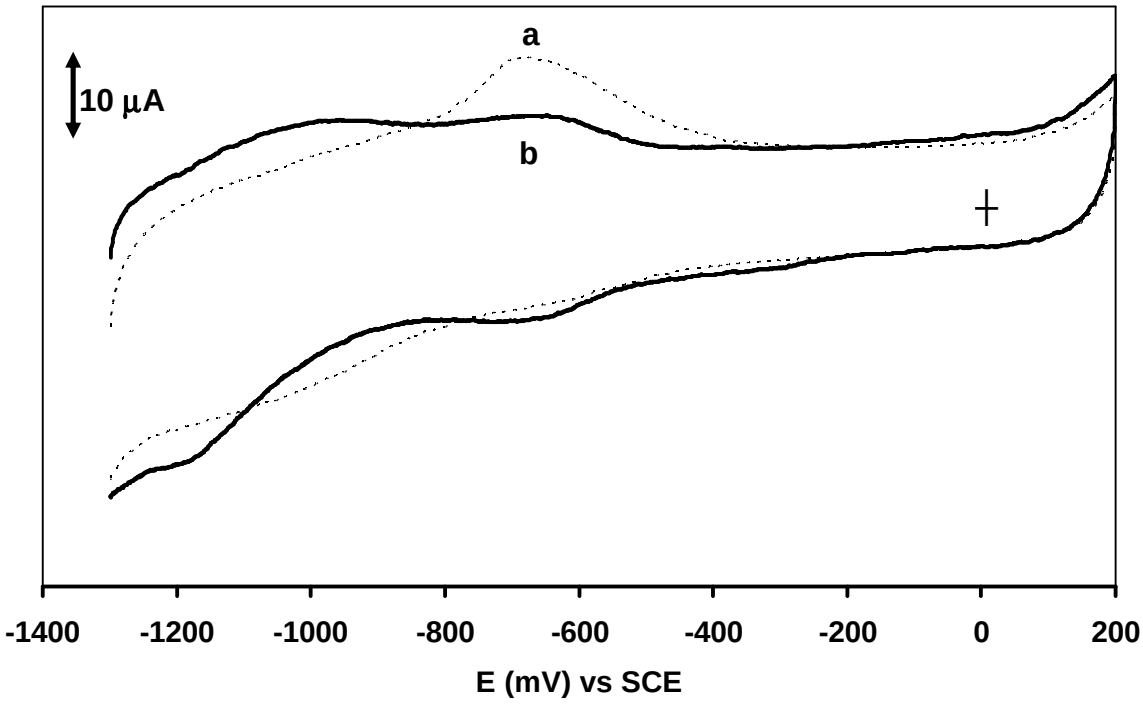

Figure 3.2: Cyclic voltammograms of OPG electrodes modified by adsorption of a) CoTPhPyrPc 6b and b) CoTEThPc 6c in 0.5 M NaOH solution showing Co(II/I) redox couples.

Fig. 3.3 shows cyclic voltammograms in the presence of 1 mM thiol solutions, namely 2-ME, CYS and GSH in 0.5 M NaOH on glassy carbon electrodes modified by 30 minute-adsorption of CoTEThPc **6c** (Fig. 3.3 A) and CoTPhPyrPc **6b** complexes (Fig. 3.3 B). In all cases, a large oxidation current was observed starting from -0.4 V for 2-ME, -0.3 V for CYS and -0.25 V/(SCE) for GSH, which is related to the electrocatalytic oxidation of the thiols at the modified electrodes. It should be noted that no thiol oxidation was observed at the bare glassy carbon electrode within the examined potential range of -1.30 to 0.20 V/(SCE).

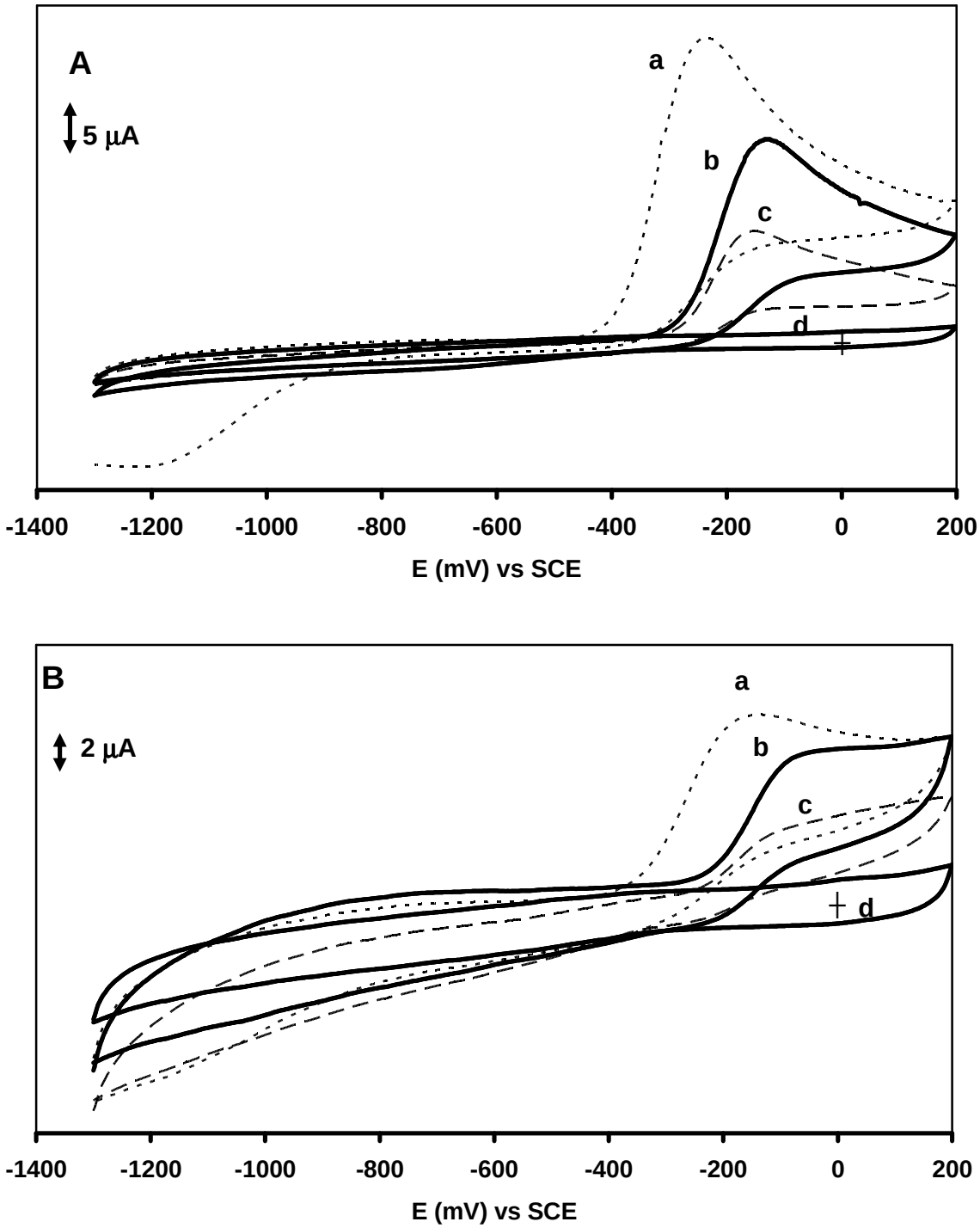

Figure 3.3: Cyclic voltammograms of oxidation of a) 2-ME, b) CYS and c) GSH in 0.5 M NaOH electrolyte solution catalyzed by adsorbed A: CoTEThPc 6c and B: CoTPhPyrPc 6b complexes on GCE. Curves d) show modified electrode in the absence of thiols in 0.5 M NaOH. Scan rate = 100 mV/s.

In the particular case of CoTEThPc-adsorbed electrode and 2-ME, the appearance of the oxidation peak at -0.3 V/(SCE) is concomitant with that of a

reduction peak at -1.18 V/(SCE), during the reverse scan. According to the previously reported studies on the electrocatalytic oxidation of 2-ME by adsorbed and electropolymerized metallophthalocyanines, the large cathodic peak can be attributed to the reduction of the corresponding disulphide[229,230]. This result clearly shows that adsorbed CoTEThPc complex **6c** not only acts as a real catalyst towards the oxidation of 2-ME but also acts as a catalyst towards the reduction of the corresponding disulphide. Similarly, the reduction of the disulphide was observed as a broad peak at ~-1.1 V/(SCE) on CoTPhPyrPc-adsorbed electrode.

Previously reported studies provided clear evidence that the oxidation of 2-ME is a monoelectronic process in basic media, which leads to the formation of 2-hydroxyethyldisulphide[159]. The assignment of the reduction peak to disulphide was clearly reported by studying the electroreduction of 2-hydroxyethyl disulphide (with no 2-ME in solution) at various electrodes modified by adsorption of cobalt phthalocyanine complexes[170]. This occurred at ~-1 V/(SCE) on such electrodes thus even in this work, it is concluded that 2-ME gets oxidized to 2-hydroxyethyldisulphide.

Quantitative analysis can be achieved from the linear variation of measured catalytic current intensity of a particular analyte as a function of its concentration. This is shown in Fig. 3.4 for 2-ME oxidation in 0.5 M NaOH.

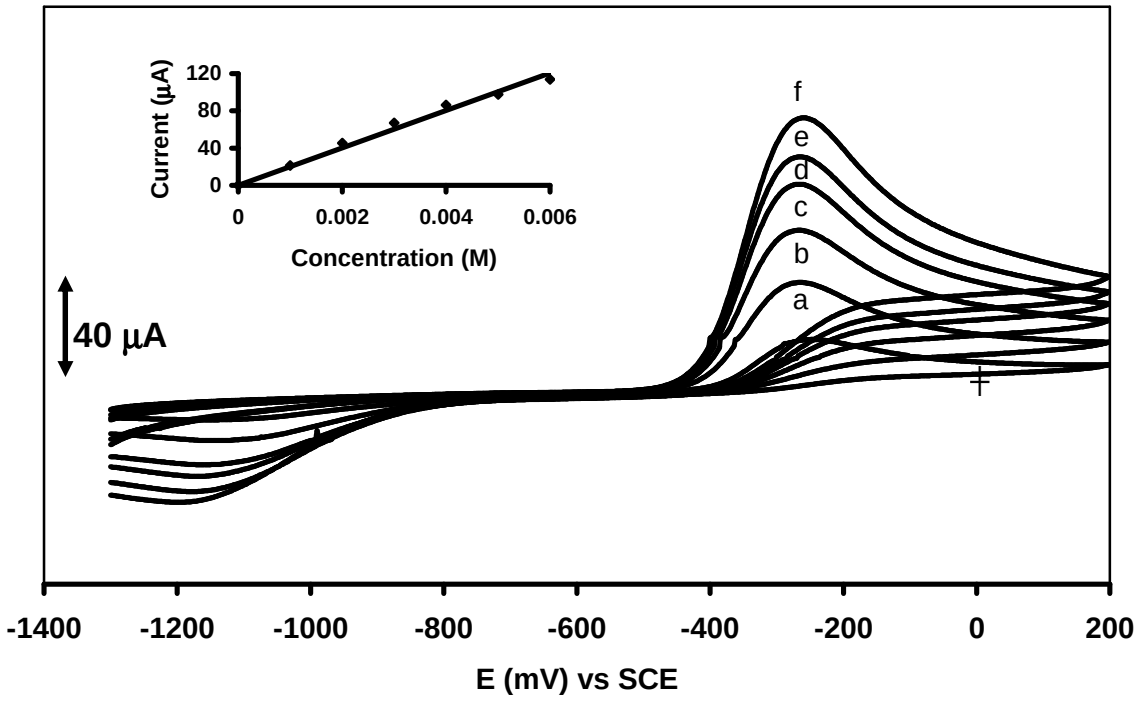

Figure 3.4: Cyclic voltammograms of catalytic oxidation of 2-ME by adsorbed CoTEThPc 6c at varying concentrations; a = 1, b = 2, c = 3, d = 4, e = 5 and f = 6 mM. Insert is a variation of current and concentration.

The electrocatalytic activity of CoTEThPc **6c** and CoTPhPyrPc **6b** adsorbed complexes towards thiol oxidation was further examined in terms of a negative shift of the peak potential and an increase of the current intensity, shown in Table 3.1. The measured oxidation peak potentials are -0.22 V, -0.11 V and -0.14 V/(SCE), for 2-ME, CYS and GSH at CoTEThPc-adsorbed electrode, respectively. In the case of CoTPhPyrPc-adsorbed electrode, the measured oxidation peak potentials are -0.12 V, -0.04 V and -0.08 V/(SCE) for 2-ME, CYS and GSH respectively. The trend in terms of peak current intensity is shown in Table 3.1.

Table 3.1: Catalytic efficiency of adsorbed CoTEThPc 6c and CoTPhPyrPc 6b in terms of oxidation peak potential E_p and current I_p in 0.5 M NaOH. Current and potential values obtained from CVs of 2.5 mM analyte solutions, Scan rate = 100 mV/s.

Thiol	Catalyst CoTEThPc **6c**		Catalyst CoTPhPyrPc **6b**	
	E_p (mV)	I_p (µA)	E_p (mV)	I_p (µA)
2-ME	-220	31	-120	7
CYS	-110	21	-40	5
GSH	-140	12	-80	3

It is clear that 2-ME is the easily oxidized thiol among the three. It is also noticeable that electrodes modified with adsorbed CoTEThPc **6c** complex had better catalytic efficiency than those modified with CoTPhPyrPc **6b**, in terms of both current and potential oxidation peak. This can be explained by the difference of structures of these two complexes. Indeed, one can imagine that the CoTEThPc **6c** complex, lies flat on the electrode, making the metal centre easily accessible to the thiol, while CoTPhPyrPc **6b** does not adopt a regular orientation because of 'twisting' of the phenoxy substituents bearing the pyrrole groups. It is for the same reason that reproducibility of catalytic activity in terms of peak potential was unachievable for CoTPhPyrPc modified electrode as the orientation of the complex within the mono-layered film is extremely sensitive to modification conditions such as electrode polishing and monomer solution.

It is important to mention that electrocatalytic activity exhibited by complexes **6b** and **6c** far exceeds what has been reported for CYS oxidation in alkaline media. Tetrasulphonated cobalt phthalocyanine, CoTSPc adsorbed onto GCE oxidized CYS at 0.20 V/(SCE)[155] compared to -0.11 V/(SCE) by complex **6c**. For complexes **6b** and **6c** oxidation of 2-ME occurred at slightly

less negative values of -0.12 and -0.22 V/(SCE) respectively compared to -0.29 and -0.32 V/(SCE) on adsorbed and polymerized cobalt tetraamino phthalocyanine (CoTAPc) respectively[155], both in alkaline media. Moreover, GSH oxidation in alkaline solutions occurred at -0.08 and -0.14 V/(SCE) catalyzed by complexes **6b** and **6c** respectively, and these were slightly less negative than observed on polymerized CoTAPc which exhibited GSH oxidation peak at -0.20 V/(SCE)[229]. This nonetheless shows that complexes **6b** and **6c** employed as electrocatalysts in this work exhibit comparable activity on average towards thiol oxidation as other complexes that have been studied before.

Electrocatalytic reactions were also performed in phosphate buffer solution at pH 7.2 so as to get information about how well our modified electrodes could behave in physiological conditions since this is one area of application. In the case of the more easily oxidized thiol, namely 2-ME, it was observed that catalytic activity is greatly decreased at pH 7.2, as shown in Fig. 3.5 both in terms of potential and current. 2-ME oxidation peak was observed at -0.22 V/(SCE) in pH 13 with current intensity of 31 μA while it occurred at 0. 13 V/(SCE) in pH 7.2 with a current intensity of 6 μA. This is not surprising since the active species that interacts with the adsorbed catalyst is RS^- anion which predominates at pH values higher than the thiol pK_a (which is in the range 9 -10[82,158]).

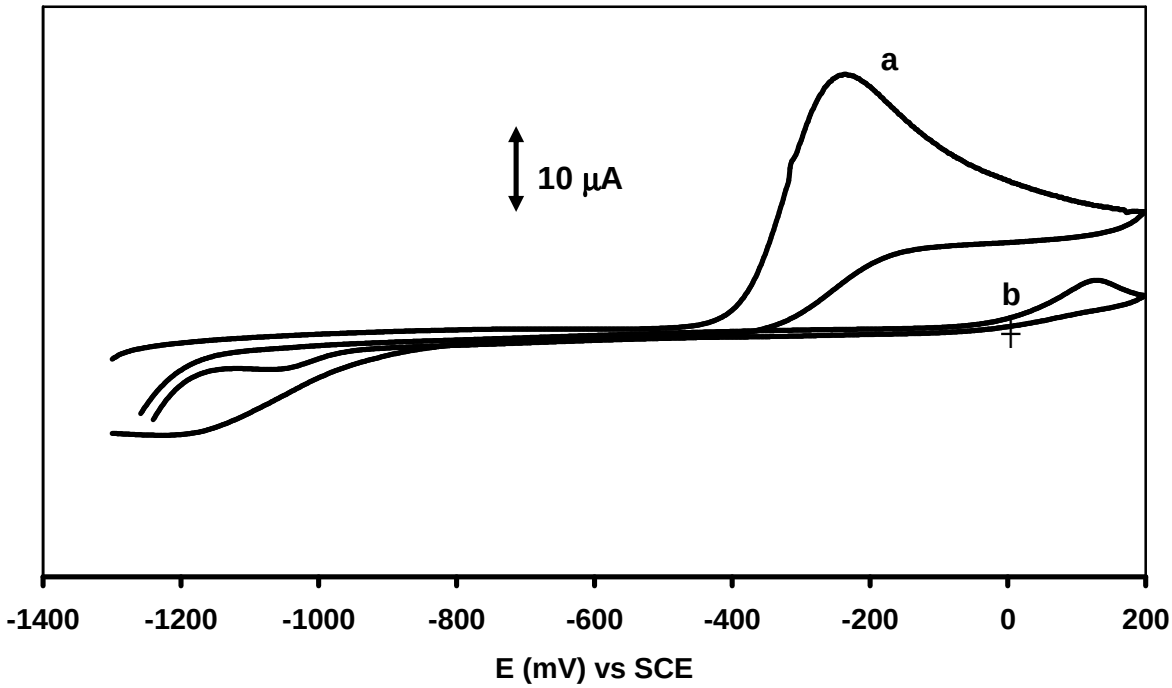

Figure 3.5: Cyclic voltammograms of oxidation of 2.5 mM 2-ME in a) 0.5 M NaOH (pH~13) and b) PBS (pH = 7.2) solution catalyzed by adsorbed CoTEThPc 6c complex. Scan rate = 100 mV/s.

Rotating disk electrodes (RDE) experiments were performed to better understand processes occurring in solution. Typical quasi-stationary current-potential curves obtained at different rotation rates are shown in Fig. 3.6. It appears that a typical diffusion plateau is observed for the catalytic oxidation current. The Levich equation, eq. 3.1 (same as eq. 1.8) was employed,

$$I_L = 0.62nFAD^{2/3}\omega^{1/2}v^{-1/6}C \qquad 3.1$$

where symbols are as described before. Linear correlations (inserts Fig. 3.6) indicating diffusion-controlled mass transport were obtained from plots of I_L vs $\omega^{½}$ and I_L vs C where I_L, ω and C represent measured limiting current intensity, electrode rotation rate and thiol concentration, respectively. The limiting current values were taken at -0.15 V for both plots. However, deviations were

observed at high thiol concentrations and electrode rotation speeds because of electrode passivation and fouling.

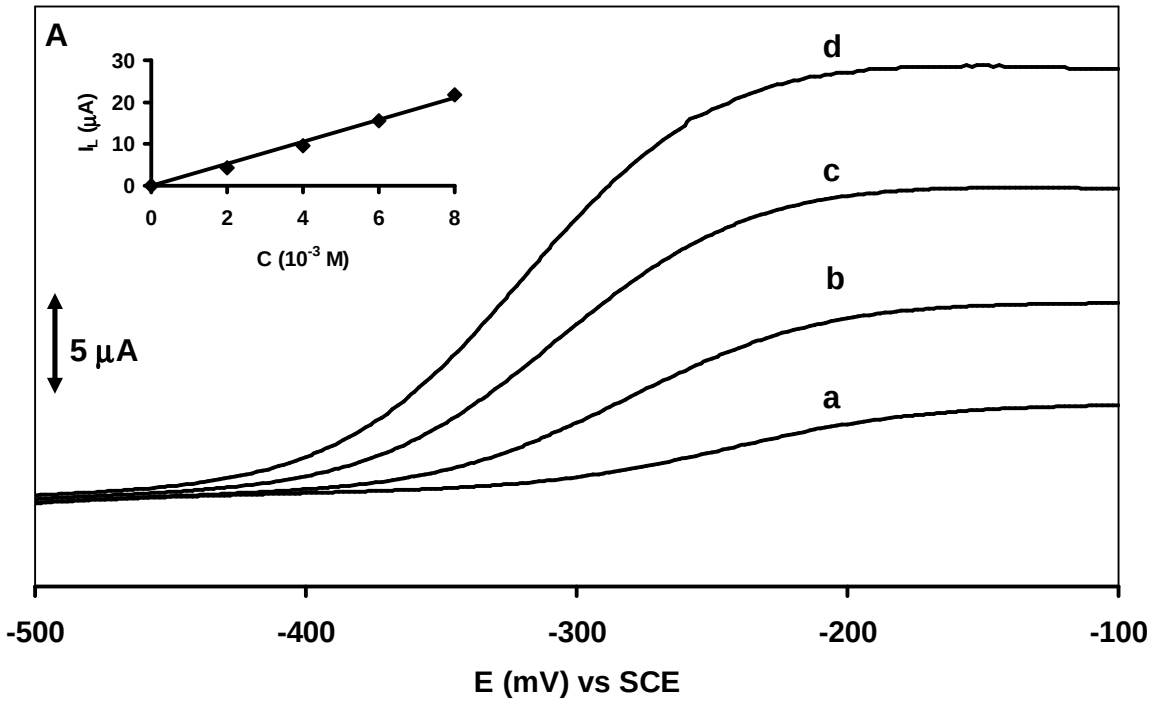

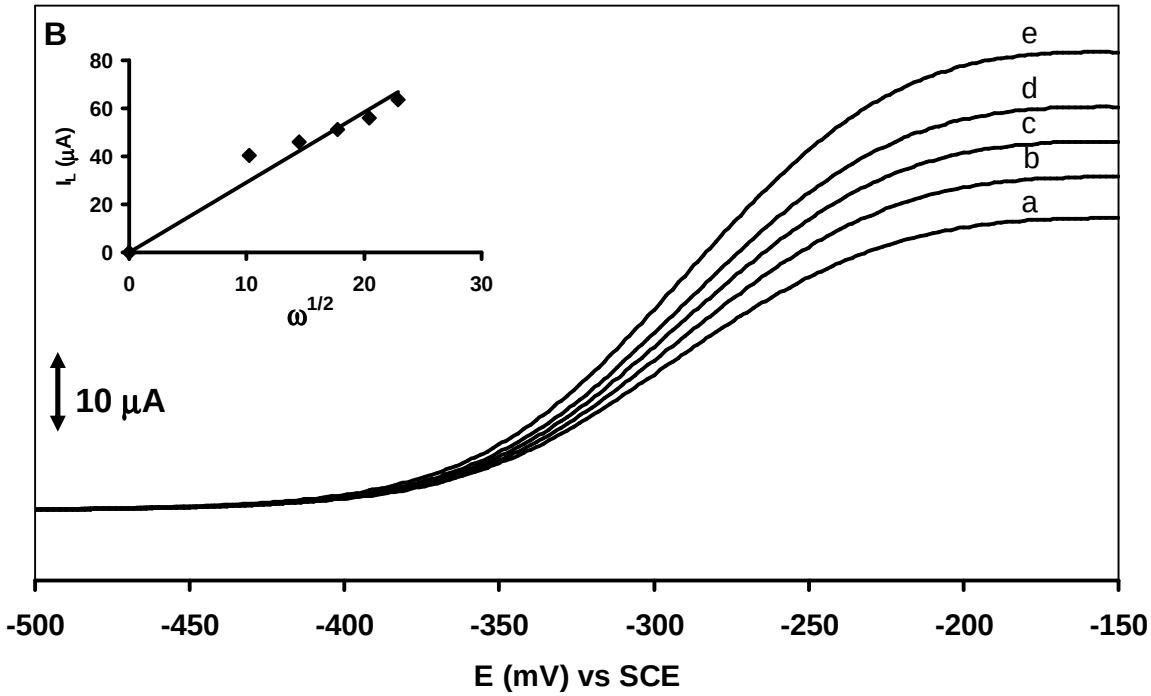

Figure 3.6: RDEs of catalytic oxidation in 0.5 M NaOH solution catalyzed by adsorbed CoTEThPc 6c at A: different concentrations of 2-ME, a = 2, b = 4, c = 6 and d = 8 mM at 5000 rpm and B: different rotation speeds of a = 1000, b = 2000, c = 3000, d = 4000 and e = 5000 rpm; 2-ME concentration = 2.5 mM. Scan rate = 10 mV/s. Inserts = Koutecky-Levich plots.

The order of the reaction is known to be equal to one for the oxidation of 2-ME[82] and *L*-cysteine[158] and this was confirmed from slope of one for the plot of log I versus log C at constant potential for 2-ME (Fig. 3.7a), based on eq. 3.2. Parallel straight lines were obtained from plots of $1/\omega^{½}$ versus 1/I, (Fig. 3.7b) further confirming the reaction order of 1. These plots were based on Koutecky-Levich equation, eq. 3.2 (same as eq. 1.13),

$$\frac{1}{I} = \frac{1}{nFCAk_c} + \frac{1}{0.62nFAD^{2/3}\omega^{1/2}v^{-1/6}C} \qquad 3.2$$

where symbols are as described before. The current for the plots in Fig. 3.7B was obtained from indicated potentials at the rising part of the curves in Fig. 3.6 for each electrode rotation rate.

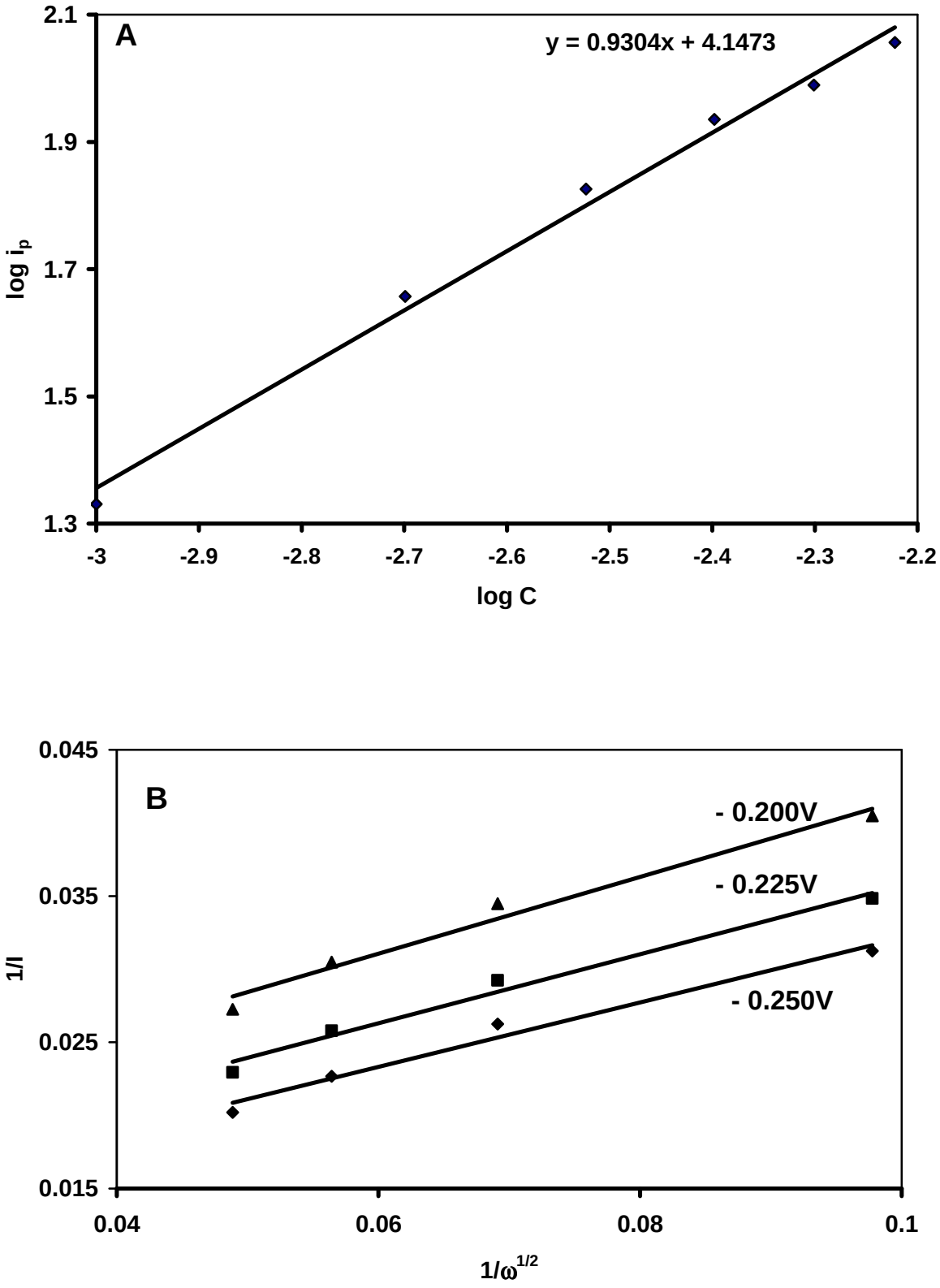

Figure 3.7: Plots of, A. log I vs log C and B. $1/\omega^{1/2}$ vs 1/I; RDE data of 2-ME catalytic oxidation on GCE modified by adsorption of CoTEThPc 6c at 1000 rpm rotation speed at indicated potential values -0.200, -0.225 and -0.250 V/(SCE) indicating reaction order of one for 2-ME oxidation.

Tafel plots (Fig. 3.8) were constructed from RDE data based on Tafel equation, eq. 3.3 (same as eq. 1.12),

$$\eta = a + b \log I \qquad 3.3$$

where symbols are as described before. Tafel plots are plots of log |I| (current) versus η(reaction overpotential) where the Tafel slope b is expressed by eq. 3.4 as,

$$b = \frac{2.3RT}{\alpha n_{\alpha} F} \qquad 3.4$$

where α is a transfer coefficient and n_{α} is number of electrons involved in a charge transfer step. Linear Tafel plots are obtained by using kinetic currents (i_K) instead, which are currents when the system is under complete kinetics, i.e. analyte transport is governed by rotation of the electrode and not diffusion. Kinetic currents are calculated and corrected for mass transport according to equation 3.5,

$$I_K = \frac{(I * I_L)}{(I_L - I)} \qquad 3.5$$

where I_L and I are the limiting current and the current at the foot of the wave, respectively, making eq. 3.3 plot of η vs. log i_K. Slopes obtained from these plots are shown in Table 3.2.

Table 3.2: Electrochemical data for thiol oxidation in 0.5 M NaOH catalyzed by complexes 6b and 6c.

Thiol	E_p mV/(SCE) **6b**	**6c**	Tafel slope (mV/decade)	α, transfer coefficient	Reaction order
2-ME	-120	-220	60.3	0.98	0.93
CYS	-40	-110	79.2	0.75	0.95
GSH	-80	-140	66.4	0.89	1.10

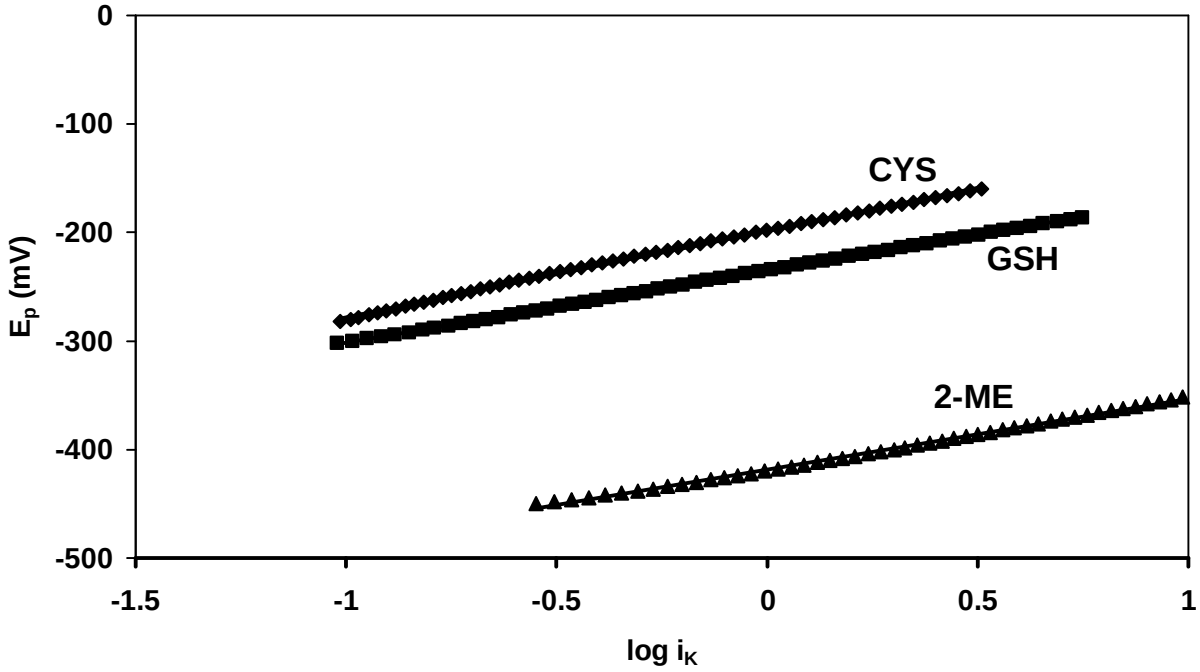

Figure 3.8: Tafel plots of thiol oxidation catalyzed by adsorbed CoTEThPc 6c; slopes are in the range of 65 to 79 mV/decade.

Slopes from Tafel plots reported in previous work[157,231] have been close to 120 mV indicating that the transfer of one electron is rate determining (for α valued at 0.5). Thus, Tafel slopes in the range 65 - 79 mV/decade shown in Table 3.2 could indicate that, i) α has high values or ii) that the rate determining step is a chemical step preceded by a fast one electron transfer (in this latter case, the slope would be 59 mV/decade). According to Table 3.2, α indeed has high values accounting for the observed range of Tafel slopes. In previous work for CoPc catalyzed thiol oxidation[229], where a similar range of Tafel slopes was observed, it was found that the slow step involved the transfer of one electron. Similarly, in this work the same mechanism is adopted and proposed in Scheme 3.1 as,

$$R\text{-}SH + OH^- \rightarrow RS^- + H_2O \quad (3.6)$$

$$RS^- + PcCo(II) \rightarrow [PcCo(I) - (SR)]^- \quad (3.7)$$

$$[PcCo(I) - (SR)]^- \xrightarrow{r.d.s} [PcCo(II) - (SR)] + e^- \quad (3.8)$$

$$[PcCo(II) - (SR)] \rightarrow [PcCo(II)] + RS^\bullet \quad (3.9)$$

$$RS^\bullet + RS^\bullet \xrightarrow{fast} RS\text{-}SR \quad (3.10)$$

where CoPc is CoTPhPyrPc **6b** and CoTEThPc **6c**, RSH is a thiol, RSSR is a disulphide and r.d.s is rate-determining step.

Scheme 3.1: Thiol oxidation mechanism in alkaline media.

The mechanism proposed for thiol oxidation is based on the following: The reactions were conducted in alkaline solutions of pH greater than pK_as of the thiols hence eq. 3.6, that describes dissociation of thiols. Involvement of Co(II/I) redox couple, eq. 3.7 is based on the fact that thiol oxidation peaks occur at the proximity of this couple. Furthermore, reductive coordination of the thiol to Co(II)Pc has been proven spectroscopically by Maree et al.[89]. Eq. 3.8 is proposed because one electron is transferred during the rate-determining step and the reaction order is one. Lastly, the RS radical will cleave from the adduct in eq. 3.9 regenerating the initial state of the CoPc complex; the RS radicals will then dimerize into the corresponding disulphide as shown by eq. 3.10.

3.1.2 Electrodeposited CoPc complexes 6b and 6c

Electropolymerization of CoTPhPyrPc **6b** and electrodeposition of CoTEThPc **6c** complexes on glassy carbon electrodes was achieved as

specified in the experimental section. Surface coverage of electrode by deposited MPc was controlled by varying the number of potential scans. Fig. 3.9 shows electropolymerization of **6b** as judged by a new polymer peak at *ca*. 0.48 V/(SCE), a pyrrole oxidation peak at *ca.* 1.1 V/(SCE) and an increase in currents of $Co^{II/I}$ and $Co^{III/II}$ redox couples located at *ca.* -0.25 and 0.70 V/(SCE), respectively. Electrodeposition of **6c** was evidenced by increase in currents of $Co^{III/II}$ redox couples located at *ca.* 0.76 V/(SCE), respectively and pyrrole oxidation peak at ca. 1.5 V/(SCE) with no new peaks observed (not shown). Polymerization is judged by formation of new peaks and an increase of monomer peak current intensities. No new peaks were observed for **6c**, only increase of monomer peak currents, implying electrodeposition and not electropolymerization.

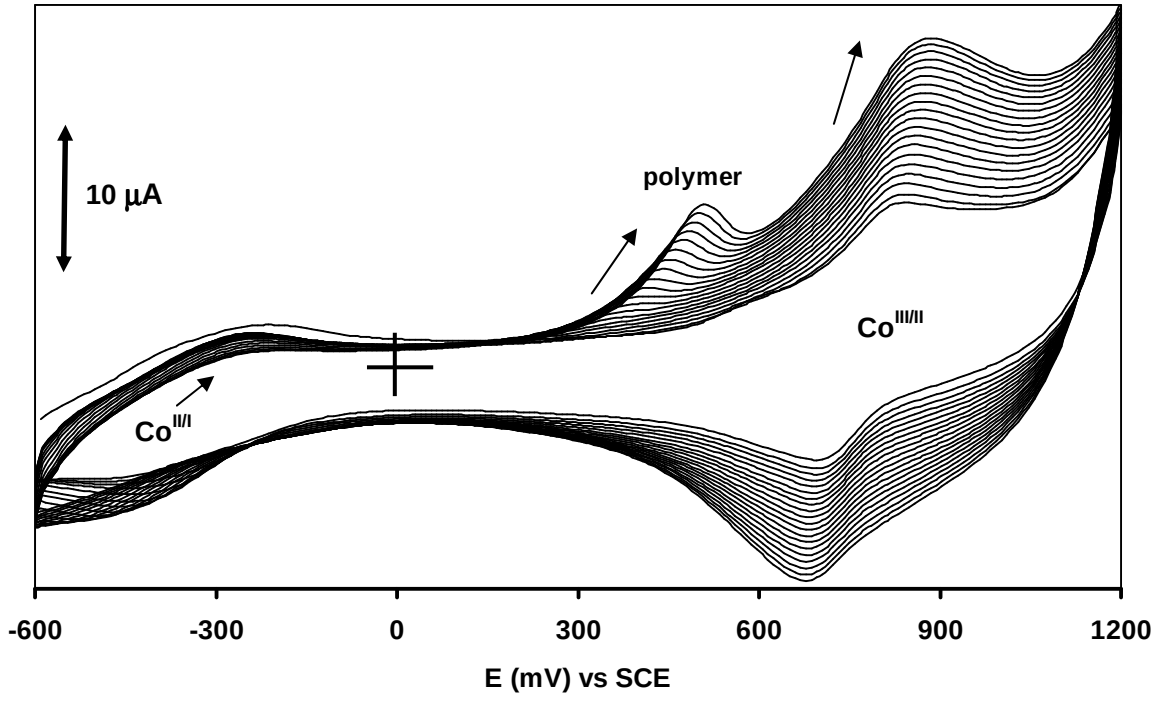

Figure 3.9: Electropolymerization of CoTPhPyrPc 6b on a glassy carbon electrode in DMF and 0.1 M $TBABF_4$ at 200 mV/s.

Pyrrole ligand forms stable polymers; in the case of CoTPhPyrPc **6b** where there is an electron-donating spacer between the pyrrole and the phthalocyanine chromophore, polymerization occurs even more readily because of increase in reactivity of radical cations as well as spatial flexibility. This enhanced polymerization has been reported for propoxy pyrrole substituted phthalocyanines, wherein better results were obtained for longer electron rich spacers[227]. CoTEThPc complex was electrodeposited, it did not electropolymerize. Electropolymerization of thiophene complexes is known to be possible using thiophenes with no substituents on the ortho positions of the pyrrole. Introduction of the ethoxy substituent at the ortho position may have produced a blocking of the polymerization process. It is also possible that the radicals formed during electrooxidation of the thiophene groups are too unstable to participate in further coupling so that no polymers are formed.

Catalytic oxidation of 2-ME, CYS and GSH, characterized by cyclic voltammetry, was observed with electropolymerized CoTPhPyrPc **6b** and electrodeposited CoTEThPc **6c** but the activity was not as high as that of the adsorbed complexes above. CVs of 2-ME on adsorbed and electrodeposited CoTEThPc **6c** (10 scans) are shown in Fig. 3.10. Peak potentials are observed at -0.22 and -0.21 V/(SCE) for adsorption and electrodeposition with current intensities of 53 and 42 μA for 2.5 mM 2-ME solution respectively. Note the difference in I_P values in Table 3.1, it is a different batch of experiments. Activity is better on electrodes modified by adsorption than electrodeposition because adsorbed films are held loosely and are less compact than their electrodeposited counterparts offering easy access for the thiol to interact effectively with the metal centre of the catalyst.

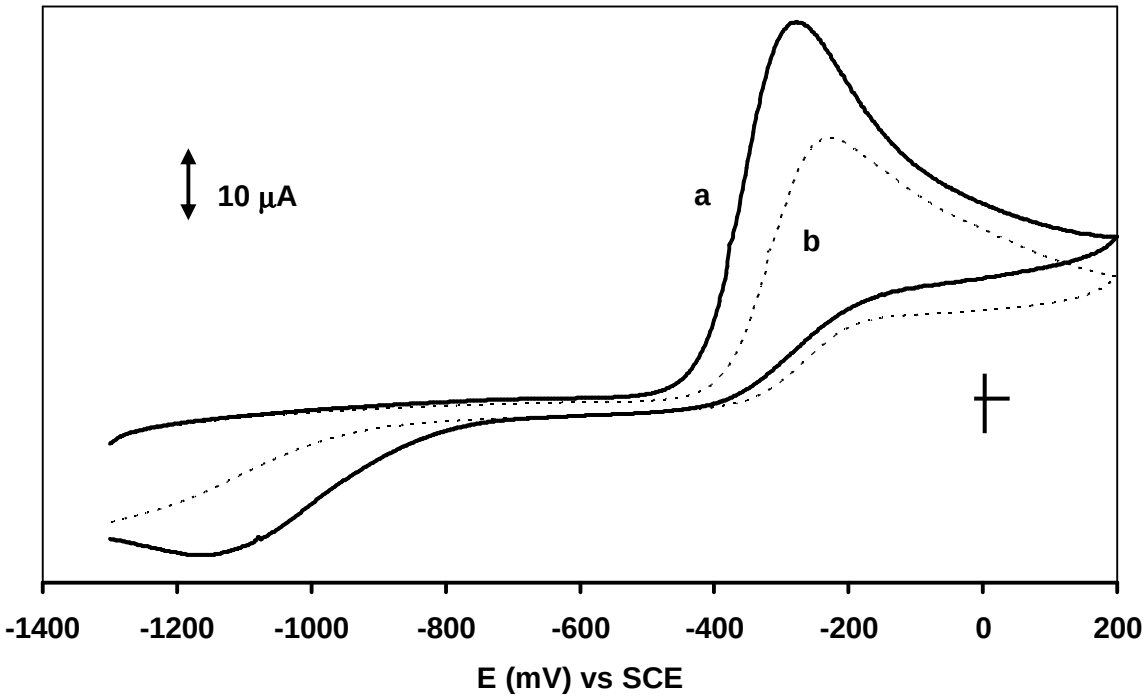

Figure 3.10: Cyclic voltammograms of 2.5 mM 2-ME oxidation on a) adsorbed and b) electrodeposited CoTEThPc complex 6c in 0.5 M NaOH. Scan rate = 100 mV/s.

Table 3.3 shows that activity was found to be dependent on MPc concentration on the electrode, assuming that it is directly proportional to number of scans. For both complexes, higher activity was observed with scan number 10, than 20 and 30. This shows that the active site is the outermost film layer not the bulk of the film on the electrode. This is in agreement with previous reports[9,113] indicating that catalytic activity does not increase with amount of modifier on the electrode. Moreover, Table 3.3 shows better catalysis in terms of current intensity with electrodeposited CoTEThPc than electropolymerized CoTPhPyrPc. This further shows that complex **6c** is a better thiol electrocatalyst than complex **6b**.

Table 3.3: Catalytic current intensities of electrodeposited CoTEThPc 6c and electropolymerized CoTPhPyrPc 6b (obtained by 10, 20 and 30 scans) on glassy carbon electrode for the electrooxidation of 2-ME.

Procedure of electrode modification	Catalyst **6c** Current[a](μA)	Catalyst **6b** Current[a](μA)
Adsorption	53	29
10 scans	42	10
20 scans	38	4
30 scans	37	3

[a]Current values obtained from CVs of 2.5 mM 2-ME in 0.5 M NaOH aqueous solutions. Scan rate = 100 mV/s.

Electrocatalytic activity of electrodeposited CoTEThPc **6c** towards thiol oxidation based on peak current intensity was found to depend on the anodic potential limit, for a given number of electrodeposition scans. Current intensity was found to be optimum when the anodic limit was 1.6 V/(SCE); it decreased by *ca.* 40 % and 50 % at 1.4 V and 1.8 V/(SCE) anodic limits, respectively. RDE experiments for both electropolymerized **6b** and electrodeposited **6c** complexes yielded the same data as their adsorbed counterparts discussed above, in that one electron was transferred during the rate-determining step and the order of the reaction was determined to be one.

Tafel slopes were 62.6, 75.0 and 70.4 mV/decade for 2-ME, CYS and GSH respectively with the corresponding transfer coefficients, α of 1.06, 1.27 and 1.19 respectively. α of 1 shows that products are even more favoured than for adsorbed complexes where it ranged from 0.75 to 0.98. In general, α of 0.5 indicates that the activated complex is exactly halfway between products and reactants on the reaction coordinate; the structure of the

activated complex reflecting reagent and product equally. α valued at 0 or 1 indicates that the activated complex has predominantly the structure of reactant or product species respectively. The same mechanism for thiol oxidation for adsorbed complexes shown in Scheme 3.1 also holds for electrodeposited complexes in alkaline media.

It must be mentioned that both electropolymerized **6b** and electro deposited **6c** were stable to poisoning. The electrodes could be used repeatedly for days without losing sensitivity and electrocatalytic activity. This is very important as stable sensors are desired for analysis. On the other hand, their adsorbed counterparts were deactivated after about 10 scans and had to be re-coated.

3.1.3 Self-assembled monolayers

Gold electrode was modified by a self-assembled monolayer of CoTEThPc **6c**. This complex was suitable because it has a sulphur moiety through which it can bind to Au, forming a very strong Au-S bond. The modified electrode was then used to catalyze thiol and thiocyanate oxidation reactions.

3.1.3.1 Characterization of SAM

Electrochemical methods used for establishing SAM formation include blockage of gold oxide formation[124,125] under-potential deposition (UPD) of metals such as copper[126] and prevention of electron transfer in redox

reactions[127,128] such as $[Fe(H_2O)_6]^{3+}/[Fe(H_2O_6)]^{2+}$. Fig. 3.11 shows blockage of (i) Au oxide formation (Fig. 3.11a), (ii) UPD of Cu (Fig. 3.11b) and (iii) $[Fe(H_2O)_6]^{3+}/ [Fe(H_2O)_6]^{2+}$ redox couple (Fig. 3.11c), indicating that SAM of CoTEThPc has been formed, since much lower currents are observed for these processes on CoTEThPc-SAM than on bare gold. Another process for checking the formation of SAM is the use of sodium sulphate in pH 4 buffer[132]. Under these conditions, gold oxide oxidation redox couple is observed near 0 volts (Fig. 3.11d (i)), and the couple is blocked on CoTEThPc-SAM (Fig. 3.11d (ii)), indicating that the SAM acts as an efficient barrier to the redox process.

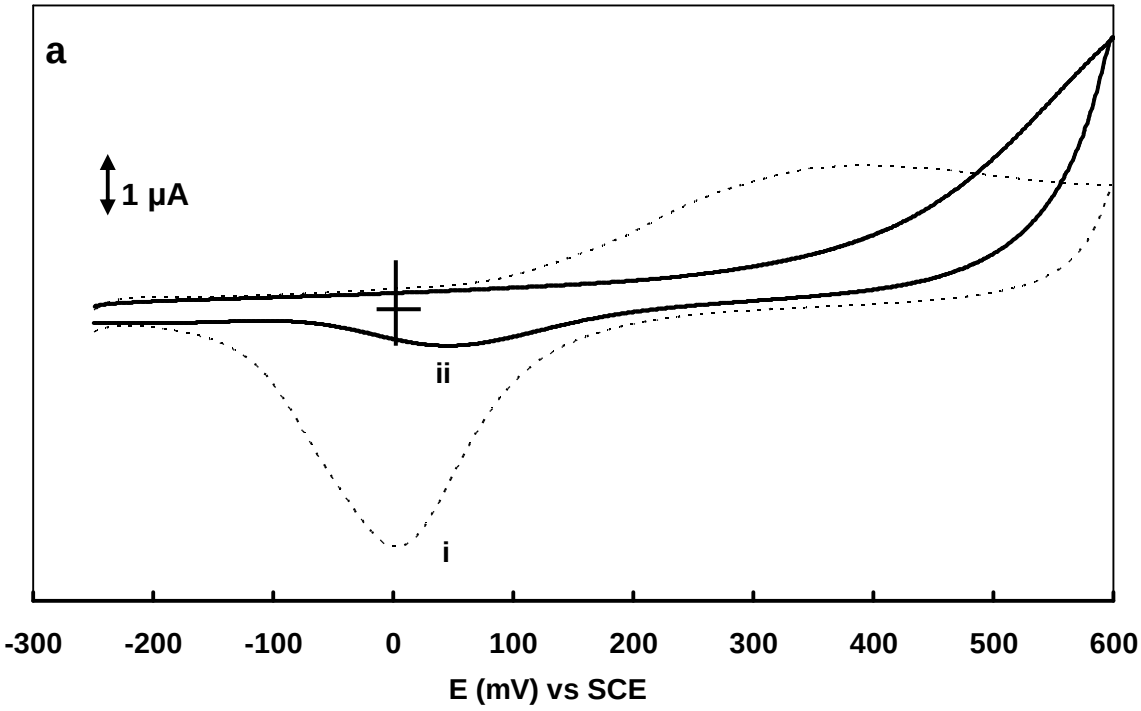
a
1 µA
ii
i
-300
-200
-100
0
100
200
300
400
500
600
E (mV) vs SCE

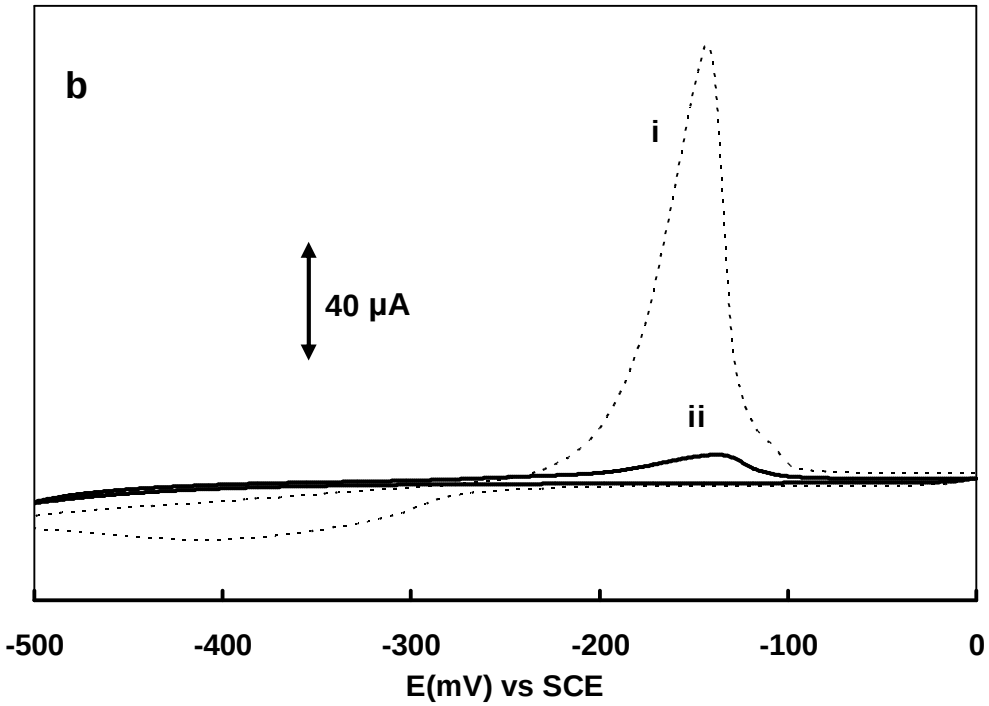
b
i
40 µA
ii
-500
-400
-300
-200
-100
0
E(mV) vs SCE

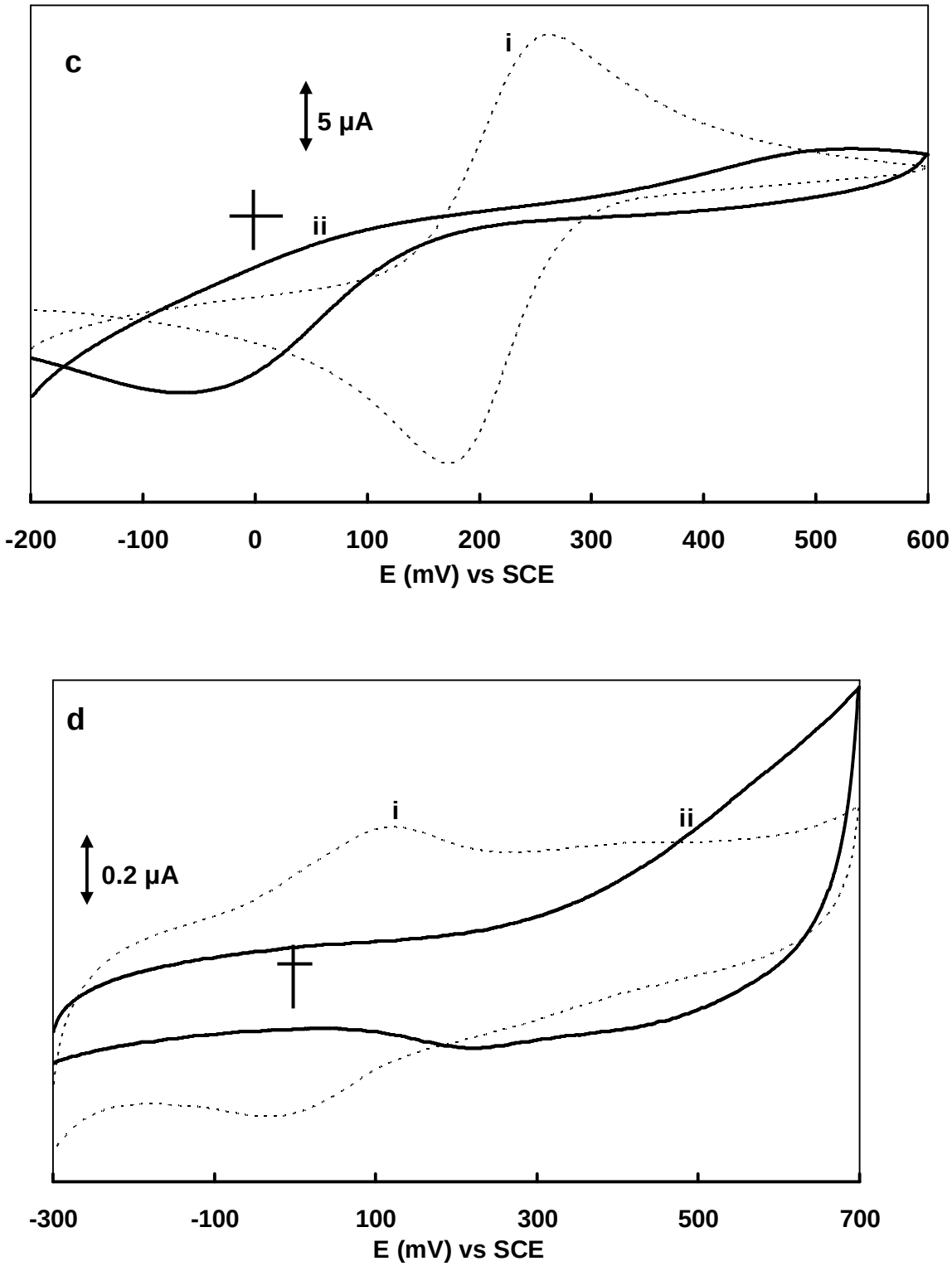

Figure 3.11: Cyclic voltammograms of i) unmodified Au electrode and ii) CoTEThPc-SAM in a) 0.01 M KOH, b)1 mM $CuSO_4$ in 0.5 M H_2SO_4, c) 1 mM $Fe(NH_4)(SO_4)_2$ in 1 mM $HClO_4$ and d) 1 mM Na_2SO_4 in pH 4 solution. Scan rate = 50 mV/s.

Fig. 3.12 shows the CV of CoTEThPc-SAM on gold electrode in pH 4 buffer alone. Broad peaks are observed at 0.37 V and ~0.7 V/(SCE). The peak at 0.37 V/(SCE) has been assigned to the Co^{III}/Co^{II} redox process in CoPc complexes[98]. The Co^{III}/Co^{II} process is known to be irreversible for adsorbed CoPc complexes, often showing no anodic component at all[98]. The weak anodic peak observed at ~0.7 V/(SCE), is in the potential range for ring oxidation ($Co^{III}Pc^{-1}/Co^{III}Pc^{-2}$) in CoTEThPc[221].

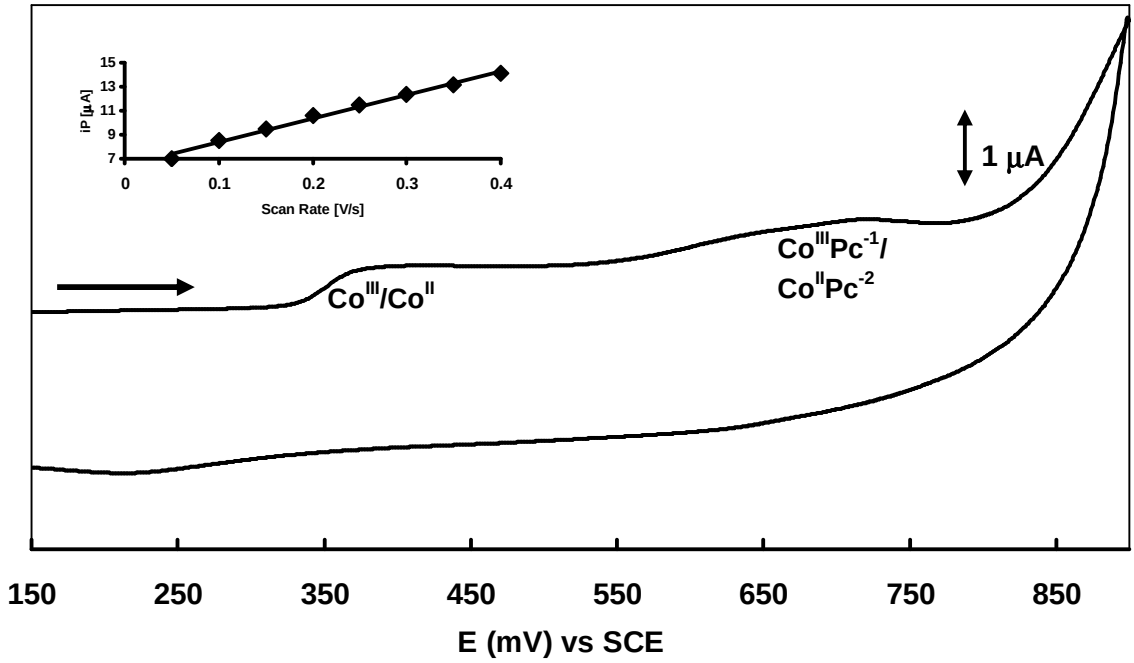

Figure 3.12: Cyclic voltammograms of CoTEThPc-SAM in pH 4 buffer solution showing redox processes related to $Co^{III/II}$ peaks. Scan rate = 50 mV/s. Insert is variation of $Co^{III/II}$ peak current with scan rate.

The currents for the Co^{III}TEThPc/Co^{II}TEThPc peak at 0.37 V/(SCE) increased linearly with scan rate as shown by Fig. 3.12 (insert), hence confirming the presence of surface confined species[158]. For this peak, the potential shifted to less positive values with increasing pH with a slope of 71 mV/pH confirming the involvement of a proton during electron transfer.

Factors used to qualitatively characterize SAMs include ion barrier factor, (Γ_{ibf}) which is calculated using eq. 3.11[129,130], which is the same as eq. 1.26,

$$\Gamma_{ibf} = 1 - \frac{Q_{SAM}}{Q_{BARE}} \qquad 3.11$$

where symbols are as defined before. This factor is a measure of how well SAMs have isolated Au electrode surface from the electrolyte, hence the disappearance of the gold oxide peak is used to establish SAM formation. Fig. 3.11a (CVs of bare Au and CoTEThPc-SAM in 0.01 KOH) and Fig. 3.11b (CVs of bare Au and CoTEThPc-SAM in 1 mM $CuSO_4$) were employed in this work to calculate ion barrier factor. Γ_{ibf} should be equal to unity for complete isolation of Au from the aqueous solution. Using Figs. 3.11a and b, Γ_{ibf} was calculated to be 0.9, which is close enough to unity indicating that the formed CoTEThPc-SAM is a relatively good barrier.

Another factor that is used to characterize SAMs is interfacial capacitance, C_s. It is a measure of ion permeability through SAM, it tells us how densely packed and defect free the SAM is[129,131]. The lower the C_s is, the fewer the defects of the SAM and hence the less permeable are the electrolyte ions to the electrode surface. A decrease in charging current observed with Au-SAMs, is attributed to the presence of a layer of low dielectric constant between the electrode and the electrolyte. C_s was calculated using eq. 3.12[132], same as eq. 1.27,

$$C_s = \frac{i_{ch}}{vA} \qquad 3.12$$

where symbols are as defined before. C_s was calculated to be 104 and 6 $\mu F/cm^2$ for bare Au and CoTEThPc-SAM, respectively, using current values

between -0.1 and -0.2 V/(SCE) (in Fig. 3.11d). The lower value for CoTEThPc-SAM compared to bare gold shows that the SAM is relatively free of defects, and again indicates a low permeability to the ions of the electrolyte.

Surface coverage of redox active film was estimated from a plot of background corrected peak current vs. scan rate according to eq. 3.13[232], introduced as eq. 1.25,

$$I_P = \frac{n^2F^2Av\Gamma_{MPc}}{4RT} \qquad 3.13$$

where symbols have their usual meaning. Γ_{MPc} was found to be 1.3 x 10^{-10} mol cm^{-2}, a value which is in the range for monolayer coverage[233,234].

3.1.3.2 L-cysteine oxidation on CoTEThPc-SAM

Fig. 3.13a shows the CV of *L*-cysteine in pH 4 buffer on CoTEThPc-SAM. No peaks due to *L*-cysteine were observed on bare gold. Two peaks are observed on CoTEThPc-SAM (Fig. 3.13a) at 0.53 V (**II**) and 0.77 V/(SCE) (**I**). The oxidation of *L*-cysteine is known to be mediated by $Co^{III}Pc/Co^{II}Pc$ couple in CoPc complexes[235]. Peak **II** at 0.53 V/(SCE) is due to *L*-cysteine oxidation, mediated by the Co^{III}/Co^{II} couple, since it is close to this couple (Fig. 3.11). This peak (**II**) was not prominent at very low pH (e.g. pH 1 in Fig. 3.13b, only **II** labeled for clarity). At pH 1, one main peak (**I**) was observed at 0.88 V/(SCE) with a shoulder (**II**) near 0.75 V/(SCE) (Fig. 3.13b). As the pH increased e.g. pH 3 in Fig. 3.13b, peak **I** shifted to less positive potentials and decreased in intensity while peak **II** become more pronounced and also shifted to less positive potentials, until only one peak remained at pH 7 (not shown). Peak **I** is in the range of ring based (Pc^{-1}) oxidation for the

CoTEThPc species, hence is catalyzed by a ring based process ($Co^{III}TEThPc^{-1}$), while **II** is catalyzed by the Co^{III}/Co^{II} couple.

Comparing the different electrodes, CoTEThPc **6c** adsorbed on GCE and its SAM on Au, Table 3.4 shows a more positive potential for 2-ME and GSH oxidation on SAMs. This is due to different electrolytes; basic media was used on GCE while an acidic one was used on SAM since SAMs desorb from electrodes in basic media. As mentioned above, thiol oxidation occurs at less positive potentials in alkaline conditions because of easy dissociation into constituent thiolate anions. However, CoTEThPc-SAM still did not fare well with CYS oxidation peak at 0.53 V/(SCE) in pH 4 in comparison with SAMs of CoOBTPc and CoOHETPc whose CYS oxidation peaks were at 0.38 and 0.46 V/(SCE), respectively (Table 3.4).

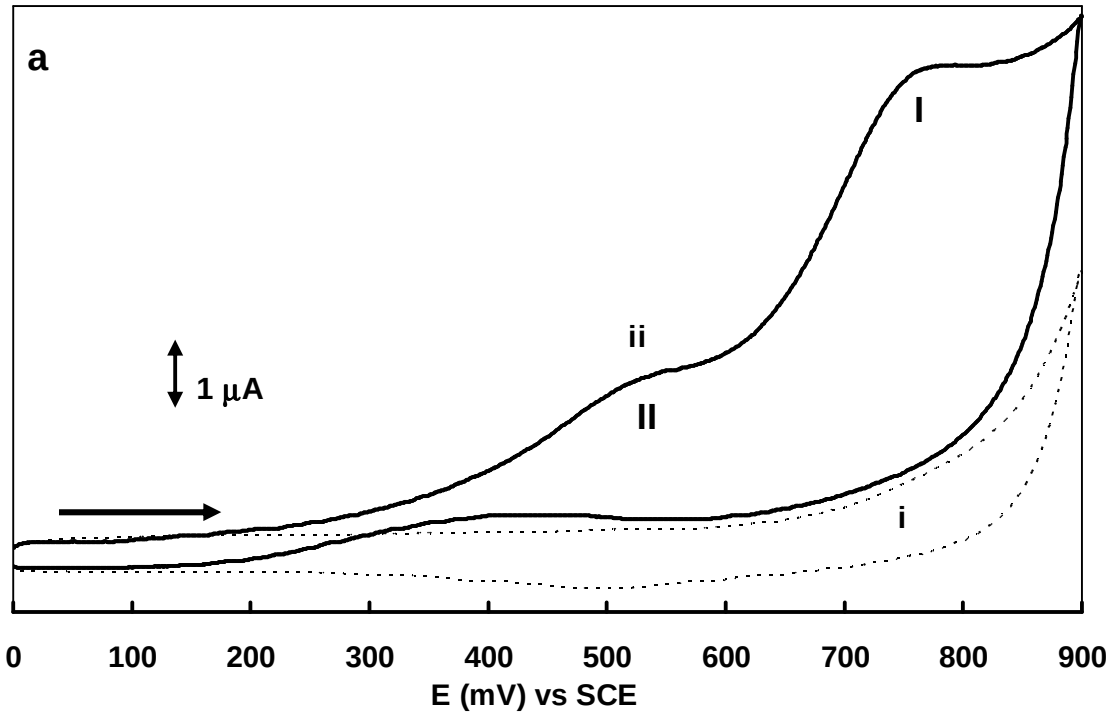

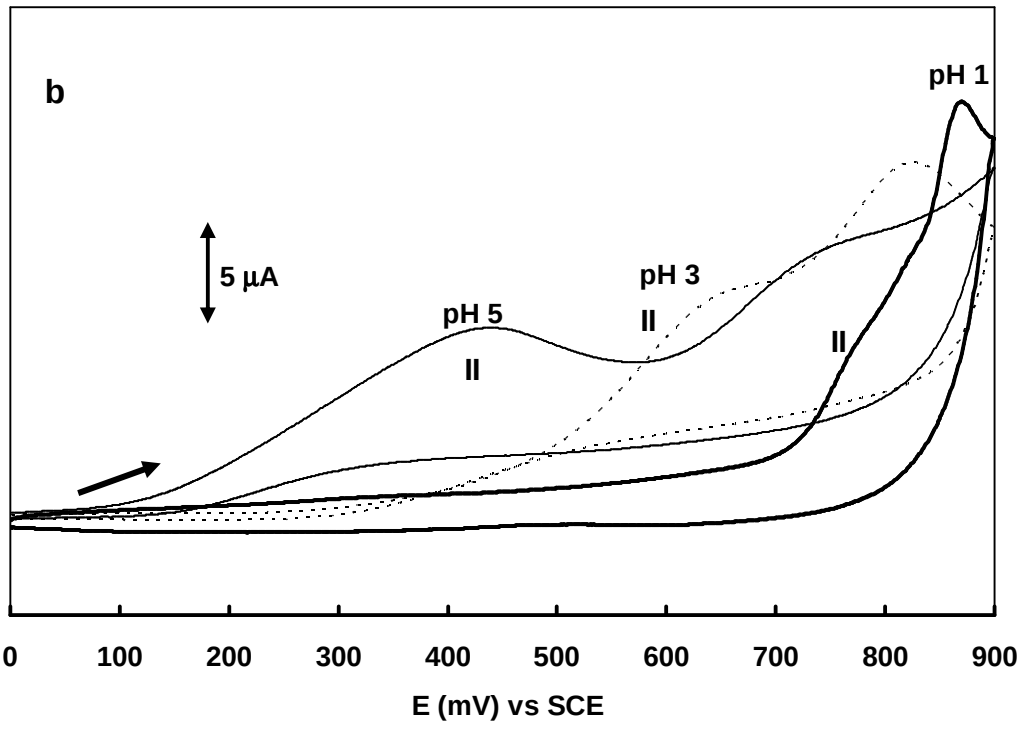

Figure 3.13: Cyclic voltammograms of *L*-cysteine on i) bare Au and ii) CoTEThPc-SAM in a) pH 4 and b) pH 1, 3 and 5 solutions. Scan rate = 50 mV/s.

Table 3.4: Electrochemical data of thiol and thiocyanate oxidation on electrodes modified by CoPc complexes.

Catalyst	Electrode	Method of modification	Media	Analyte	E_P V/(SCE)
6a	OPG	Adsorption	pH 7.4	GSH	0.050
	SPC	Composite paste	pH 7.4	GSH	0.47
				2-ME	0.18
			pH 13	GSH	0.05
				2-ME	-0.34
6b	GC	Adsorption & Polymerization (10 scans)	pH 13	2-ME	-0.12
				CYS	-0.04
				GSH	-0.08
6c	GC	Adsorption & Polymerization (10 scans)	pH 13	2-ME	-0.22
				CYS	-0.11
				GSH	-0.14
	Au	SAM	pH 4	SCN^-	0.64
				CYS	0.53, 0.77
				2-ME	0.78
CoOBTPc[a]	Au	SAM	pH 4	CYS	0.38
CoOHETPc[a]	Au	SAM	pH 4	CYS	0.46

[a]Data excerpted from reference[155].

Abbreviations: OBT; octabutylthio ($SC_4H_9)_8$, OHET; octahydroxyethylthio ($SC_2H_4OH)_8$, GC; glassy carbon, OPG; ordinary pyrolytic graphite, SPC; screen printed carbon, SAM; self-assembled monolayer, 2-ME; 2-mercaptoethanol, CYS; *L*-cysteine, GSH; reduced glutathione and SCN^-; thiocyanate.

The potentials of both peaks in Fig. 3.13 become less positive as pH increased as shown by Fig. 3.14 with slopes of 30 mV/pH for **I** and 60 mV/pH for **II**, showing that process **II** involves one electron and one proton, and

process **I** involves two electrons and two protons. Tafel slope was calculated using an equation (eq. 3.14) for a totally irreversible process [236,237],

$$E_P = \frac{b}{2} \log v + \text{constant} \qquad 3.14$$

where ν is the scan rate and b is the Tafel slope. Tafel slope was found to be 230 mV/pH ($\alpha = 0.26$) from the plot E_p versus log ν for both **I** and **II**, confirming the involvement of one electron in the rate determining step[235]. As stated above, Tafel slopes greater than the normal 30 – 120 mV/decade are known[83,238] to be due to the substrate-catalyst interactions, where the substrate binds very strongly to the catalyst during the interaction as the reaction step. Thus the high Tafel slope suggests interaction between CoTEThPc and *L*-cysteine, which is also confirmed by UV-Vis spectroscopy below.

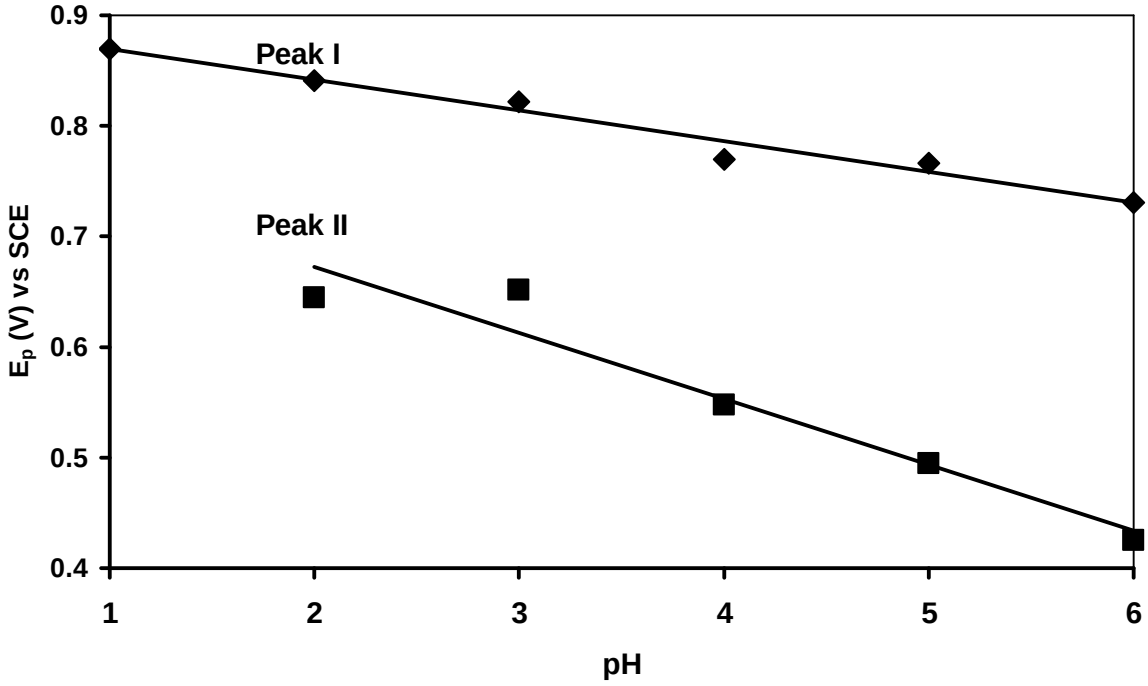

Figure 3.14: Pourbaix diagram (E_p vs pH) for 1 mM *L*-cysteine on CoTEThPc-SAM.

From the well known mechanism for catalytic oxidation of *L*-cysteine on CoPc complexes[89,239] and the fact that the oxidation of *L*-cysteine (process **II**, Fig. 3.13) occurs at the potentials for the Co^{III}/Co^{II} process for CoTEThPc, the following mechanism (Scheme 3.2) is proposed for the oxidation of *L*-cysteine in acidic media on CoTEThPc-SAM catalyzed by the Co^{III}/Co^{II} couple (process **II**);

$$Co^{II}TEThPc^{-2} \xrightarrow{r.d.s} [Co^{III}TEThPc^{-2}]^{+} + e^{-} \qquad 3.15$$

$$[Co^{III}TEThPc^{-2}]^{+} + RSH \rightarrow [RHS\text{-}Co^{III}TEThPc^{-2}]^{+} \qquad 3.16$$

$$[RHS\text{-}Co^{III}TEThPc^{-2}]^{+} \rightarrow Co^{II}TEThPc^{-2} + RS^{\bullet} + H^{+} \qquad 3.17$$

$$RS^{\bullet} + RS^{\bullet} \xrightarrow{fast} RSSR \qquad 3.18$$

where RSH is *L*-cysteine, RSSR is *L*-cystine and r.d.s is rate-determining step.

Scheme 3.2: Mechanism of *L*-cysteine oxidation in acidic media catalyzed by $Co^{III}Pc/Co^{II}Pc$ redox couple.

Equation 3.15 is proposed since catalytic oxidation of *L*-cysteine occurs at potentials in the stability range of the Co^{III}/Co^{II} couple (Fig. 3.11). It is also the rate-determining step since Tafel slopes showed transfer of one electron during this step. The coordination of *L*-cysteine to $Co^{III}TEThPc^{-2}$ (eq. 3.16) was confirmed by UV/Visible spectroscopy as follows: Addition of *L*-cysteine to chemically generated $Co^{III}TEThPc^{-2}$ species (using bromine) resulted in small bathochromic shifts associated with coordination of *L*-cysteine to the $Co^{III}TEThPc$ species, Fig. 3.15; such spectral changes are associated with axial ligation in MPc complexes[25]. No spectral changes were observed on addition of *L*-cysteine to the $Co^{II}TEThPc^{-2}$ species. These

observations suggest that *L*-cysteine coordinates to $Co^{III}TEThPc^{-2}$ as proposed in eq. 3.16 and not to the $Co^{II}TEThPc^{-2}$ species.

The thiol RSH then cleaves from the coordinate adduct regenerating the initial $Co^{II}TEThPc^{-2}$ species as shown in eq. 3.17. The resulting thiol radical cations then dimerize into corresponding disulphide, eq. 3.18. It must be noted that thiol oxidation reaction in acidic media occurs via a different mechanism from alkaline media reactions in that the catalytic redox couples are Co(III/II) in acid and Co(II/I) in alkaline media, hence the differences in Schemes 3.1 and 3.2.

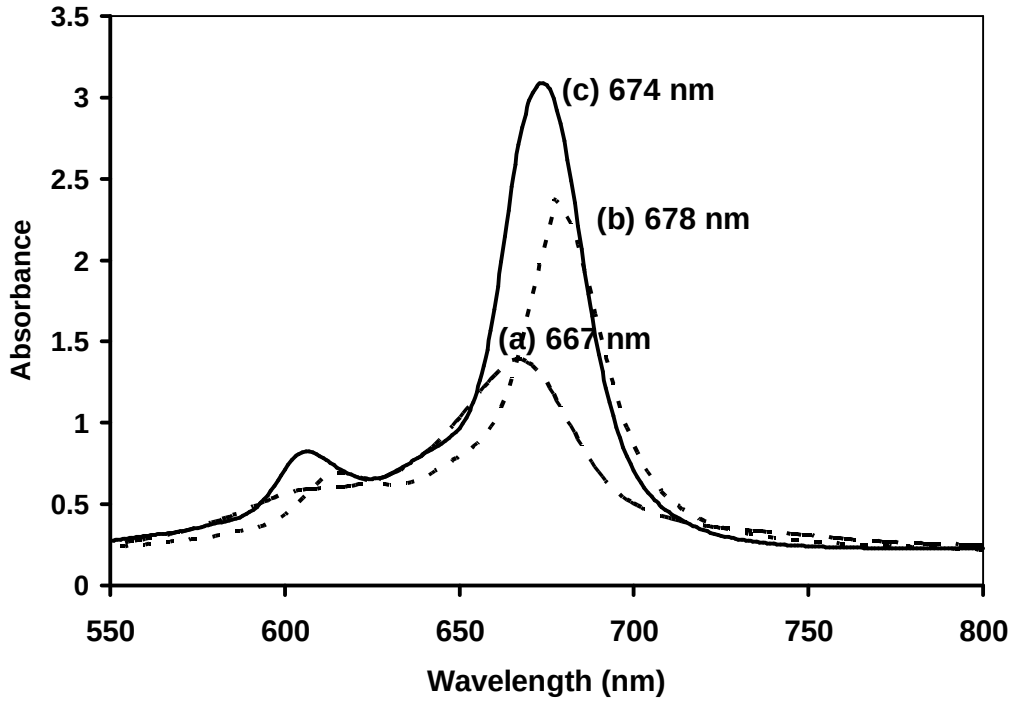

Figure 3.15: UV-Vis spectral changes observed on addition of *l*-cysteine to solutions of CoTEThPc in DMF. Spectrum of a) Co^{II}TEThPc in the absence of *l*-cysteine , b) Co^{III}TEThPc generated by bromine oxidation in the absence of *l*-cysteine and c) Co^{III}TEThPc in the presence of *l*-cysteine. Solvent = DMF.

The oxidation of *L*-cysteine catalyzed by CoPc ring-based processes (process **I**, Fig. 3.12) in acidic media may be represented by the following mechanism (Scheme 3.3).

$$Co^{II}TEThPc^{-2} \xrightarrow{r.d.s} [Co^{III}TEThPc^{-2}]^{+} + e^{-} \quad 3.19$$

$$[Co^{III}TEThPc^{-2}]^{+} \rightarrow [Co^{III}TEThPc^{-1}]^{2+} + e^{-} \quad 3.20$$

$$[Co^{III}TEThPc^{-1}]^{2+} + 2RSH \rightarrow Co^{II}TEThPc^{-2} + RS^{\bullet} + 2H^{+} \quad 3.21$$

$$RS^{\bullet} + RS^{\bullet} \xrightarrow{fast} RSSR \quad 3.22$$

where r.d.s denotes rate-determining step, RSH is the thiol and RSSR is the disulphide.

Scheme 3.3: Mechanism of *L*-cysteine oxidation in acidic media catalyzed by $Co^{III}Pc^{-1}$ /$Co^{III}Pc^{-2}$ redox couple.

Eqs. 3.19 and 3.20 are proposed because *L*-cysteine oxidation occurs in the range of $Co^{III}Pc^{-1}/Co^{III}Pc^{-2}$ couple, Fig. 3.12. Two electrons are transferred during oxidation as evidenced by slopes of 30 mV/pH in Fig. 3.14, for process **I**. Eq. 3.21 shows oxidation of the thiol with regeneration of the initial $Co^{II}TEThPc^{-2}$ catalytic species and formation of thiol radicals which subsequently dimerize into the disulphide according to eq. 3.22. Coordination of RSH to the $Co^{III}TEThPc^{-2}$ is possible as shown by Fig. 3.15.

Lastly, it must be mentioned that both peaks **I** and **II** in Fig. 3.13 for *L*-cysteine oxidation are both diffusion-controlled in the studied pH range of 1 – 7, as evidenced by the linear plot of peak current versus square root of scan rate (Fig. 3.16). Detection limits were determined using 3σ criterion and were valued at 2.5×10^{-8} M. CoTEThPc-SAM was very stable and could be re-used for longer than a month, exhibiting reproducible electrocatalytic activity. It was rinsed and stored in pH 4 buffer solutions in between experiments.

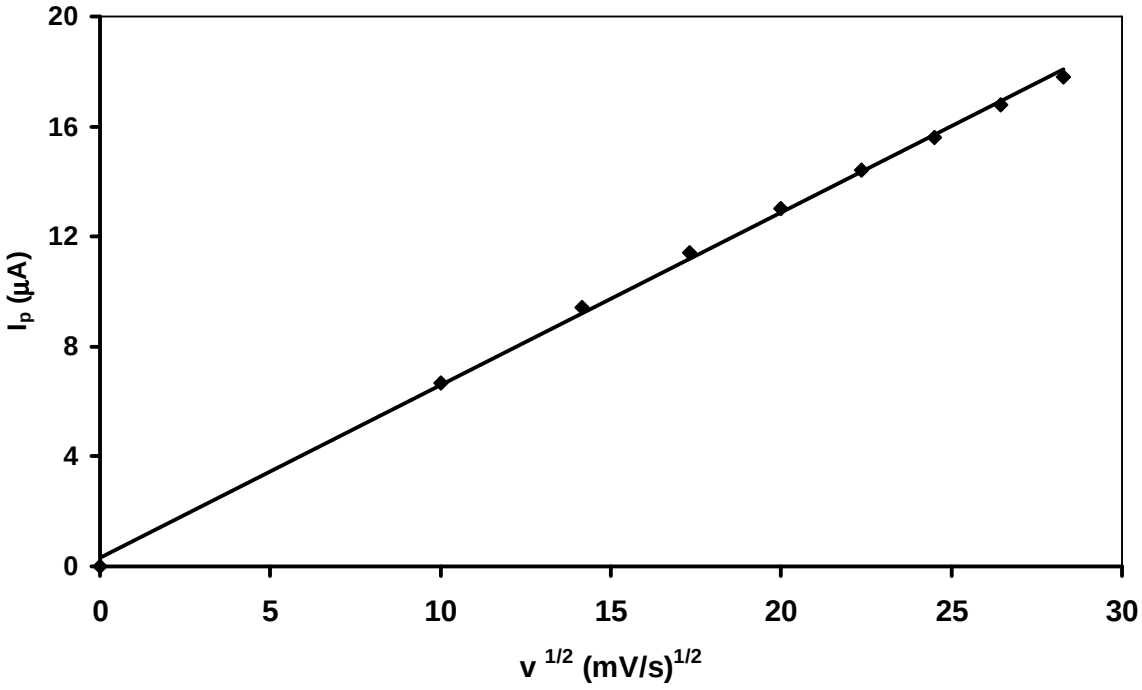

Figure 3.16: Plot of square root of scan rate versus peak current for 1 mM *L*-cysteine oxidation on CoTEThPc-SAM in pH 4.

3.1.3.3 2-Mercaptoethanol oxidation on CoTEThPc-SAM

2-ME oxidation was performed in buffer solutions in the pH range 1 – 7, because SAMs desorb from electrode surfaces in alkaline pH. Under these conditions, the analyte is in its protonated form ($HSCH_2CH_2OH$). Fig. 3.17 shows the CV of 2-ME in pH 4 buffer. The oxidation peak for 2-ME was observed at 0.78 V/(SCE) and the peak for the reduction of the oxidation product (2-hydroxyethyl disulphide) was observed at -0.6 V/(SCE). The high potential compared to oxidation on adsorbed CoTEThPc (-0.22 V/(SCE)) is due to acid conditions which are unfavourable for dissociation of the thiol and easy interaction with the catalyst thereafter.

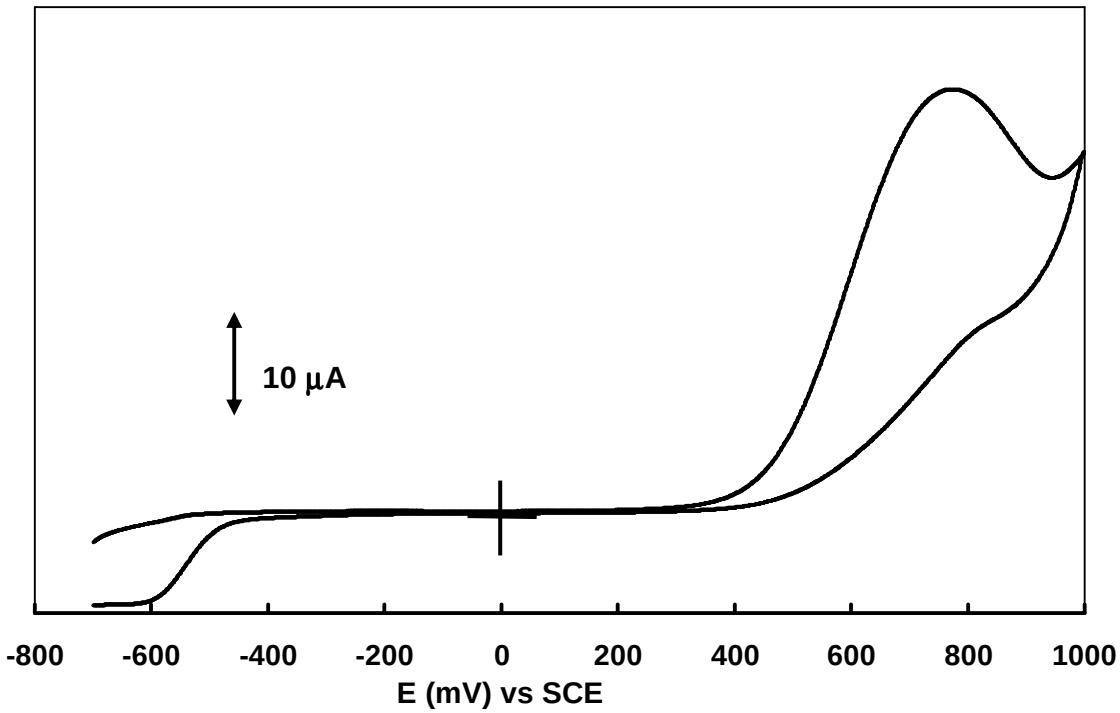

Figure 3.17: Cyclic voltammograms of 2-ME in pH 4 solution on CoTEThPc-SAM.

Fig. 3.18 shows that at pHs between pH 1 and 3, the peak potential was independent of pH, the oxidation occurred via electron transfer that did not involve proton transfer. But from pH 4 onwards, the potential shifts to less negative values with increase in pH, and two electrons were transferred accompanied by two proton transfers as evidenced from slopes valued at 28 mV/pH of E_p vs pH plot (Pourbaix diagram), Fig. 3.18. Furthermore, the mode of transport of 2-ME was found to be diffusion-controlled in the pH range of 1 - 7, confirmed from a linear variation of peak current versus square root of scan rate (similar to Fig. 3.16). Note that in basic media for adsorbed MPcs, one electron oxidation of 2-ME occurred but in this section, in acidic media, two electrons were involved.

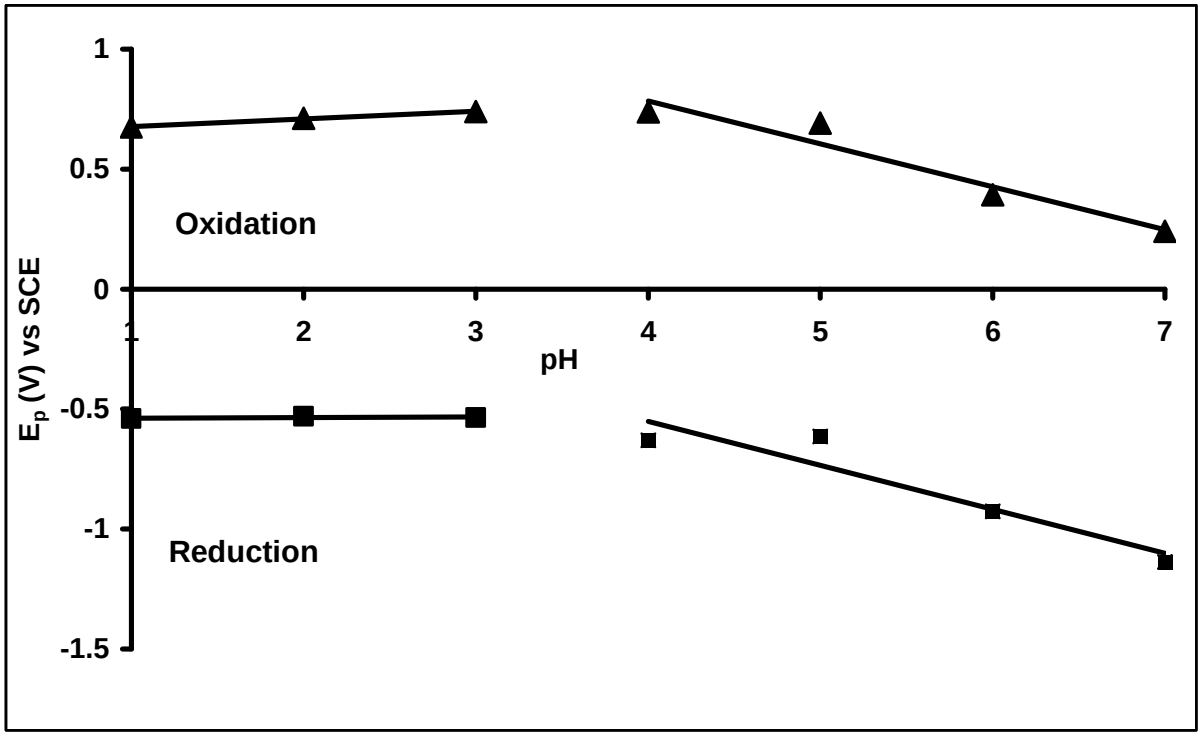

Figure 3.18: Pourbaix diagram for 1 mM 2-mercaptoethanol on CoTEThPc-SAM.

As stated above, the 2-ME catalytic peak is observed at 0.78 V/(SCE), Fig. 3.17 whereas the $Co^{III}Pc/Co^{II}Pc$ and $Co^{III}Pc^{-1}/Co^{III}Pc^{-2}$ redox couples occur at 0.37 and 0.70 V/(SCE) in Fig. 3.12, respectively. Since two electrons are involved in the electrocatalysis of 2-ME oxidation based on the slopes of the Pourbaix diagram, Fig. 3.18, and the initial state of the central metal of the catalyst being +2, it can be concluded that $Co^{III}Pc^{-1}/Co^{III}Pc^{-2}$ process catalyzes the oxidation. Such behaviour has been observed before for catalytic oxidation of thiols on CoPc complexes[98], where the thiol oxidation peak occurs in the potential range of ring-based processes.

A Tafel slope of 0.180 V/decade was obtained from a plot of E_p versus log scan rate, based on eq. 3.14, suggesting transfer of one electron during the rate-determining step. The transfer coefficient (α) was 0.35, suggesting that product formation is unfavoured. Again the high Tafel slope suggests strong substrate-catalyst interactions, as discussed above for *L*-cysteine

electrocatalytic oxidation. 2-ME oxidation in acidic media therefore occurs via the same mechanism proposed for *L*-cysteine oxidation catalyzed by ring-based processes postulated in Scheme 3.3.

Lastly, it must be emphasized that 2-ME oxidation reaction is conducted for the first time in acidic media in this work. GSH oxidation in acidic media on CoTEThPc-SAM is not reported because of poor catalysis. This is unlike **6b** and **6c** adsorbed on GCE where it occurred successfully as described in sections 3.1.1 and 3.1.2. The CoTEThPc-SAM was very stable and yielded reproducible electrocatalytic activity for 2-ME oxidation, similar to *L*-cysteine oxidation discussed above.

3.1.4 Screen printed carbon electrodes

Screen printed carbon electrodes (SPCEs) were prepared by printing graphite powder dissolved in an appropriate solvent onto ceramic tiles, as elaborated in the experimental section. These electrodes are cheap, small, amendable to mass production and disposable. They offer advantages of avoidance of tiresome electrode cleaning and enable easy manouvering because of their size, which makes them legible candidates for use in biological systems. Suitable catalysts can be incorporated into the graphite ink, fine-tuning catalytic behaviour of the SPCEs towards specific analytes. In this work, SPCEs were employed for oxidation of *reduced*-glutathione and 2-mercaptoethanol reactions.

CoPc **6a** was incorporated into the graphite powder during fabrication to afford CoPc-SPCEs which were then used for thiol oxidation electro

catalysis. CoPc was so chosen because phthalocyanine complexes with cobalt as the metal centre have been reported to exhibit exceptional electro catalytic behaviour towards thiol oxidation compared to other transition metals such as Fe and Mn. Moreover, this complex is readily available; it can be purchased at a low price. It should be noted that modification of SPCEs with MPcs requires large quantitites of complexes, for instance 100 mg of CoPc was used to make CoPc-SPCEs employed in this work. It is for this reason that CoTPhPyrPc **6b** and CoTEThPc **6c** complexes were not used as modifiers because their synthesis is difficult and results in minute product yields.

Incorporation of CoPc into the graphite ink mixture of the SPCEs was confirmed by probing reversibility of a well-known reversible $Fe^{III/II}$ redox couple of the ferricyanide system. Indeed, the couple was more resolved and had a smaller peak separation on CoPc-SPCE than on unmodified SPCE (Fig. 3.19), confirming presence of CoPc on the electrode surface. Also cyclic voltammograms of CoPc-SPCEs were recorded in pH 7.4 buffer solution. These exhibited $Co^{II/I}$ redox couple peaks at ~-0.70 V /(SCE) (Fig. 3.20a (i)), proving the presence of CoPc on the SPCE surfaces. Note that this couple has been observed at -0.66 and -0.68 V /(SCE) for CoTPhPyrPc **6b** and CoTEThPc **6c** adsorbed on OPG electrodes in 0.5 M NaOH solution. The variation in potential is due to different complexes and media, as well as electrode material.

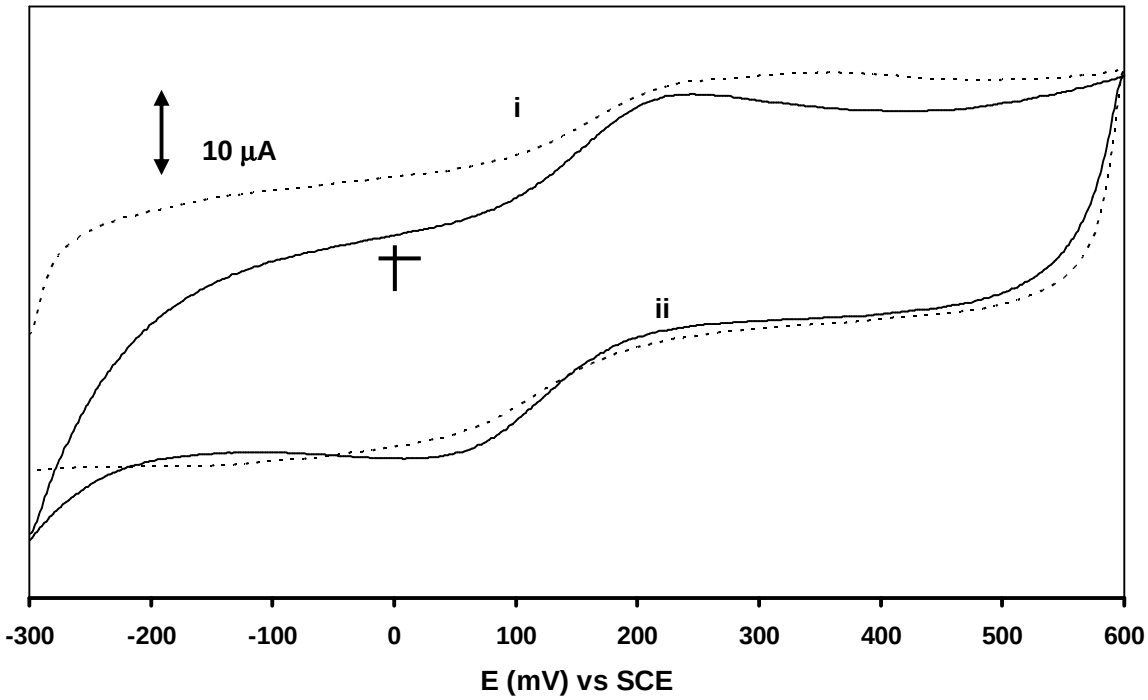

Figure 3.19: Cyclic voltammograms of 1 mM $Fe(CN)_6^{3-}/Fe(CN)_6^{4-}$ in 0.1 M KCl on i) bare SPCE and ii) 5 % CoPc-SPCE. Scan rate = 100 mV/s.

Electrooxidation of GSH and 2-ME was performed on 5% CoPc-SPCEs (prepared from CoPc dissolved in cyclohexanone solution) in neutral and in alkaline solution. Fig. 3.20 shows the cyclic voltammograms of GSH and 2-ME in 0.1 M NaOH (pH ~13). Electrooxidation peaks of GSH and 2-ME were observed at 0.05 and -0.34 V/(SCE), respectively. Note that in neutral solution (phosphate buffer, pH 7.4), the peaks were observed at 0.47 V and 0.18 V/(SCE) for GSH and 2-ME, respectively (Fig. 3.21). As expected, reaction overpotentials were greatly reduced in alkaline media[240]. In both cases, it should be noted that oxidation of GSH and 2-ME was not observed at bare SPCEs (without CoPc) in the investigated potential range (data not shown).

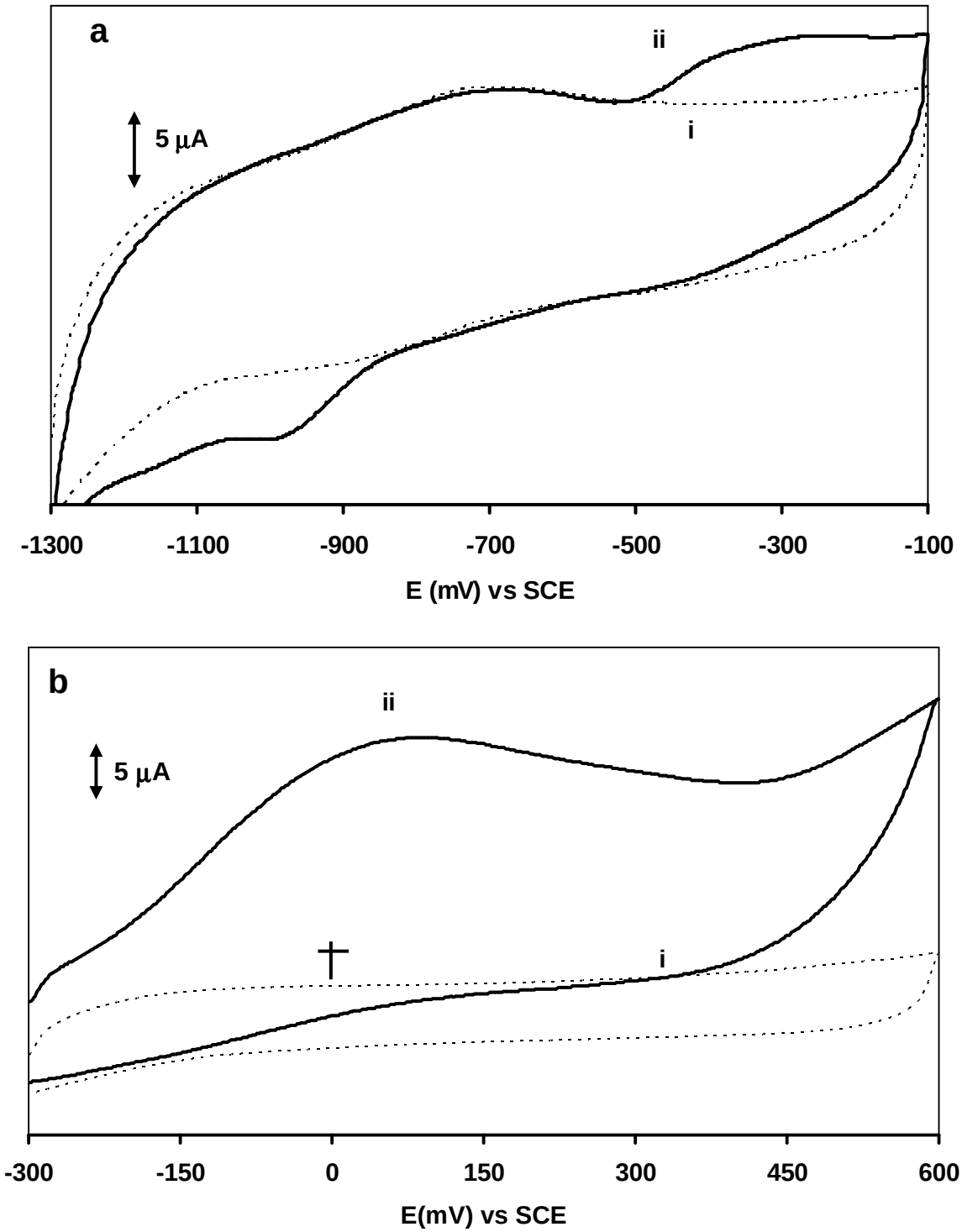

Figure 3.20: Cyclic voltammograms of a) 2 mM 2-ME (curve ii) and b) 0.01 M GSH (curve ii) in 0.1 M NaOH (pH~13) on 5 % CoPc-SPCE at 50 mV/s. Curve (i) is in the absence of thiols.

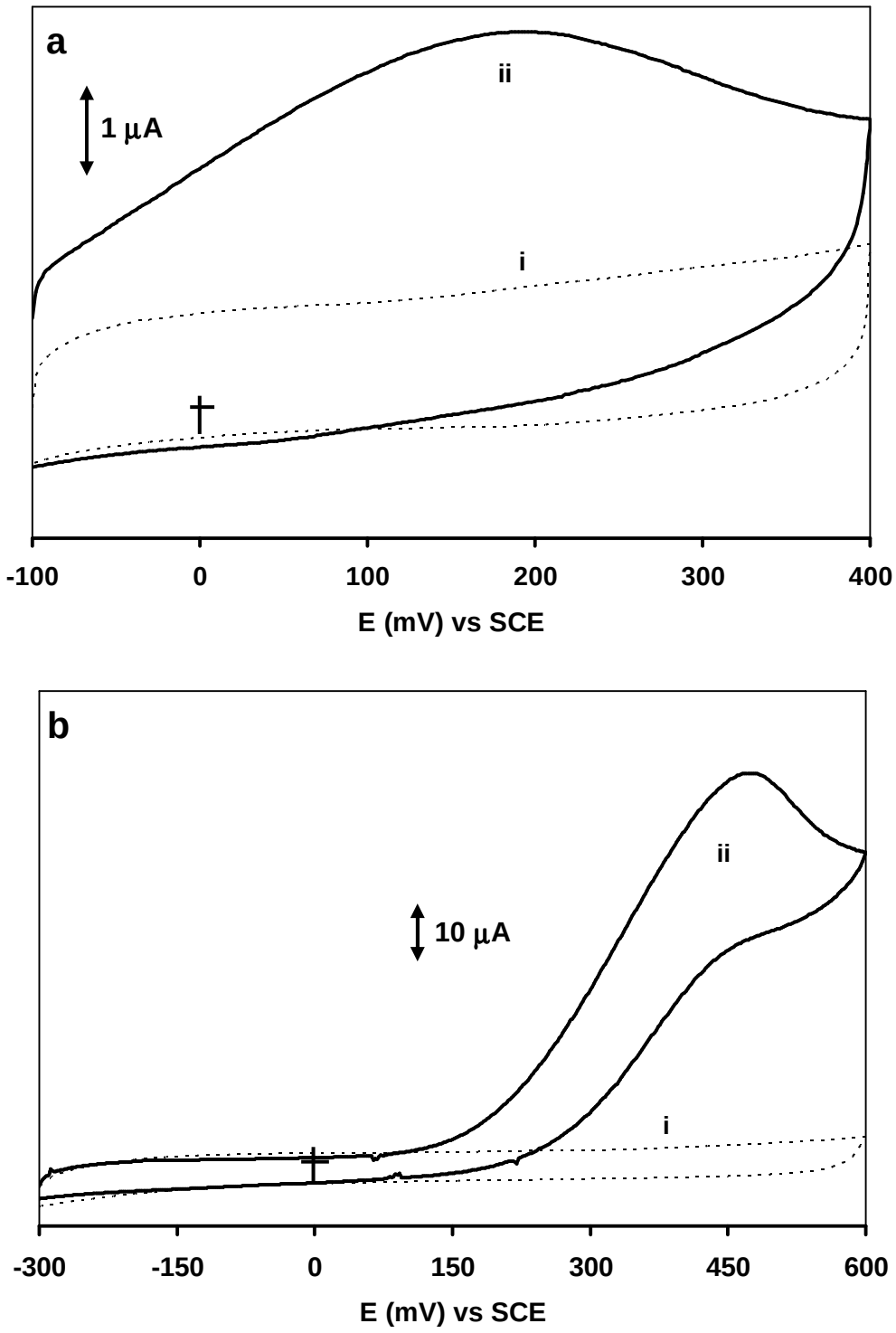

Figure 3.21: Cyclic voltammograms of a) 3 mM 2-ME (curve ii) and b) 0.01 M GSH (curve ii) in PBS (pH = 7.4) on 5 % CoPc-SPCE at 50 mV/s. Curve (i) is in the absence of thiols.

GSH was oxidized at -0.08 and -0.14 V/(SCE) in alkaline solutions (pH ~ 13) on glassy carbon electrodes modified by adsorption of complexes **6b** and **6c** respectively (Table 3.4), whereas on CoPc-SPCE, the reaction

occurred at 0.050 V/(SCE). This shows that GSH gets oxidized more easily on CoPc-modified GCE than on SPCE. The oxidation of 2-ME in alkaline media occurred at -0.12 and -0.22 V/(SCE) on **6b** and **6c** adsorbed-GCE respectively, Table 3.4, while on CoPc-SPCE, it occurred at -0.34 V/(SCE). It can therefore be concluded that it is easier to oxidize 2-ME on CoPc-SPCEs than on GCE modified by adsorption of **6b** and **6c**.

CoPc adsorbed on GCE showed oxidation of 2-ME at a potential of -0.32 V/ (SCE)[230] showing that SPCEs do improve catalytic activity marginally. The additional advantage of SPCEs is their disposability and their potential use in biological systems. Electrocatalytic activity towards thiol oxidation on CoPc-SPCEs cannot be compared with that of CoTEThPc-SAM because reactions were conducted in acidic media on the latter electrode where dissociation of thiols is unlikely and oxidation more difficult.

Furthermore, cyclic voltammograms were recorded at various 2-ME concentrations at fixed scan rate (Fig. 3.22a). A linear variation was obtained between concentration and peak current at a potential of -0.34 V (Fig. 3.22b), rendering the calibration curve useful for quantitative analysis of 2-ME.

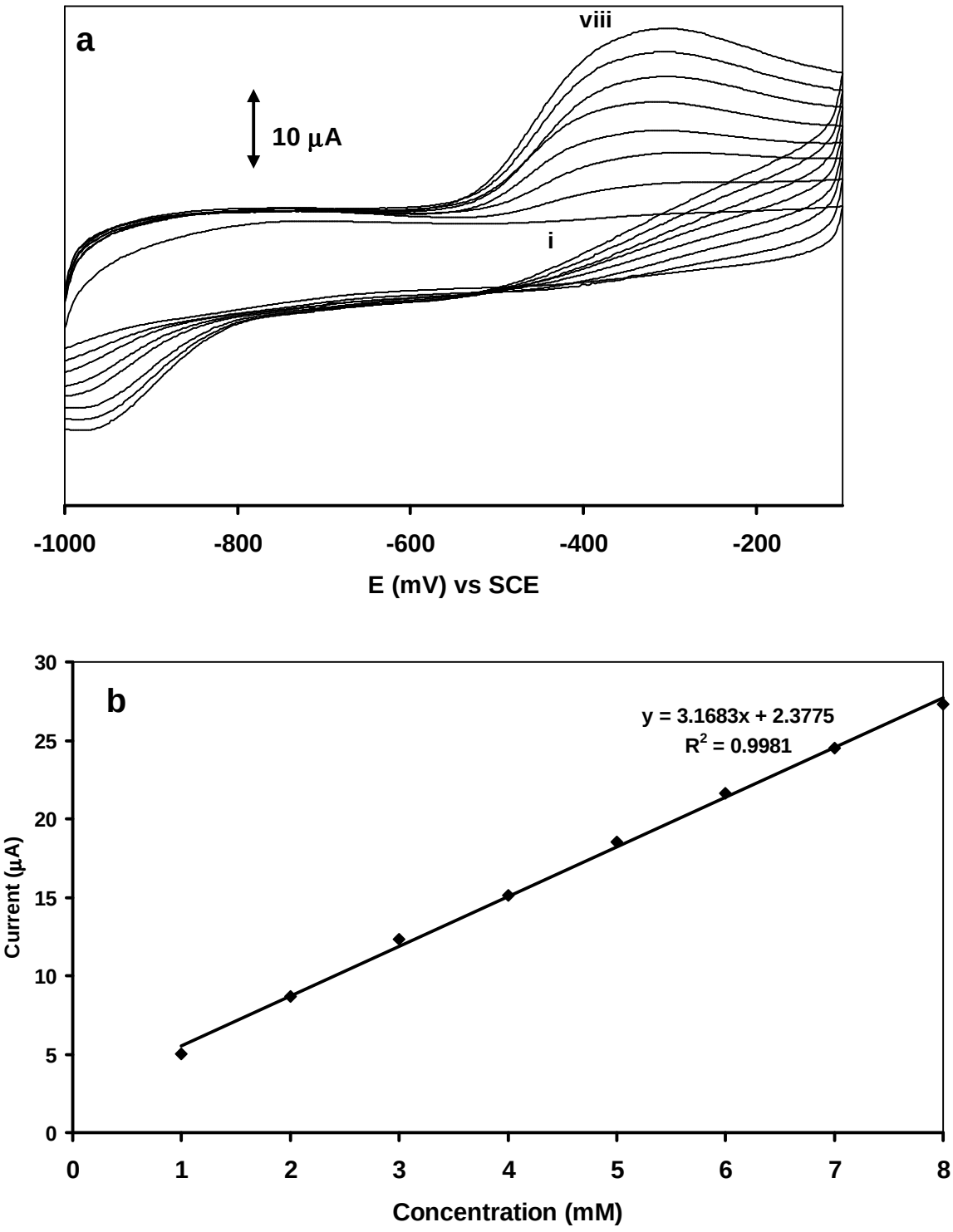

Figure 3.22: a) Cyclic voltammograms of concentrations 1 - 8 mM (i - viii) 2-ME in 0.1 M NaOH (pH ~ 13) on 5 % CoPc-SPCE at 50 mV/s. b) Variation of concentration and peak current for 2-ME oxidation in 0.1 M NaOH on 5 % CoPc-SPCE.

These results show that the examined CoPc-SPCEs are good electrocatalysts towards 2-ME and GSH oxidation in alkaline media, and they

are better than CoPc-GCE for 2-ME. In order to further assess the catalytic activity that stemmed from CoPc incorporated in the SPCEs, electrooxidation reactions were performed on SPCEs of various CoPc % composition of 1.0, 2.5 and 5.0 % prepared from CoPc dissolved in chloroform. Fig. 3.23 shows the cyclic voltammograms of GSH recorded at 1 %, 2.5 % and 5 % CoPc-SPCEs in neutral and alkaline solutions. In both cases, electrode loading of 5% CoPc-SPCEs showed the poorest catalytic activity, in terms of current intensity.

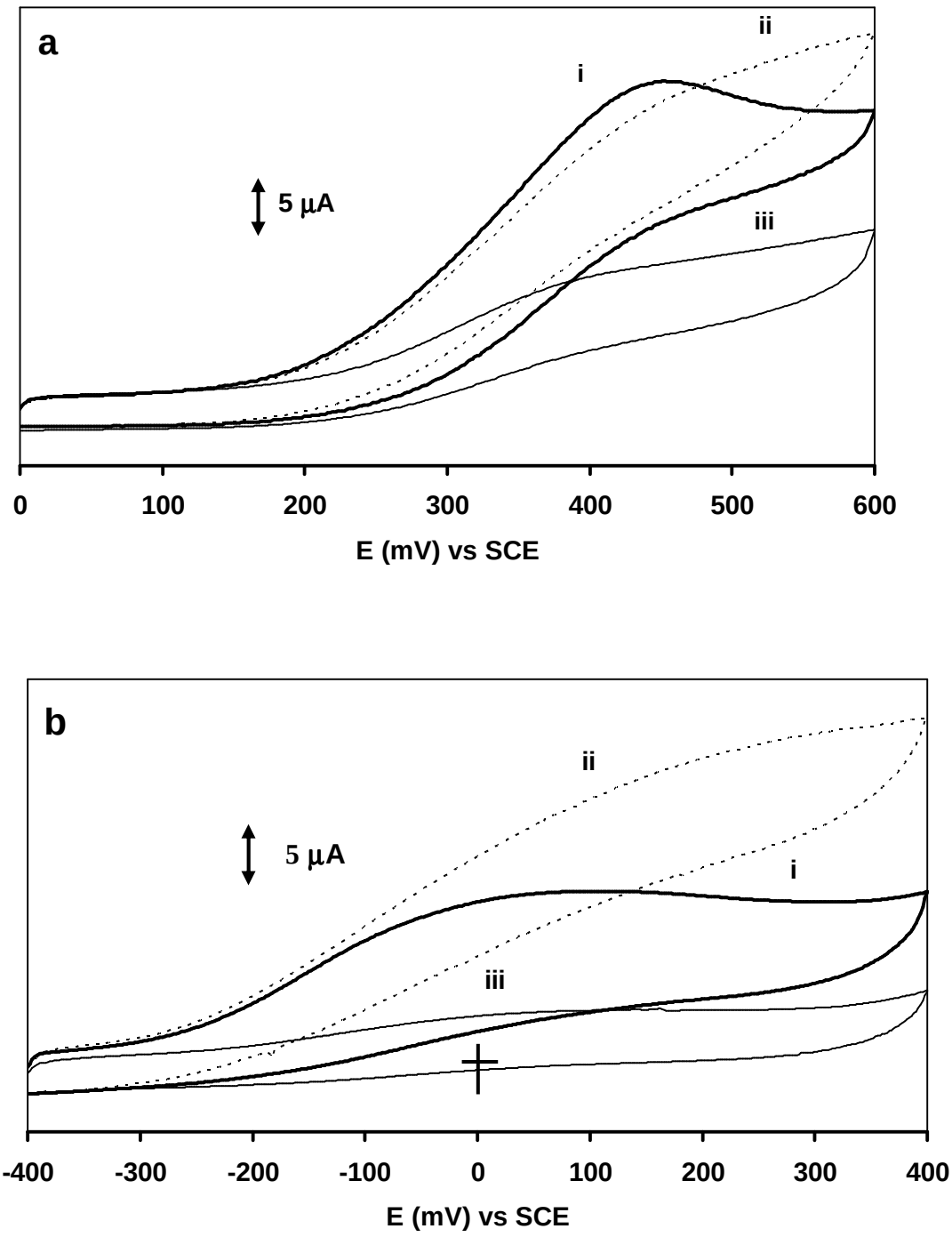

Figure 3.23: Cyclic voltammograms of 50 mM GSH at 1% CoPc-SPCE (curve i), 2.5% CoPc-SPCE (curve ii) and 5% CoPc-SPCE (curve iii) in a) PBS (pH 7.4) and b) 0.1 M NaOH aqueous solutions.

To ascertain that thiol current intensity results from various amounts of CoPc incorporated in the inks of SPCEs, peak intensity of the well known

$Fe(CN)_6^{3-}/Fe(CN)_6^{4-}$ reversible redox was used for calibration. If similar cyclic voltammograms of this system were obtained for CoPc-SPCE of different batches of the same % CoPc composition, then any observed thiol oxidation activity will be attributed to % CoPc composition. Figs. 3.24 and 3.25 show the cyclic voltammograms of GSH and 2-ME respectively, obtained in neutral solution at different batches of 1% (i, ii) and different batches of 2.5% (iii, iv) CoPc-SPCEs. In both cases, the cyclic voltammograms were compared with those obtained by the same electrodes in neutral solutions containing a given concentration of $K_4Fe(CN)_6$.

It must be mentioned that cyclic voltammograms were conducted first in the ferricyanide solutions, then in thiol solutions. This was done to avoid drawing erroneous conclusions because SPCEs were easily poisoned by the thiols and not by the ferricyanide solutions. However, SPCE poisoning by thiols is not that much of a threat because the electrodes are disposable and cheap.

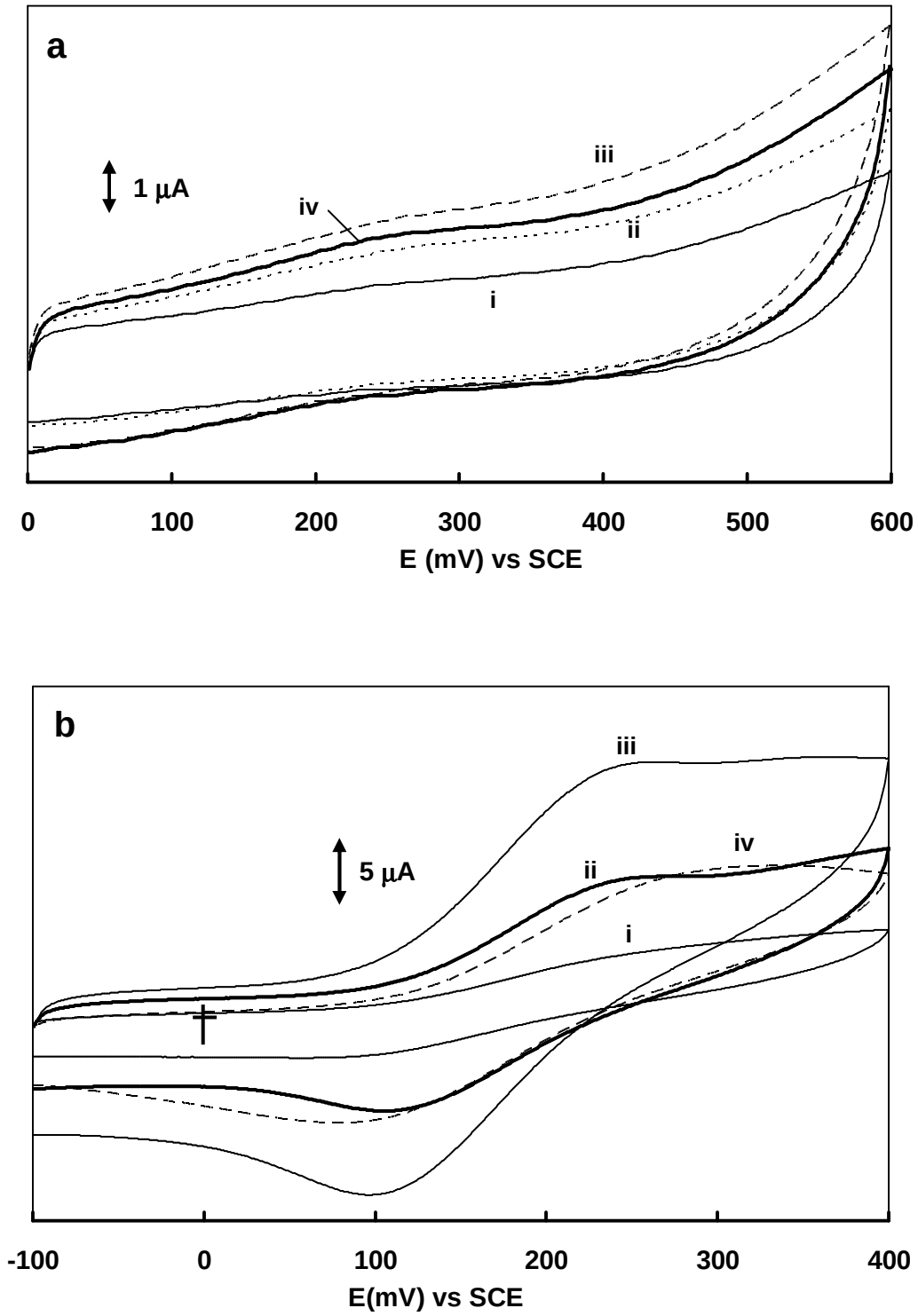

Figure 3.24: Cyclic voltammograms of a) 10 mM GSH and b) 1 mM $K_4Fe(CN)_6$ in PBS (pH 7.4) at different batches of 1% CoPc-SPCE (i & ii) and different batches of 2.5% CoPc-SPCE (iii & iv). The same electrodes were used for GSH and $K_4Fe(CN)_6$ oxidation reactions.

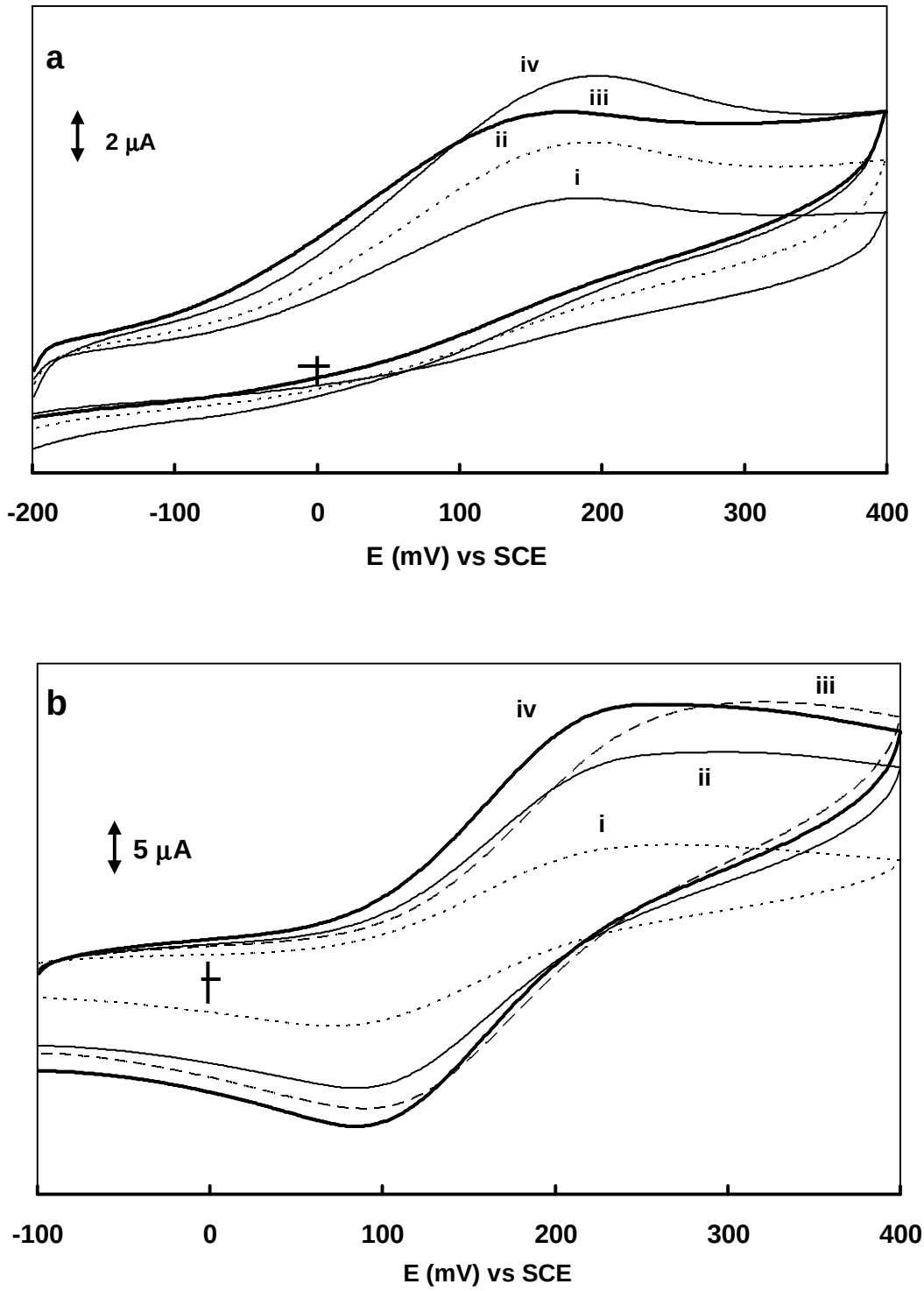

Figure 3.25: Cyclic voltammograms of a) 3 mM 2-ME and b) 1 mM $K_4Fe(CN)_6$ in PBS (pH 7.4) at batches of different 1% CoPc-SPCE (i & ii) and different batches of 2.5% CoPc-SPCE (iii & iv). The same electrodes were used for GSH and $K_4Fe(CN)_6$ oxidation reactions.

Cyclic voltammograms of SPCEs of the same CoPc % composition did not have the same peak intensities of the $Fe(CN)_6^{3-}/Fe(CN)_6^{4-}$ redox probe as shown in Figs. 3.24b and 3.25b, nor of thiol oxidation reactions (Figs. 3.24a and 3.25a). Thus varying electrocatalytic activity in terms of peak current intensities towards thiol oxidation could not be attributed to varying amounts of CoPc incorporated in SPCEs, much to the disagreement of the stated hypothesis above. However to rationalize the obtained results, a catalytic factor *f* was used (Table 3.5), which is defined as the ratio $\Delta I/\Delta I_p$ where ΔI is the difference between the highest and lowest measured oxidation current of a given thiol at a given potential (0.1 V and 0.2 V/(SCE) for 2-ME and GSH, respectively), on different batches of electrodes of the same CoPc % composition. ΔI_p is the difference between the peak intensities for $Fe(CN)_6^{3-}/Fe(CN)_6^{4-}$ reduction process on different batches of electrodes of the same CoPc % composition.

Table 3.5: Catalytic factor (f) calculated for the oxidation of GSH and 2-ME in neutral aqueous solution for different CoPc-SPCEs.

% CoPc-SPCE	Thiol (mM)	Catalytic factor, *f*
1	GSH (10 mM)	0.41
2.5	GSH (10 mM)	0.66
1	2-ME (3 mM)	1.11
2.5	2-ME (3mM)	3.01

The higher the f value, the more efficient is the catalyst. The largest f factor was observed for 2.5 % CoPc-SPCE, which also had the highest catalytic currents than 1.0 % CoPc-SPCE in Figs. 3.24 and 3.25, meaning that

the 2.5 % composition was more efficient than the 1.0 % composition. It should be noted that in all cases, the electrodes (i.e. 2.5 % CoPc-SPCE) that exhibited the highest activities towards the thiol oxidation also exhibited the highest peak intensities for the reference redox probe ($Fe(CN)_6^{3-}/Fe(CN)_6^{4-}$). The inverse holds for the 1.0 % CoPc-SPCE, which exhibited lowest activities for thiol oxidation and ferricyanide redox process.

3.2 Decomposition of *S*-nitrosoglutathione

In this work, decomposition reaction of *s*-nitrosoglutathione (GSNO) which results in formation of thiols is studied in physiological pH. $NaBH_4$ is used as a reducing agent whereas Cu^{2+} is used as a source of catalytically active Cu^{+} cations. This is a similar study to the previous section in that thiols are detected, though indirectly as opposed to the previous methods that involved detection of thiols that have been added to analyte solutions. The reaction is monitored by electrochemical detection of the formed thiol by cyclic voltammetry. This will be afforded by use of an ordinary pyrolytic graphite (OPG) electrode that has been modified by adsorption of CoPc.

CoPc-OPG electrode has been used successfully for detection of GSH in physiological media before[161]. Moreover, CoPc is readily available and the media used in this study is harsh for substituted MPc complexes as the substituents can detach or complex with components of the reaction solution leading to interferences. In this context, the possibility of electrochemically detecting GSH oxidation formed upon Cu^{+}-catalyzed decomposition of GSNO

is shown. Thus CoPc-modified electrodes are employed in indirect detection of thiols as opposed to direct methods discussed above.

OPG electrode was modified by adsorption of 10 mM CoPc solution in DMF. Fig. 3.26 (curve a) shows typical cyclic voltammograms of OPG after adsorption of CoPc in phosphate buffer of pH 7.4. The cyclic voltammogram exhibits a well-defined pair of peaks at *ca*. -0.64 V/(SCE) that is related to the reversible redox couple of $Co^{II/I}Pc$[161]. A slight shift in potential from -0.7 V/(SCE) observed for CoPc on SPCEs should be noted (Fig. 3.20); this is due to a different electrode material. Fig. 3.26 (curve b) shows the CV of CoPc-adsorbed OPG in PBS containing 1 mM GSH solution. A peak at ~0.05 V/(SCE) is observed indicating the electrocatalytic oxidation of GSH[161]. No oxidation peak of GSH is observed on unmodified OPG in the potential range studied (-1.1 V to 0.3 V/(SCE).

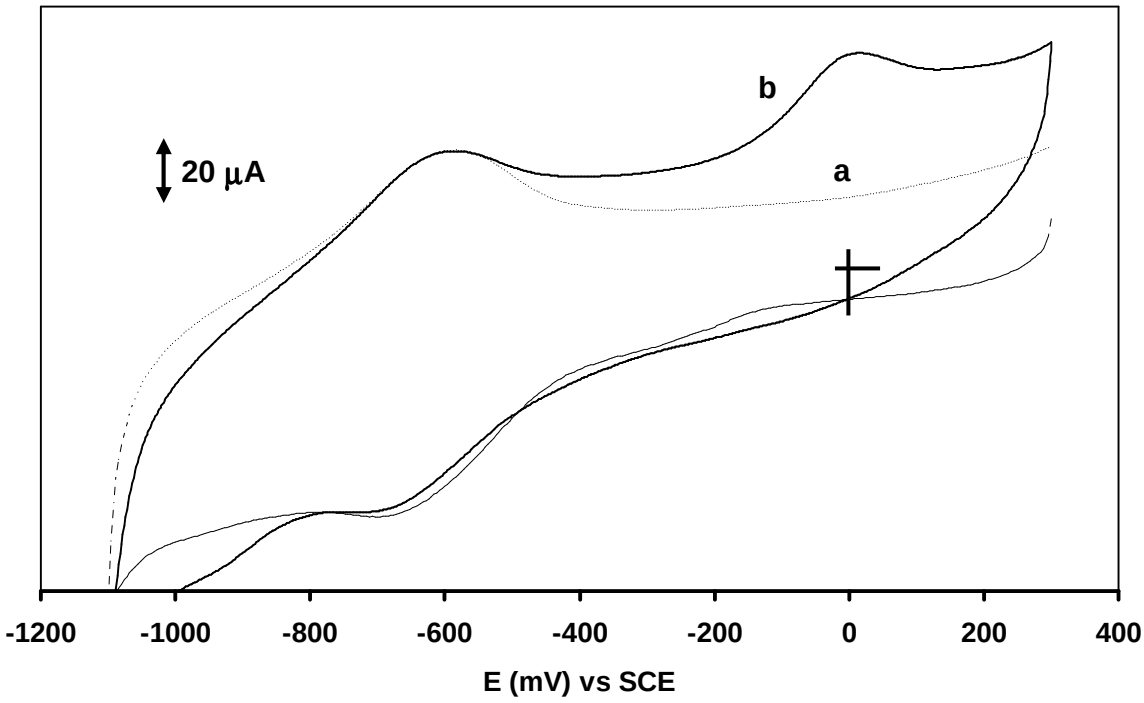

Figure 3.26: Cyclic voltammograms of CoPc adsorbed on OPG in argon-deaerated phosphate buffer (pH 7.4) at 50 mV/s. Curve a): without GSH; curve b): in presence of 1 mM GSH.

GSNO decomposition has been reported in the presence of $Cu(NO_3)_2$ and $NaBH_4$ reducing agent to form the catalytically active species Cu^+ cations[166]. Fig. 3.27a shows the cyclic voltammogram of CoPc adsorbed on OPG in phosphate buffer solution, Fig. 3.27b shows the CV when glucose was added to the physiological buffered solution for nutriment reasons. Fig. 3.27c shows the CV of adsorbed CoPc onto OPG with $Cu(NO_3)_2$ added to the electrolyte. No peaks, other than those related to $Co^{II/I}Pc$ were observed due to the added reagents in the potential range studied. Fig. 3.27d shows GSH oxidation peak at 0.05 V/(SCE). This clearly shows that GSH oxidation occurs in this potential range without any complications from the copper procatalyst, glucose or any other electrochemical interference at the OPG electrode modified by adsorption of the CoPc complex.

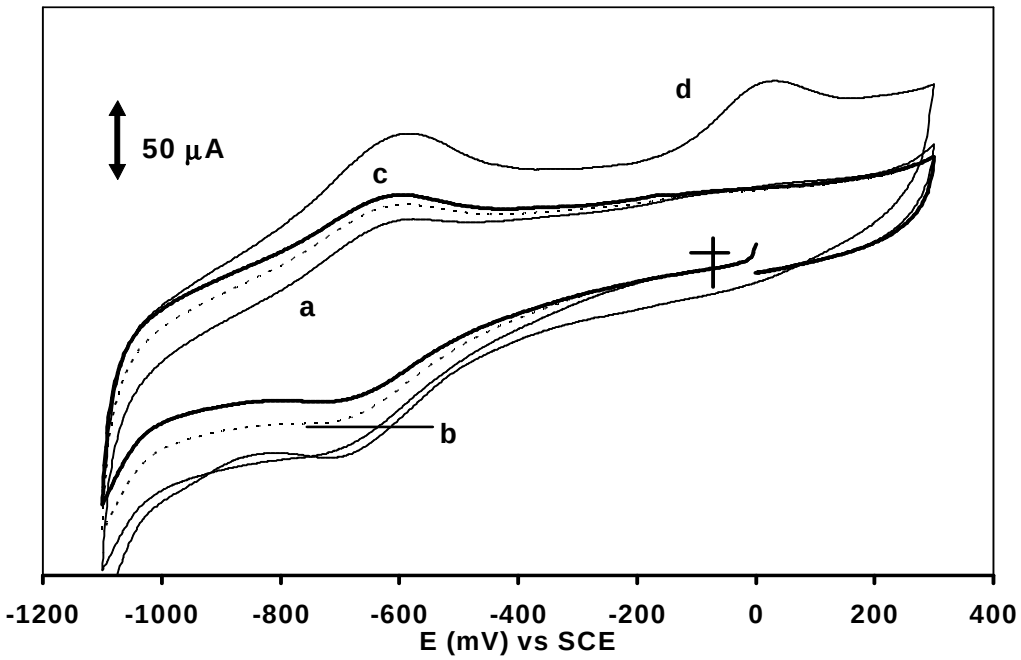

Figure 3.27: Cyclic voltammograms of CoPc adsorbed on OPG in commercial Dulbecco phosphate buffer saline (pH 7.4) without (curve a) and with: 5 mM glucose (curve b); 5 mM glucose + 10 µM $Cu(NO_3)_2$ (curve c) and 5 mM glucose + 10 µM $Cu(NO_3)_2$ + 1 mM GSH (curve d). Scan rate = 50 mV/s.

Fig. 3.28 (curve a) shows the cyclic voltammogram of CoPc adsorbed on OPG electrode in phosphate buffer of pH 7.4. These studies were conducted in the presence of atmospheric oxygen to mimick biological systems where the electrodes will be eventually used. Upon addition of 1 mM GSNO, a new reduction peak is observed at -0.9 V/(SCE), Fig. 3.28, curve b. This is due to a redox activity of GSNO. Indeed, similar reductive peak was recently reported in the case of GSNO on a hanging mercury electrode[241]. But the most remarkable result is that no redox process occurs in the potential range where the GSH is expected to be oxidized.

An oxygen reduction peak is observed at -0.23 V/(SCE). Also, it is important to note that no changes in the cyclic voltammogram were observed when 0.025 mM of the procatalyst Cu^{2+} was added (Fig. 3.28, curve c). Upon addition of 1 mM $NaBH_4$ (Fig. 3.28, curve d), a large anodic peak at *ca.* 0.05 V/(SCE) appeared. With time, this peak decreased in intensity (Fig. 3.28, curve e) until it diminished completely within 2 minutes. The GSNO reduction peak also decreased in intensity with time, but it stabilized (by *ca.* 25%) when the GSH oxidation peak was no longer observed. This shows that, after addition of $NaBH_4$ to Cu^{2+}, the products formed upon the decomposition of GSNO are unstable and short-lived.

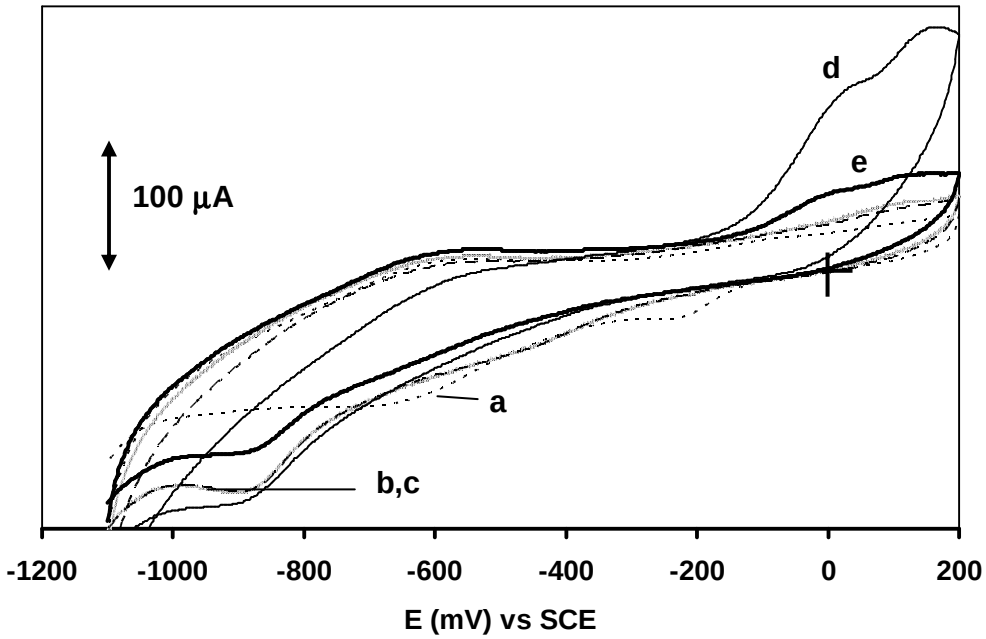

Figure 3.28: Cyclic voltammograms in aerobic phosphate buffer (pH 7.4) of CoPc adsorbed on OPG without (curve a) and in the presence of 1 mM GSNO (curve b); 1 mM GSNO + 0.025 mM $Cu(NO_3)_2$ (curve c) and after immediate addition of 1 mM $NaBH_4$ (curve d) and 1 minute later (curve e) . Scan rate = 50 mV/s.

The Cu^+-catalyzed decomposition of GSNO as a rule leads to the formation of NO and GSSG. But $NaBH_4$ is a strong reducing agent that reduces disulphide for analysis and quantification of total plasma thiols[242,243], it reduces GSSG to GSH. The oxidation of the reduced glutathione can thus be transiently observed at the electrode through its peak at 0.05 V/(SCE) (Figs. 3.28d and 3.28e). Since $NaBH_4$ is primarily involved in reducing Cu^{2+} and the formed GSSG/GSH undergo several side reactions such as complexation with cupric and cuprous ions[244,245], it is conceivable that the peak due to the oxidation of GSH does not last longer than for a few minutes. It is highly likely that the formed disulphide GSSG got reduced on this electrode. The reduction of GSSG has been reported to occur at -0.92

V/(SCE)[161] on CoPc-adsorbed OPG electrode in pH 7.4, but it overlaps with the reduction peak observed upon the initial addition of GSNO.

3.3 Thiocyanate oxidation

Thiocyanate oxidation was studied on CoTEThPc-SAM because SAMs have been reported to lower SCN^- oxidation potentials successfully[106]. This reaction was conducted on bare Au electrode and occurred at E_p = 0.70 V/(SCE) in pH 4, Fig. 3.29a. However, the peak due to the oxidation of thiocyanate was observed at a lower potential (E_p = 0.64 V/(SCE)) on CoTEThPc-SAM, Fig. 3.29b, indicating that CoTEThPc-SAM electrocatalyzes the oxidation of thiocyanate. The oxidation was irreversible. A large increase in currents was also observed confirming electrocatalytic behaviour (Fig. 3.29b). The voltammograms were recorded in solutions of pH ranging between 1 and 7, since in basic media, SAMs desorb from electrode surfaces.

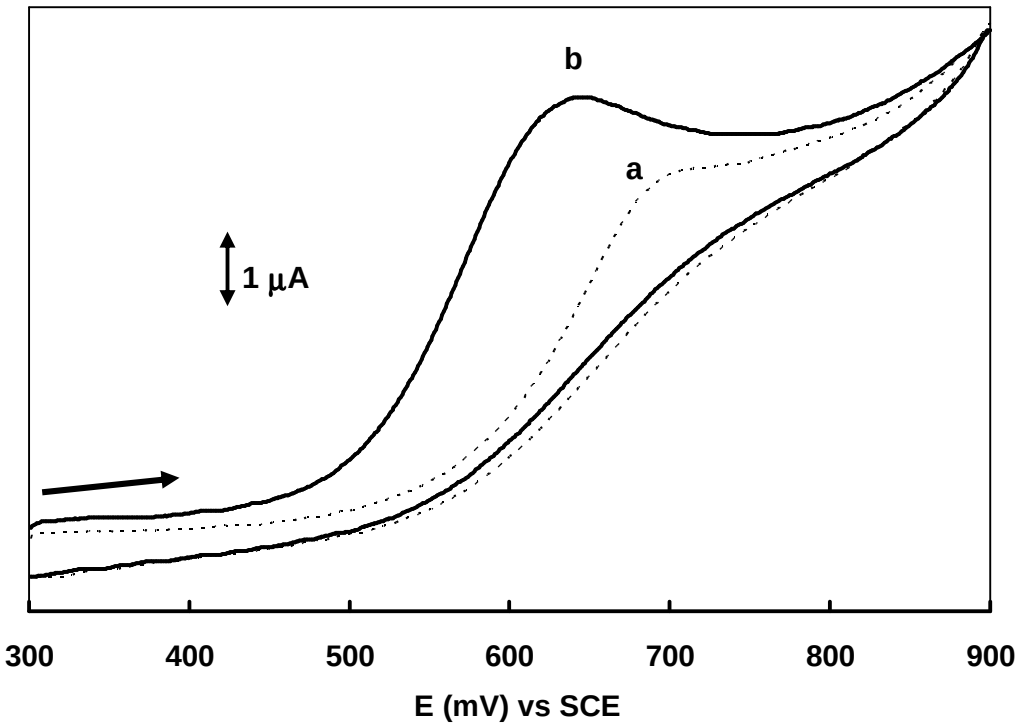

Figure 3.29: Cyclic voltammograms of 1 mM thiocyanate in pH 4 solution on a) bare Au and b) CoTEThPc-SAM. Scan rate = 50 mV/s.

Fig. 3.30 shows the dependence of SCN^- oxidation peak potential on pH. Two linear regions were observed: pH 1 to 4 and pH 4 to 7. The least positive potential was observed for pH 4, hence this pH was employed for further SCN^- studies. The slope of the plot between pH 1 and 4 was 30 mV/pH, suggesting the involvement of two electrons. Based on the equal number of protons and electrons transferred principle, it can therefore be concluded that number of protons transferred is also two.

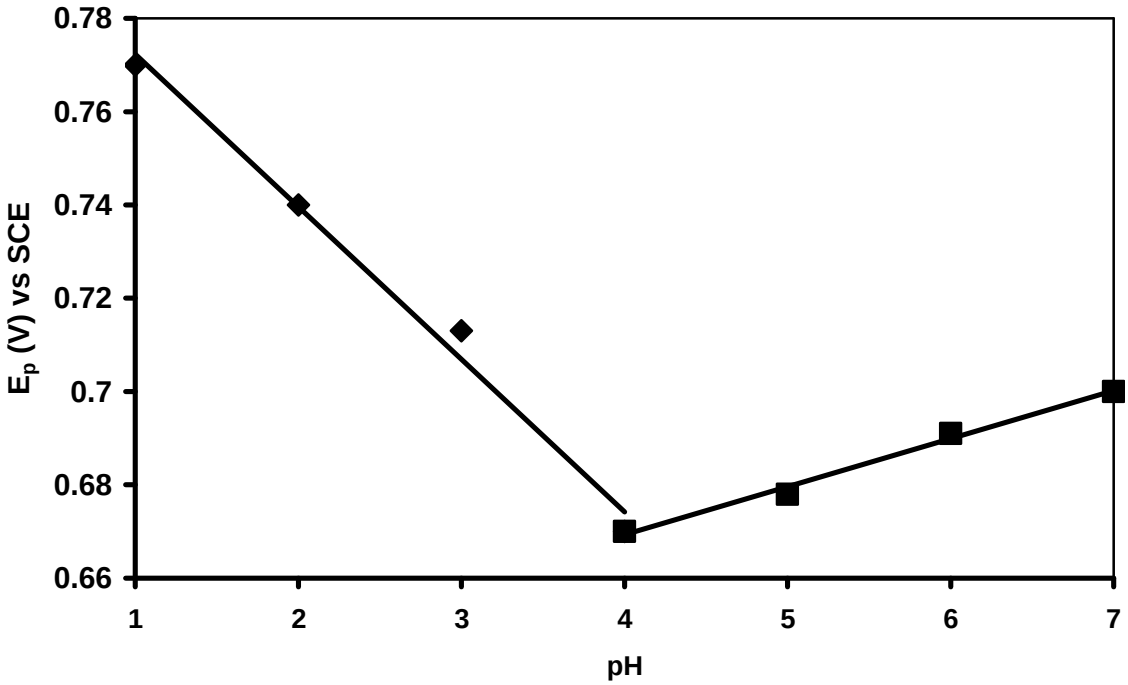

Figure 3.30: Pourbaix diagram (E_p vs pH) of 1 mM thiocyanate solution on CoTEThPc-SAM.

The oxidation of SCN^- is known to occur by two one-electron steps when catalyzed by horse radish peroxidase[148]. Direct one step two-electron oxidation of SCN^- in the presence of Fe(V) or Fe(III) has been reported[147,153]. Thus the observation of a two-electron oxidation of SCN^- evidenced in Fig. 3.30 is in accordance with literature. The oxidation of SCN^- is known to result in the intermediate formation of radicals which dimerize to form $(SCN)_2$, which further hydrolyzes to form CN^- and sulphate ions[147,148]. The oxidation process for thiocyanate was diffusion controlled as judged by the linearity of the plot of peak current versus square root of scan rate (similar to Fig. 3.16).

In order to determine the Tafel slope, the usual equation (Eq. 3.14) for a totally irreversible process was employed[236,237]. A plot of E_p vs log ν (Fig. 3.31a) gave a linear relationship. The Tafel slope ($b = 0.059/\alpha n$) of 116

mV/decade was obtained, indicating one electron transfer is involved in the rate-determining step. The electrocatalysis of thiocyanate was found to be diffusion-controlled based on the slope of one from a plot of log i_p versus log SCN^- concentration (Fig. 3.31b), based on Koutecky-Levich equation (eq. 3.2).

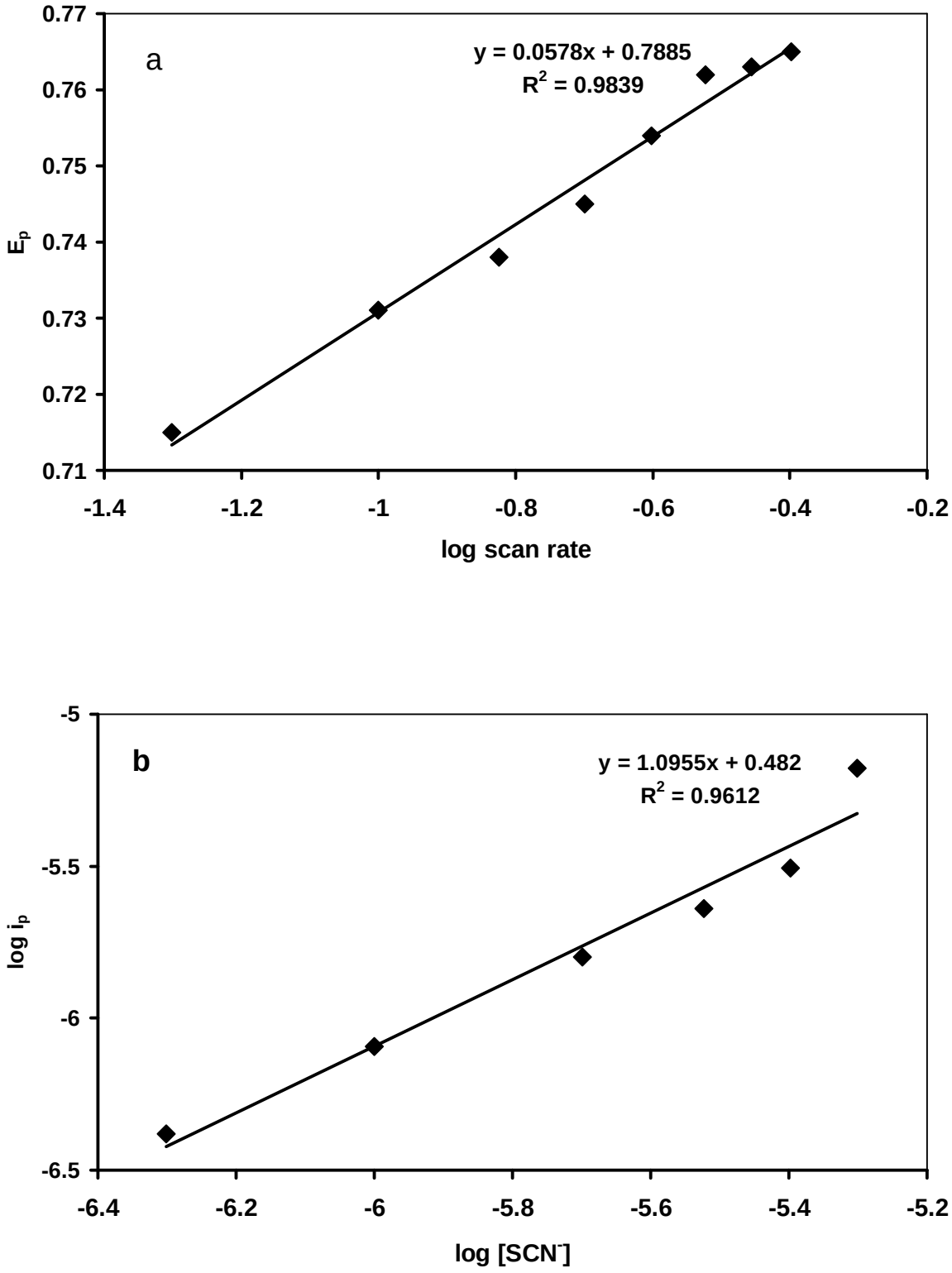

Figure 3.31: Plots of a) E_p versus log υ and b) log i_p vs log [SCN^-] for oxidation of thiocyanate on CoTEThPc-SAM in pH 4.

From Figs. 3.12 and 3.29, it is evident that the electrocatalytic oxidation peak for thiocyanate occurred at a potential range of the ring ($Co^{III}TEPhPc^{-1}$/ $Co^{III}TEPhPc^{-2}$) processes. Thus this process catalyzes the oxidation of thiocyanate. Since the oxidation of thiocyanate requires two electrons as discussed above, the following mechanism is proposed for electrocatalytic oxidation of thiocyanate (Scheme 3.4):

$$Co^{II}TEThPc^{-2} \rightarrow Co^{III}TEThPc^{-2} + e^- \quad 3.23$$

$$Co^{III}TEThPc^{-2} \rightarrow Co^{III}TEThPc^{-1} + e^- \quad 3.24$$

$$Co^{III}TEThPc^{-1} + 2SCN^- + 2H^+ \rightarrow Co^{II}TEThPc^{-2} + 2HSCN \quad 3.25$$

Scheme 3.4: Thiocyanate oxidation mechanism in acidic media catalyzed by $Co^{III}Pc^{-1}$ /$Co^{III}Pc^{-2}$ redox couple.

Equations 3.23 and 3.24 are proposed because oxidation of thiocyanate occurs at potentials of MPc ring oxidation and requires two electrons. Ring involvement in catalytic reactions involving CoPc has been reported before[9]. No significant changes (Fig. 3.32) were observed in the UV-Vis spectra of $Co^{II}TEThPc$ or $Co^{III}TEThPc$ (generated by bromine oxidation) on addition of SCN^-. Small spectral changes are expected due to axial coordination of ligands to MPc complexes[25]. Thus there was no evidence of coordination of SCN^- to the CoTEThPc complexes.

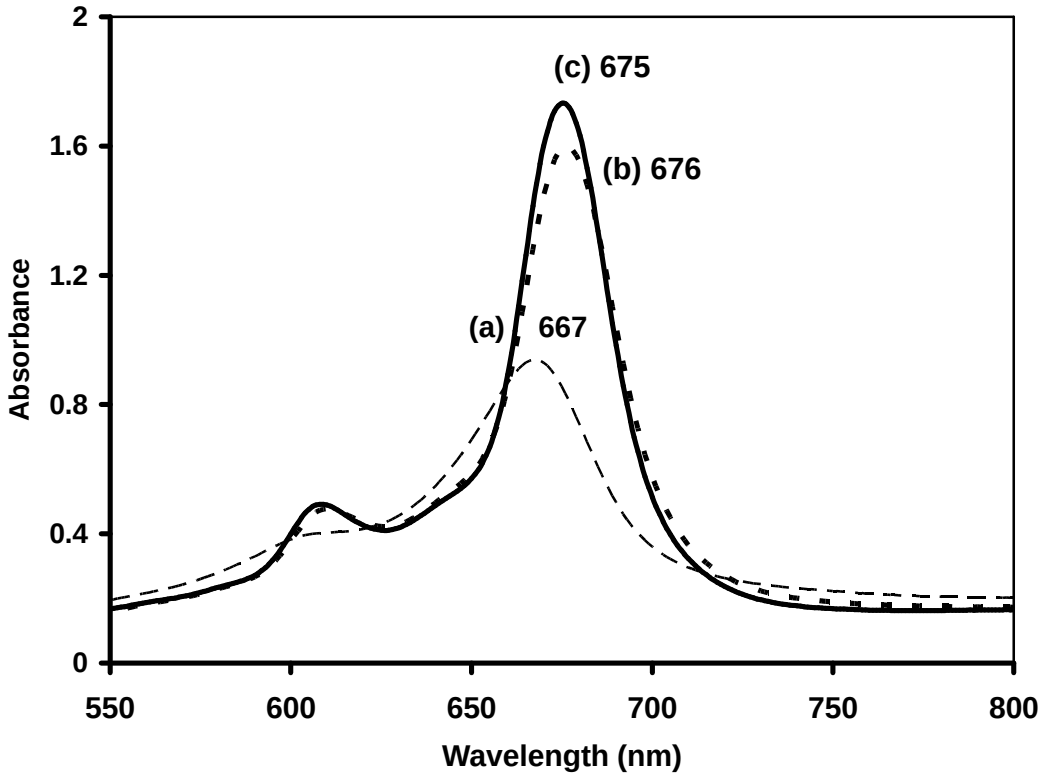

Figure 3.32: UV-Vis spectral changes observed on addition of SCN^- to solutions of CoTEThPc in DMF. Spectrum of a) Co^{II}TEThPc in the absence of SCN^-, b) Co^{III}TEThPc generated by bromine oxidation in the absence of SCN^- and c) Co^{III}TEThPc in the presence of SCN^-.

The fact that the electrocatalytic process showed first order behaviour and the Tafel plot showed the involvement of one electron for the rate determining step, yet an overall two electron transfer was observed, suggests that in equation 3.25, the electron transfer from thiocyanate to the $Co^{III}TEThPc^{-1}$ species, occurs in a stepwise manner. The involvement of protons in equation 3.25 is proposed to account for the need of protons as shown by Fig. 3.30. However the weak peak due to the HSCN species reported before[246], was not observed. The formation of $(SCN)_2$ cannot be ruled out[147,148], however, the involvement of protons cannot be explained if this species is formed.

Detection limits for the analysis of thiocyanate were determined using 3σ criterion and were valued at 3.4 x 10^{-7} M, which is in the same range as reported before[246]. Similar to *L*-cysteine and 2-ME oxidation on CoTEThPc-SAM discussed above, the modified electrode was very stable and exhibited reproducible electrocatalytic activity towards thiocyanate oxidation.

3.4 Oxygen reduction

Reduction of oxygen is an important reaction in industry because it forms the basis of operation of fuel cells; emission free energy sources. It is studied in this work on glassy carbon electrodes which are easy to clean and re-use. It is catalyzed by manganese phthalocyanines, Mn has half filled d-orbitals of energy that allows constructive overlap and energy transfer with p-orbitals of oxygen[189]. The aim is to achieve four electron transfer leading to formation of water that results in high energy output and not the two electron transfer that leads to formation of hydrogen peroxide, with less energy. The MnPc complexes employed as electrocatalysts for reduction of oxygen in this work are shown in Fig. 3.33.

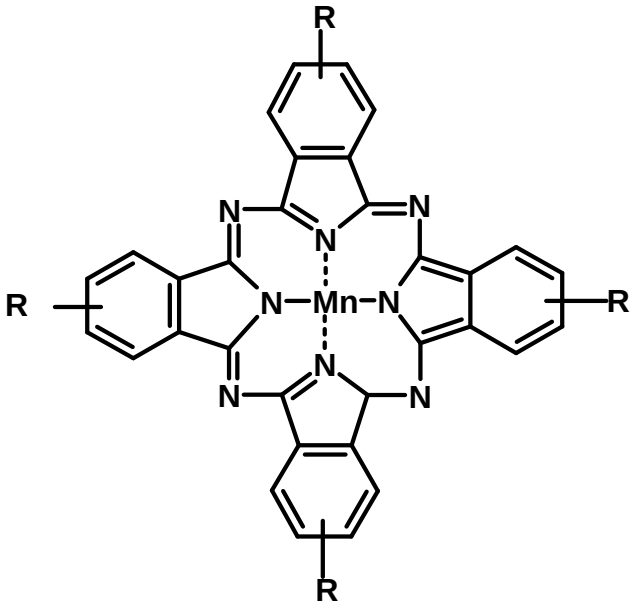

Complex	R	Abbreviation
7a	H	MnPc
7b	NH_2	MnTAPc
7c	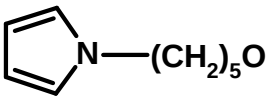	MnTPePyrPc
7d	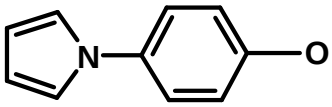	MnTPhPyrPc
7e	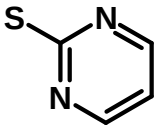	MnTMerPyPc
7f	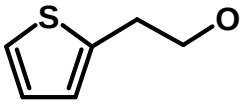	MnTEThPc

Figure 3.33: Molecular structures of phthalocyanine complexes used in electrocatalytic reduction of oxygen; MnPc (manganese phthalocyanine), MnTAPc (manganese tetraamino phthalocyanine), MnTPePyrPc (manganese tetrapentoxy pyrrole phthalocyanine), MnTPhPyrPc (manganese tetraphenoxypyrrole phthalocyanine), MnTMerPyPc (manganese tetramercaptopyrimidine phthalocyanine) and MnTEThPc (manganese tetraethoxythiophene phthalocyanine).

3.4.1 Characterization of new MnTPePyrPc, complex 7c

The synthesis of **7c** has not been reported before, unlike that of the other complexes. The synthetic procedure is outlined in Scheme 3.5, following the method employed by Trombach et al.[227]. The initial step was synthesis of the pyrrolyl pentoxy ligand. 5-Pyrrol-1-yl pentan-1-ol **12** was afforded from a reaction of 5-aminopentanol and dimethoxy tetrahydrofuran **11** in acetic acid. Compound **12** was then reacted with 4-nitrophthalonitrile resulting in 5-pyrrol-1-ylpentoxy phthalonitrile **13**, the latter was then cyclotetramerized into a metal-free phthalocyanine **14**, followed by metallation with Mn yielding **7c**.

IR spectroscopy was employed in characterizing the synthesized compounds. The nitrile (C≡N) stretch at 2229 cm^{-1} of **13** disappeared upon formation of the phthalocyanine. The ether stretching frequencies were prominent in the phthalonitrile (1244 cm^{-1}, **13**) and the resulting phthalocyanines (1235 cm^{-1}, **14** and 1244 cm^{-1}, **7c**). Complex **7c** was axially ligated with chloride anion and evidenced by a Mn-Cl vibration at 285 cm^{-1}. UV/Vis spectrum of **7c** in DMF showed a Q-band at 641 nm and a shoulder around 700 nm (Fig. 3.34). The former is μ-oxo dimer species $PcMn^{III}$-O-$Mn^{III}Pc$ while the latter is the Mn^{III} species, based on the well-documented UV/Vis spectra of MnPc complxes[25]. Moreover, ^{1}H NMR spectra of the H_2TPePyrPc **14** showed 1,4 protons at 9.00 and 2,3 protons at 8.41 ppm. Elemental analysis confirmed the formation of complex **7c**.

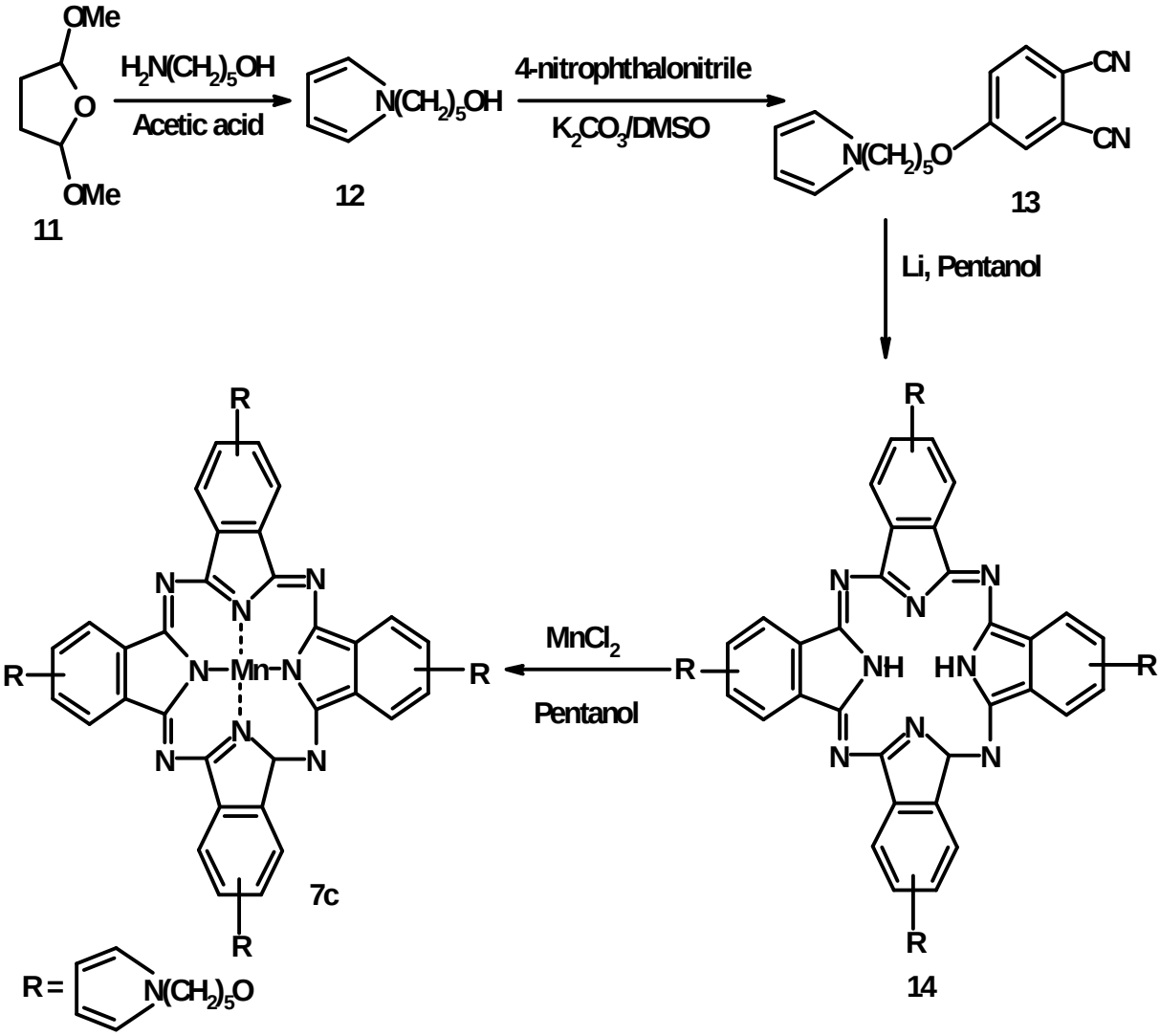

Scheme 3.5: Synthesis of MnTPePyrPc, 7c.

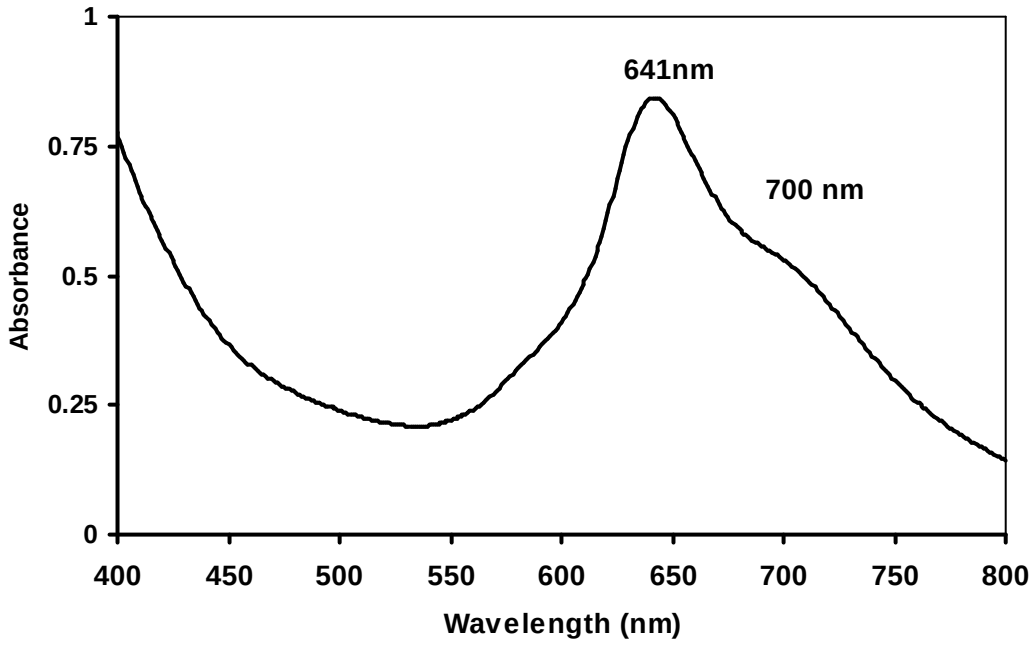

Figure 3.34: UV/Visible spectrum of MnTPePyrPc 7c in DMF.

3.4.2 Characterization of adsorbed MnPc complexes

MnPc complexes **7a** to **7f** (Fig. 3.33) were used to electrocatalyze oxygen reduction reaction. Cyclic voltammograms of MnPc complexes adsorbed on glassy carbon electrodes were run in nitrogen-purged buffer solutions in the pH range 1 - 13 for characterization purposes. Only studies in pH 5 are shown in Fig. 3.35 (curves i). The adsorbed MnPc derivatives exhibited $Mn^{III/II}$ processes (labeled **I**) at -0.35, -0.25[112], -0.12, -0.29[101], -0.26[222] and -0.41 V/(SCE)[221] for complexes **7a** to **7f**, respectively, in comparison with literature. The second peak labeled **II** is associated with ring based reduction and the formation of $Mn^{II}Pc^{-2}/Mn^{II}Pc^{-3}$.

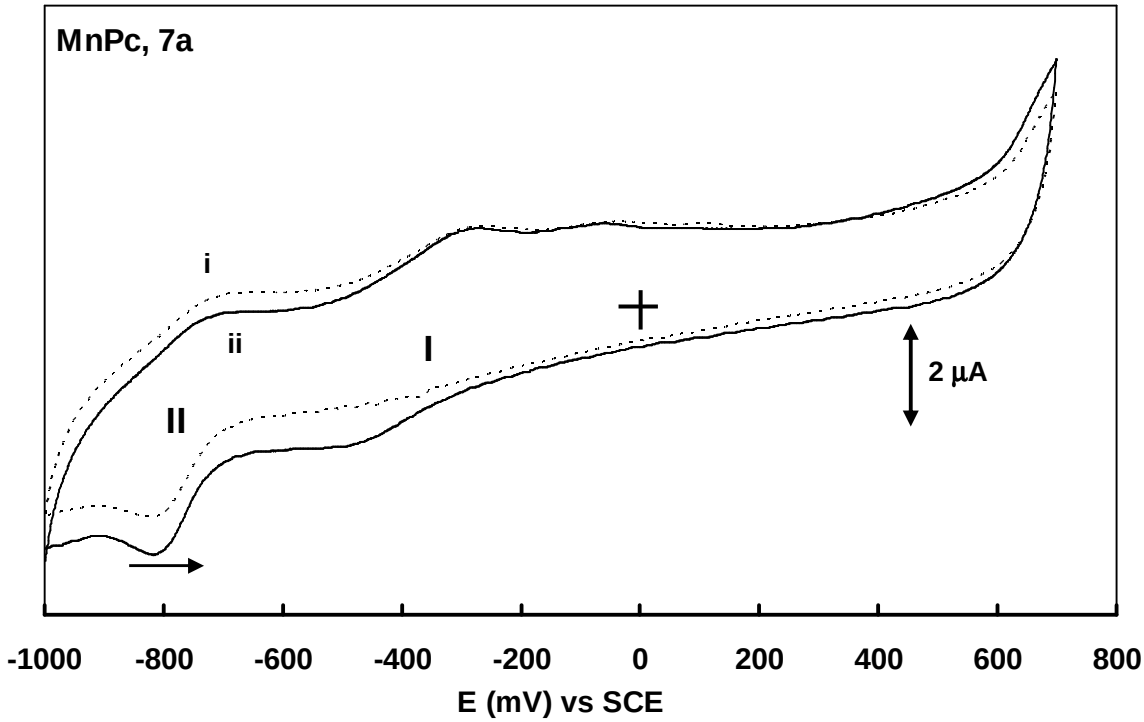
MnPc, 7a
i
ii
I
II
2 µA
-1000
-800
-600
-400
-200
0
200
400
600
800
E (mV) vs SCE

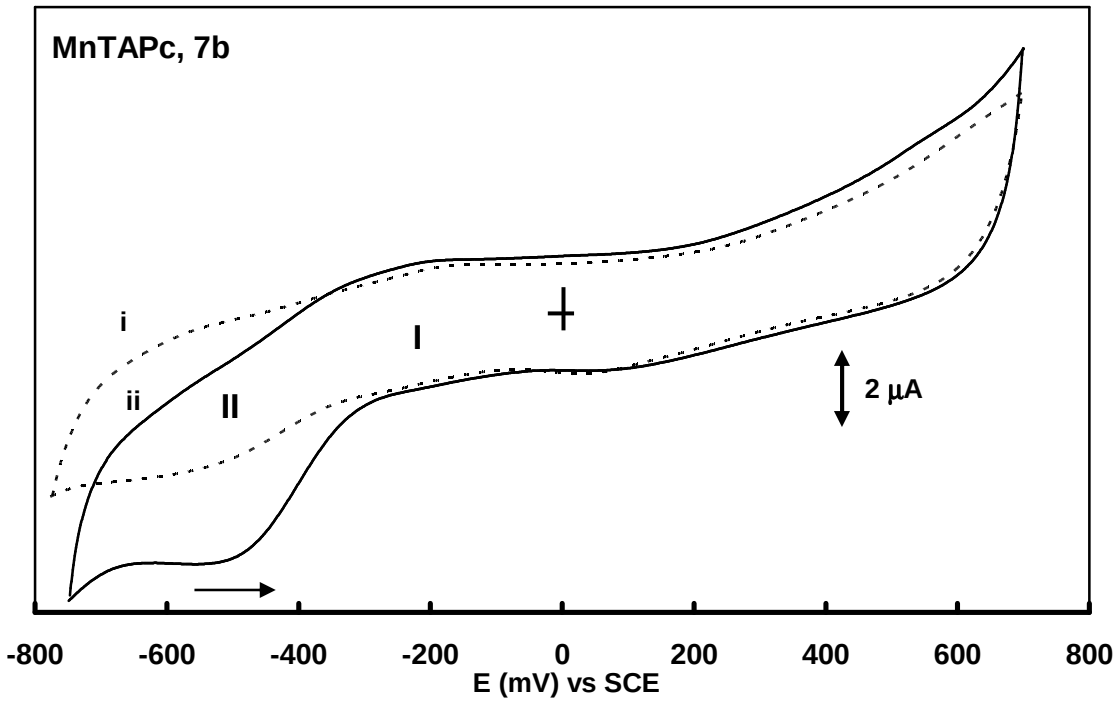
MnTAPc, 7b
i
ii
I
II
2 µA
-800
-600
-400
-200
0
200
400
600
800
E (mV) vs SCE

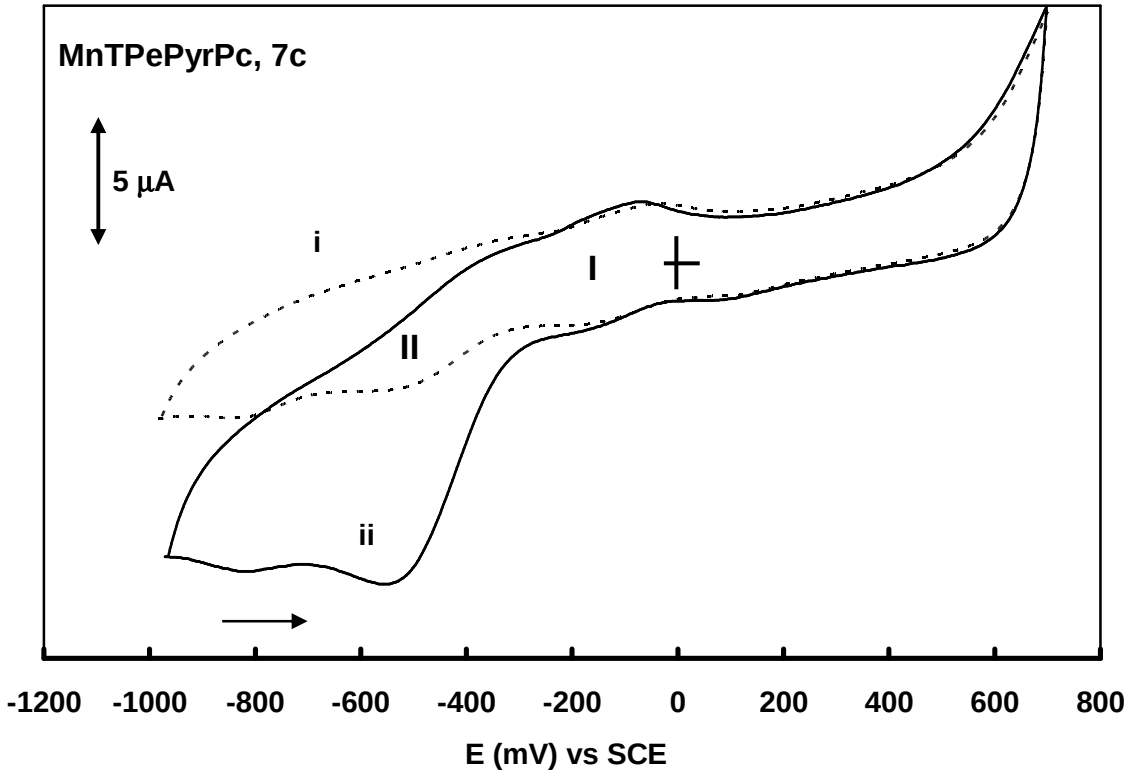
MnTPePyrPc, 7c
5 µA
i
I
II
ii
-1200 -1000 -800 -600 -400 -200 0 200 400 600 800
E (mV) vs SCE

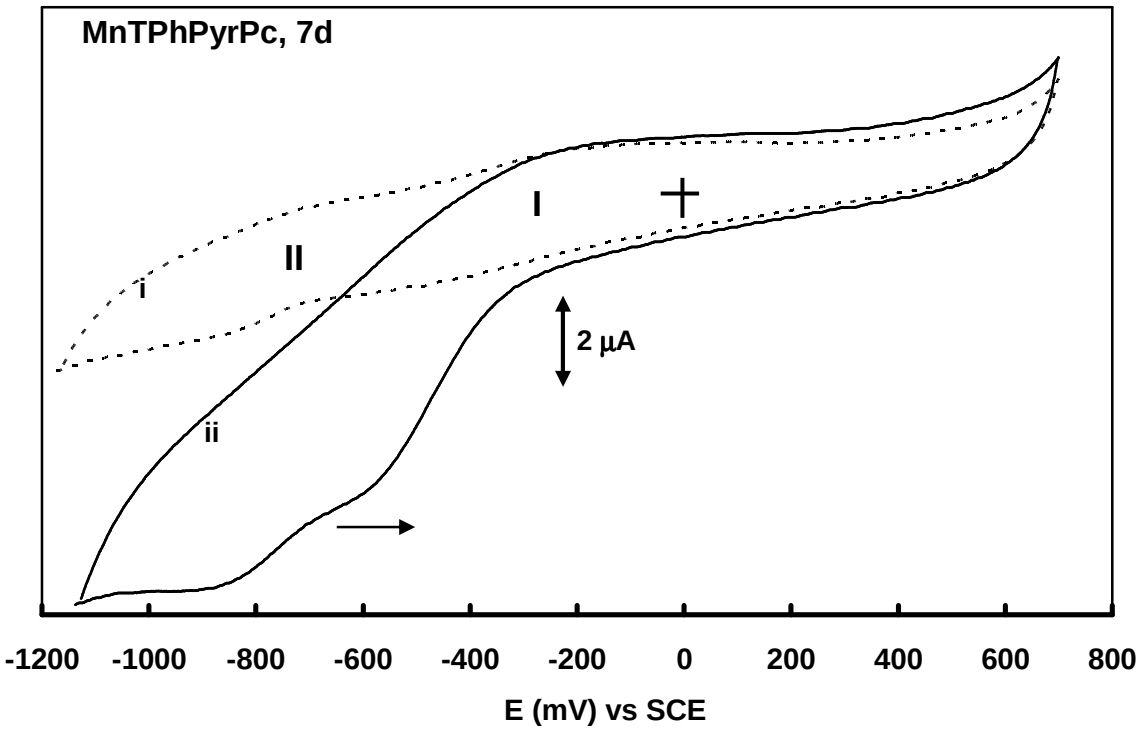
MnTPhPyrPc, 7d
I
II
i
2 µA
ii
-1200 -1000 -800 -600 -400 -200 0 200 400 600 800
E (mV) vs SCE

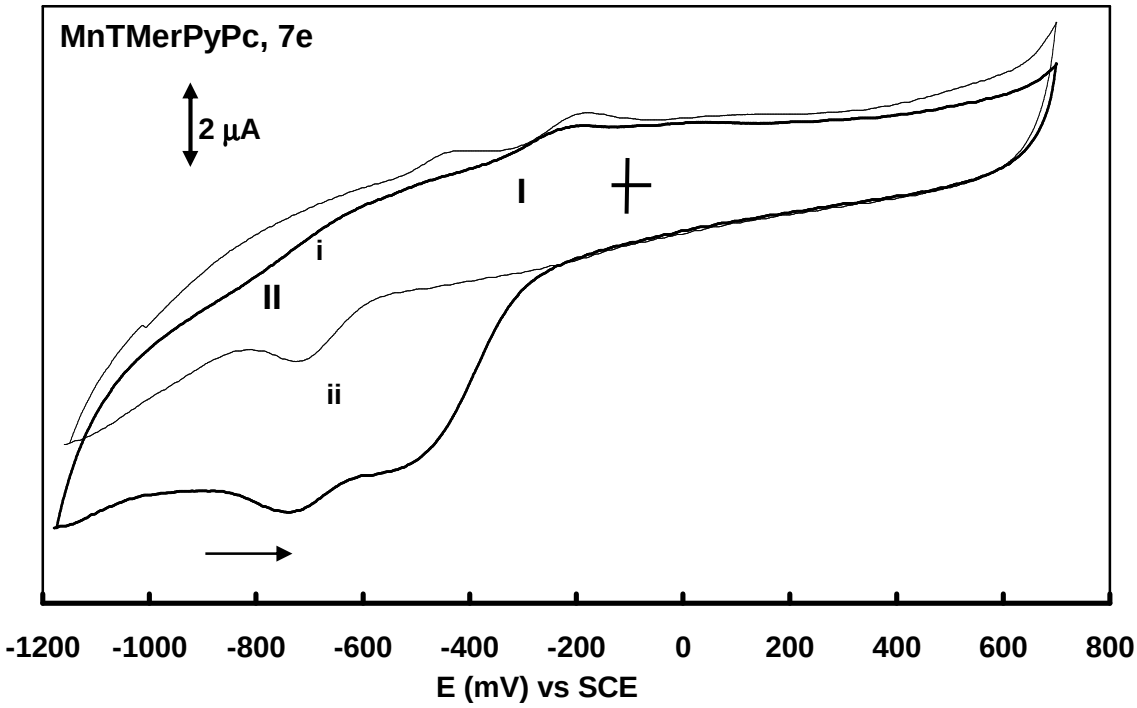

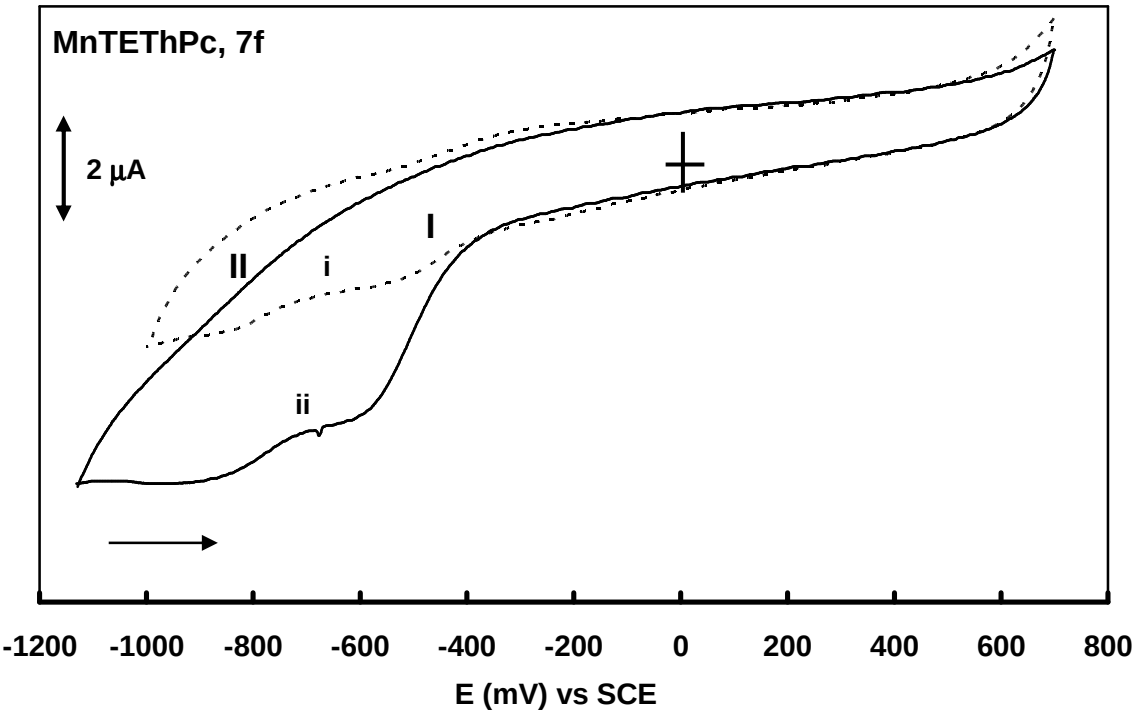

Figure 3.35: Cyclic voltammograms in i) nitrogen-purged and ii) oxygen saturated pH 5 buffer solutions of complexes 7a to 7f. Scan rate = 50 mV/s.

Peak potentials for the $Mn^{III/II}$ couple shifted to the negative with increasing pH, an average slope of ~-0.06V/pH was observed for all complexes in the pH range of 1 to 6 indicating a transfer of one proton and one electron. This is shown in Fig. 3.36 for MnTPePyrPc, **7c**.

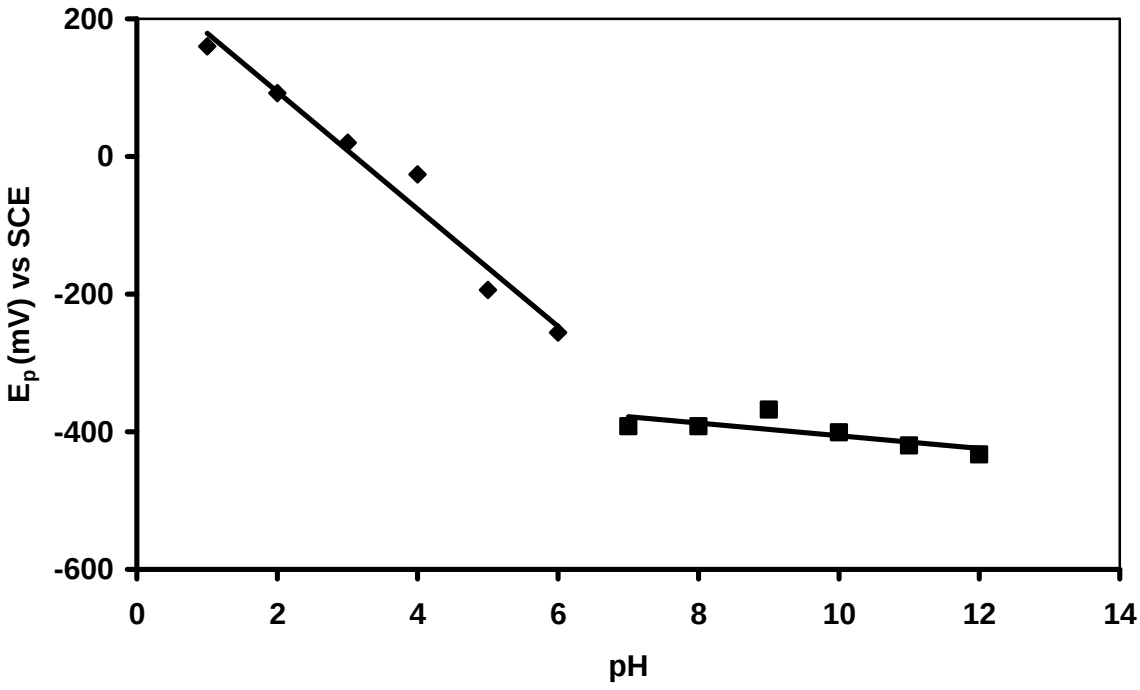

Figure 3.36: Pourbaix diagram (E_p vs pH) for $Mn^{III/II}$ couple of complex 7c.

The surface coverage of adsorbed films was probed by recording the CVs of **7a** to **7f** at different scan rates based on equation 3.13[232]. This is shown for complex **7c** in Fig. 3.37. Surface coverage was calculated from the plots of I_p versus ν to be 3.6, 1.1, 4.8, 7.6, 8.2 and 6.8 x 10^{-10} for complexes **7a** to **7f** respectively, Table 3.6, indicating monolayer thickness. Linearity of the I_p versus ν plots indicated surface confined adsorbed species[158], further confirming adsorption of MPc complexes.

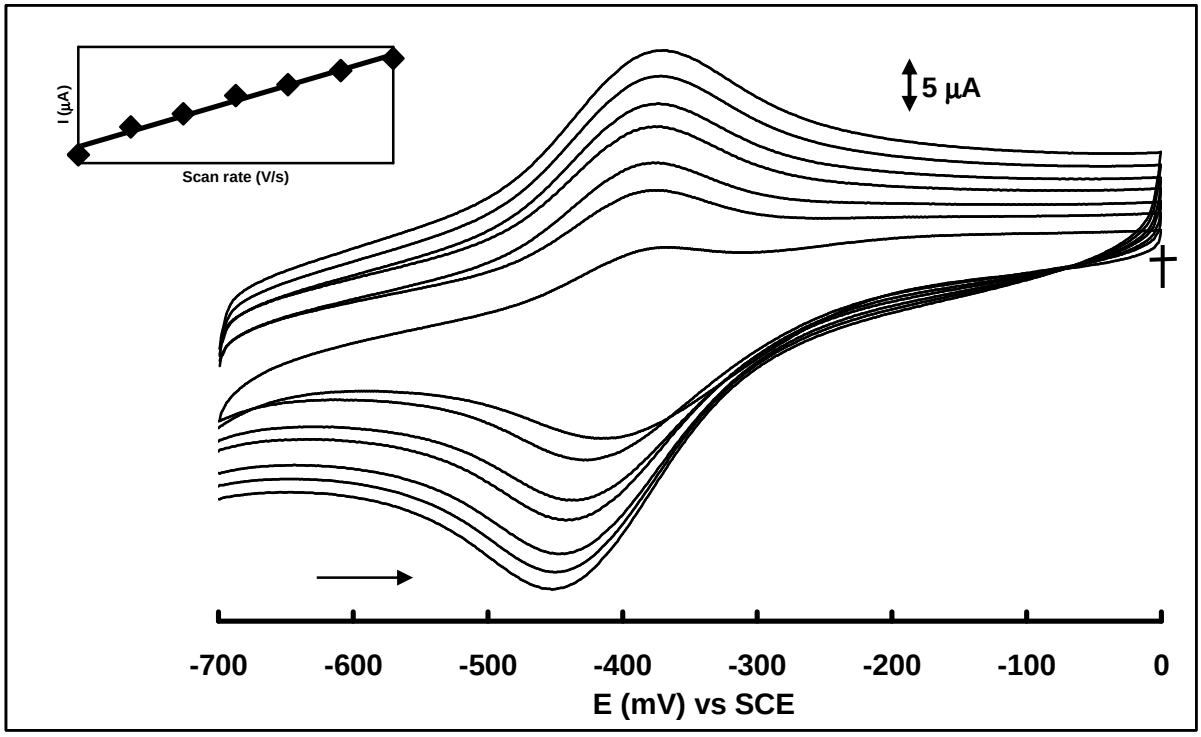

Figure 3.37: Cyclic voltammogram of 7c showing $Mn^{III/II}$ couple in pH 12 at scan rates of 100 - 400 mV/s. Insert is a plot of peak current versus scan rate.

Table 3.6: Oxygen reduction data in pH 5 for complexes 7a to 7f adsorbed on GCE.

MPc	Γ_{MPc} (10^{-10})	$Mn^{III/II}$ V/(SCE)	O_2 / H_2O_2 V/(SCE)	Total no. e^-s	Tafel Slope	α	k_c (10^{-5})
7a	3.6	-0.35	-0.49 (-0.45)	2.6	-115	0.51	13.5
7b	1.1	-0.25	-0.54 (-0.50)	2.0	-218	0.27	7.3
7c	4.8	-0.12	-0.51 (-0.47)	2.2	-177	0.33	6.8
7d	7.6	-0.29	-0.59 (-0.63)	2.8	-129	0.46	7.5
7e	8.2	-0.26	-0.51 (-0.43)	2.1	-148	0.40	5.7
7f	6.8	-0.41	-0.58 (-0.58)	1.8	-130	0.45	5.2

Data in parentheses is in pH 12 for the O_2 – H_2O process.

3.4.3 Oxygen reduction on MnPc complexes

Oxygen gets reduced to hydrogen peroxide, followed by reduction of the latter to water on MPc modified electrodes[247], each step requiring two electrons. In acid and slightly alkaline media, the CV for oxygen reduction on MPc modified electrodes shows two peaks due to oxygen reduction to hydrogen peroxide and subsequent hydrogen peroxide reduction to water[247]. In highly alkaline solutions, the reaction goes to completion with only one peak observed due to four electron reduction of oxygen to water[247]. In this study, a similar trend in activity was observed. Fig. 3.35 shows enhancement of currents of the MnPc complexes in the presence of oxygen, confirming catalytic reduction of oxygen.

Two peaks are observed for all complexes (except **7b**) due to the formation of hydrogen peroxide and water. The presence of the two peaks in the range for $Mn^{III}Pc^{-2}/Mn^{II}Pc^{-2}$ and the ring process $Mn^{II}Pc^{-2}/Mn^{II}Pc^{-3}$ confirms that both of these processes catalyze the oxygen reduction, as has been reported before[247]. However, in highly alkaline solutions (pH 9 - 13), there is only one peak for all complexes (Fig. 3.38), due to reduction of oxygen to water. Based on the ease of the reduction (shifting of potential to less negative values) of oxygen to water in Fig. 3.38, which reflects the efficiency of these molecules as catalysts for the process, the MnPc complexes may be ranked as follows in pH 12 (Table 3.6): **7e ≈ 7a ≈ 7c** > **7b** > **7f** > **7d**. The ease of reduction of oxygen is not directly related to the redox potential of the $Mn^{III}Pc/Mn^{II}Pc$ couple, which followed this trend in pH 5 buffer (Table 3.6): **7f** (-0.41 V) > **7a** (-0.35 V) > **7d** (-0.29 V) > **7e** (-0.26 V) > **7b** (-0.25) > **7c** (-0.12

V/(SCE)). Note that the $Mn^{III}Pc/Mn^{II}Pc$ redox couple of the complexes was not clearly defined in pH 12 buffer solutions.

Plots of peak current versus square root of scan rate for the reduction of oxygen were linear for all studied complexes in the pH range 1 - 13 indicating oxygen reduction to hydrogen peroxide or water is diffusion-controlled. This is shown for MnPc in pH 12 in Fig. 3.39.

Rotating disc electrode (RDE) experiments were conducted to further elucidate studied reactions. These experiments were conducted in pH 5, 8 and 12 (Fig. 3.40 shown for pH 5 and 12) since in these solutions, different mechanisms were highly probable as explained above. Unfortunately only single runs at low rotation speeds were done because the catalyst was lost from the surface. However, runs were done in triplicates and averages are reported.

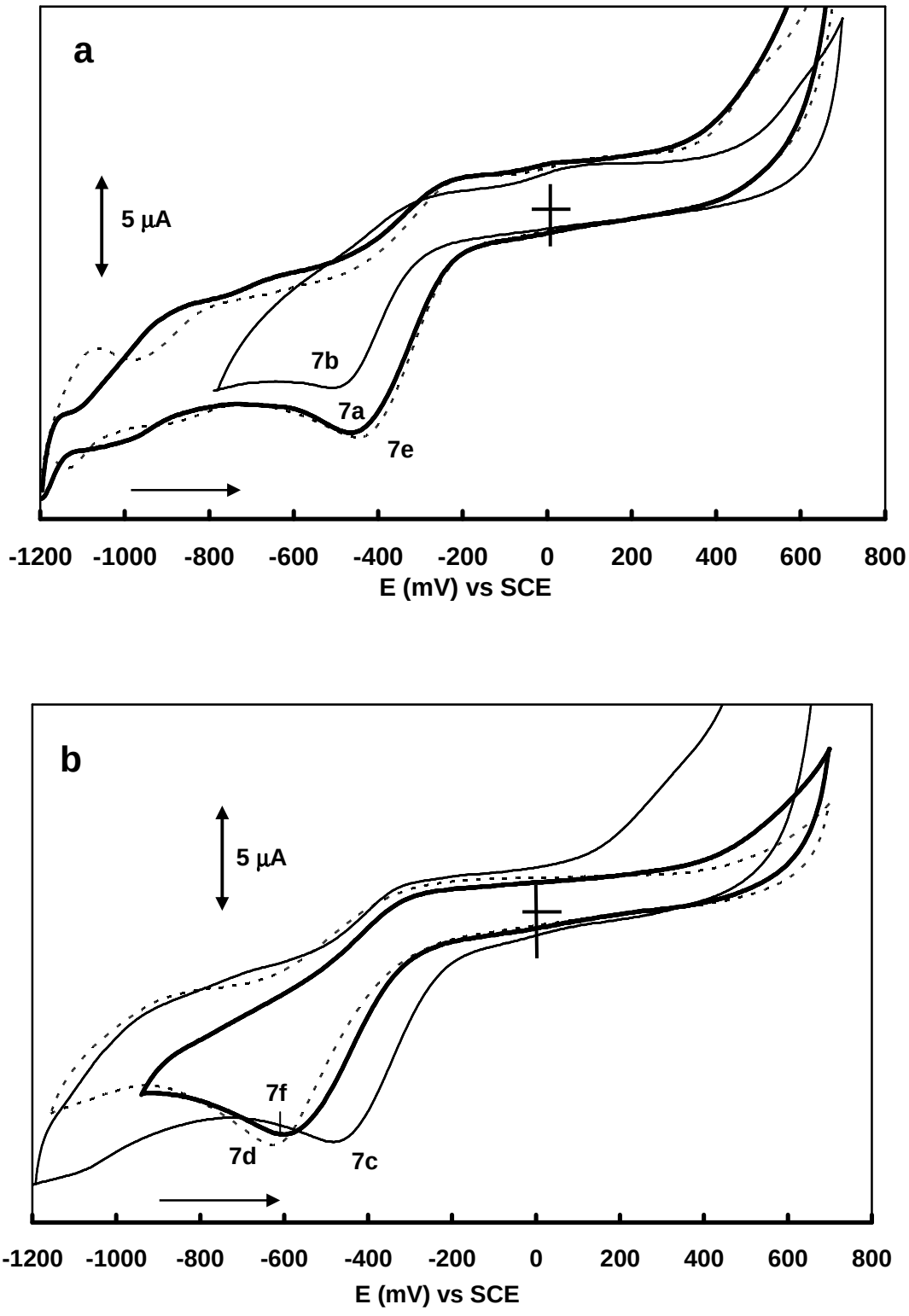

Figure 3.38: Cyclic voltammograms of oxygen reduction in pH 12 for adsorbed MnPc complexes a) 7a, 7b and 7e, b) 7c, 7d and 7f. Scan rate = 50 mV/s. Numbers on the CV scans are complex numbers.

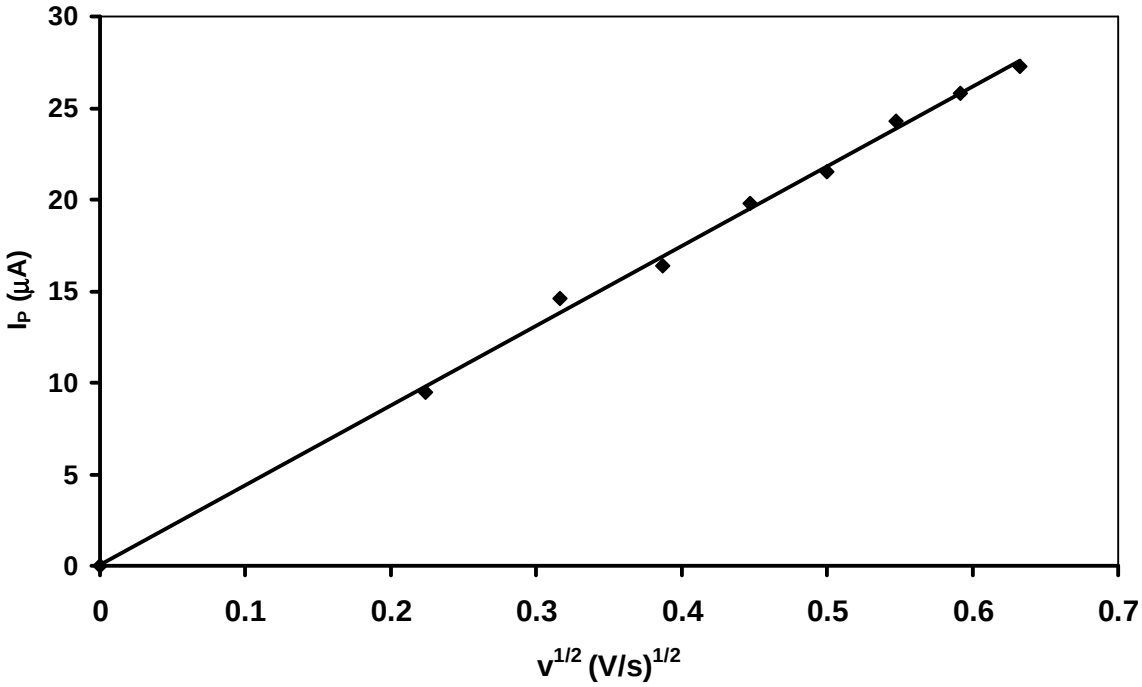

Figure 3.39: Plot of square root of scan rate versus peak current for oxygen reduction on MnPc in pH 12.

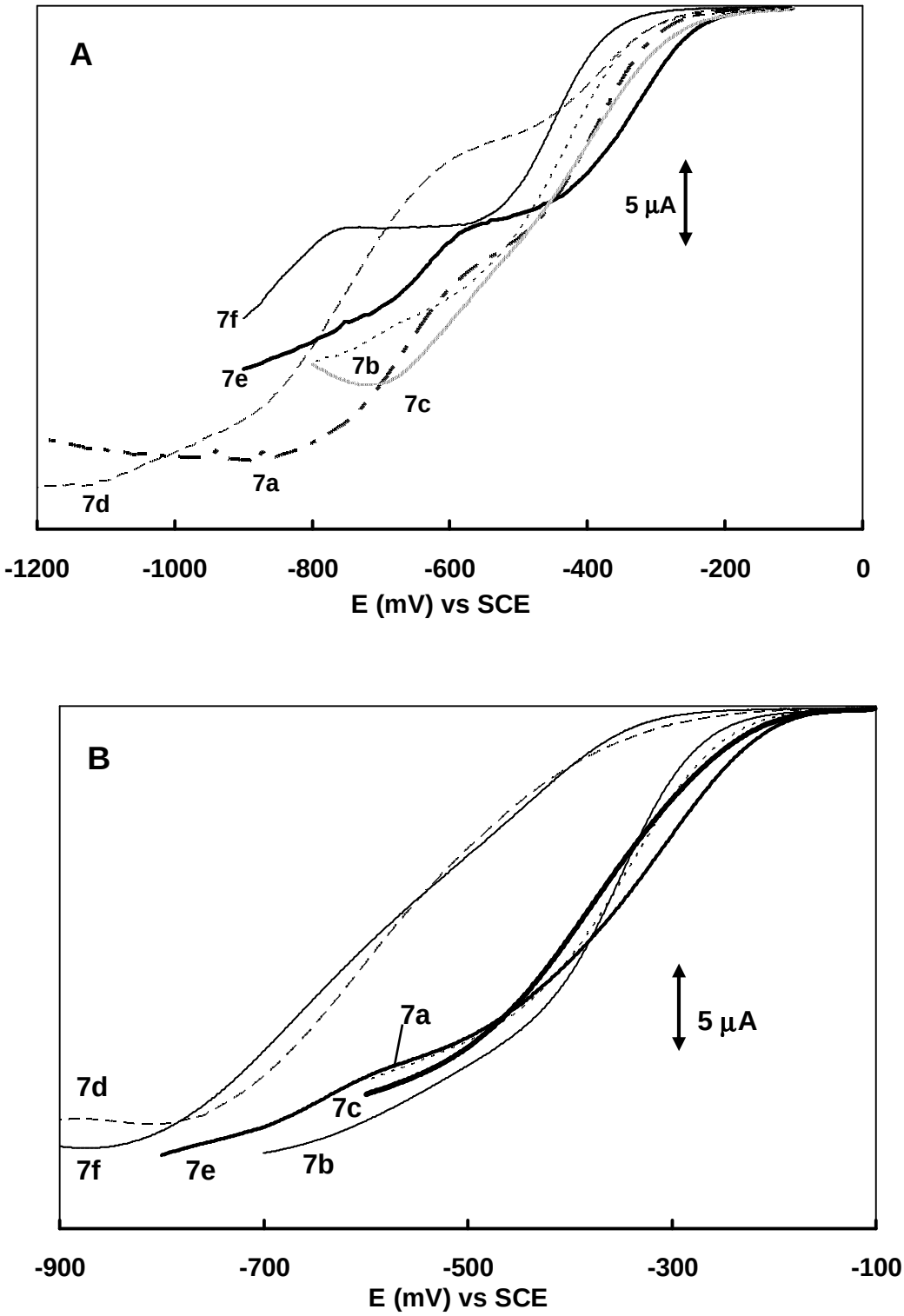

Figure 3.40: Rotating disk electrode voltammograms of adsorbed MnPc complexes in pH a) 5 and b) 12 oxygen saturated solutions at rotation rate of 400 r.p.m and scan rate of 20 mV/s. Numbers on the CV scans are complex numbers.

The number of electrons transferred during oxygen reduction was calculated from the magnitude of limiting current at 400 rotations per minute (r.p.m.). This was based on Levich equation (eq. 3.1), where D, C and v values are 1.67 x 10^{-5}, 1.3 μM and 9.97 x 10^{-3} cm^2/s respectively as reported in literature for oxygen[178,248]. The total number of electrons transferred was calculated to be on average 2 in pHs 1 to 5 and 4 in pHs greater than 5, Table 3.6.

Tafel slopes were calculated from the same RDE data. These were obtained from plots of log $|i_K|$ versus η, based on Tafel equation, eq. 3.3. Calculated Tafel slopes in pH 5 are shown in Table 3.6. The values of the Tafel slopes suggest the involvement of one electron in the rate determining step. However these values are larger than the expected 120 mV/decade in some cases suggesting strong binding of the analyte to the catalyst[80,83]. Electron transfer coefficients, α were calculated from Tafel slopes using eq. 3.4, they were on average close to 0.5 indicating an equal chance of the activated complex to go to the product or reactant side.

The reaction order m was determined using equation 3.26, introduced as eq. 1.14[83] in Chapter 1,

$$\log I = \log I_K + m \log\left(1 - \frac{I}{I_L}\right) \qquad 3.26$$

where symbols have their usual meaning. Log I versus log $(1 - I/I_L)$ could not be plotted because RDEs could not be recorded at various rotation speeds due to loss of adsorbed catalysts from the electrode surface. The reaction order was found to be one for all studied complexes in the pH range 1 – 13, by substituting variables in eq. 3.26. I_L values were taken from the plateau of

the RDE voltammograms of oxygen reduction reaction at 400 r.p.m whereas I values were taken from the same RDE plot at the oxygen reduction peak potential, determined from cyclic voltammograms; these values are listed in Table 3.6 for reactions conducted in pHs 5 and 12. It should be noted that eq. 3.26 was used for determintation of reaction order instead of 3.2 where log of peak current is plotted against log of analyte concentration because concentration of oxygen could not be varied and measured accurately.

Rate constants of cathodic oxygen reduction reaction were determined using equation 3.27, which was introduced as eq. 1.11 in Chapter 1,

$$i_K = nFCAk_c \qquad 3.27$$

where symbols have their usual meaning. The electron transfer constant k_c was found to be in the 10^{-5} range (Table 3.6) for all complexes in the pH range studied indicating slow reaction kinetics. The obtained kinetic parameters are used to derive a mechanism for oxygen reduction reaction electrocatalyzed by manganese phthalocyanine complexes that will be provided below.

3.4.4 Oxygen reduction on a selection of CoPc and FePc complexes

Complexes selected for use as electrocatalysts of oxygen reduction were CoPc **6a**, CoTPhPyrPc **6b**, CoTEThPc **6c**, FePc **8** and $FePc(Cl)_{16}$ **9**. The activity of unsubstituted complexes **6a** and **8** will be compared to that of MnPc **7a** to determine the effect of central metal on catalytic efficiency. The other substituted complexes offer investigation of substituent effect.

3.4.4.1 Characterization of adsorbed MPc complexes

For characterization purposes, cyclic voltammograms of adsorbed MPc complexes were run on GCE in nitrogen-purged buffer solutions in the pH range 1 - 13. MPc redox processes were observed in pH 7 buffer solution only for unsubstituted complexes (CoPc and FePc), Fig. 3.41. It is usually difficult to observe redox couples of MPcs adsorbed onto glassy carbon electrodes because the electrode material is not as porous as ordinary pyrolytic graphite for instance, that was used for characterization of **6b** and **6c** in section 3.1.1. $Co^{III/II}$ process was observed at ~0.2 V/(SCE), $Co^{II/I}$ at ~-0.69 V/(SCE) and $Co^{I}Pc^{-2}/Co^{I}Pc^{-3}$ was observed at ~-0.93 V/(SCE), Fig. 3.41a. Process X is unknown, it has been observed by other researchers and has not been properly assigned[178]. For FePc, $Fe^{III/II}$ process was observed at ~0.055 V/(SCE), $Fe^{II/I}$ at ~-0.71 V/(SCE) and $Fe^{I}Pc^{-2}/Fe^{I}Pc^{-3}$ was at ~-0.95 V/(SCE), Fig. 3.41b and Table 3.7. All the peak assignments are in relation to literature reports[63,79]. No clear redox processes were observed for $FePc(Cl)_{16}$.

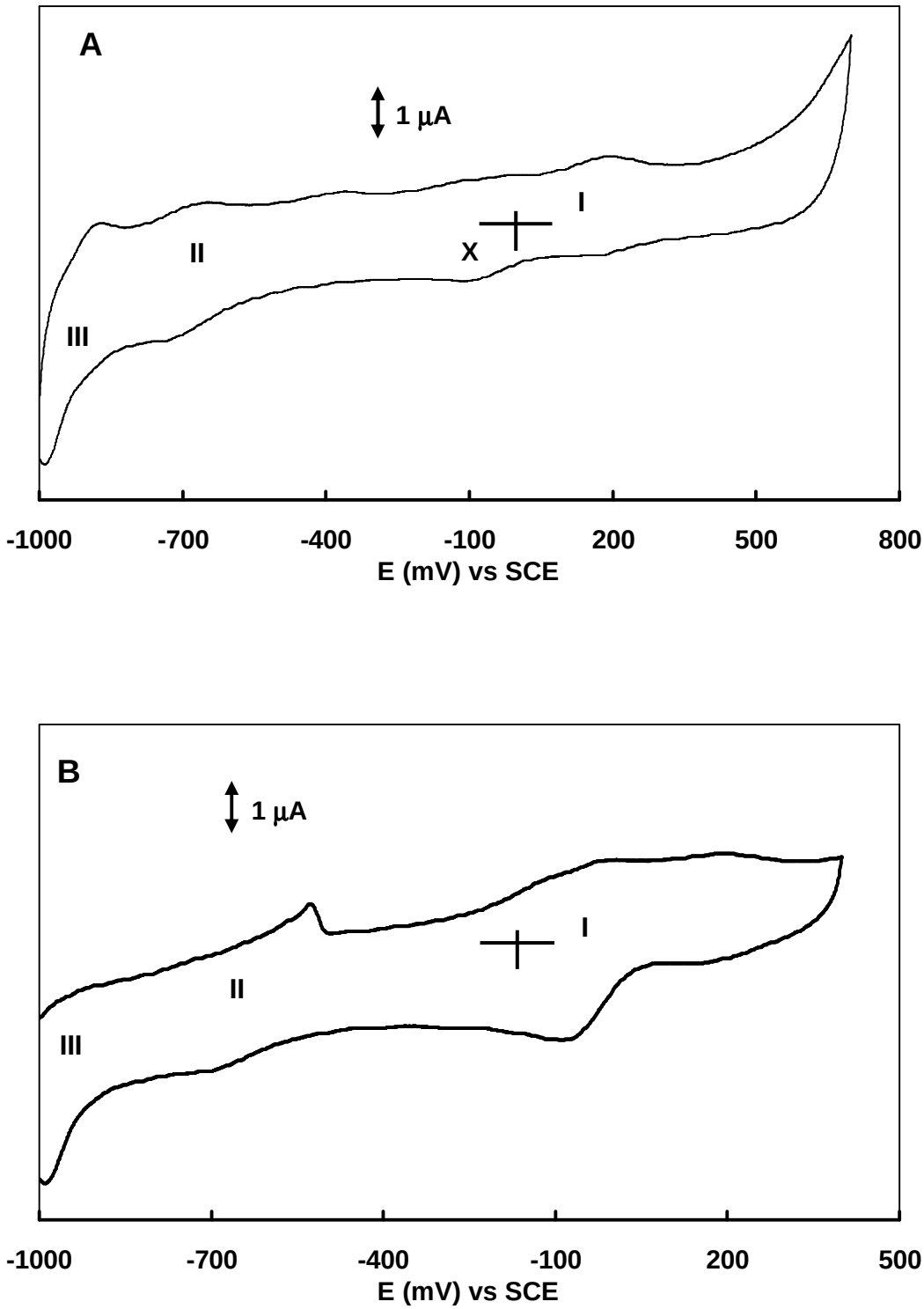

Figure 3.41: Cyclic voltammograms in nitrogen-purged pH 7 buffer solution of glassy carbon electrodes modified by adsorption of a) CoPc 6a and b) FePc 8. Scan rate = 50 mV/s.

Surface coverage, Γ_{MPc} of CoPc and FePc adsorbed films was probed by recording their CVs at different scan rates based on equation 3.13. Surface coverage was calculated from the plots of I_p versus v, Fig. 3.42 to be 6.58 and 7.94 x 10^{-10} for CoPc and FePc respectively, Table 3.7. Surface coverage values determined in section 3.1.1 are also listed in Table 3.7. Values in the 1 x 10^{-10} range indicate monolayer thickness. Moreover, linearity of I_p versus v plots indicates surface confined adsorbed species[158], confirming adsorption of the MPc complexes.

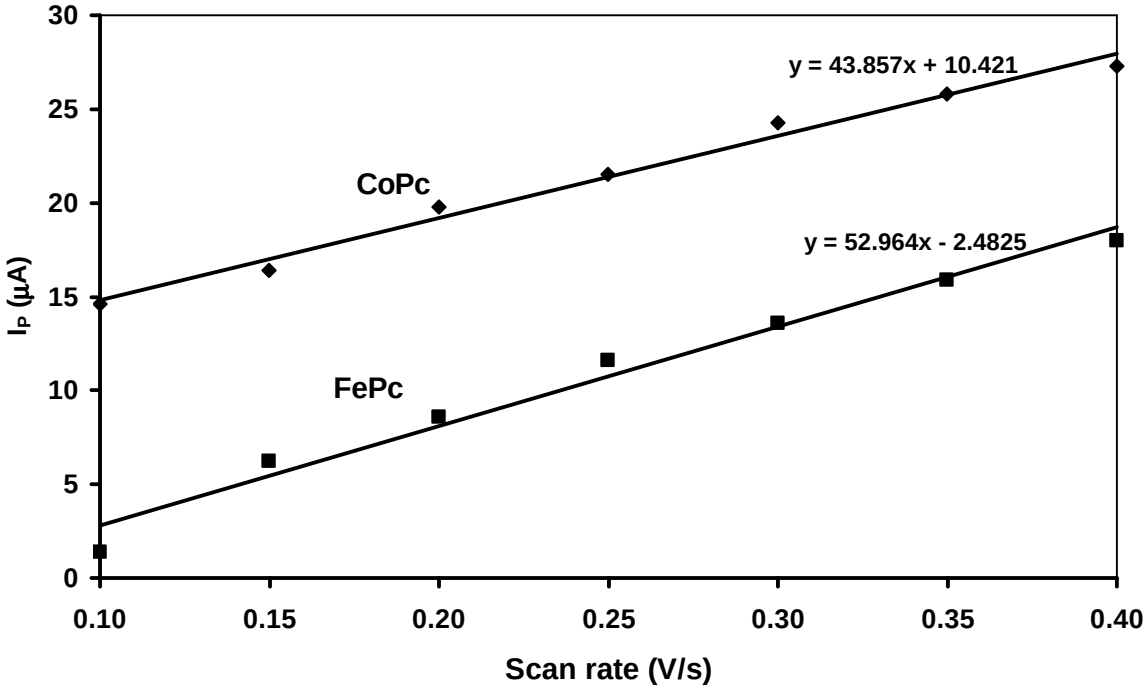

Figure 3.42: Plots of I_p versus ν for $M^{III/II}$ peak of a) CoPc and b) FePc adsorbed on GCE in pH 7 buffer solution.

3.4.4.2 Oxygen reduction

Oxygen reduction reactions were performed in buffer solutions of pH range 1 - 13 on bare and MPc-adsorbed glassy carbon electrodes. Data from pH 2, 7 and 12 is shown in Table 3.7 as examples. In pH 7, oxygen reduction

occurred at ~-0.64 V/(SCE) on unmodified glassy carbon electrode. However, it occurred at -0.082, -0.41, -0.40, -0.090, and -0.19 V/(SCE) on CoPc **6a**, CoTPhPyrPc **6b**, CoTEThPc **6c**, FePc **8**, $FePc(Cl)_{16}$ **9** modified glassy carbon electrodes respectively, Fig. 3.43. The fact that the reaction occurs at less negative potentials on modified electrodes (Table 3.7) indicates that the adsorbed complexes are indeed electrocatalysts, as is known for MPc complexes. The trend of MPcs in increasing catalytic efficiency based on the least negative oxygen reduction potentials is as follows: **6a** > **8** > **9** > **6c** ~ **6b** in pH 7, and **8** > **6a** > **9** > **6c** ~ **6b** in pH 12. Thus the MPc catalytic efficieny is pH dependant.

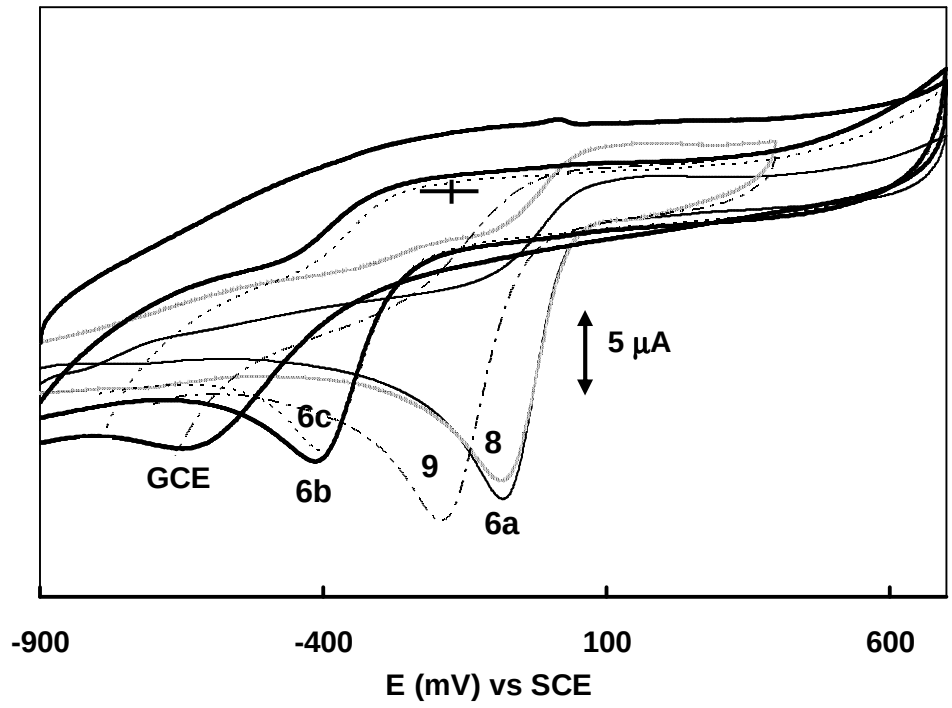

Figure 3.43: Cyclic voltammograms of oxygen reduction reaction in oxygen saturated pH 7 buffer solutions on GCE, CoPc 6a, CoTPhPyrPc 6b, CoTEThPc 6c, FePc 8 and $FePc(Cl)_{16}$ 9. Scan rate = 50 mV/s.

Metal couples involved in catalysis appear at the proximity of oxygen reduction peaks. Metal redox processes were assigned on comparison with

literature reports as stated above. The Co(II/I) redox process of adsorbed CoPc was observed at ~-0.69 V/(SCE) while the Co(III/II) process was at ~0.2 V/(SCE) in pH 7 (Fig. 3.41a). For FePc, the Fe(III/II) redox process was observed at 0.06 V/SCE while that of Fe(II/I) was at ~-0.71 V/SCE, Fig. 3.41b. In both cases, oxygen reduction peaks were situated in between M(III/II) and M(II/I) peaks (Fig. 3.43), but since the oxygen reduction peaks lie negative of the M(III/II) redox processes, it can be concluded that the M(III/II) redox processes are involved in catalysis of oxygen reduction.

Oxygen reduction peak position was observed to vary with pH as shown in Fig. 3.44. In acidic media, slope of E_p vs pH is 60 mV/pH on average was observed but in neutral and alkaline media, the potential remained constant with increase in pH. The observed trend is in agreement with literature reports[178], and it was attributed to pH dependence of a product formed in acidic media as opposed to the pH-independent one formed in alkaline conditions. Plots of peak current versus square root of scan rate for the reduction of oxygen were linear, similar to Fig. 3.39, for all studied complexes in the pH range 1 - 13 indicating that oxygen reduction reaction is diffusion-controlled.

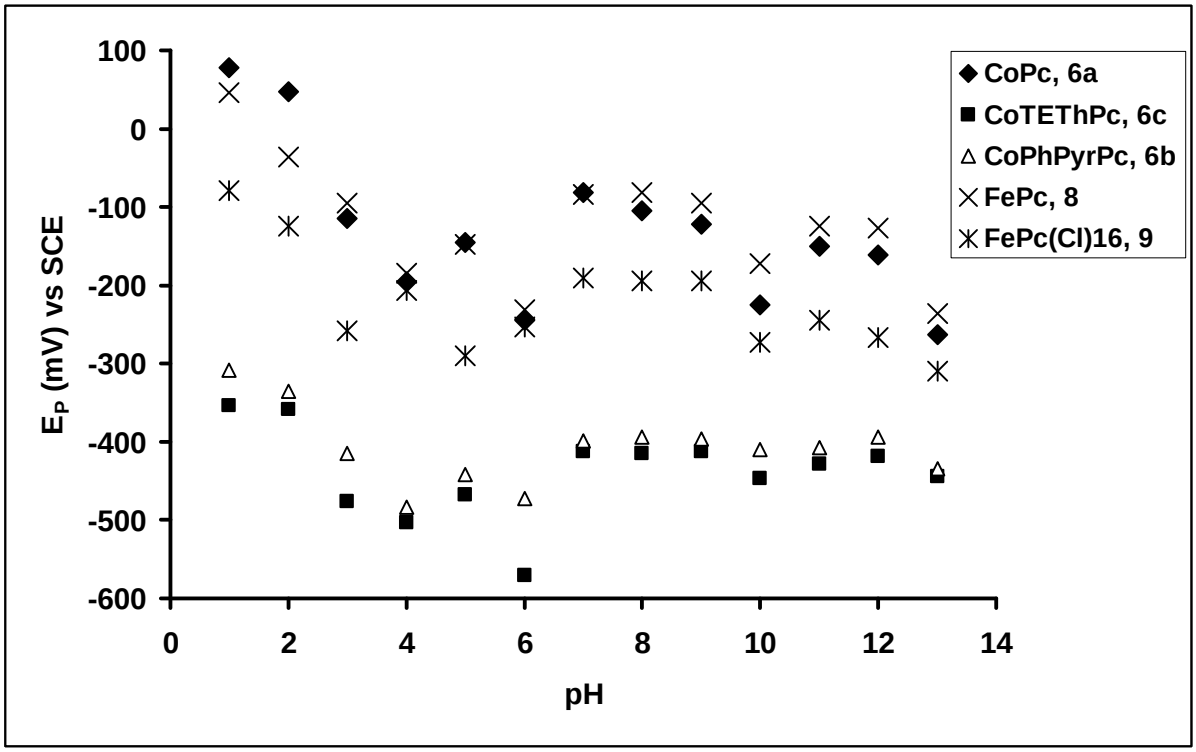

Figure 3.44: Pourbaix diagram of oxygen reduction reaction electrocatalyzed by complexes 6a, 6b, 6c, 8 and 9.

Rotating disc electrode (RDE) experiments were conducted to further elucidate studied reactions. These experiments were conducted in buffer solutions of pH 1 - 13 at 400 rotations per minute (r.p.m.). Fig. 3.45 shows RDE voltammograms of all complexes in pH 12. Only single runs at low rotation speeds were done because the catalyst was lost from the surface. However, runs were done in triplicates and averages are reported.

The number of electrons transferred during oxygen reduction was calculated from the magnitude of limiting current at 400 r.p.m, from rotating disc electrode voltammograms based on Levich equation, eq. 3.1. The total number of electrons transferred was calculated to be 2 in all pHs for the substituted cobalt complexes CoTPhPyrPc **6b** and CoTEThPc **6c**. However, for CoPc **6a**, FePc **8** and $FePc(Cl)_{16}$ **9**, it was found to be 2 in pHs below 5,

above this pH the number of electrons was 4. Two electron transfer reaction leads to formation of hydrogen peroxide while four electron transfer leads to formation of water. This shows that unsubstituted CoPc **6a**, FePc **8** and $FePc(Cl)_{16}$ **9** are best catalysts as they result in a complete four-electron oxygen reduction.

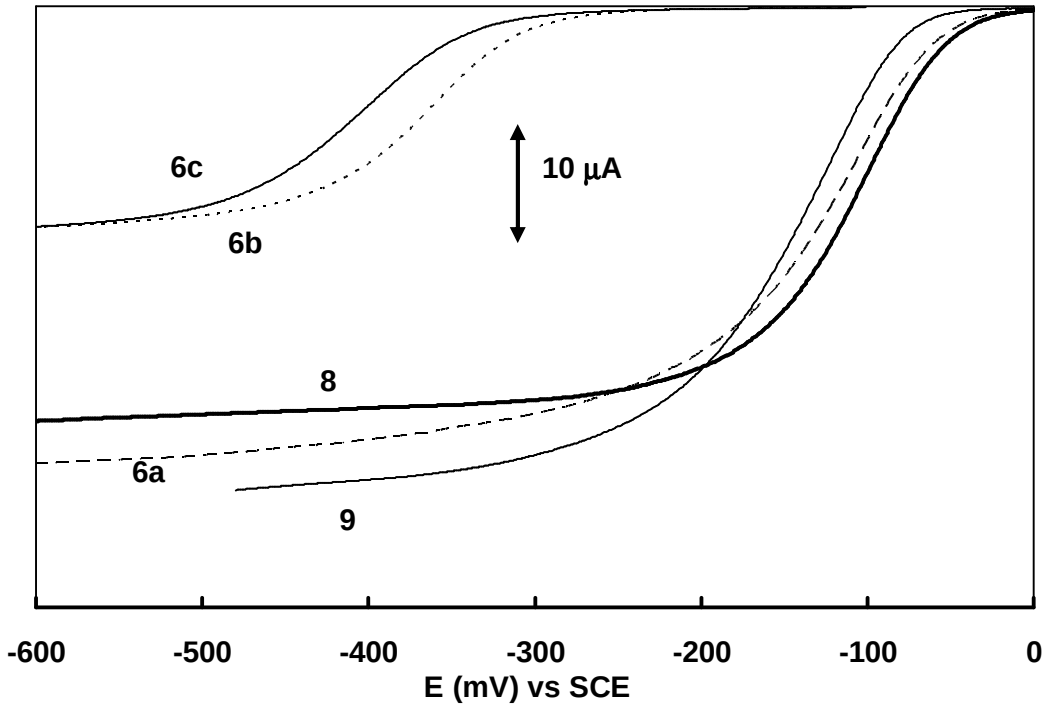

Figure 3.45: Rotating disc electrode voltammograms of oxygen reduction reaction in pH 12, on adsorbed MPc complexes at rotation rate of 400 r.p.m. and scan rate of 20 mV/s. Numbers on the CV scans are complex numbers.

Tafel slopes were obtained from Tafel plots (Fig. 3.46, plots of log $|i_K|$ versus η), based on the RDE data. Calculated Tafel slopes in pH 2, 7 and 12 are shown in Table 3.7. All complexes had slopes in the range 100 - 175 mV/decade in pH range of 1 – 4, Table 3.7a (pH 2). In neutral and slightly basic solutions, unsubstituted CoPc **6a** and FePc **8** exhibited slopes close to 60 mV/decade while those of their substituted counterparts were close to 120

mV/decade, Table 3.7b (pH 7). In strongly alkaline solutions, CoPc **6a**, FePc **8** and $FePc(Cl)_{16}$ **9** had Tafel slopes close to 60 mV/decade whereas for substituted CoPcs, CoTPhPyrPc **6b** and CoTEThPc **6c**, Tafel slopes were close to 120 mV/decade, Table 3.7c.

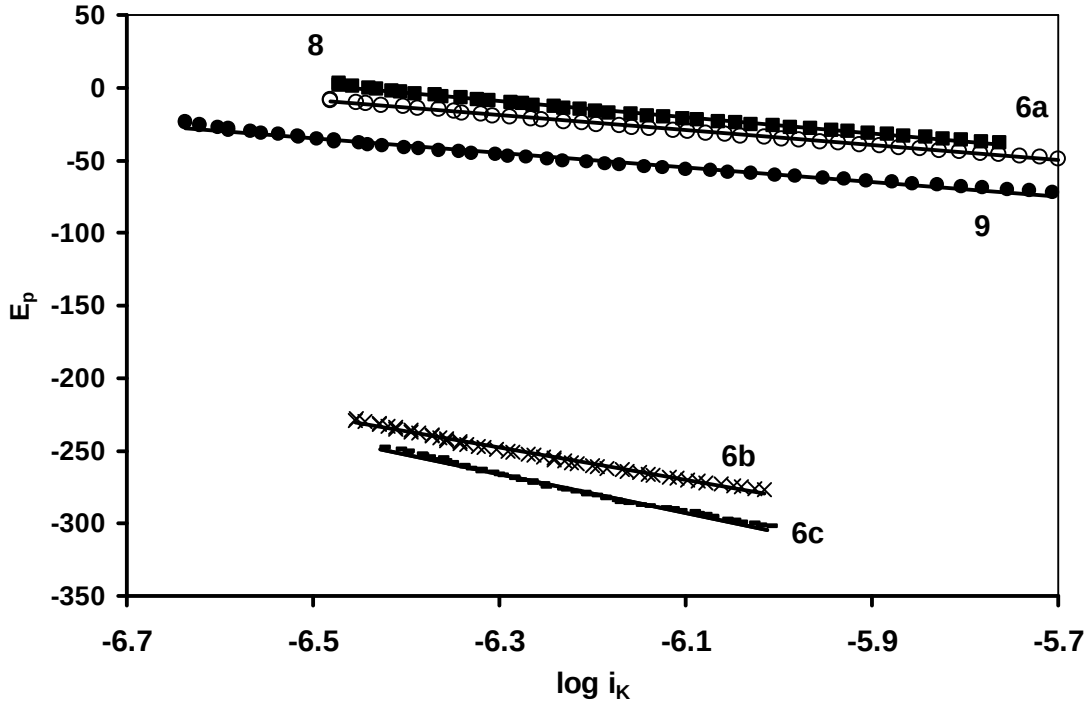

Figure 3.46: Tafel slopes of oxygen reduction reaction electrocatalyzed by complexes 6a, 6b, 6c, 8 and 9 in pH 12 buffer solutions.

Thus substituted cobalt complexes (**6b** and **6c**) exhibited Tafel slopes equal to approximately 120 mV/decade and two electron transfer in the pH range studied. For CoPc, FePc and $FePc(Cl)_{16}$ in pH above 4, number of electrons transferred was 4 and Tafel slopes were ~60 mV/decade. These complexes only exhibited slopes of ~120 mV/decade in acidic solutions where only two electrons were transferred. A Tafel slope of 120 mV/decade suggests the involvement of one electron in the rate determining step whereas that of 60 mV/decade indicates that the fast electron transfer is followed by a slow chemical step[9,102]. However, for some complexes, Tafel slopes are larger than

the expected 120 mV/decade suggesting strong binding of the analyte to the catalyst[80,83].

Electron transfer coefficients (α) were calculated from Tafel slopes using equation 3.4 described above for an irreversible process. The calculated values for pH 2, 7 and 12 are shown in Table 3.7. Generally, when one electron is involved in the rate-determining step (i.e. $n_\alpha = 1$), which is the case for oxygen reduction reaction, α is equal to 0.5 for Tafel slopes of 120 mV/decade. But for slopes of 60 mV/decade, α is equal to 1. α valued at approximately 0.5 indicates that there is an equal probability that the reaction activated transition state can form either products or reactants. This holds for substituted cobalt complexes **6b** and **6c** in the pH range studied and for other complexes, **6a**, **8** and **9** in pHs below 5, Table 3.7.

Transfer coefficients values of approximately 1 were found for CoPc **6a**, FePc **8** and $FePc(Cl)_{16}$ **9** in pHs greater than 5, shown for pHs 7 and 12 in Table 3.7. This implies that the reaction equilibrium favours product formation only. This therefore shows that the transfer coefficient is pH dependant for these complexes, in agreement with a literature report[178]. The reaction order was determined using equation 3.26 described above and it was found to be one on average for all studied complexes in pH range 1 - 13. Heterogeneous electron transfer rate constants k_c of cathodic oxygen reduction reaction were determined using RDE data based on eq. 3.27. k_c was found to be in the 10^{-5} range for all complexes in the pH range studied (Table 3.7), indicating that reaction kinetics are slow.

Table 3.7: Oxygen reduction data for complexes 6a, 6b, 6c, 8 and 9 in pHs 2, 7 and 12.

A. pH 2

MPc	Γ_{MPc} (10^{-10})	E_P V/(SCE)	Total no. of e^-s	Tafel Slope mV/decade	k_c (10^{-5})	α
6a	6.58	0.10	2.3	113	3.38	0.52
8	7.94	0.10	2.4	107	3.48	0.55
9	-	-0.17	2.1	152	3.99	0.39
6b	9.85	-0.30	2.2	150	3.56	0.39
6c	1.23	-0.39	2.3	173	3.66	0.34

B. pH 7

MPc	E_P V/(SCE)	Total no. of e^-s	Tafel Slope mV/decade	k_c (10^{-5})	α
6a	-0.082	3.7	60	1.73	0.96
8	-0.090	3.7	60	2.74	0.96
9	-0.19	3.5	95	3.50	0.62
6b	-0.41	2.1	136	2.92	0.43
6c	-0.40	2.0	148	3.16	0.40

C. pH 12

MPc	E_P V/(SCE)	Total no. of e^-s	Tafel Slope mV/decade	k_c (10^{-5})	α
6a	-0.14	3.8	56	2.77	1.0
8	-0.13	3.5	52	2.65	1.1
9	-0.25	3.9	51	2.87	1.2
6b	-0.43	1.9	111	3.94	0.53
6c	-0.42	1.9	133	3.71	0.44

3.4.5 Mechanism of oxygen reduction

Oxygen reduction is an inner sphere process, meaning the reactant must interact with an active site on the surface of the electrode[157,184]. Oxygen is an acceptor while MPc is a donor. The interaction becomes possible when the symmetry of the involved frontier orbitals is right and relative energy levels are close. The 2p electrons of oxygen interact with electrons in the partially filled d-orbitals of the metal of the MPc, accompanied by intramolecular electron transfer from the metal to oxygen. This happens between molecular orbital (MO) of the central metal M in MPc complexes and oxygen; this interaction is more prominent for Mn compared to other transition metals such as Fe and Co because Mn has lower energy d-orbitals. Energy gap between participating MOs of oxygen and MnPc is described in terms of hardness[157,184]. This is expressed as half the difference between lowest unoccupied molecular orbital of the acceptor (oxygen in this case) and highest occupied molecular orbital of the donor (MPc in this case); $\frac{1}{2}\{E_{LUMO(A)} - E_{HOMO(D)}\}$[157,184]. The larger the gap, the higher the hardness and the more stable the system is, hence low reactivity.

Substituents on the MPc have an effect on the MO energy levels. Electron-withdrawing groups lower the energy of the MO of MPc, while their electron-donating counterparts increase it[189]. Lowering of energy levels of MO of MPc minimizes the gap between MO of MPc and that of oxygen. The system becomes soft, the interaction is enhanced and thus reactivity increases. It is therefore theoretically expected that electron withdrawing ligands will increase catalytic activity of MPcs towards oxygen reduction.

Electron-donating substituents are expected to have an opposite effect. Log k (k = rate constant) of oxygen reduction catalyzed by CoPcs with electron donating substituents was found to decrease when plotted against sum of Hammett parameters of the substituents[184].

In this work, effect of substituents on electrocatalytic activity towards oxygen reduction was investigated by comparison of reaction peak potentials. For the MnPc complexes in this work, the ease of reduction of oxygen in pH 12 based on reaction peak potentials followed the order, stated above: **7a** (-0.45) **≈ 7c** (-0.47) **≈ 7e** (-0.43) > **7b** (-0.51) > **7f** (-0.58) > **7d** (-0.63), showing that the unsubstituted complex **7a**, is a better catalyst than for example **7b** (which contains electron-donating substituents) in agreement with literature. For other complexes FePc **8** and $FePc(Cl)_{16}$ **9**, peak potentials were at -0.13 and -0.25 V/(SCE) respectively, in pH 12. It is therefore obvious that this electron withdrawing group Cl^- does not enhance electrocatalytic activity since oxygen reduction occurs at more negative potentials. In the case of CoPc **6a** and its substituted counterparts CoTPhPyrPc **6b** and CoTEThPc **6c**, oxygen reduction occurred in pH 12 at -0.14, -0.43 and -0.42 V/(SCE) respectively. This shows that electrocatalytic activity was greatly reduced in the presence of substituents.

Similarly the effect of central metal of the phthalocyanine catalysts was probed by comparison of oxygen reduction peak potentials. In pH 12, oxygen reduction peaks were observed at -0.45 (Table 3.6), -0.13 and -0.14 V/(SCE) (Table 3.7) for MnPc, CoPc and FePc, respectively. The catalytic activity trend is more conspicuous in pH 7 where oxygen reduction peaks are observed at -0.49, -0.082 and -0.090 V/(SCE) for MnPc, CoPc and FePc, respectively. This

is not in agreement with perturbation theory wherein Mn is expected to exhibit the highest electrocatalytic activity by virtue of good orbital overlap with oxygen, compared to Fe and Co. However, a similar trend in catalytic activity of Mn, Fe and Co phthalocyanines towards reduction of oxygen has been observed before[171].

Interaction of oxygen with MPcs

It has been reported that when MnPcs interact with oxygen, either the superoxide or the μ-oxo-bridged dimer are formed[249,250]. This has been confirmed with UV/Vis spectroscopy[251,252]. Furthermore, it has been reported that oxygen adsorption on the electrode can involve electron transfer leading to its activation as shown in Scheme 3.6, eq. 3.28. It can also occur without electron transfer (eq. 3.29); the former has been proven spectroscopically[253].

$$S + O_2 = S\text{-}O_2^- \qquad 3.28$$

$$S + O_2 = S\text{-}O_2, \qquad 3.29$$

where S is the electrode surface.

Scheme 3.6: Oxygen adsorption onto an electrode.

In this study, formation of adducts upon interaction of MPc complexes with oxygen was probed using UV/Vis spectroscopy, Fig. 3.47. In all MnPc complexes, the starting species is the $Mn^{III}Pc$ as evidenced by the red shifted Q band with λ > 700 nm. Oxygen was bubbled to $Mn^{III}Pc$ solutions and no shifts of spectral bands were observed for all MnPc complexes, curves ii. Fresh solutions of the complexes were reduced using sodium borohydride,

curves iii, and oxygen bubbled, curves iv. After reduction (and before bubbling of oxygen, curves iii), two peaks are observed for complexes **7a**, **7d**, **7e** and **7f**. From the well documented UV/Vis spectra of MnPc complexes[25], the low energy peak ranging from 674 to 688 nm, is assigned to $Mn^{II}Pc$ species for complexes **7a**, **7d**, **7e** and **7f**. This peak was however very weak for complex **7e**.

The higher energy peak ranging from 615 to 626 nm (for **7a**, **7d**, **7e** and **7f**) is assigned to the μ-oxo complex. Decomposition was observed for complex **7b** on reduction with sodium borohydride, hence its spectra are not included in Fig. 3.47. For complex **7c**, the μ-oxo complex was observed as the main peak at 641 nm, even before reduction. When oxygen was bubbled to the reduced species, the $Mn^{II}Pc$ peaks generally decreased in intensity, and the peak due to the μ-oxo species increased in intensity or remained the same. Based on the ability to form μ-oxo species (which is related to the ability to bind and reduce oxygen), as judged by the relative intensities of the μ-oxo dimer and Mn(II)Pc species, the MnPc complexes may be ranked as follows: **7c** > **7e** > **7d** > **7a** and **7f.** This is related to the ease of oxygen reduction discussed above (**7a ≈ 7c ≈ 7e** > **7b** > **7f** > **7d**) in that complexes **7c** and **7e** are high on both trends, while complexes **7d** and **7f** are low.

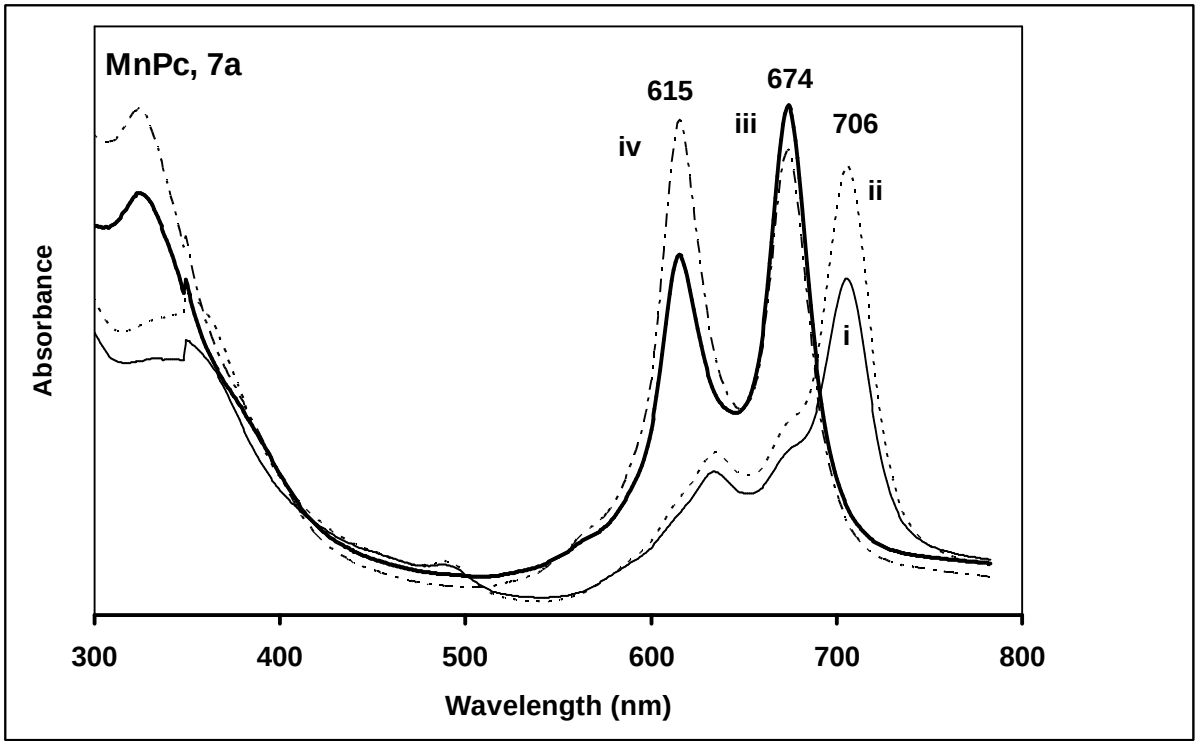
MnPc, 7a
615
674
706
iv
iii
ii
i
Absorbance
300
400
500
600
700
800
Wavelength (nm)

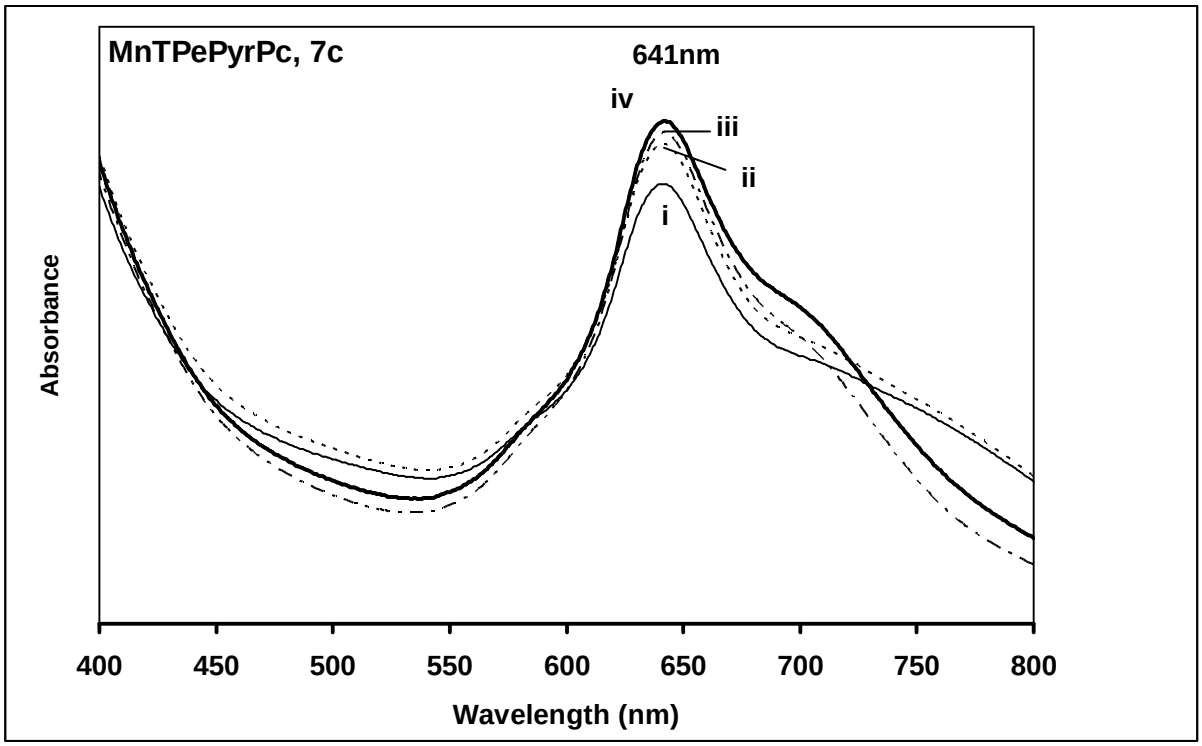
MnTPePyrPc, 7c
641nm
iv
iii
ii
i
Absorbance
400
450
500
550
600
650
700
750
800
Wavelength (nm)

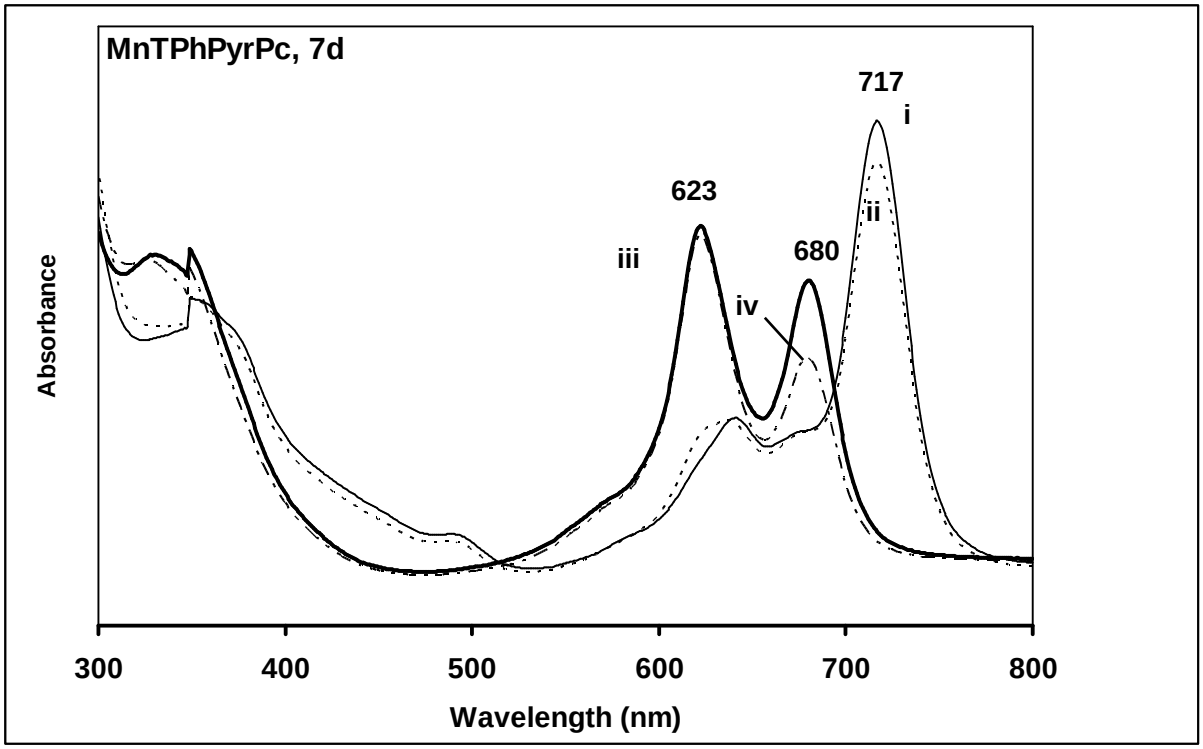
MnTPhPyrPc, 7d
717
i
623
ii
iii
680
iv
Absorbance
300
400
500
600
700
800
Wavelength (nm)

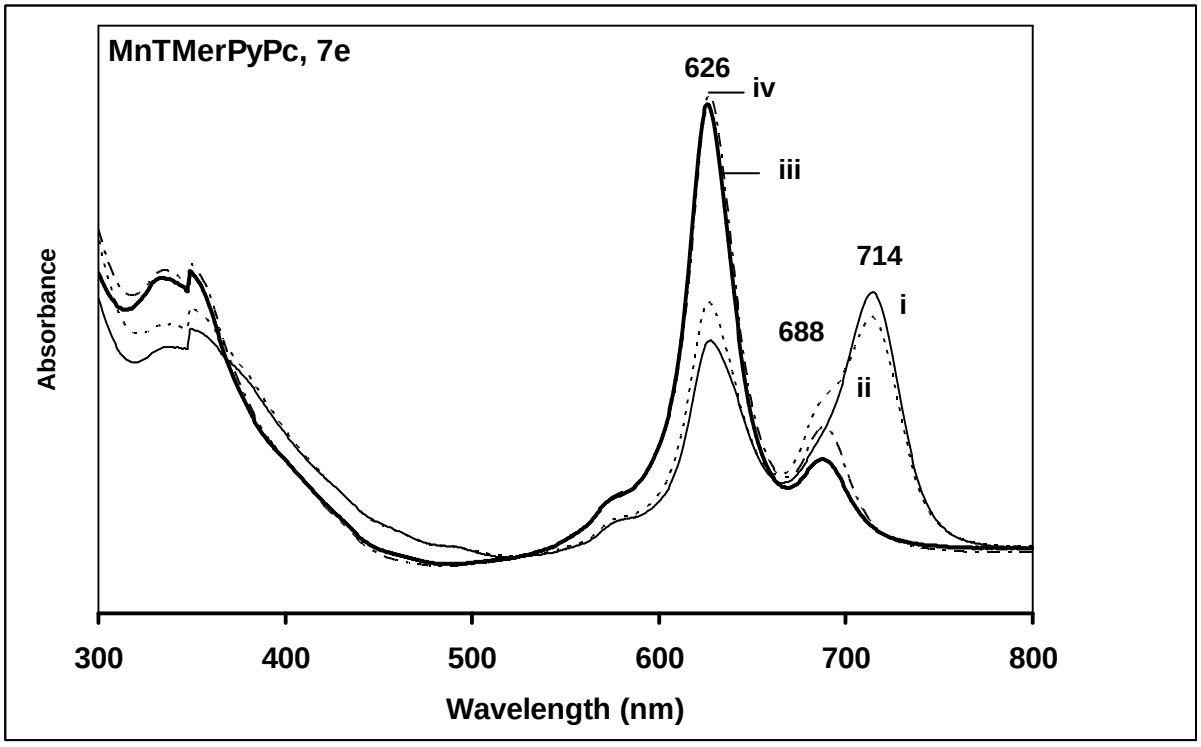
MnTMerPyPc, 7e
626
iv
iii
714
i
688
ii
Absorbance
300
400
500
600
700
800
Wavelength (nm)

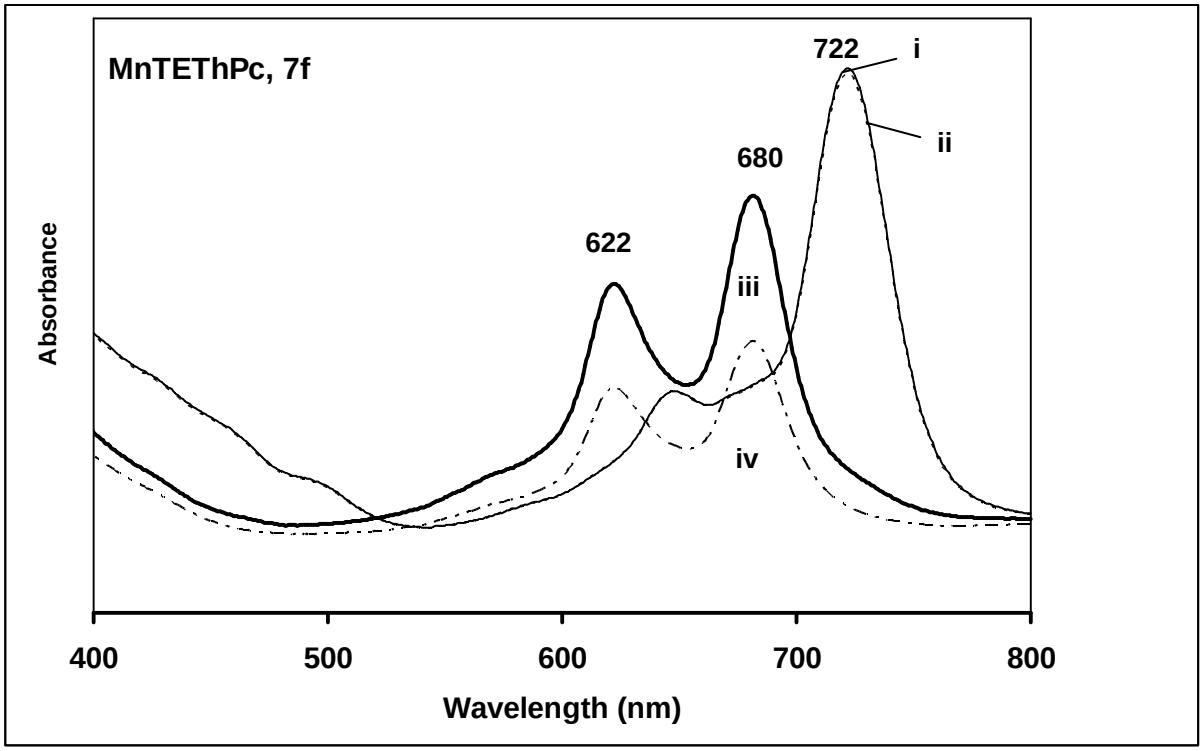

Figure 3.47: UV/Visible spectra of complexes 7a, 7c to 7f in DMF. i) starting spectrum, ii) oxygen bubbled to (ii), iii) $NaBH_4$ added to (i), and iv) oxygen bubbled to (iii).

Based on the following observations: (i) in acid and slightly alkaline solutions, two peaks were observed on cyclic voltammograms for oxygen reduction, each due to two electron reduction of oxygen to hydrogen peroxide, and subsequently to water, (ii) Tafel plots proved that one electron transfer occurs during the rate determining step, (iii) protons are involved during the electron transfer and (iii) spectroscopy proved the formation of μ-oxo complexes which results from $O_2Mn^{II}Pc$ adduct and that this adduct is best represented as $O_2^{-}Mn^{III}Pc$[25], the following mechanism for oxygen reduction on MnPc complexes and formation of hydrogen peroxide is proposed (Scheme 3.7):

$$Mn^{III}Pc + e^{-} \rightarrow Mn^{II}Pc \quad 3.30$$

$$Mn^{II}Pc + O_2 \rightarrow (O_2)Mn^{II}Pc \rightarrow (O_2^{-})Mn^{III}Pc \quad 3.31$$

$$(O_2^{-})Mn^{III}Pc + H^{+} \rightarrow (O_2H)\,Mn^{III}Pc \quad 3.32$$

$$(O_2H)Mn^{III}Pc + e^{+} + H^{+} \rightarrow Mn^{III}Pc + H_2O_2 \quad 3.33$$

where MnPc represents complexes **7a** – **7f**.

Scheme 3.7: Mechanism of oxygen reduction catalyzed by MnPc complexes.

For CoPc and FePc complexes, their interaction with oxygen was also probed using UV/Vis spectroscopy (Fig. 3.48), just like MnPc complexes. UV/Vis spectra of all the complexes were recorded in DMF. Q bands of CoPc **6a**, CoTPhPyrPc **6b** and CoTEThPc **6c** were observed at 660, 666 and 665 nm respectively. No spectral changes were observed upon bubbling oxygen into the Co(II)Pc solutions. Chemical oxidation with bromine caused a Q-band shift of **6a** from 660 to 665 nm, indicating oxidation from Co(II) to Co(III) species[25,63]. Oxygen was then bubbled into the Co(III)Pc solution but no changes were observed, except the peak intensified probably due to enhanced solubility. For the substituted CoPc complexes, similar spectral changes were observed, Fig. 3.48. Oxidation using bromine led to a Q-band shift from 666 to 675 nm for CoTPhPyrPc **6b**, and a shift from 665 to 670 nm for CoTEThPc **6c.** Bubbling of oxygen to the Co(III) solutions caused an increase in peak intensity. These observations show no coordination of oxygen with the CoPc complexes.

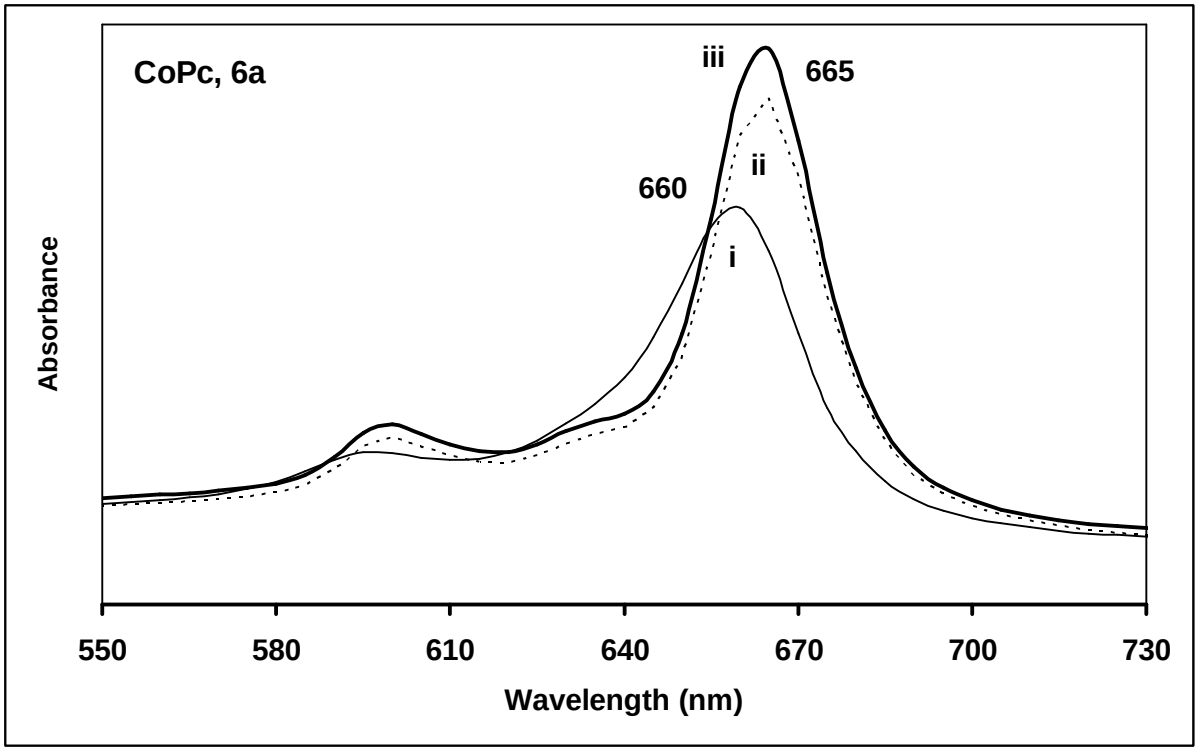
CoPc, 6a
iii
665
ii
660
i
Absorbance
550
580
610
640
670
700
730
Wavelength (nm)

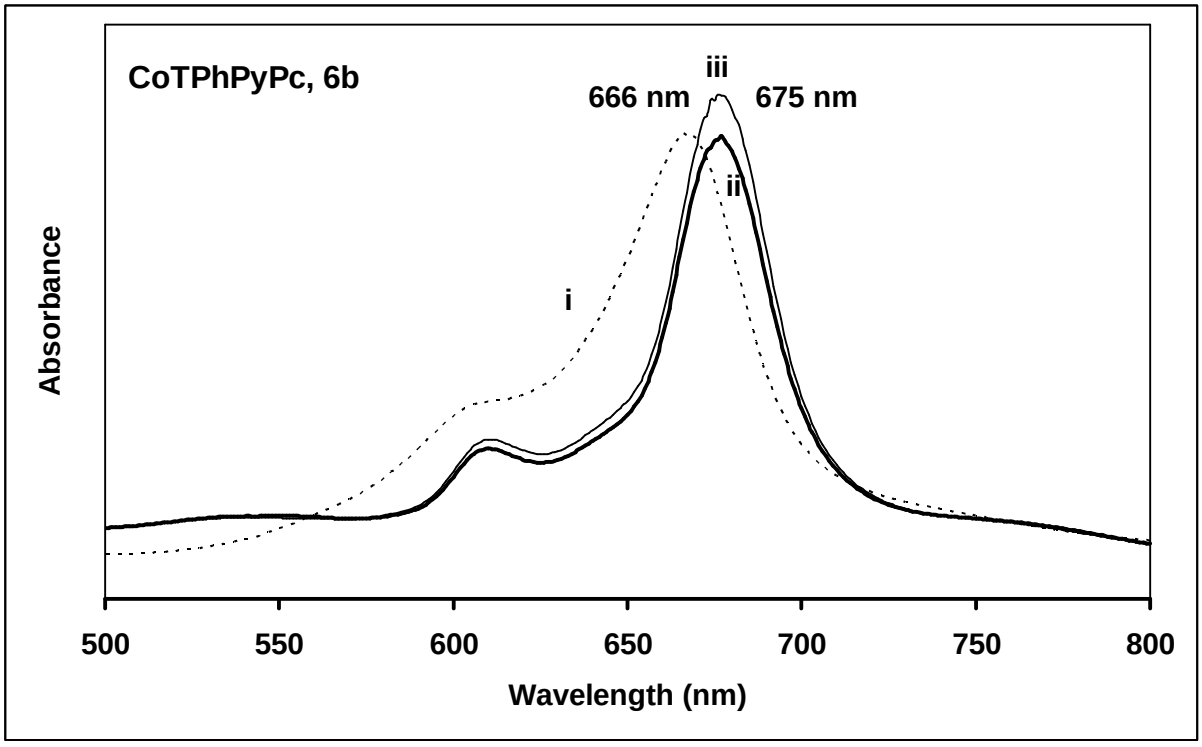
CoTPhPyPc, 6b
iii
666 nm
675 nm
ii
i
Absorbance
500
550
600
650
700
750
800
Wavelength (nm)

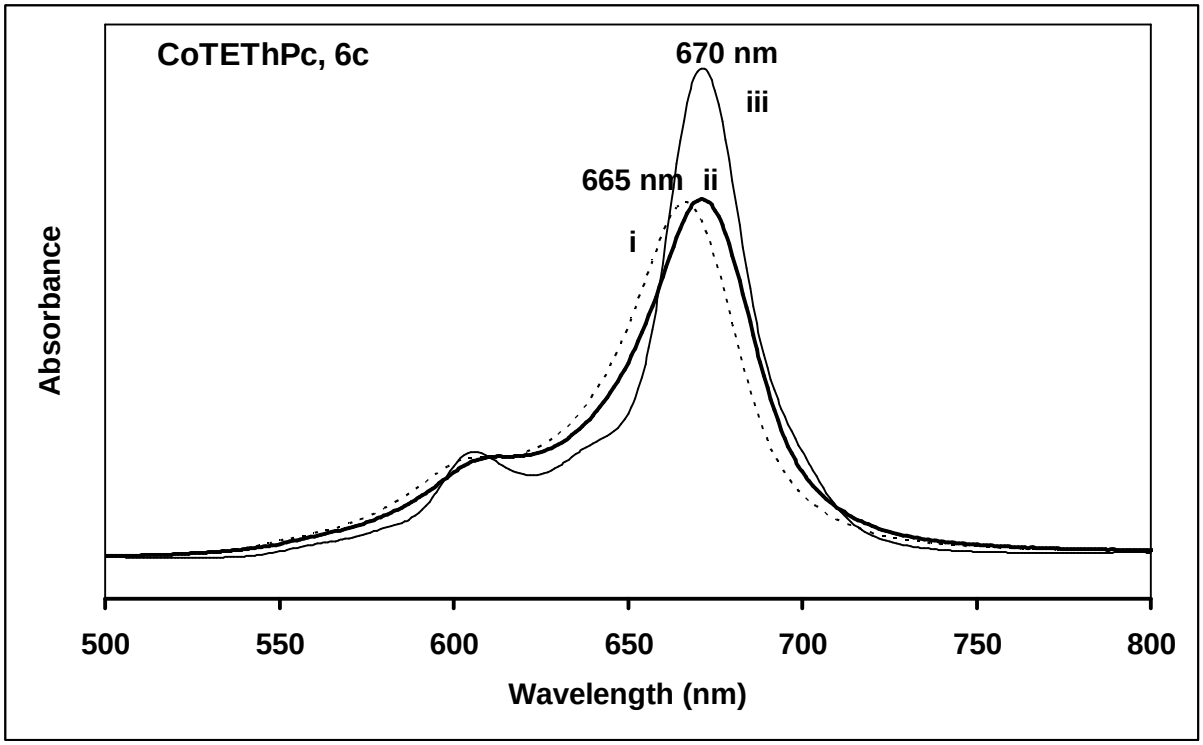

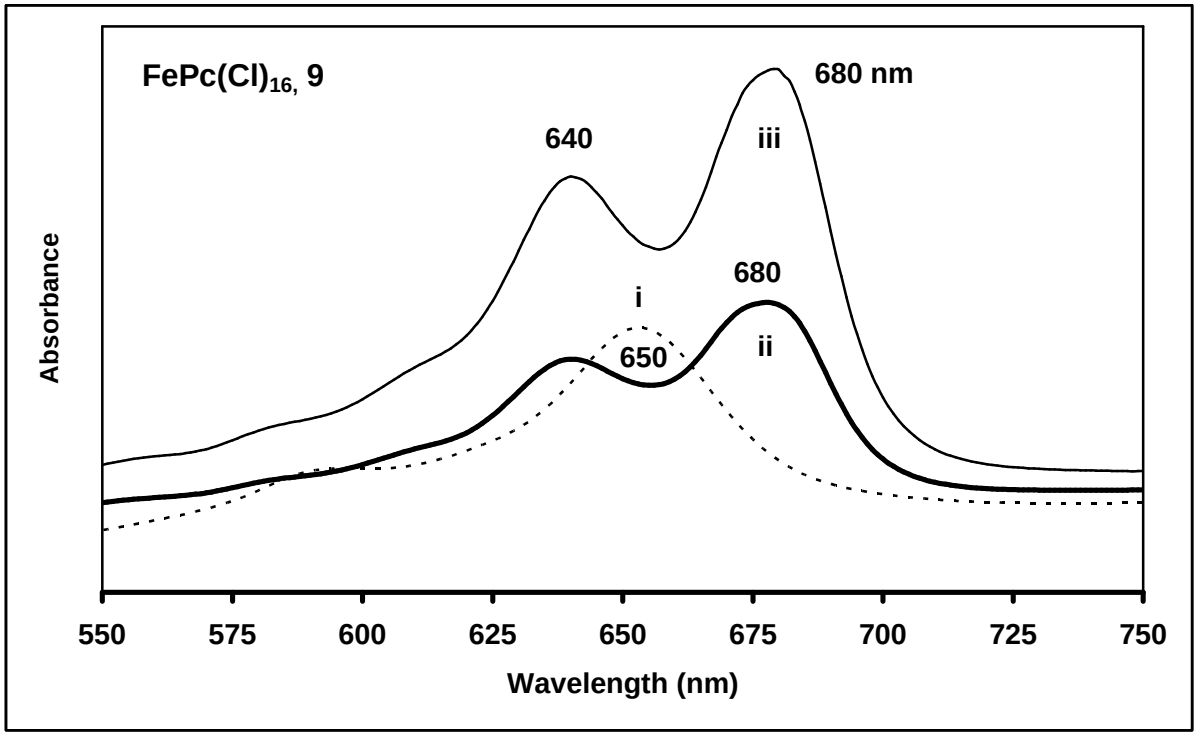

Figure 3.48: UV/Visible spectra of complexes 6a, 6b, 6c and 9 in DMF. i) starting spectrum, ii) bromine added to (i) and iii) oxygen bubbled to (ii).

The Q band of $FePc(Cl)_{16}$ **9** was observed at 650 nm in DMF. The band split upon oxidation using bromine into components at 640 and 680 nm. The split Q band indicates oxidation to Fe (III). The lower energy component denotes formation of Fe (III) while its counterpart at higher energy is attributed to the μ-oxo dimer[25,63]. Both peaks intensified upon oxygenation. Similar spectral changes were observed for FePc. These studies show that interaction of oxygen with iron (II) complexes leads to formation of Fe (III) μ-oxo dimers, confirming involvement of the Fe (III/II) redox couple in oxygen reduction reactions.

In summary, Co (III/II) and Fe (III/II) couples were involved in catalysis based on their CV peak positions relative to the oxygen reduction peaks. Oxygen is electrocatalytically reduced to hydrogen peroxide in buffer solutions of pHs below 5 by all studied complexes, Table 3.7. Water is formed at higher pH by CoPc **6a**, FePc **8** and $FePc(Cl)_{16}$ **9** as judged four electron transfer, Table 3.7, whereas substituted cobalt complexes, **6b** and **6c** form only hydrogen peroxide in all pH range studied. Protons were also involved in the reaction, this is shown by the Pourbaix diagram in Fig. 3.44. For hydrogen peroxide formation, Tafel slopes of 120 mV/decade were obtained indicating that one electron transfer occurs during the rate determining step for complexes **6a**, **8** and **9** at pH less than 5. Tafel slopes of 60 mV/decade were obtained when water is the product at pH greater than 5, implying that one electron transfer is followed by a slow chemical step.

Based on the above observations, the following mechanism (Scheme 3.8) based on literature reports[81,185] is therefore proposed for oxygen

reduction catalyzed by iron phthalocyanine complexes when two electrons are transferred and Tafel slopes are 60 mV/decade:

$$[Fe^{III}Pc]^+ + e^- \rightarrow Fe^{II}Pc \quad 3.34$$

$$Fe^{II}Pc + O_2 \xrightarrow{r.d.s} (O_2^-)Fe^{III}Pc \quad 3.35$$

$$(O_2^-)Fe^{III}Pc + H^+ \rightarrow [(O_2H)Fe^{III}Pc]^+ \quad 3.36$$

$$[(O_2H)Fe^{III}Pc]^+ + e^- + H^+ \rightarrow [Fe^{III}Pc]^+ + H_2O_2 \quad 3.37$$

For oxygen reduction catalyzed by cobalt phthalocyanine complexes involving transfer of two electrons and 60 mV/decade Tafel slopes, the mechanism is as follows:

$$[Co^{III}Pc]^+ + e^- \rightarrow Co^{II}Pc \quad 3.38$$

$$Co^{II}Pc + O_2 + 2e^- + 2H^+ \xrightarrow{r.d.s} [Co^{III}Pc]^+ + H_2O_2 \quad 3.39$$

Scheme 3.8: Mechanism of oxygen reduction catalyzed by CoPc and FePc complexes.

At the beginning of oxygen reduction reactions, positive potential is applied that oxidizes the catalysts, hence eqs. 3.34 and 3.38 are proposed that involve reduction of the MPcs from M(III) to M(II). The reduced species then interact with oxygen whereby the formed adduct of the iron species will be in the +3 state, eq. 3.35. This superoxide species does not exist for Co as reported in literature[185]; oxygen does not coordinate with the Co metal centre as proven by UV/Vis spectroscopy, Fig. 3.48. The $(O_2^-)Fe^{III}Pc$ adduct is then protonated (eq. 3.36), followed by cleavage of the (O_2H) and subsequent protonation leading to formation of hydrogen peroxide, eq. 3.37. The peroxide can then undergo further two electron transfer to form water.

The same oxygen reduction mechanism holds for 120 mV/decade Tafel slopes, the difference lies in the rate-determining step which will be eq. 3.36.

The difference in Tafel slopes stems from different adsorption conditions. For 120 mV/decade slopes, the reaction occurs under Langmuir adsorption conditions while for Tafel slopes of 60 mV/decade, it occurs under Temkin adsorption conditions[81,179].

In conclusion, oxygen reduction is catalyzed by MnPc, CoPc and FePc complexes. The best electrocatalytic activity in terms of peak potentials and complete reduction via four electron transfer was afforded by unsubstituted Co, Fe and Mn phthalocyanines. Substitution with either electron-donating or electron-withdrawing ligands lowers electrocatalytic efficiency of the catalysts. Substituted CoPcs produced H_2O_2 in all pHs whereas unsubstituted CoPc and FePc produced it in pHs below 5, and above this pH, they formed water. MnPc complexes form the peroxide in acidic and slightly alkaline media, but at high pH, they form water.

Chapter 4

Biomimetic catalysis

This section describes results obtained from use of metallo-phthalocyanines as biomimetic catalysts for oxidation of cyclohexene in the presence of chemical oxidants.

This work has been published as;

Nthapo Sehlotho and Tebello Nyokong
Catalytic activity of iron and cobalt phthalocyanine complexes towards the oxidation of cyclohexene using *tert*-butylhydroperoxide and chloroperoxybenzoic acid.
***J. Mol. Cat. A: Chem.,* 209 (2004) 51-57.**

4.1 Oxidation of cyclohexene

The use of *tert*-butylhydroperoxide (TBHP) as an oxidant was based on the earlier studies on the oxidation of cyclohexane[196], this oxidant was found to cause minimal destruction of the phthalocyanine catalyst, and to give better selectivity of the products. For comparative purposes, chloroperoxybenzoic acid (CPBA) was also employed as an oxidant. $FePc(Cl)_{16}$ was employed as a biomimetic catalyst because the metal centre Fe is the catalytic moiety in Cytochrome P450 enzymes. Ring substitution with electron withdrawing ligands stabilizes the catalyst against oxidative degradation as explained in the introduction. A 3:7 DMF-CH_2Cl_2 solvent mixture was employed for the reactions. $FePc(Cl)_{16}$ dissolves completely in DMF; moreover it coordinates with the solvent thereby being further protected against oxidative degradation. However, it has been reported that no biomimetic reaction products were detected in DMF[196] hence the CH_2Cl_2 component in the solvent mixture. Alkane oxidation has been reported to occur fast and at high yields in DCM[205].

Thus oxidation of cyclohexene catalyzed by $FePc(Cl)_{16}$ in the presence of TBHP was conducted in the 3:7 DMF-CH_2Cl_2 solvent mixture. Three products were clearly identified using gas chromatography by both spiking and comparison with standards. These products are cyclohexene oxide **a**, 2-cyclohexen-1-ol **b**, 2-cyclohexen-1-one **c** and adipic acid **d** (Fig. 4.1), in order of elution. Product yields, selectivities and turnover numbers are shown in Table 4.1.

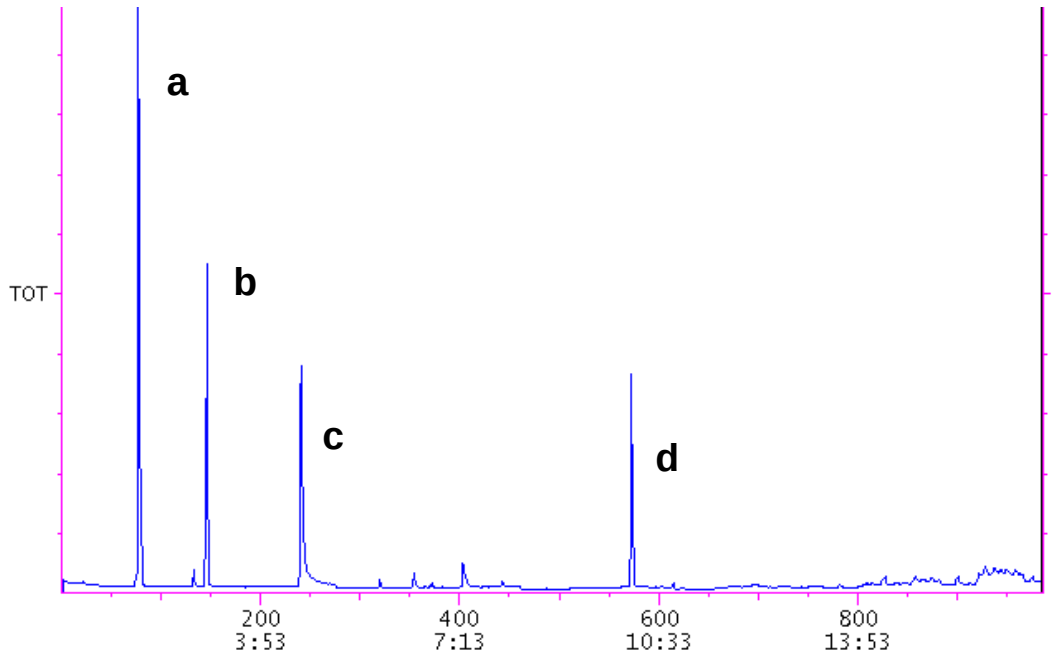

Figure 4.1: Gas chromatograms for biomimetic oxidation of cyclohexene using TBHP as an oxidant and $FePc(Cl)_{16}$ as the catalyst. Obtained products are a) cyclohexene oxide, b) 2-cyclohexen-1-ol, c) 2-cyclohexen-1-one and d) adipic acid, in order of elution.

Product identification was confirmed by mass spectra, which showed M-1 peak at 97 m/z for cyclohexene oxide and cyclohexen-1-ol, and M^+ peak at 96 m/z for cyclohexen-1-one. Reported products for the oxidation of cyclohexene in the presence of metallo tetra-*tert*-butylphthalocyanine complexes are cyclohexene oxide and 2-cyclohexen-1-one, with the former being the major product[207]. This work shows the formation of 2-cyclohexen-1-ol in addition to cyclohexene oxide and 2-cyclohexen-1-one when iron hexadecachlorophthalocyanine ($FePc(Cl)_{16}$) is employed as a catalyst. After prolonged reaction time, a new peak was formed which was identified by GC

and GC-MS as being due to adipic acid. It was also confirmed by GC that TBHP oxidant is converted to tert-butanol during the catalytic process.

Table 4.1: Product yields (based on the substrate), selectivities and turnover numbers for the oxidation of 1.6 mol dm^{-3} cyclohexene using 0.5 mol dm^{-3} TBHP as an oxidant (unless stated otherwise) and 1.7 mg/mL $FePc(Cl)_{16}$ as the catalyst. Reaction time is 8 hours unless stated otherwise.

Product	% yield	% yield[a]	% yield[b]	% selectivity	Turnover number
Cyclohexene oxide	3.5 (51.0)	8.5	7.5	7.8	39.8
2-Cyclohexen-1-ol	9.1 (3.0)	78.6	2.5	20.0	209
2-Cyclohexen-1-one	32.7 (1.0)	98.9	3.0	72.2	494

[a] Reaction time = 4 weeks.
[b] CPBA as oxidant.
[c] Literature values in parentheses, ref.[255]

The nature and the relative yields of the products formed by catalytic oxidation of cyclohexene using porphyrins vary considerably depending on the catalyst and oxidant. When iron porphyrin containing nitrate or perchlorate as axial ligands was employed for the oxidation of cyclohexene using CPBA, large yields of cyclohexene oxide were obtained (68 - 78 %), but when chloride axial ligands were employed using the same oxidant, the yields of cyclohexene oxide were less than 2 %[254]. Higher yields of cyclohexene oxide relative to the other products were observed for most porphyrins using oxidants such as CPBA or iodosylbenzene[192,204]. However photooxygenation of cyclohexene using titanium porphyrins resulted in the formation of cyclohexene hydroperoxide as a major product, with cyclohexene oxide being

one of the side products[219]. Table 4.1 shows that the catalyst, $FePc(Cl)_{16}$ favoured the formation of 2-cyclohexen-1-one to the rest of the products.

The yields for the formation of allylic oxidation products shown in Table 4.1 are higher than those reported for oxidation of cyclohexene using iron (III) porphyrin and hydrogen peroxide as an oxidant, in the presence of imidazole[255]. The yields of products using $FePc(Cl)_{16}$ catalyst reported in Table 4.1 are after 8 hours and 4 weeks of catalysis. The product yields increased steadily with time and improved to total yield values greater than 100 % after 4 weeks. Yields consistently higher than 100 % have been reported for porphyrin catalysts and attributed to auto-oxidation[204]. Thus after prolonged catalysis, the yields obtained for Pc catalysts are comparable to porphyrins with the advantage of added stability for the former.

The yields observed for the formation of cyclohexene oxide from the oxidation of cyclohexene in the presence of Mn (III), Co (II) and Fe (II) tetra-*tert*-butylphthalocyanines (MTTBPc) and in the presence of a reducing agent, isobutylaldehyde[207] are higher than those reported in this work. Cyclohexene oxide yields are 38, 21 and 57 % after 8 hours of reaction for MTTBPc where M is Mn, Co and Fe complexes respectively (Table 1.4). However the yields obtained using the MTTBPc as catalysts stabilized after about 10 hours[207], while as has been been discussed above, the yields for the cyclohexen-1-one, cyclohexene oxide and cyclohexen-1-ol increased even after 4 weeks of the reactions. The fact that the $FePc(Cl)_{16}$ catalyst is selective to the formation of 2-cyclohexen-1-one over that of cyclohexene oxide and maintained stability of the active form of the catalyst even after prolonged use, is a very useful

observation. High turn-over values were obtained for the catalytic process employing $FePc(Cl)_{16}$, Table 4.1.

The biomimetic catalytic activity of $FePc(Cl)_{16}$ was compared to that of unsubstituted FePc and CoPc after 8 hours of reaction time. FePc showed selectivity towards cyclohexen-1-ol not cyclohexen-1-one observed for perchlorinated $FePc(Cl)_{16}$, Table 4.2. Unsubstituted CoPc, however showed selectivity towards the cyclohexen-1-one, Table 4.2. When CPBA was employed as an oxidant, $FePc(Cl)_{16}$ was found to be selective towards cyclohexene oxide, instead of cyclohexen-1-one observed when TBHP was employed for the same catalyst. Product yields are also tabulated in Table 4.2; these are comparable for the three catalysts. However, yields for FePc and CoPc levelled off after 24 hours of reaction due to degradation of catalysts, unlike $FePc(Cl)_{16}$ whose yields are tabulated in Table 4.1 after 4 weeks of reaction. This shows therefore that ring halogenation does indeed stabilize biomimetic catalysts against oxidative degradation, rendering them useful over extended periods.

Table 4.2: Product selectivities and yields (in parentheses) for oxidation of 1.6 mol dm^{-3} cyclohexene using 1.7 mg/mL $FePcCl_{16}$ 9, FePc 8 and CoPc 6a as catalysts and 0.5 mol dm^{-3} TBHP as an oxidant. Reaction time is 8 hours.

Product	$FePc(Cl)_{16}$	$FePc(Cl)_{16}$[a]	FePc	CoPc
Cyclohexene oxide	7.8 (3.5)	57.7	3.8 (4.7)	5.5 (4.5)
2-Cyclohexen-1-ol	20.0 (9.1)	19.2	71.2 (26.0)	33.7 (8.9)
2-Cyclohexen-1-one	72.2 (32.7)	23.1	25.0 (27.1)	60.8 (46.1)

[a] CPBA as an oxidant.

Catalytic reactions of MPc complexes may be assumed to be accompanied by coordination of the oxidant to the central metal of the catalyst, in a similar manner to porphyrins[255]. MPc complexes containing different central metal ions will have varying coordination abilities and this may result in varying modes and rates of cleavage of the MPc-oxidant bonds hence resulting in different product selectivities.

It has been shown that CPBA oxidant coordinates to the Fe porphyrin complex during catalysis, followed by heterolytic O-O band cleavage to afford the active μ-oxo Fe-O-Fe species[256]. The rate of O-O bond cleavage was found to be lower for Fe porphyrin complexes containing electron withdrawing ring substituents. Since it has been proposed that the mechanism of alkene epoxidation using phthalocyanine catalysts may be similar to that of porphyrins[256], the presence of electron withdrawing groups could affect the rate of formation of active intermediates in FePc derivatives, resulting in different selectivities of products for the FePc and $FePc(Cl)_{16}$ complexes.

Experiments were carried out with varying amounts of the $FePc(Cl)_{16}$ catalyst, oxidant or substrate and using fixed amounts of the other two reagents. Fig. 4.2 shows that for fixed oxidant and substrate molar ratio, the yield for all the products increased with time, and showed slowing down after eight hours. However, the yields of the products: cyclohexen-1-one, cyclohexene oxide and cyclohexen-1-ol showed slow increase even after four weeks of the reaction.

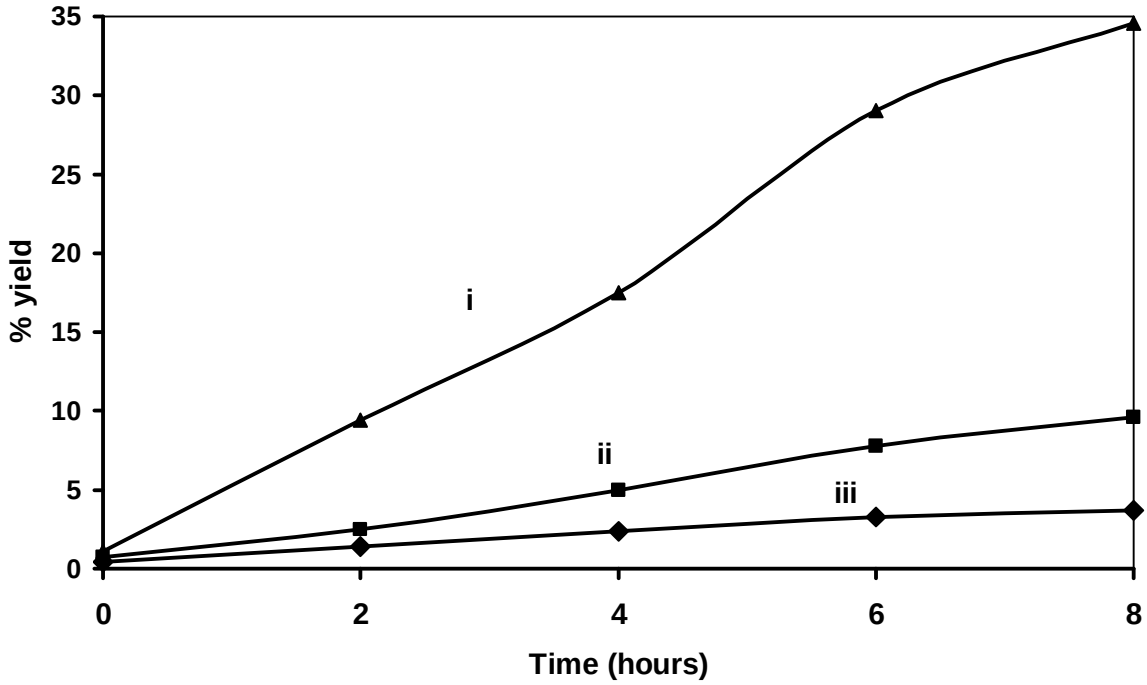

Figure 4.2: Variation of product yield with time for i) 2-cyclohexen-1-one, ii) 2-cyclohexen-1-ol and iii) cyclohexene oxide. Starting concentrations: cyclohexene = 1.6 mol dm^{-3} and TBHP = 0.5 mol dm^{-3}. Catalyst = $FePc(Cl)_{16}$ (1.7 mg/mL) in dimethylformamide-dichloromethane (3:7) solvent mixture.

When the concentration of cyclohexene substrate is larger than that of the oxidant with fixed amount of catalyst, the product yield showed no significant dependence on the substrate to oxidant ratio, Fig. 4.3. The yield generally increased with catalyst concentration as shown in Fig. 4.4. The highest catalyst concentration used 5mg/3mL since at high concentrations, $FePc(Cl)_{16}$ aggregates and this may affect its efficiency and hence product yields.

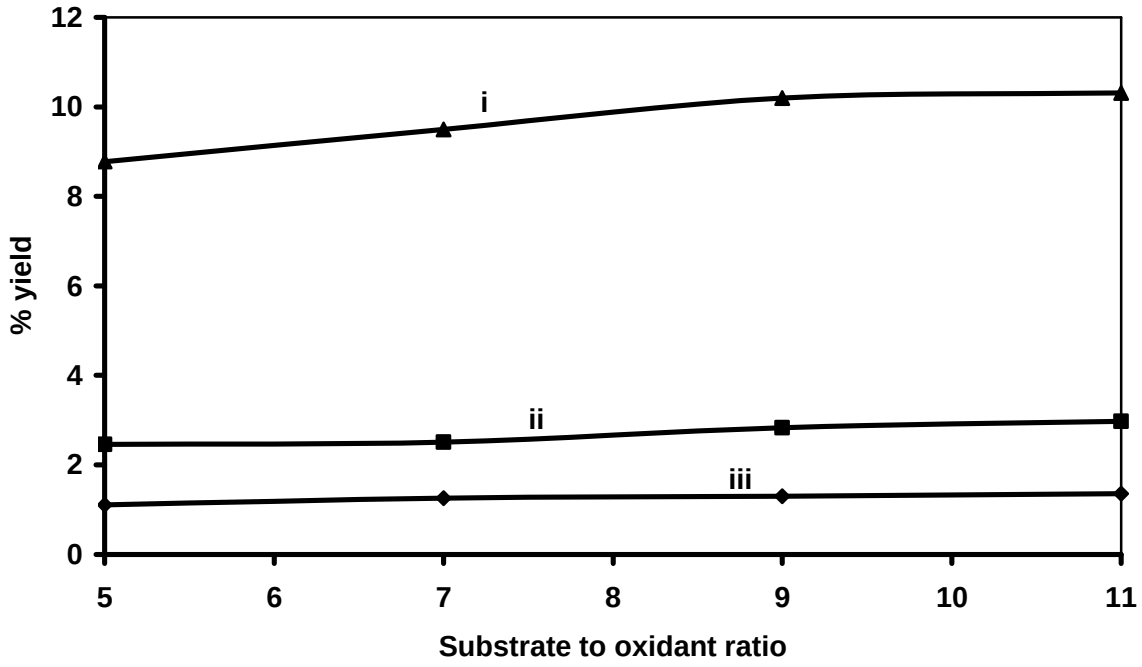

Figure 4.3: Variation of product yield with substrate to oxidant molar ratios (substrate in excess) for i) 2-cyclohexen-1-one, ii) 2-cyclohexen-1-ol and iii) cyclohexene oxide. Catalyst = 1.7 mg/mL $FePc(Cl)_{16}$. Solvent mixture is dimethylformamide - dichloromethane (3:7) and reaction time = 8 hours.

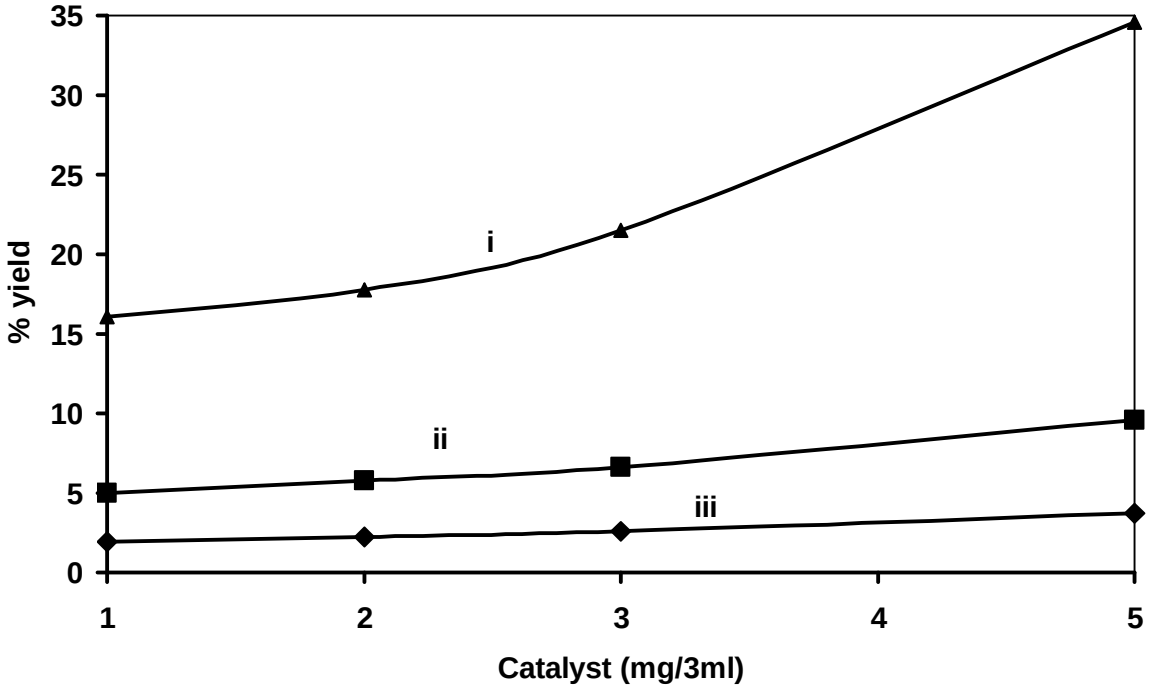

Figure 4.4: Variation of product yield with the amount of catalyst for i) 2 cyclohexen-1-one, ii) 2-cyclohexen-1-ol and iii) cyclohexene oxide. Starting concentrations: cyclohexene = 1.6 mol dm^{-3} and TBHP = 0.5 mol dm^{-3}. Solvent mixture is dimethylformamide-dichloromethane (3:7) and reaction time = 8 hours.

When unsubstituted FePc or CoPc were employed as catalysts, the products were formed within a very short time, but the product yield did not increase significantly with time even after about four hours, Fig. 4.5.

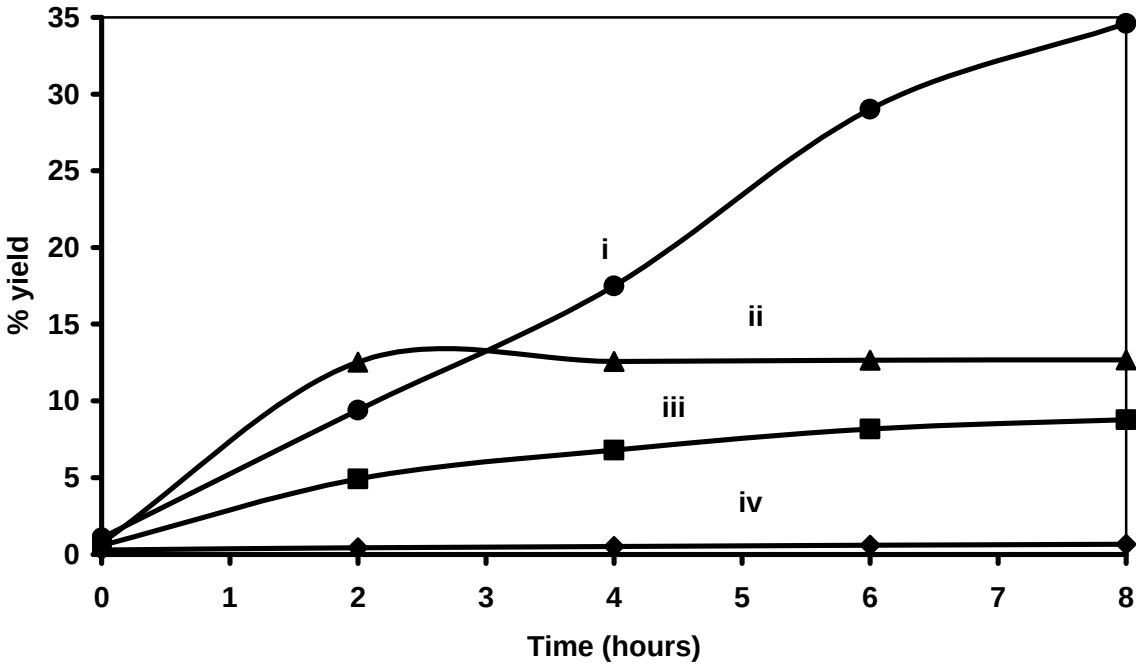

Figure 4.5: Effect of the nature of catalyst on the cyclohexen-1-one product yield. i) $FePc(Cl)_{16}$, ii) FePc, iii) CoPc and iv) no catalyst. Starting concentrations: catalyst 1.7 mg/mL, cyclohexene = 1.6 mol dm^{-3} and TBHP = 0.5 $moldm^{-3}$ in 3:7 dimethylformamide-dichloromethane solvent mixture.

4.2 Fate of the catalysts

The UV/Vis spectra of iron phthalocyanines has been a subject of several reports and much controversy[30,63]. In the absence of oxygen, the spectra of $FePc(Cl)_{16}$ in DMF consists of a sharp Q band due to the monomeric species[63]. In the presence of oxygen the spectra broadens and shifts to the blue due to the formation of μ-oxo dimeric species of the form $Cl_{16}PcFe^{III}$-O-$Fe^{III}PcCl_{16}$[63]. Fig. 4.6a shows spectral changes observed for the catalyst $FePc(Cl)_{16}$ during the catalytic oxidation of cyclohexene in the presence of TBHP as oxidant. The spectrum in Fig. 4.6a (i) is typical of the monomeric form of the $Fe^{II}Pc(Cl)_{16}$ complex before the start of the catalytic process with a Q band at 681 nm. Immediately after addition of oxidant, the Q

band decreased in intensity and it became split (Fig. 4.6a (ii)). The split components were observed at 648 and 678 nm. The split in the Q band is typical of the oxidation of $Fe^{II}Pc$ to $Fe^{III}Pc$ species[25]. Thus spectral changes shown in Fig. 4.6a are consistent with the oxidation of the $Fe^{II}Pc(Cl)_{16}$ and the formation of the $Fe^{III}Pc(Cl)_{16}$ species.

Following the split of the Q band, the 678 nm band decreased in intensity and finally disappeared as the catalytic process proceeded, Fig. 4.6b. The 648 nm band on the other hand gradually shifted to lower wavelengths and after about eight hours, this band was observed at 636 nm, Fig. 4.6b (ii). Oxidants such as iodosobenzene are known to convert $Fe^{II}Pc$ species to the μ-oxo species, $PcFe^{III}$-O-$Fe^{III}Pc$[30], which is characterized by a low intensity broad Q band at ~ 630 nm. Thus the final spectrum in Fig. 4.6b (ii) is typical of the μ-oxo species, confirming that the final form of the catalyst following the oxidation of cyclohexene using TBHP oxidant, is the $Cl_{16}PcFe^{III}$-O-$Fe^{III}PcCl_{16}$ species. The oxidation is probably accompanied by some degradation of the catalyst as judged by the decrease in the Q band intensity, though the $PcFe^{III}$-O-$Fe^{III}Pc$ species typically show a weak Q band.

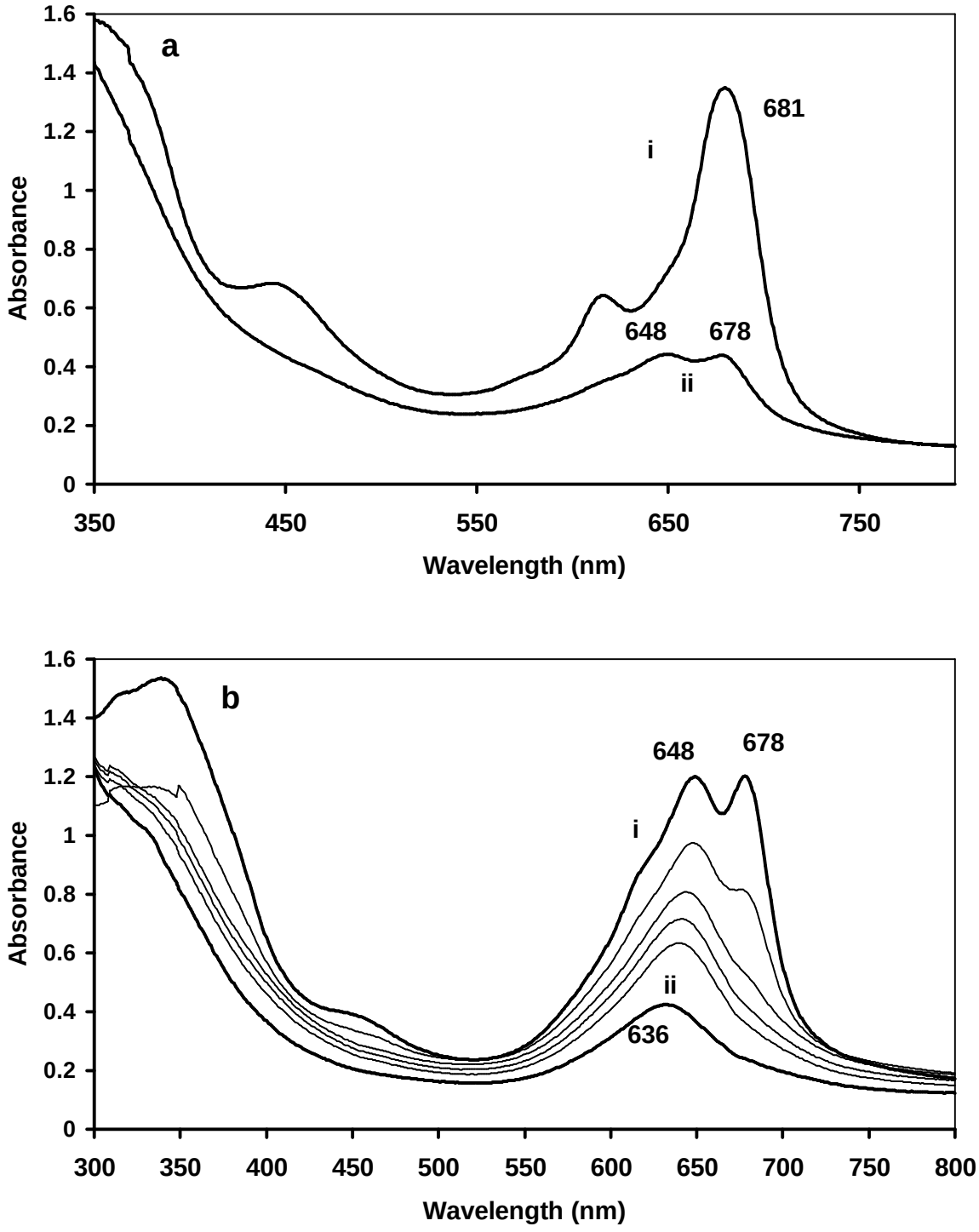

Figure 4.6: Absorption spectral changes observed on addition of 0.5 moldm^{-3} TBHP oxidant to a reaction mixture containing 1.7 mg/mL $FePc(Cl)_{16}$ catalyst and 1.6 mol dm^{-3} cyclohexene. For spectral measurements, the solution made of these reagents was diluted a hundred fold. (a) i) before addition and ii) immediately after addition of TBHP to catalyst-substrate mixture. (b) i) same as spectrum (ii) in Fig 4.6a and (ii) spectrum eight hours after addition of TBHP to catalyst/substrate mixture.

The catalyst was still present even after four weeks of catalysis, with the yields of the products still increasing. The solution turned from blue to brown, even though the 636 nm band was still present after four weeks of catalysis. When CPBA was employed as an oxidant for cyclohexene oxidation using $Fe^{II}Pc(Cl)_{16}$ catalyst, fast degradation of the catalyst was observed, with the final formation of a weak high energy band at 636 nm, Fig. 4.7, hence confirming the formation the μ-oxo species as was the case with TBHP. However complete disappearance of 636 nm band was observed within two hours when CPBA was employed as an oxidant, showing that this oxidant degrades the phthalocyanine molecule more readily than TBHP.

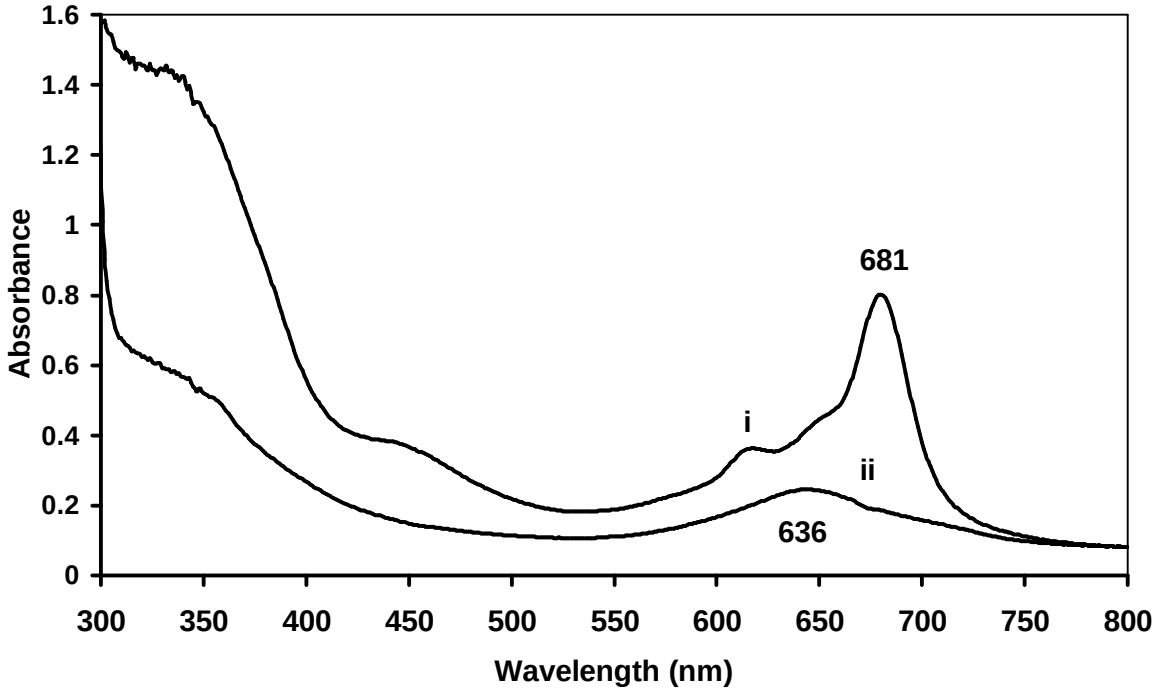

Figure 4.7: Absorption spectral changes observed on addition of 0.5 moldm^{-3} CPBA oxidant to a reaction mixture containing 1.7 mg/mL $FePc(Cl)_{16}$ catalyst and 1.6 mol dm^{-3} cyclohexene. For spectral measurements, the solution made of these reagents was diluted a hundred fold. i) before addition and ii) immediately after addition of CPBA to catalyst-substrate mixture.

Oxidation of cyclohexane using the $FePc(Cl)_{16}$ catalyst and chloro-peroxybenzoic acid oxidant[196], showed different spectral features from those reported here in that the μ-oxo dimer was not formed, only the $Fe^{III}Pc$ species was observed. Thus the formation of the μ-oxo species following oxidation of $Fe^{II}Pc$ species may be determined by both the nature of the substrate and the oxidant.

The CoPc and FePc catalysts were readily deactivated, with the solutions changing from blue to brown in a very short time (within two hours). For FePc catalyzed-cyclohexene oxidation, the Q band of FePc at 660 nm shifted to 675 nm on addition of TBHP oxidant, consistent with the formation of the $Fe^{III}Pc$ species (Fig. 4.8a). However the latter degraded very fast, based on the abrupt decrease in peak intensity. For the CoPc catalyst, an initial shift of the Q band from 660 nm to 670 nm, typical of oxidation of $Co^{II}Pc$ to $Co^{III}Pc$[25] was observed (Fig. 4.8b). Thereafter, total disappearance of the Q band within an hour was observed. Thus for both CoPc and FePc, the $M^{III}Pc$ species are implicated in the catalytic process. However both of these catalysts are readily degraded and hence the unsubstituted CoPc and FePc catalysts are not efficient for the catalytic oxidation of cyclohexene. This therefore shows that ring substitution with electron-withdrawing ligands indeed enhances metallophthalocyanine stability against oxidative degradation.

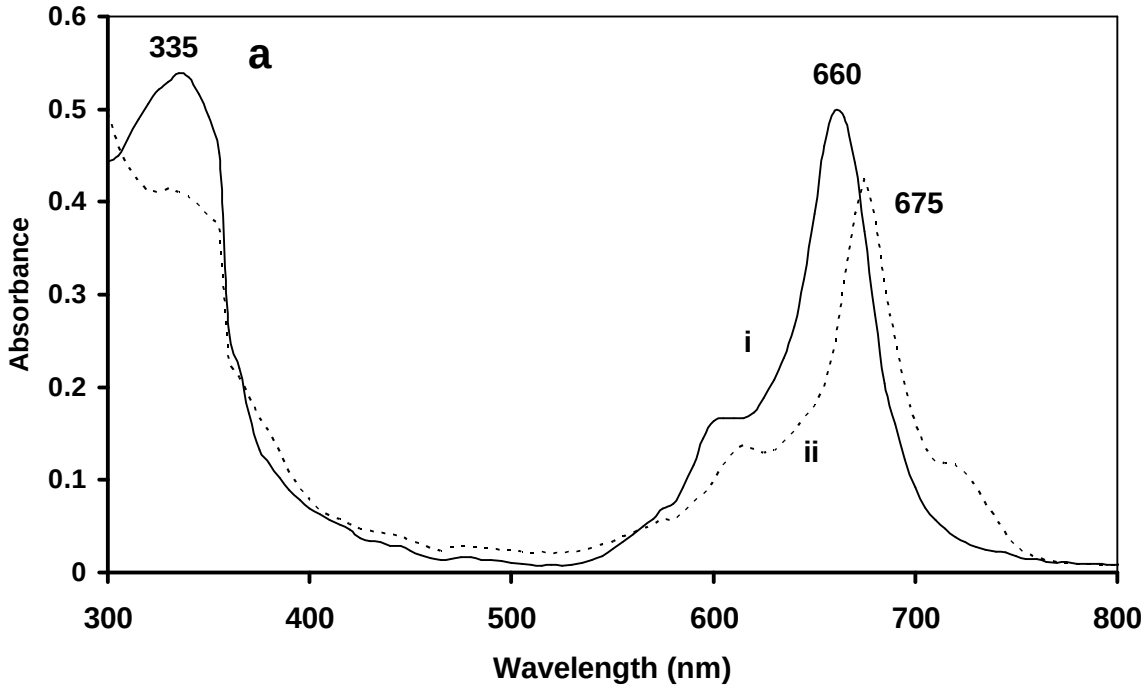

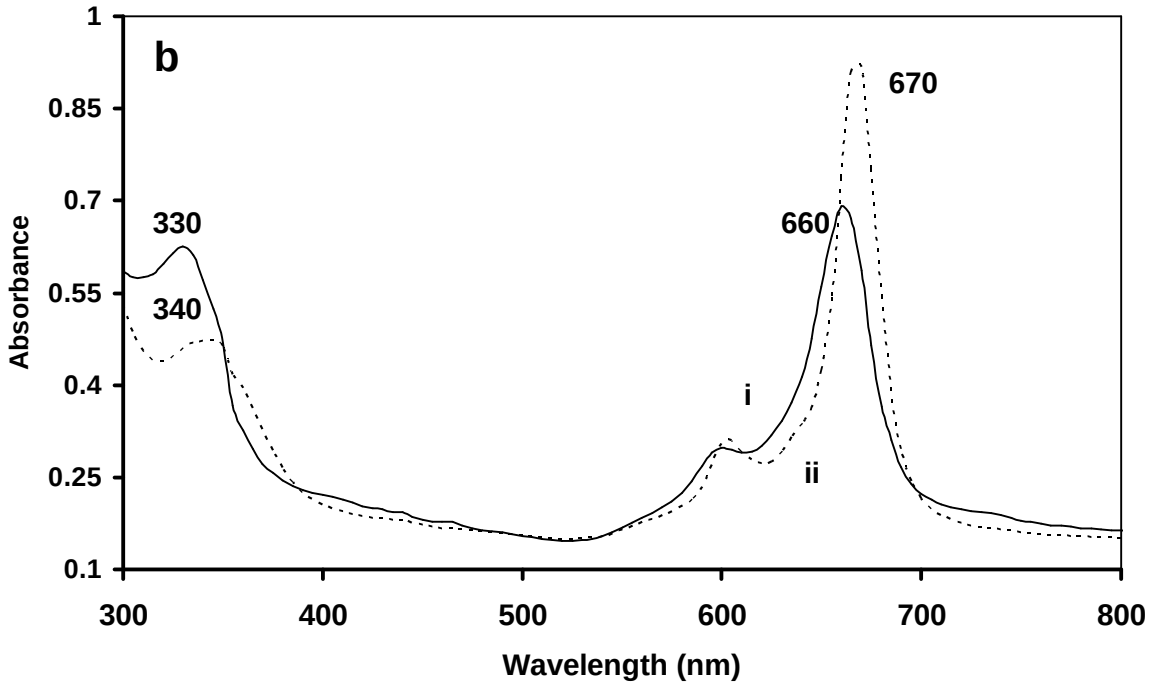

Figure 4.8: Absorption spectral changes observed on addition of 0.5 moldm^{-3} TBHP oxidant to a reaction mixture of 1.7 mg/mL a) FePc and b) CoPc catalysts and 1.6 mol dm^{-3} cyclohexene. For spectral measurements, the solution made of these reagents was diluted a hundred fold. i) before addition and ii) immediately after addition of TBHP to catalyst-substrate mixture.

Spectral changes shown in Fig. 4.6 suggest the following mechanism for the $Fe^{II}Pc(Cl)_{16}$ catalyst, Scheme 4.1:

$$Fe^{II}Pc(Cl)_{16} + ROOH \xrightarrow{-ROO^{\bullet}, RO^{\bullet}} Fe^{III}Pc(Cl)_{16} \qquad 4.1$$

$$Fe^{III}Pc(Cl)_{16} \xrightarrow{ROOH} Cl_{16}PcFe^{III}\text{-}O\text{-}Fe^{III}PcCl_{16} \qquad 4.2$$

Scheme 4.1. The mechanism for $Fe^{II}Pc(Cl)_{16}$ transformation during the catalytic oxidation of cyclohexene. ROOH represents oxidants, TBHP or CPBA.

It is expected that $ROO^{\bullet}$ and $RO^{\bullet}$ radicals will be formed, since these have been suggested as the species involved in the catalytic processes involving phthalocyanines and porphyrins[257]. When a radical scavenger diazabicyclooctane (DABCO) was added to the reaction mixture, there was a decrease in product yield, confirming the involvement of radicals in the mechanism for the catalytic oxidation of cyclohexene. It has also been shown that when $Fe^{III}Pc$ is employed as a catalyst, with iodosylbenzene as an oxidant, an $O=Fe^{IV}Pc$ species is an intemediate in the epoxidation of alkenes[206]. However there is no spectroscopic evidence for the formation of an $O=Fe^{IV}Pc$ intermediate in this work.

Product formation for the transformation of cyclohexene in the presence of $FePc(Cl)_{16}$ and TBHP (or CPBA) oxidant may be represented by Scheme 4.2 as follows:

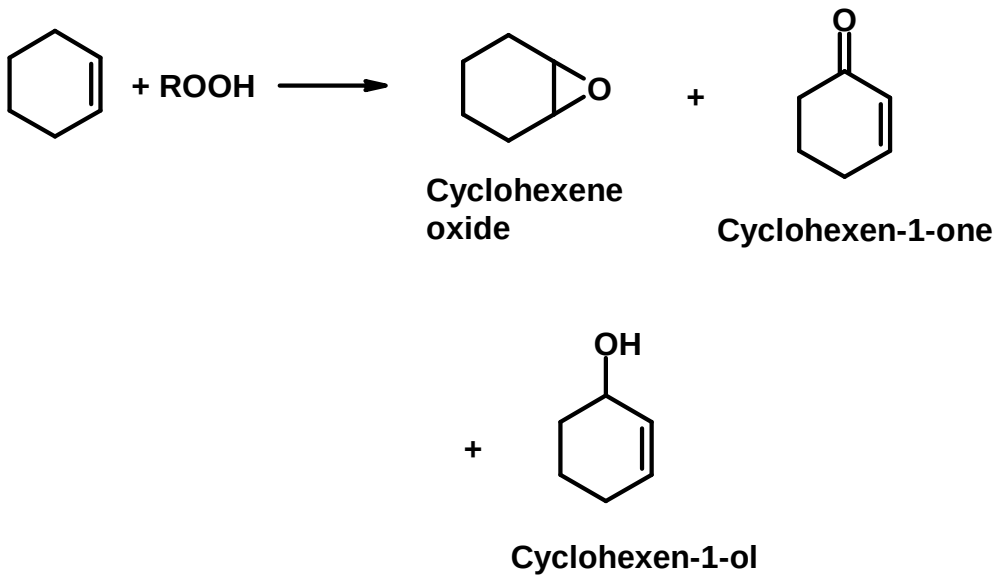

Scheme 4.2. Products formed from oxidation of cyclohexene by TBHP or CPBA oxidants (ROOH) in the presence of $FePc(Cl)_{16}$, CoPc or FePc catalysts.

In conclusion, oxidation of cyclohexene using TBHP or CPBA oxidants catalyzed by $FePc(Cl)_{16}$, FePc and CoPc leads to the formation of cyclohexene oxide, 2-cyclohexen-1-ol and 2-cyclohexen-1-one. Product selectivity varied with the nature of the catalyst and oxidant. CPBA degraded the catalysts faster than TBHP. Ring substitution with electron-withdrawing ligands stabilizes FePc against oxidative degradation.

Chapter 5

Photocatalysis

In this section, an account of results obtained from zinc phthalocyanine (ZnPc) photo-catalyzed oxidation of cyclohexene is outlined.

This work has been published as;

Nthapo Sehlotho and Tebello Nyokong

Zinc phthalocyanine photocatalyzed oxidation of cyclohexene

***J. Mol. Cat. A: Chem.*, 219 (2004) 201- 207.**

5.1 Photo-oxidation of cyclohexene

ZnPc was employed as a photocatalyst for cyclohexene oxidation because the central metal Zn is diamagnetic and its excited singlet state is known to undergo intersystem crossing to the triplet state readily, where it can transfer its energy to oxygen generating sufficient catalytic singlet oxygen. Singlet oxygen quantum yields (ϕ_Δ) of ZnPc are high, for instance ϕ_Δ has been reported to be ~ 0.6 in DMF[215]. Experiments were done using white and visible light in the presence and absence of ZnPc catalyst, to probe the efficiency of ZnPc as a photocatalyst. Light of different wavelengths and intensities was used to investigate their effect on the photocatalytic efficiency of the system towards cyclohexene oxidation.

Experiments were conducted in a number of solvents, namely 1,4-dioxane, THF, benzene and 3:7 DMF-CH_2Cl_2 mixture. Criteria of solvent choice was as follows: For 1,4-dioxane, THF and benzene, photochemical and fluorescenece studies of ZnPc and its derivatives have been studied before[51,57]. They were found to be photostable in these solvents, and hence it was interesting to explore their photocatalytic behaviour. ZnPc is very soluble in the 3:7 DMF-CH_2Cl_2 solvent mixture. Moreover, this solvent mixture has been employed in biomimetic oxidation of cyclohexene, thus this forms a basis for comparison of catalytic efficiency towards cyclohexene oxidation using different methods but the same solvent system.

Fig. 5.1 shows a gas chromatogram under white light irradiation of cyclohexene oxidation reaction catalyzed by ZnPc in 1,4-dioxane. Products were identified to be cyclohexene oxide **a**, 2-cyclohexen-1-ol **b**, 2-cyclohexen-

1-one **c** and *trans*-cyclohexane diol **d** in order of elution, by comparison of GC traces of standards with that of the reaction mixture, spiking with standards and GC-MS. Cyclohexene hydroperoxide was identified by iodine liberation methods under white light irradiation.

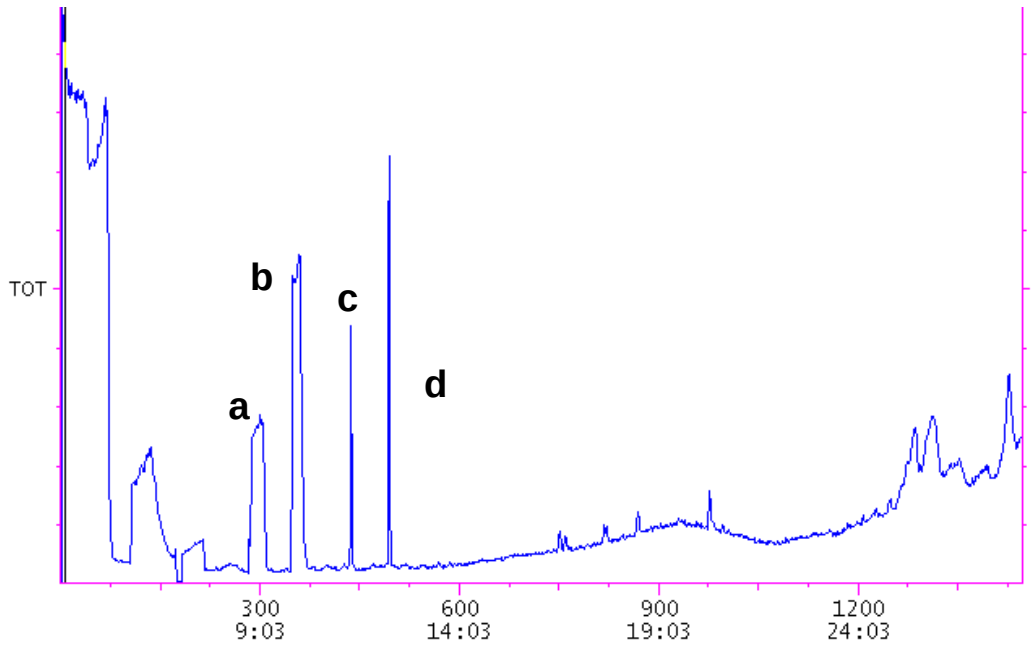

Figure 5.1: Gas chromatogram of cyclohexene oxidation photocatalyzed by ZnPc in 1,4-dioxane under white light irradiation. Obtained products are a) cyclohexene oxide, b) 2-cyclohexen-1-ol, c) 2-cyclohexen-1-one and d) *trans*-cyclohexane diol, in order of elution.

It was observed that cyclohexene gets oxidized in 1,4-dioxane by white light in the absence of a catalyst to cyclohexene oxide, cyclohexenol and cyclohexenone. The increase in the products was insignificant after 45 minutes. When ZnPc was employed as a catalyst for oxidation of cyclohexene in 1,4-dioxane in the presence of white or red light, the reaction occurred faster and yields of cyclohexene oxide, cyclohexenol and cyclohexenone

increased compared to in the absence of ZnPc. This proves that ZnPc is indeed a photocatalyst. Data reported in this work is therefore corrected for cyclohexene oxidation in the absence of ZnPc catalyst. In the presence of the catalyst following white light irradiation, *trans*-cyclohexane diol and cyclohexene hydroperoxide were observed in addition to cyclohexene oxide, cyclohexenol and cyclohexenone, which are observed in the absence of the catalyst. Thus the presence of the catalyst results in the formation of a wider range of products.

It should be mentioned that the same oxidation products were obtained with red light irradiation except cyclohexene hydroperoxide, even though the product yields were higher with white light irradiation than with red light. Fig. 5.2 shows an increase in % yields of 2-cyclohexen-1-one over time with white (i) and red (ii) light. White light irradiation exhibits higher % yields than red light irradiation. The products formed using ZnPc as a photocatalyst are similar to those formed during the photo-oxygenation of cyclohexene in the presence of titanium (IV) porphyrins except that *trans*-cyclohexanediol was not obtained using the latter catalyst[219].

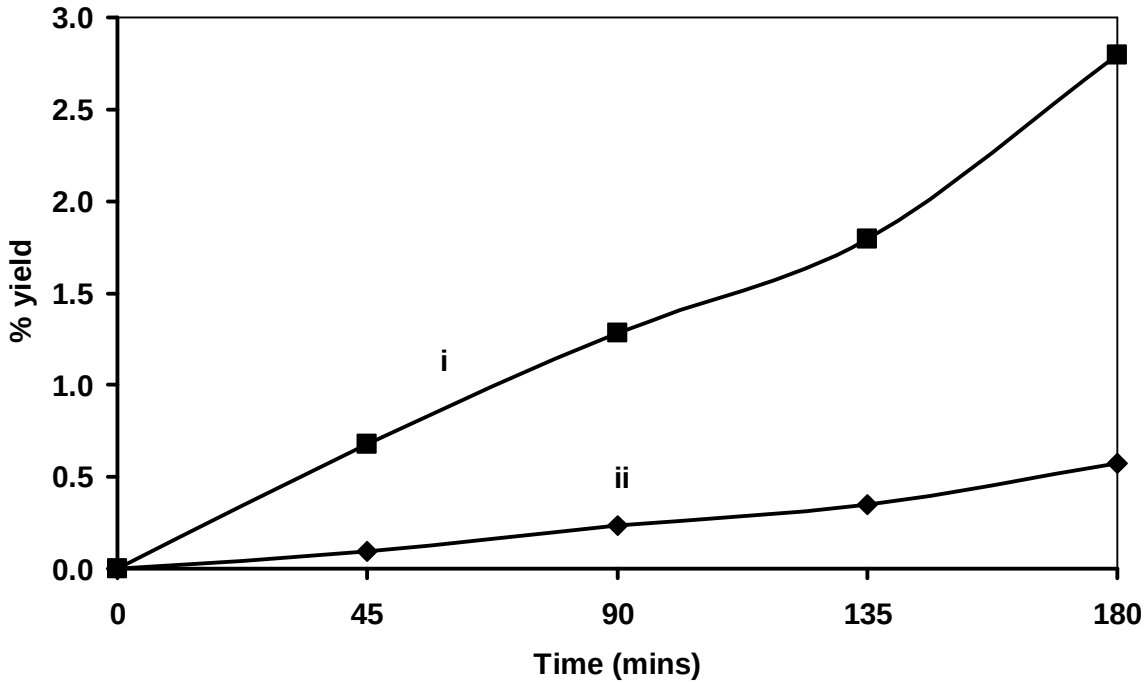

Figure 5.2: Variation of cyclohexenone with time on photolysis with i) white or ii) red (λ > 600 nm) light and in the presence of 0.004 mg/mL ZnPc photocatalyst. Reaction time is 3 hours. Starting concentration of cyclohexene in 1,4-dioxane is 0.9 mol dm^{-3}.

As explained above and in the experimental section, the products (cyclohexene oxide, cyclohexenol, cyclohexenone and *trans*-cyclohexanediol) were identified by comparison of their GC retention times with those of standards. Further product confirmation was afforded by GC-MS which showed M-1 peak at m/z = 97 for cyclohexene oxide and cyclohexenol, and $M^{\bullet+}$ at m/z = 96 and a major α cleavage fragment at m/z = 68 for cyclohexenone. Cyclohexene hydroperoxide was identified using the iodine liberation method described in the experimental section. No peroxide was obtained on photolysis of solutions containing ZnPc in the absence of cyclohexene, confirming that the peroxide was not due to radicals formed through Type I mechanism, Scheme 5.1.

$^3MPc^* + {}^3O_2 \rightarrow O_2^{-\bullet} + MPc^{+\bullet}$ 5.1

$^3MPc^* + Subs \rightarrow MPc^{-\bullet} + Subs^{+\bullet}$ 5.2

$MPc^{-\bullet} + {}^3O_2 \rightarrow O_2^{-\bullet} + MPc$ 5.3

$O_2^{-\bullet} \xrightarrow{H^+} HO_2^{\bullet}$ 5.4

$HO_2^{\bullet} + Subs \rightarrow H_2O_2 + Subs^{\bullet}$ 5.5

$Subs^{+\bullet}, Subs^{\bullet}, H_2O_2 \rightarrow$ Oxidation products 5.6

Scheme 5.1: Type I mechanism of photo-catalysis. Subs is substrate, cyclohexene in this case.

Only cyclohexene oxide, cyclohexenol and cyclohexenone have been obtained as products using phthalocyanines as biomimetic catalysts in the presence of oxygen donors[207]. In addition to cyclohexene oxide, cyclohexenol and cyclohexenone, adipic acid was formed as discussed in Chapter 4 for cyclohexene oxidation catalyzed by $FePc(Cl)_{16}$. In ZnPc-photocatalyzed oxidation of cyclohexene in white light, cyclohexene hydroperoxide and *trans*-cyclohexanediol were formed in addition to cyclohexene oxide, cyclohexenol and cyclohexenone. This shows that $FePc(Cl)_{16}$ and ZnPc catalysts employed in this work for oxidation of cyclohexene result in a wider variety of products.

Table 5.1 shows the yields obtained for white light irradiation in the presence of ZnPc catalyst and after 3 hours of irradiation. The yields for cyclohexene photooxidation are lower than those observed from biomimetic oxidation using MPc complexes such as $FePc(Cl)_{16}$, FePc and CoPc and an oxidant (Table 4.2). It is however important to note that the yields will be highly dependent on the nature of the catalyst, solvent and on reaction time.

Table 5.1: Comparison of 0.9 mol/dm^3 cyclohexene oxidation product yields in the various solvents at light intensity = 0.52 x 10^{17} photons s^{-1} cm^{-2} catalyzed by 0.2 mg/mL ZnPc. Reaction time is 3 hours with white light irradiation.

Solvent	% Yield[a] Cyclohexen-1-one	Cyclohexen-1-ol	Cyclohexane diol	Cyclohexene hydroperoxide	Cyclohexene Oxide
1,4-dioxane Intensity:					
i) 0.52	4.4	1.0	0.30	1.1	0.08
ii) 1.0[b]	4.6	1.2	0.37	1.8	0.04
iii) 1.9[b]	5.1	1.6	0.27	1.4	0.02
THF	4.3	1.0	0.58	2.8	0.19
Benzene	1.8	0.4	0.11	0.4	0.03
DMF-CH_2Cl_2	6.6	1.6	0	0.7	0.08

[a] Product yields based on the substrate cyclohexene.

[b] Different light intensities, 10^{17} photons s^{-1} cm^{-2}.

It has been mentioned that product yields were higher for white light irradiation than with the red light (shown in Fig. 5.2). This is because white light has higher energy than the red ($E = h\upsilon$) to drive the reaction. Moreover, this could be attributed to increased amount of radicals in solution due to occurrence of redox reactions that have been characterized as abstractions of hydrogen from appropriate hydrogen donors (SH_2), by photoexcited MPc complexes, leading to the formation of Pc radicals[258], Scheme 5.2. In photooxidation reactions, SH_2 is more likely to be solvents and substrates. For 1,4-dioxane in particular which is not a proton donor, the substrate will donate hydrogens.

$$MPc \xrightarrow{h\nu} {}^{*}MPc \quad 5.7$$

$${}^{*}MPc \xrightarrow{SH_2} MPc\text{-}H^{\bullet} + SH^{\bullet} \quad 5.8$$

Scheme 5.2. Hydrogen abstraction and formation of MPc radicals.

Fig. 5.3 compares the yields formed with time for the various products. The highest yields were obtained for cyclohexenone (Table 5.1). The following trend in product yield based on the substrate (cyclohexene) was obtained:

Cyclohexenone > cyclohexene hydroperoxide > cyclohexenol > *trans*-cyclohexane diol > cyclohexene oxide.

The high yields of cyclohexenone compared to cyclohexenol could be due to the fact that the latter is known to phototransform to the former[218]. Thus, once cyclohexenol has been produced by photolysis, it will be transformed to cyclohexenone with time. This was investigated by photolyzing cyclohexenol alone; indeed it was oxidized to cyclohexenone. It is thus possible that both cyclohexenone and cyclohexenol are generated from the parent cyclohexene, but in addition, cyclohexenol is converted to cyclohexenone as photolysis proceeds, hence the much higher yields of the ketone relative to that of the alcohol.

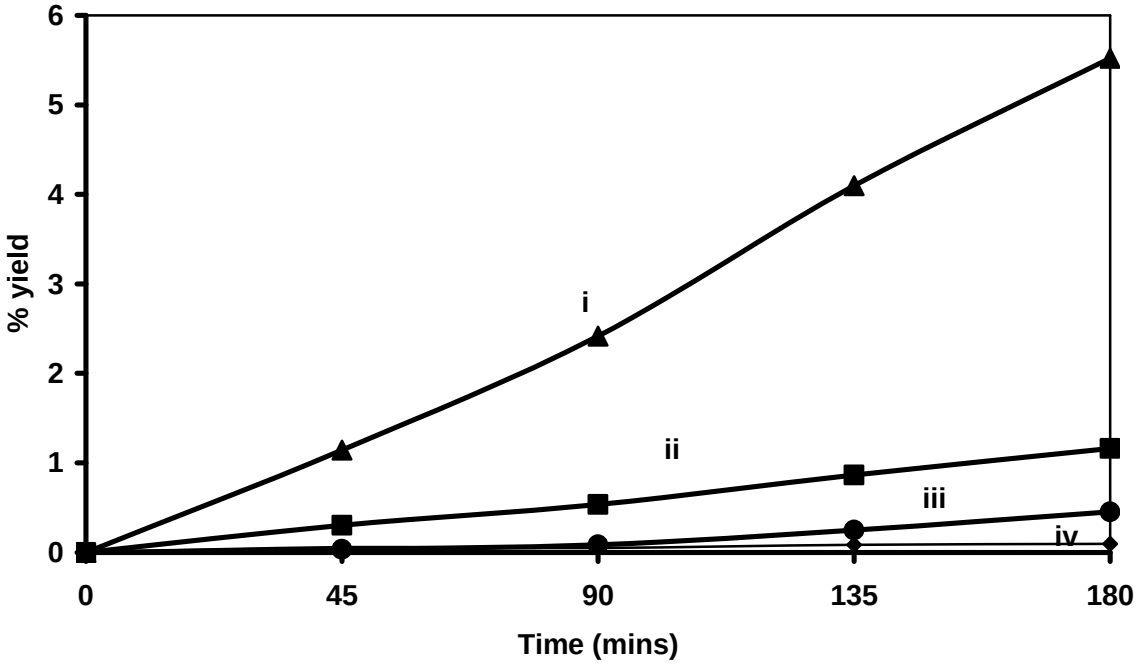

Figure 5.3: Variation of product yield with time for i) 2-cyclohexen-1-one ii) 2-cyclohexen-1-ol iii) *trans*-cyclohexanediol and iv) cyclohexene oxide under white light irradiation of 0.52 x 10^{17} photons/s.cm^2. Starting concentrations in 1,4-dioxane; cyclohexene = 0.9 mol dm^{-3} and ZnPc catalyst = 0.3 mg/mL.

It was observed that reactions continued in the dark following irradiation of solutions containing cyclohexene and ZnPc. It was also observed that product yields improved with increasing light intensity (Table 5.1) even though catalyst degradation was enhanced as will be discussed below. These two observations suggest that once reaction intermediates are formed upon interaction of singlet oxygen or radicals with the substrate, the reaction can still proceed in the dark in the presence or absence of the original form of the catalyst. Cyclohexene did not form products in the dark in the absence of the catalyst.

5.2. Solvent effects

Studies using porphyrin catalysts have shown that the nature and relative yields of products formed by catalytic photo-oxygenation of cyclohexene vary depending on the type of catalyst, oxidant, solvent, irradiation wavelength, irradiation period and light intensity[217,220]. The products obtained in this work for the ZnPc photocatalyzed oxidation of cyclohexene in 1,4-dioxane were similar to those obtained in THF and benzene, except lower yields on average were obtained for benzene (Table 5.1). When the 3:7 solvent mixture of DMF and CH_2Cl_2 was employed for the photo catalytic reaction, the yields of cyclohexene oxide, cyclohexenol and cyclohexenone were generally higher than for benzene and 1,4-dioxane (Table 5.1).

Chlorinated solvents are known to quench triplet states[259] of porphyrins and phthalocyanines according to Scheme 5.3, eq. 5.9[260,261], hindering generation of singlet oxygen. However photo-oxidation still occurred in the presence of dichloromethane, suggesting that it is not only singlet oxygen which is involved in the generation of products from cyclohexene, but that the radical mechanism is also important as will be discussed below.

$$Pc^* + RCl \rightarrow Pc^{\bullet+} + R^{\bullet} + Cl^{-} \qquad 5.9$$

$$Pc^{\bullet+} + R^{\bullet} + Cl^{-} + \text{Substrate} \rightarrow \text{Oxidation products} \qquad 5.10$$

where RCl is the chlorinated solvent.

Scheme 5.3. Quenching of excited states by chlorinated solvents.

As mentioned earlier, catalytic activity was lower in benzene, compared to other solvents, THF and 1,4-dioxane. It would be expected that

for the reaction to occur effectively, the solvent should be able to stabilize the formed intermediates. It has been reported that low polarity solvents do not stabilize the excited triplet state of the MPc (^{3}MPc*) formed by Type II mechanism, Scheme 5.4), nor radicals formed upon interaction of ^{3}MPc* with oxygen or substrate as effectively as high polarity solvents[202], Type I mechanism, Scheme 5.1. This accounts for low yields in the non-polar benzene compared to the other solvents. THF is more polar than 1,4-dioxane (dipole moment (μ) = 1.69 and 0.45 respectively[211]), but the former gave larger product yields in general.

$$MPc \xrightarrow{h\nu} {}^1MPc^* \xrightarrow{ISC} {}^3MPc^* \qquad 5.11$$

$$^3MPc^* + {}^3O_2 \rightarrow {}^1O_2 + MPc \qquad 5.12$$

$$^1O_2 + \text{substrate} \rightarrow \text{Oxidation products} \qquad 5.13$$

Scheme 5.4: Type II mechanism of photo-catalysis.

Photostability of the MPc molecule is known to affect catalytic activity: The less photostable the MPc is, the less catalytic it will be. ZnPc is known to photodecompose on irradiation using red light with high photobleaching quantum yields[57]. Excitation of phthalocyanines with visible light populates the triplet state resulting in generation of singlet oxygen which subsequently attacks the Pc complexes, resulting in decomposition[202]. The study of the photostability of ZnPc in the absence of substrate under visible light in 1,4-dioxane and THF showed degradation of the B and Q bands as shown in Fig. 5.4. Photobleaching quantum yields, ϕ_P were determined using a method discussed in the experimental section and using equation 5.14 that was introduced as eq. 2.4 in Chapter 2,

$$\phi_P = \frac{(C_0 - C_t)V}{I_{abs}t} \qquad 5.14$$

where symbols are as described before. The photobleaching quantum yields of ZnPc were determined to be valued at 1.2 x 10^{-6} and 1.56 x 10^{-4} in 1,4-dioxane and THF respectively. This implies that ZnPc is more photo-stable in the former solvent than in the latter[51].

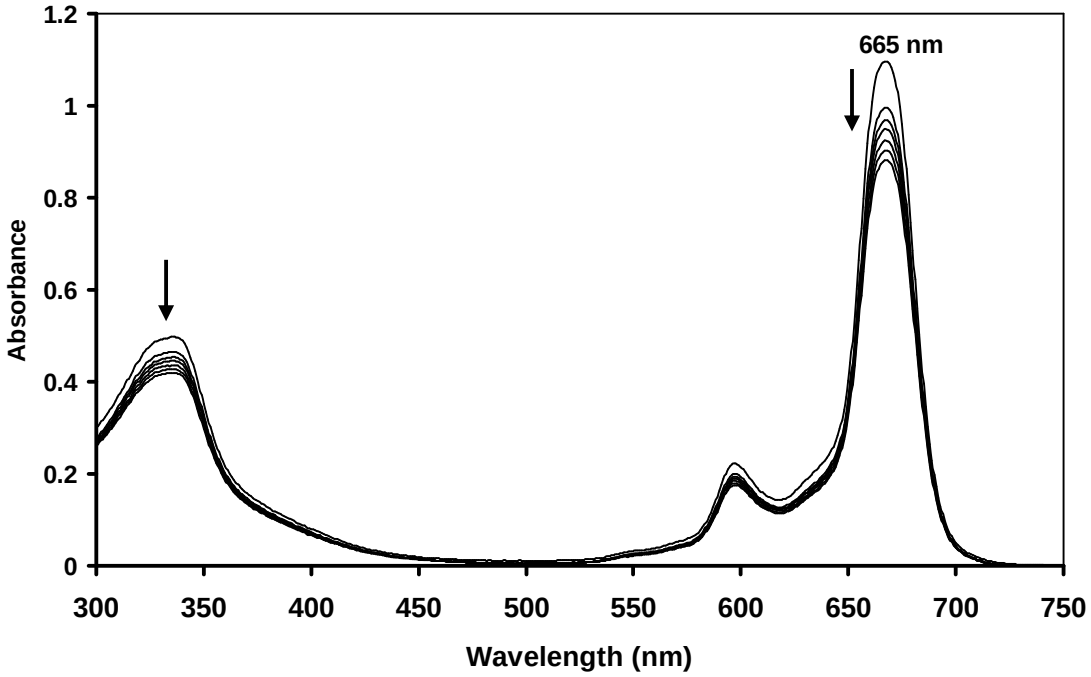

Figure 5.4: Photodegradation of ZnPc in 1,4-dioxane with visible light.

Triplet lifetime (τ_T) of the catalyst is another attributing factor since the longer it is, the larger the generation of the catalytic singlet oxygen. τ_T is the time needed for the concentration of the catalyst to decrease to 1/e of its original value. Fig. 5.5 shows the triplet absorption curve for ZnPc in THF, whose data was fitted onto ORIGINPro 7.5 software to determine the triplet lifetime. The τ_T values of ZnPc were found to be almost equal in THF and 1,4-

dioxane, i.e. 240 μs, hence explaining the almost similar product yields in some cases in these solvents.

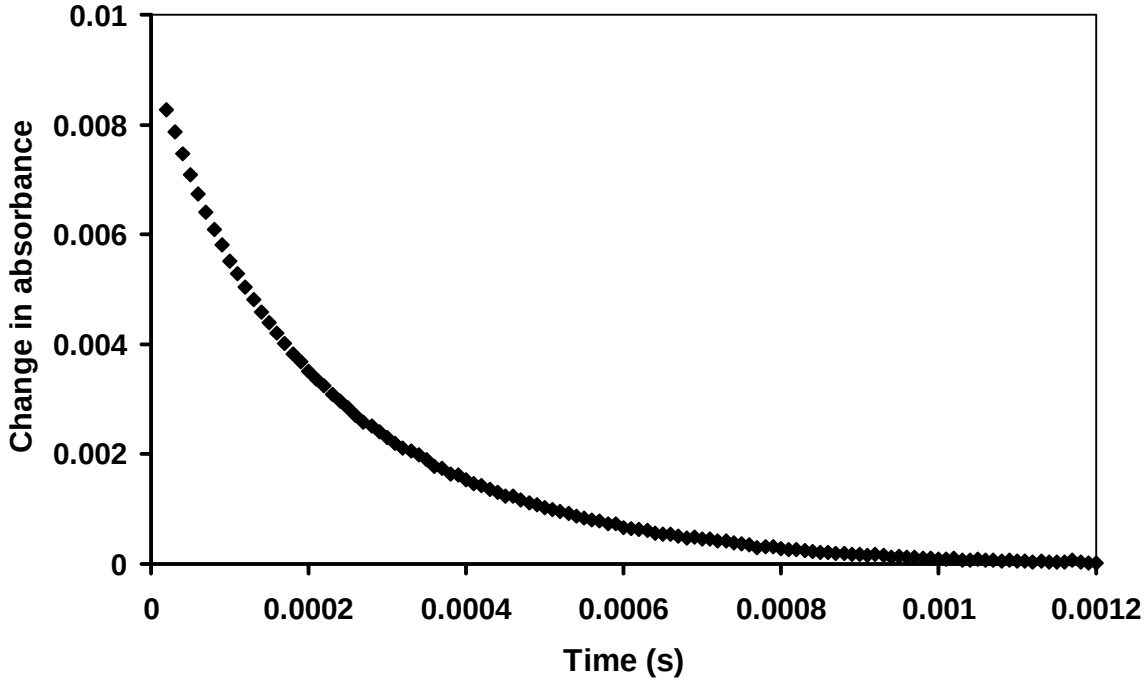

Figure 5.5: A triplet absorption curve of ZnPc in THF.

5.3. Fate of the ZnPc catalyst

The fate of the ZnPc catalyst during the photocatalysis of cyclohexene oxidation in 1,4-dioxane was monitored by UV/Vis spectroscopy. The ZnPc complex tended to decompose as photolysis progressed. This was evidenced by the decrease in the intensities of both the Q and Soret bands, with both red and white light irradiation, similar to changes shown in Fig. 5.4. However, the degradation was more pronounced with white light when compared with red light.

The rate of decomposition of the catalyst depended on light intensity as shown by Fig. 5.6. For low light intensity, the decomposition was minimal,

and the data reported in this work was undertaken using light intensity of 5.2 x 10^{16} photons $s^{-1}cm^{-2}$ which was low enough to avoid photodegradation of the catalyst. The rate of photodegradation of ZnPc using red light was the same as when white light was employed at the above-mentioned light intensity. The kinetic curve for red light was similar to that for white light of 5.2 x 10^{16} photons $s^{-1}cm^{-2}$ intensity in Fig. 5.6, suggesting that it is the photoexcitation of the ZnPc complex in the visible region which results in photodegradation.

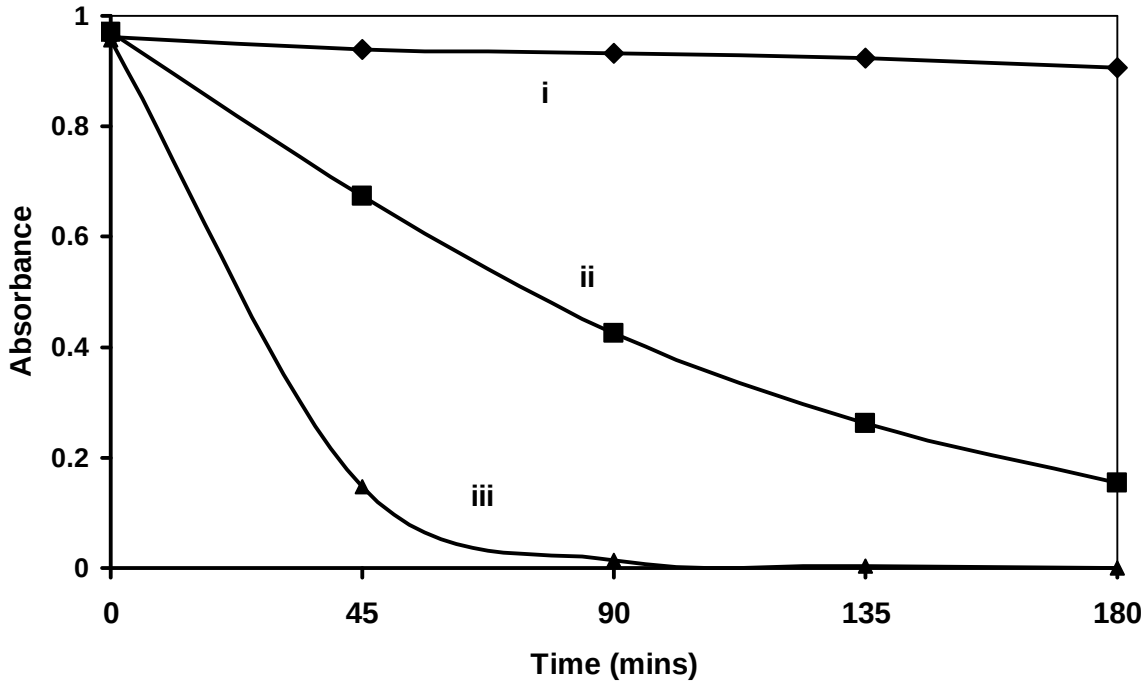

Figure 5.6: Variation of absorbance of ZnPc photocatalyst with time upon white light photolysis at various light intensities i) 0.52 ii) 1.0 and iii) 1.9 x 10^{17} photons s^{-1} cm^{-2}. Starting concentrations in 1,4-dioxane; cyclohexene = 0.9 mol dm^{-3} and ZnPc catalyst = 0.003 mg/mL.

5.4. Singlet oxygen versus radical mechanisms

In order to elucidate the mechanism (singlet oxygen, Type II or radical, Type I) for the ZnPc photocatalyzed oxidation of cyclohexene, experiments

were performed in; (i) air, (ii) bubbled oxygen, (iii) bubbled nitrogen, (iv) radical and singlet oxygen scavenger DABCO and (v) singlet oxygen scavenger, DPBF, Fig. 5.7. The experiments were performed in 1,4-dioxane. For all the products, yields in the presence of DPBF, a singlet oxygen quencher and DABCO, both a singlet oxygen and radical quencher were much lower, more especially in the latter situation. This indicates that both singlet oxygen and radicals are needed for the photocatalytic reaction to proceed faster. Fig. 5.7 shows that the highest yields were obtained in air.

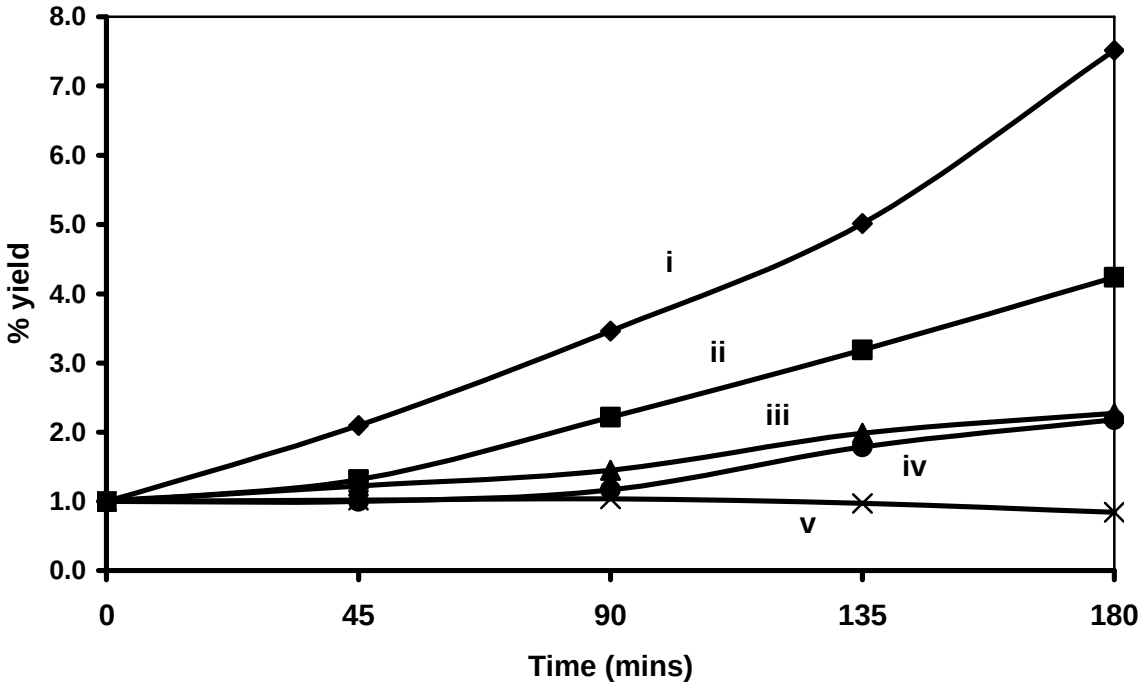

Figure 5.7: Kinetic curves for product formation from the ZnPc-photocatalyzed oxidation of cyclohexene in 1,4-dioxane under white light irradiation conditions in the presence of i) air, ii) nitrogen, iii) bubbled oxygen, iv) DPBF (0.03 g/mL) and v) DABCO (0.01 g/mL). Starting concentrations; cyclohexene = 0.9 mol dm^{-3} and ZnPc catalyst = 0.4 mg/mL.

When oxygen was bubbled to the solution, faster decomposition of the catalyst was observed than in air. As mentioned above, it is known that singlet oxygen adds to the macrocyclic ring of porphyrins and phthalocyanines

leading to cleavage and degradation[202]. The product of degradation is a phthalimide, shown in Scheme 5.5. The low product yields obtained in the presence of DPBF, show that singlet oxygen generated from ground state oxygen by ZnPc catalyst is needed for the reactions. However, the lower yields obtained in the presence of bubbled oxygen show that photodegradation of the catalyst by the generated singlet oxygen becomes a limiting factor in the formation of the products. Thus for the photocatalytic reactions discussed in this work, singlet oxygen should be in moderation not to cause oxidative degradation of the catalyst. When nitrogen was bubbled through the solution containing ZnPc and cyclohexene, the yields of the products decreased, again confirming that oxygen is needed for the reactions.

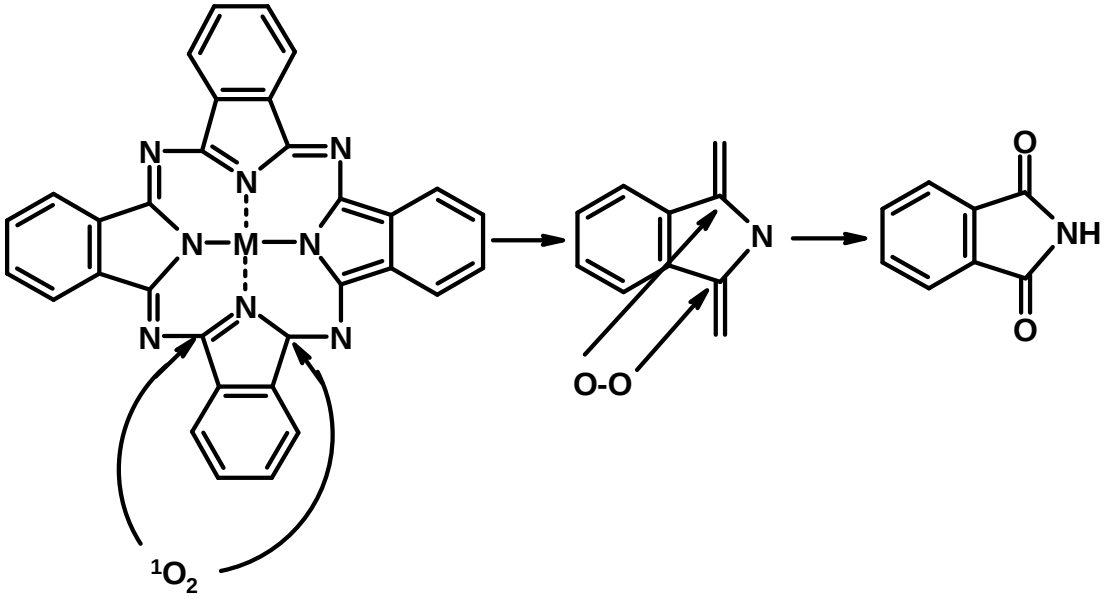

Scheme 5.5: Degradation of MPc by singlet oxygen.

It has been reported that intermediates such as endo-peroxides[262], dioxetanes[263], zwitterions[264], biradicals[265], and peroxiranes[266] are formed upon interaction of singlet oxygen with ethylenes. Using these types of intermediates, it is proposed in this work that cyclohexene hydroperoxide,

trans-cyclohexanediol and cyclohexene oxide are formed as shown by Scheme 5.6;

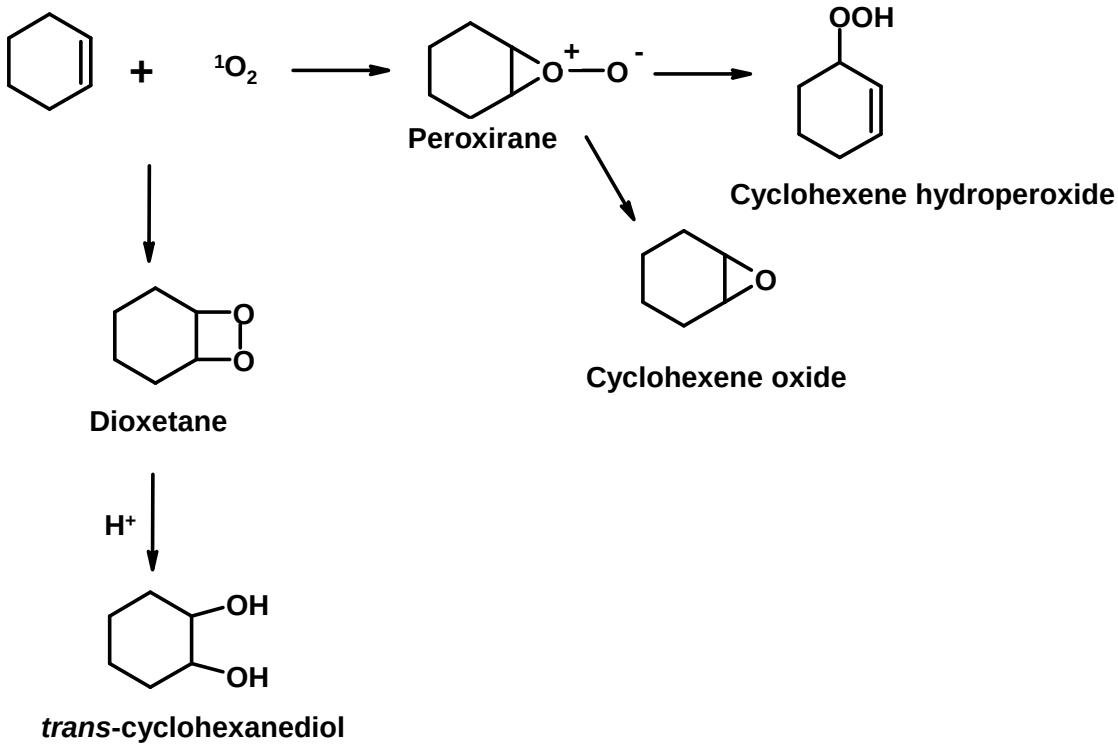

Scheme 5.6: Suggested mechanism for the formation of photolysis products.

Formation of cyclohexene hydroperoxide results from the 'ene' reaction, (proton abstraction and addition) while that of cyclohexene oxide results from loss of oxygen atom inductively. Protonation of dioxetane, which may form as an intermediate, could give t*rans*-cyclohexanediol as shown by Scheme 5.6.

It can be concluded that photooxidation of cyclohexene under white light irradiation catalyzed by ZnPc leads to formation of cyclohexene oxide, 2-cyclohexen-1-ol, 2-cyclohexen-1-one, cyclohexene hydroperoxide and *trans*-1,2-cyclohexane diol. Product yields were dependent on the nature of solvent, irradiation wavelength, light intensity and irradiation period. Cyclohexene oxide was not formed when red light was used, and product yields were lower

with red light irradiation. Product yields were observed to increase with light intensity, though care should be taken that it is not too intense so as not to degrade the catalyst.

Chapter 6

Conclusions

Conclusions

The main aim of the project was to use metallophthalocyanine complexes as electrocatalysts towards thiol and thiocyanate oxidation as well as reduction of oxygen. Electrodes were successfully modified with the MPc catalysts. Glassy carbon electrode was modified by adsorption, electrodeposition and electropolymerization of CoTEThPc and CoTPhPyrPc complexes, and employed in oxidation of 2-mercaptoethanol (2-ME), *L*-cysteine (CYS) and *reduced* glutathione (GSH). Co(II/I) redox couple was involved in the catalysis. CoTEThPc exhibited higher catalytic activity towards thiol oxidation than CoTPhPyrPc in terms of peak potentials and current intensities.

It was also observed that adsorbed complexes showed higher catalytic activity than their electrodeposited counterparts, indicating that thiols could interact easily with the metal centre of the catalysts in adsorbed, loosely held films as opposed to the compact films obtained with electrodeposition. Concentration of MPc complex on the electrodes was observed not to increase the catalytic activity which indicated that only the external layers are active and the analyte does not have access to the bulk of the film. The order of thiol activation (in terms of potential and current) was found to be 2-ME > CYS > GSH, for both MPc complexes. Moreover, catalytic activity was found to be pH dependent and it involved interaction of analyte with the metal centre in the complex. Thiol oxidation was found to be a first order reaction.

This study offers a new range of cobalt substituted phthalocyanines as possible electrocatalysts for the highly demanded oxidation of thiols in aqueous solutions.

Screen printed carbon electrodes incorporated with CoPc electrocatalyzed oxidation of GSH and 2-ME in neutral and alkaline solutions. Co(II/I) redox couple was involved in catalysis, but activity was better for 2-ME oxidation compared to CoTEThPc and CoTPhPyrPc complexes adsorbed onto glassy carbon electrodes. Lifetime and integrity of CoPc-SPCEs depended on the solvent in which CoPc was dissolved during fabrication. This work shows use of SPCEs in thiol oxidation reactions, forming a platform for application in biological studies.

CoPc adsorbed onto an ordinary pyrolytic graphite electrode detected *oxidized*-glutathione (GSSG) formed from decomposition of *s*-nitroso glutathione (GSNO). Moreover, oxidation of *reduced*-glutathione (GSH) was observed concurrently on the CoPc-OPG electrode. Thus this electrode achieved indirect detection of thiols as opposed to direct methods where thiols are detected in solutions in which they are added. Moreover, this approach provides a new route for analysis of GSNO decomposition, other than studying the amount of released NO. Although additional experiments are needed in order to start building a dual electrode system to sense both NO and GSH/GSSG, these results are very promising.

A self-assembled monolayer of CoTEThPc complex electrocatalyzed irreversible oxidations of thiocyanate (SCN^-), CYS and 2-ME in acidic media. The oxidation of 2-ME in acid media is not common since it occurs with more

difficulty than in basic media. This work provides a workable electrode for analysis of this species in acid media. A detection limit of the order of 10^{-7} M was obtained for SCN^- and 10^{-8} M for CYS and 2-ME. The oxidation of thiocyanate involved transfer of two electrons and was catalyzed by $Co^{III/}Co^{II}$ and $Co^{III}Pc^{-1}/Co^{III}Pc^{-2}$ redox processes. The oxidation of 2-ME was mediated by the $Co^{III}Pc^{-1}/Co^{III}Pc^{-2}$ redox process in CoTEThPc and involved transfer of two electrons. For *L*-cysteine, both Co^{III}/Co^{II} and $Co^{III}Pc^{-1}/Co^{III}Pc^{-2}$ redox processes were involved. For all three analytes, a reaction order of 1 was obtained.

Moreover, manganese, iron and cobalt phthalocyanine complexes substituted with different ring ligands were adsorbed on glassy carbon electrodes and used for oxygen reduction to hydrogen peroxide in acidic or slightly alkaline media and to water in highly alkaline media. The number of electrons transferred was calculated to be 2 and 4 for the peroxide and water respectively. Tafel slopes near 60 and 120 mV/decade were obtained, implying that a fast electron transfer is followed by a slow chemical step, for the former, and one electron is transferred during the rate determining step, for the latter. Oxygen reduction occurs via different mechanisms on MnPc, CoPc and FePc complexes.The reaction order was found to be one in the pH range 1 -13.

Metallophthalocyanine complexes were also employed as biomimetic catalysts for oxidation of cyclohexene. The reaction was conducted using *tert*-butylhydroperoxide (TBHP) or chloro-peroxybenzoic acid (CPBA) oxidants in the presence of $FePc(Cl)_{16}$, FePc and CoPc catalysts. Formed products were cyclohexene oxide, 2-cyclohexen-1-ol and 2-cyclohexen-1-one, with adipic

acid formed over a long time. Product selectivity varied with the nature of the catalyst and the oxidant: $FePc(Cl)_{16}$ and CoPc showed selectivity towards cyclohexen-1-one, while FePc favoured formation of cyclohexen-1-ol when TBHP was employed as an oxidant. Cyclohexene oxide was favoured when CPBA oxidant was used. Generally, better selectivity was obtained when TBHP was used as an oxidant other than CBPA.

When $FePc(Cl)_{16}$ was employed as catalyst and TBHP as oxidant, the highest yields were obtained for the 2-cyclohexen-1-one, whereas cyclohexene oxide was the major product when CPBA was used. Product yields were lower when CPBA was used as an oxidant; this is because it degraded MPc catalysts faster than TBHP. However, $FePc(Cl)_{16}$ did not degrade as fast as the other complexes during the course of the reaction, confirming that indeed ring substitution with electron-withdrawing ligands stabilizes MPcs against oxidative degradation. The $FePc(Cl)_{16}$ catalyst was transformed to the $Cl_{16}PcFe^{III}$-O-$^{III}FePcCl_{16}$ species during the catalytic process. $Fe^{III}Pc$ and $Co^{III}Pc$ species were implicated as intermediates when the FePc and CoPc were employed as catalysts.

When ZnPc was employed as a photocatalyst for oxidation of cyclohexene, the following products were formed under white light irradiation, cyclohexene oxide, 2-cyclohexen-1-ol, 2-cyclohexen-1-one, *trans*-1,2-cyclohexane diol and cyclohexene hydroperoxide. Product yields were dependent on the nature of solvent, irradiation wavelength, light intensity and irradiation period. Reaction mechanism involved both singlet oxygen and radicals. The range of products formed was larger for the photocatalytic transformation of cyclohexene in the presence of ZnPc when compared to

biomimetic catalysis. It could be concluded that new products cyclohexene hydroperoxide and *trans*-cyclohexanediol were formed via singlet oxygen mechanism while cyclohexene oxide, cyclohexenol and cyclohexenone were formed via radical mechanism. Thus the use of photocatalysis could assist the petroleum industry in achieving a wider variety of useful products.

As a general conclusion, metallophthalocyanine complexes were used successfully as electrocatalysts for oxidation of thiocyanate, *L*-cysteine, 2-mercaptoethanol and *reduced* glutathione, decomposition of *s*-nitroso glutathione as well as reduction of oxygen. They were also employed with great success as biomimetic and photo-catalysts of cyclohexene oxidation.

References

1. M.J. Stillman, in *Phthalocyanines: Properties and applications,* C.C. Leznoff and A.B.P. Lever (Ed.s), Vol. 3, VCH Publishers, New York, 1993.
2. P. Erk and H. Hengelsberg, in *The Porphyrin Handbook,* K.M. Radish, K.M. Smith and R. Guilard (Ed.s), Vol. 19, Academic Press, San Diego, 2003.
3. J. Simon and T. Toupance, in *Comprehensive supra-molecular chemistry,* D.N. Reinhoudt (Ed.), Vol. 10, Pergamon, London, 1996.
4. N.B. McKeown, in *The Porphyrin Handbook,* K.M. Radish, K.M. Smith and R. Guilard (Ed.s), Vol. 15, Academic Press, San Diego, 2003.
5. I. Rosenthal, *Photochem. Photobiol.,* **6** (1991) 859.
6. E. Luk'yanets, *J. Porphyrins Phthalocyanines,* **3** (1999) 424.
7. S.R. Flom, in *The Porphyrin Handbook,* K.M. Radish, K.M. Smith and R. Guilard (Ed.s), Vol. 19, Academic Press, San Diego, 2003.
8. N.S. Nalwa and J.S. Shirk, in *Phthalocyanines: Properties and applications,* Ed. C.C. Leznoff and A.B.P. Lever, Vol. 4, VCH Publishers, New York, 1996.
9. S. Griveau, J. Pavez, J. Zagal and F. Bedioui, *J. Electroanal. Chem*., **497** (2001) 75.
10. C.A. Caro, J.H. Zagal and F. Bedioui, *J. Electrochem. Soc.,* **150** (2003) E95.
11. M. Kimura and H. Shirai, in *The Porphyrin Handbook,* K.M. Radish, K.M. Smith and R. Guilard (Ed.s), Vol. 19, Academic Press, San Diego, 2003.

12. K. Kasuga, K. Mori, T. Sugimori and M. Handa, *Bull. Chem. Soc. Jpn.,* **73** (2000) 939.

13. J.D. Spikes, *Photochem. Photobiol. B: Biol.,* **6** (1990) 259.

14. R. Hagen and T. Bieringer, *Adv. Mater.,* **13** (2001)1805.

15. F.H. Moser and A.L. Thomas, in *Phthalocyanine Compounds,* Reinhold: New York, Chapman and Hall, London, 1963.

16. F.H. Moser and A.L. Thomas, in *The Phthalocyanines,* Vol.s 1&2, CRC, Boca Raton, 1983.

17. M. Hanack and M. Lang, *Adv. Mat.,* **6** (1994) 819.

18. D. Wohrle, G. Schnurpfeil and G. Knothe, *Dyes and Pigments*, **18** (1992) 91.

19. P. Yiru, H. Fenghua, L. Zhipeng, C. Naisheng and H. Jinling, *Inorg. Chem. Commun.,* **7** (2004) 967.

20. A. Lützen, S.D. Starnes, D.M. Rudkevich and J. Rebeck Jr., *Tet. Lett.,* **41** (2000) 3777.

21. F. Yilmaz, D. Atilla and V. Ahsen, *Polyhedron*, **23** (2004) 1931.

22. N.B. Mckeown, in *Phthalocyanine Materials: Synthesis, Structure and Function*, Cambridge University Press, London, 1998.

23. J. Mack and M.J. Stillman, *J. Am. Chem. Soc.,* **116** (1994) 1292.

24. K. Walzer and M. Hietschold, *Surf. Sci.,* **471** (2001) 1.

25. M.J. Stillman and T. Nyokong, in *Phthalocyanines: Properties and applications,* C.C. Leznoff and A.B.P. Lever (Ed.s), Vol. 1, VCH Publishers, New York, 1989.

26. I. Seotsanyana-Mokhosi, N. Kuznetsova and T. Nyokong, *Photochem. Photobiol. A: Chem.,* **140** (2001) 215.

27. G. de la Torre, M.V. Martinez-Diaz and T. Torres, *J. Porphyrins Phthalocyanines,* **3** (1999) 560.

28. S. Maree, D. Phillips and T. Nyokong, *J. Porphyrins Phthalocyanines,* **6** (2002) 17.

29. Z. Zhao, K. Ozoemena, M.D. Maree and T. Nyokong, *Dalton Trans.,* (2005) 1241.

30. V.N. Nemykin, V.Y. Chernii, S.V. Volkov, N.I. Bundina, O.L. Kaliya, V.D. Li and E.A. Luk'yanets, *J. Porphyrins Phthalocyanines,* **3** (1999) 87.

31. J. Jiang, W. Liu and D.P. Arnold, *J. Porphyrins Phthalocyanines,* **7** (2003) 459.

32. K. Durr and M. Hanack, *J. Porphyrins Phthalocyanines,* **3** (1999) 224.

33. N. Kobayashi, A. Muranaka, and V.N. Nemykin, *Tet. Lett*., **42** (2001) 913.

34. P. Matlaba and T. Nyokong, *Polyhedron*, **21** (2002) 2463.

35. P.N. Day, Z. Wang and R. Pachter, *J. Mol. Struc. (THEO-Chem),* **455** (1998) 33.

36. T. Nyokong, Z. Gasyna and M.J. Stillman, *Inorg. Chem.,* **26** (1987) 548.

37. T. Nyokong, Z. Gasyna, and M.J. Stillman, *Inorg. Chem.,* **26** (1987) 1087.

38. E.A. Ough, T. Nyokong, K.A. Creber and M.J. Stillman, *Inorg. Chem.,* **27** (1988) 2724.

39. E.A. Ough, Z. Gasyna and M.J. Stillman, *Inorg. Chem.,* **30** (1991) 2301.

40. E.A. Ough and M.J. Stillman, *Inorg. Chem.,* **33** (1994) 573.

41. M. Gouterman, in *The Porphyrins,* D. Dolphin (Ed.), Physical Chemistry, Part A, Vol. 3, Academic Press: New York, 1978.

42. F.R. Fan and L.R. Faulkner, *J. Am. Chem. Soc*., **101** (1979) 4779.

43. K. Kasuga, N. Matsura, K. Inoue, M. Handa, T. Sugimori, K. Isa and M. Nakata, *Chem. Lett.,* (2002) 352.

44. G.A. Kumar, J. Thomas, N.V. Unnikrishnan, V.P.N. Nampouri and C.P.G. Vallabhan, *J. Porphyrins Phthalocyanines,* **5** (2001) 456.

45. M. Stillman, J. Mack and N. Kobayashi, *J. Porphyrins Phthalocyanines,* **6** (2002) 296.

46. M. Gouterman, *J. Mol. Spectrosc.,* **6** (1961) 138.

47. A. Ogunsipe, J.-Y. Chen and T. Nyokong, *New J. Chem.,* **28** (2004) 822.

48. Z. Zhao, A. Ogunsipe, M.D. Maree and T. Nyokong, *J. Porphyrins Phthalocyanines,* **9** (2005) 186.

49. M.D. Maree, N. Kuznetsova and T. Nyokong, *Photochem. Photobiol. A: Chem.,* **140** (2001) 117.

50. M.J. Cook, *Chem. Rec.,* **4** (2002) 225.

51. A. Ogunsipe and T. Nyokong, *J. Mol. Struc.,* **689** (2004) 89.

52. A. Beeby, S. FitzGerald and C.F. Stanley, *J. Chem. Soc. Perkin Trans.,* **2** (2001) 1978.

53. W.–F. Law, R.C.W. Liu, J. Jiang and D.K.P. Ng., *Inorg. Chim. Acta.,* **256** (1997) 6349.

54. N. Kobayashi and H. Konami, in *Phthalocyanines: Properties and applications,* C.C. Leznoff and A.B.P. Lever (Ed.s), Vol. 4, VCH Publishers, New York, 1999.

55. F.R. Fronczek, R.J. Johnson and R.M. Strongin, *Acta Cryst.,* **E57** (2001) 447.

56. J.G. Calvert and J.N. Pitts, in *Photochemistry,* John Wiley & Sons, Inc., New York, 1966.

57. A. Ogunsipe, D. Maree and T. Nyokong, *J. Mol. Struc.,* **650** (2003) 131.

58. A.B.P. Lever, E.R. Milaeva and G. Speier, in *Phthalocyanines: Properties and applications,* C.C. Leznoff and A.B.P. Lever (Ed.s), Vol. 3, VCH Publishers, New York, 1989.

59. A.B.P. Lever, M.R. Hempstead, C.C. Leznoff, W. Liu, M. Melnik, W.A. Nevin and P. Seymour, *Pure Appl. Chem.,* **58** (1986) 1467.

60. M. L'Her and A. Pondaven. in *The Porphyrin Handbook*, K.M. Kadish, K.M. Smith and R. Guilard (Ed.s), Vol. 16, Academic Press, San Diego, 2003.

61. A.B.P. Lever, S. Licoccia, K. Magnell, R.C. Minor and B.S. Ramaswamy, *ACS Symp. Ser.,* **201** (1982) 237.

62. T. Nyokong, *S.A. J. Chem.,* **48** (1995) 23.

63. M.N. Golovin, P. Seymour, K. Jayaraj, Y.S. Fu and A.B.P. Lever, *Inorg. Chem.,* **29** (1990) 1719.

64. T. Nyokong, *Polyhedron,* **12** (1993) 375.

65. T. Kuwana, R.K. Darlington and D.W. Leedy, *Anal. Chem*., **36** (1964) 2023.

66. J. Obirai and T. Nyokong, *J. Electroanal. Chem.,* **573** (2004) 77.

67. D.B. Hibbert, in *Introduction to Electrochemistry*, Macmillan, London, 1993.

68. L. Gaffo, M.J.S.P. Brasil, F. Cerdeira, C. Giles and W.C. Moreira, *J. Porphyrins Phthalocyanines,* **9** (2005) 89.

69. J.W. Dodd and N.S. Hush, *J. Chem. Soc.,* (1964) 4607.

70. L.D. Rollman and R.T. Iwamoto, *J. Am. Chem. Soc.,* **90** (1968) 1455.

71. D.W. Clack and J.R. Yandle, *Inorg. Chem.,* **11** (1972) 1738.

72. G. Inzelt, in *Electroanalytical methods: Guide to experiments and applications,* F. Scholz (Ed.), Springer 2002.

73. H. Kahlert, in *Electroanalytical methods: Guide to experiments and applications*, F. Scholz (Ed.), Springer 2002.

74. W.R. Heineman and P.T. Kissinger, in *Laboratory Techniques in Electroanalytical-chemistry*, 2nd ed, P.T. Kissinger and W.R. Heineman (Ed.s), Marcel Deccer Inc., New York, 1996.

75. A.J. Bard and L.R. Faulkner, in *Electrochemical Methods: Fundamentals and Applications,* John Willey & Sons, Toronto, 1996.

76. J. O'M. Bockris and S.U.M. Khan, in *Surface electrochemistry: A molecular level approach,* Plenum Press, New York, 1993.

77. V.G. Levich, in *Physicochemical hydrodynamics* (English translation), Prentice Hall, New Jersey, 1962.

78. C.M.A. Brett and A.-M.O. Brett, in *Electrochemistry, principles, methods and applications,* Oxford University Press, 1993.

79. M.J. Aguirre, M. Isaacs, F. Armijo, L. Basaez and J.H. Zagal, *Electroanalysis,* **14** (2002) 356.

80. B. Wermeckers and F. Beck, *Electrochim. Acta,* **30** (1985) 1491.

81. J.H. Zagal, *Coord. Chem. Rev.,* **119** (1992) 89 and references cited therein.

82. J.H. Zagal and C. Paez, *Electrochim. Acta,* **34** (1989) 243.

83. J.-M. Zen, A.S. Kumar and M.-R. Chang, *Electrochim. Acta,* **45** (2000)1691.

84. J. Zagal, R.K. Sen and E. Yeager, *J. Electroanal. Chem*., **83** (1977) 207.

85. M. Gulppi, F. Bedioui and J.H. Zagal, *Electroanalysis,* **13** (2001) 1136.

86. N.B. McKeown, *Chem. Ind.,* (1999) 92.

87. J. Oni and T. Nyokong, *Anal. Chim. Acta,* **434** (2001) 9.

88. J. Zagal, P. Bindra and E. Yeager, *J. Electrochem. Soc.,* **127** (1980) 1506.

89. S. Maree and T. Nyokong, *J. Electroanal. Chem.,* **492** (2000) 120.

90. M. Sekota and T. Nyokong, *Polyhedron*, **16** (1997) 3279.

91. S. Ledru, N. Ruillé and M. Boujtita, *Biosens. Bioelectron.,* **21** (2006) 1591.

92. C.D. Kuhnline, M.G. Gangel, M.K. Hulvey and R.S. Martin, *Analyst,* **131** (2006) 202.

93. A. Napier and J.P. Hart, *Electroanalysis,* **8** (1996) 1006.

94. T.J. Mafatle and T. Nyokong, *J. Electroanal. Chem.,* **408** (1996) 213.

95. M.J. Cook, *Pure Appl. Chem*., **71** (2002) 2145.

96. X. Lu, K.W. Hipps, X.D. Wang and U. Mazur, *J. Am. Chem. Soc.*, **118** (1996) 7197.

97. M.J. Cook, *J. Mater. Chem.,* **6** (1996) 677.

98. C.A. Caro, F. Bedioui and J.H. Zagal, *Electrochim. Acta*, **47** (2002) 1489.

99. K.I. Ozoemena, P. Westbroek and T. Nyokong, *Electrochem. Commun.,* **3** (2001) 529.

100. B.J. Hwang, R. Santhanam and Y.W. Chang, *Electroanalysis,* **14** (2002) 363.

101. J. Obirai, N. Pereira-Rodrigues, F. Bedioui and T. Nyokong, *J. Porphyrins Phthalocyanines,* **7** (2003) 508.

102. S. Griveau and F. Bedioui, *Electroanalysis,* **13** (2001) 253.

103. M.J. Cook and A. JafariFini, *J. Mater. Chem*., **7** (1997) 5.

104. Z. Li and M.Lieberman, *Langmuir*, **17** (2001) 4887.

105. X. Li, W. Xu, X. Wang, H. Jia, B. Zhao, B. Li and Y. Ozaki, *Thin Solid Films,* **457** (2004) 372.

106. K.I. Ozoemena and T. Nyokong, *J. Electroanal. Chem.,* **579** (2005) 283.

107. Z. Li and M. Lieberman in *Fundamental and applied aspects of chemically modified surfaces,* J.P. Blitz and C.B. Little (Eds), Royal society of chemistry. Lettchworth, UK, 1999.

108. K.I. Ozoemena and T. Nyokong, *Talanta,* **67** (2005) 162.

109. B. Liedberg and P. Tengvall, *Langmuir*, **11** (1995) 3821.

110. M.P. Somashekarappa, J. Keshavayya and S. Sampath, *Pure Appl. Chem.*, **74** (2002) 1609.

111. M. Thamae and T. Nyokong, *J. Electroanal. Chem.,* **579** (1999) 126.

112. J. Obirai and T. Nyokong, *Electrochim. Acta*, **49** (2004) 1417.

113. S. Griveau, V. Albin, T. Pauporte, J.H. Zagal and F. Bedioui, *J. Mater. Chem.,***12** (2002) 225.

114. J. Obirai, F. Bedioui and T. Nyokong, *J. Electroanal. Chem.,* **576** (2005) 323.

115. E. Crouch, D.C. Cowell, S. Hoskins, R.W. Pittson and J.P. Hart, *Anal. Biochem.,* **347** (2005) 17.

116. J. Wang and P.V.A. Pamidi, *Talanta,* **42** (1995) 463.

117. S. Miserere, S. Ledru, N. Ruillé, S. Griveau, M. Boujtita and F. Bedioui, *Electrochem. Comm.,* **8** (2006) 238.

118. J.R. de Sousa, A.A. Batista, I.C.N. Diogenes, G.F.S. Andrade, M.L.A. Temperini, L.G.F. Lopes and I. D.-S. Moreira, *J. Electroanal. Chem.,* **543** (2003) 93.

119. J. Chen, J. Su, W. Wang and M.A. Reed, *Physica E*, **16** (2003) 17.

120. Y. Naitoh, T. Matsumoto, K.-I. Sugiura, Y. Sakata and T. Kawai, *Surf. Sci.,* **487** (2001) L534.

121. M.S. El-Deab and T. Ahsaka, *Electrochem. Commun.,* **5** (2003) 214.

122. X. Huang, Y. Liu, S. Wang, S. Zhou and D. Zhu, *Chem. Eur. J.*, **8** (2002) 4179.

123. F. Bedioui, J. Devynck and C. Bied-Charreton, *Acc. Chem. Res.,* **28** (1995) 30 and references cited therein.

124. K. Nishiyama, S.I. Tahara, Y. Uchida, S. Tanoue and I. Taniguchi, *J. Electroanal. Chem*., **478** (1999) 83.

125. K.V. Gothelf, *J. Electroanal. Chem*., **494** (2000) 147.

126. H.O. Finklea in Electroanalytical Chemistry, A.J. Bard, I. Rubenstein (Eds), Vol 19 (and references therein), Marcel Dekker, New York, 1996.

127. E. Sabatani and I. Rubinstein, *J. Phys. Chem.,* **91** (1987) 6663.

128. M.D. Porter, T.B. Bright, D. Allara and C.E.D. Chidsey, *J. Am. Chem. Soc*., **109** (1987) 3559.

129. D. Losic, J.G. Shapter and J.J. Gooding, *Langmuir*, **17** (2001) 3307.

130. J. Wang, J.L.P. Paz and M. Jiang, *Langmuir*, **15** (1999) 1884.

131. D.L. Pilloud, X. Chen, P.L. Dutton and C.C. Moser, *J. Phys. Chem. B,* **104** (2000) 2868.

132. K.I. Ozoemena and T. Nyokong, *Electrochim. Acta,* **47** (2002) 4035.

133. H. Ohmori and I. Yamamoto, *J. Exp. Med.,* **155** (1982) 1277.

134. W.A. Kleinman and J.P. Richie, *Biochem. Pharmacol.,* **60** (2000) 19.

135. A. Meister, *J. Biol. Chem.,* **263** (1988) 17205.

136. I. Chatti, A. Ghorbel, P. Grange and J.M. Colin, *Catal. Today,* **75** (2002) 113.

137. P.M. Schweizer-Berberich, S. Vaihinger and W.Gopel, *Sens. Actuators,* **B18-19** (1994) 282.

138. D.L.H. Williams, *Chem. Soc. Rev.*, **14** (1985) 171.

139. C.M. Venturini, R.M. Palmer and S. Moncada, *J. Pharmacol. Exp. Ther.,* **266** (1993) 1497.

140. M.W. Radomski, D.D. Rees, A. Dutra and S. Moncada, *Br. J. Pharmacol.,* **107** (1992) 745.

141. E.J. Langford, A.S. Brown, A.J. de Belber, R.E.A. Smith, J.F. Martin, R.J. Wainwright, M.R. Thomas, M.W. Radomski and S. Moncada, *Lancet,* **344** (1994) 1458.

142. A.D. Belber, C. Lees, J. Martin, S. Moncada and S. Campbell, *Lancet*, **345** (1995) 124.

143. S. Modi, S.S. Deodhar, D.V. Behere and S. Mitra, *Biochemistry,* **30** (1991) 118.

144. D. Gao, J.-Z. Li, and R.-Q. Yu, *Anal. Chem.,* **66** (1994) 2245.

145. M.K. Amini, S. Shahrokhian and S. Tangestaninejad, *Anal. Chim. Acta*, **402** (1999) 137.

146. N. Phougat and P. Vasudevan, *J. Power Sources,* **69** (1997) 161.

147. E. Itabashi, *Inorg. Chem*., **24** (1985) 4024.

148. S. Adak, A. Mazumdar and R.K. Banerjees, *J. Biol. Chem.,* **272** (1997) 11049.

149. T.M. Aune and E.L. Thomas, *Eur. J. Biochem.,* **80** (1977) 209.

150. E.L. Thomas, *Biochemistry,* **20** (1981) 3273.

151. S. Modi, D.V. Behere and S. Mitra, *Biochemistry,* **28** (1989) 4689.

152. S. Modi, D.V. Behere and S. Mitra, *J. Biol. Chem.,* **264** (1989) 19677.

153. V.K. Sharma, D.B. O'Connor and D. Cabelli, *Inorg. Chimica Acta,* **357** (2004) 4587.

154. T. Ohta, T. Kamachi, Y. Shiota and K. Yoshizawa, *J. Org. Chem.,* **6** (2001) 4122.

155. T. Nyokong in *N_4-macrocyclic metal complexes,* J.H. Zagal, F. Bedioui and J-P. Dodelet (Ed.s), Springer, New York, 2006.

156. K.I. Ozoemena, T. Nyokong and P. Westbroek, *Electroanalysis,* **14** (2003) 1.

157. G.I. Cardenas-Jiron, M.A. Gulppi, C.A. Caro, R. del Rio, M. Paez and J.H. Zagal, *Electrochim. Acta,* **46** (2001) 3227.

158. D. Mimica, F. Bedioui and J.H. Zagal, *Electrochim. Acta*, **48** (2002) 323.

159. X. Qi and R.P. Baldwin, *J. Electrochem. Soc.,* **143** (1996) 1283.

160. M.A. Gulppi, M.A. Paez, J.A. Costamagna, G.I. Cardenas-Jiron, F. Bedioui and J.H. Zagal, *J. Electroanal. Chem.,* **580** (2005) 50.

161. N. Pereira-Rodrigues, R. Cofré, J.H. Zagal and F. Bedioui, *Bioelectrochem*., 2006, in press.

162. D. Giustarini, A. Milzani, R. Colombo, I. Dalle-Donne and R. Rossi, *Clin. Chim. Acta,* **330** (2003) 85.

163. M.P. Gordge, J.S. Hothersall, G.H. Neild and A.A.N. Dutra, *Br. J. Pharmacol.*, **119** (1996) 533.

164. P.D. Wood, B. Mutus and R.W. Redmond, *Photochem. Photobiol*., **64** (1996) 518.

165. R.J. Singh, N. Hogg, J. Joseph and B. Kalyanaraman, *J. Biol. Chem.*, **271** (1996) 18596.

166. M. David-Dufihlo, A. Brunet and F. Bedioui, *Electroanalysis*, **18** (2006) 1827.

167. Y. Hou, J. Wang, F. Arias, L. Echegoyen and P. G. Wang, *Bioorg. Med. Chem. Lett.,* **8** (1998) 3065.

168. S. Pfeiffer, A. Schrammel, K. Schmidt and B. Mayer, *Anal. Biochem.,* **258** (1998) 68.

169. H. Ikezawa, E. Miki, K. Mizumachi, T. Ishimori, T. Nagai and M. Tanaka, *Bull. Chem. Soc. Jpn*., **66** (1993) 89.

170. J.H. Zagal, M.A. Gulppi and G. Cardenas-Jiron, *Polyhedron,* **19** (2000) 2255.

171. J.A.R. van Veen and C. Visser, *Electrochim. Acta,* **24** (1979) 921.

172. G. Lalande, G. Faubert, R. Cote, D. Guay, J.P. Dodelet, L.T. Weng and P. Bertrand, *J. Power Sources,* **61** (1996) 227.

173. S. Baranton, C. Coutanceau, C. Roux, F. Hahn and J.M. Leger, *J. Electroanal. Chem.,* **577** (2005) 223.

174. F. Beck, *J. Appl. Electrochem*., **7** (1977) 239.

175. G. Lalande, R. Cote, G. Tamizhmani, D. Guay, J.P. Dodelet, L. Dignard-Bailey, L.T. Weng and P. Bertrand, *Electrochim. Acta,* **40** (1995) 2635.

176. K. Kinoshita, in *Electrochemical oxygen technology*, 1992, Wiley, New York.

177. S. Popovici, W. Leyffer and R. Holze, *J. Porphyrins Phthalocyanines,* **2** (1998) 249.

178. Y. Tse, P. Janda, H. Lam, J. Zhang, W.J. Pietro and A.B.P. Lever, *J. Porphyrins Phthalocyanines,* **1** (1997) 3.

179. C. Coutanceau, P. Crouigneau, J.M. Leger and C. Lamy, *J. Electroanal. Chem.,* **379** (1994) 389.

180. J.H. Zagal, R.K. Sen and E. Yeager, *J. Electroanal. Chem.,* **83** (1977) 207.

181. K. Oyaizu, A. Haryono, J. Natori and E. Tsuchida, *J. Chem. Soc., Faraday Trans.,* **94** (1998) 3737.

182. J.H. Zagal, M. Paez, A.A. Tanaka, J.R. dos Santos and C.A. Linkous, *J. Electroanal. Chem.,* **339** (1992) 13.

183. J.H. Zagal, M.J. Aguirre, L. Basaez and J. Pavez, in *Oxygen Electrochemistry, The Electrochem. Soc. Symposium Series,* R.R. Adzic, F.C. Anson and K. Kinoshita (Ed.s), Vol. 95(26), 1995.

184. J.H. Zagal and G.I. Cardenas-Jiron, *J. Electroanal. Chem*., **489** (2000) 96.

185. J.H. Zagal, M.A. Paez and J.F. Silva, in *N_4-macrocyclic metal complexes,* J.H. Zagal, F. Bedioui and J.-P. Dodelet (Ed.s), Springer, New York, 2006.

186. N. Kobayashi, P. Janda and A.B.P. Lever, *Inorg. Chem.,* **31** (1992) 5172.

187. P. Janda, N. Kobayashi, P.R. Auburn, H. Lam, C.C. Leznoff and A.B.P. Lever, *Can. J. Chem.,* **67** (1989) 1109.

188. J. Pavez, M. Paez, A. Ringuede, F. Bedioui and J.H. Zagal, *J. Solid State Electrochem.,* **9** (2005) 21.

189. J.H. Zagal, M. Gulppi, M. Isaacs, G. Cardenas-Jiron and M.J. Aguirre, *Electrochim. Acta,* **44** (1998) 1349.

190. X.-B. Zhang, C.-C. Guo, J.-B. Xu and R.-Q. Yu, *J. Mol. Cat. A: Chem.,* **154** (2000) 31.

191. K.T. Moore, I.T. Horváth and M.J. Therien, *Inorg. Chem.*, **39** (2000) 3125.

192. F.G. Doro, J.R.L. Smith, A.G. Ferreira and M.D. Assis, *J. Mol. Cat. A: Chem.*, **164** (2000) 97.

193. H.C. Sacvo, Y. Iamamoto and J.R.L. Smith, *J. Chem. Soc. Perkin Trans*., **2** (2001) 181.

194. Y.-W. Chan and R.B. Wilson Jr., *ACS Natl. Meeting*, **33** (1988) 453.

195. S. Seelan, M.S. Agashe, D. Srinivas and S. Sivasanker, *J. Mol. Catal. A: Chem.*, **168** (2001) 61.

196. N. Grootboom and T. Nyokong, *J. Mol. Catal. A: Chem.,* **179** (2002) 113.

197. K.E. Simmons and D.E. van Sickle, *J. Am. Chem. Soc.,* **95** (1973) 7759.

198. R.R. Diaz, K. Selby and D.J. Waddington, *J. Chem. Soc. Perkin. Trans.,* **2** (1975) 758.

199. W. Nam, Y.M. Goh, Y.J. Lee, M.H. Lim and C. Kim, *Inorg. Chem.,* **38** (1999) 3238.

200. M. Salavati-Niasari, F. Farzaneh and M. Ghandi, *J. Mol. Catal. A: Chem.,* **186** (2002) 101.

201. M.E. Nino, S.A. Giraldo and E.A. Paez-Mozo, *J. Mol. Cat. A: Chem.,* **175** (2001) 139.

202. J.-W. Huang, W-Z. Huang, W-J. Mei, J. Liu, S-G. Hu and L-N. Ji, *J. Mol. Catal. A: Chem.*, **156** (2000) 275.

203. N.A. Kuznetsova, N.S. Gretsova, V.M. Derkachera, O.L. Kaliya and E.A. Luk'yanets, *J. Porphyrins Phthalocyanines,* **7** (2003) 147.

204. M.A. Schiavon, Y. Iamamoto, O.R. Nascimento and M. D. Assis, *J. Mol. Cat. A: Chem.*, **174** (2001) 213.

205. A.N. de Sousa, M.E.M.D. de Carvalho and Y.M. Idemori, *J. Mol. Cat. A: Chem.,* **169** (2001) 1.

206. N. Safari and F. Bahadoran, *J. Mol. Cat. A: Chem.,* **171** (2001) 115.

207. K. Kasuga, K. Tsuboi, M. Handa, T. Sugimori and K. Sogabe, *Inorg. Chem. Comm.,* **2** (1999) 507.

208. A. Jablonski, *Nature,* **131** (1933) 839.

209. A. Jablonski, *Z. Phys.,* **73** (1931) 460.

210. R. Bonnett, *Chem. Soc. Rev.,* **24** (1995) 19.

211. R. Bonnett, in *Chemical Aspects of Photodynamic Therapy: Advanced Chemistry Texts,* D. Phillips, P. O'Brein and S. Roberts (Ed.s), Vol. 1, Gordon & Breach, Germany, 2000.

212. A.K.Sobbi, D. Wohrle and D. Schlettwein, *J. Chem. Soc. Perkin Trans.,* **2** (1993) 481.

213. I. Rosenthal and E. Ben-Hur, *Int. J. Radiat. Biol.,* **67** (1995) 85.

214. J.A.S. Cavaleiro, M.G.P.S. Neves, M.J.E. Hewlis and A.H. Jackson, *J. Chem. Soc. Perkin Trans.,* **1** (1990) 1937.

215. W. Spiller, H. Kliesch, D. Wohrle, S. Hackbarth, B. Roder and G. Schnurpfeil, *J. Porphyrins Phthalocyanines,* **1** (1997) 159.

216. N.A. Kuznetsova, E. Makarova, S. Dashkevich, N. Gretsova, V. Negrimovsky, O. Kaliya and E. Luk'yanets, *Zh. Obshch. Khim.,* **70** (2000) 140.

217. T. Shiragami, K. Kubomura, D. Ishibashi and H. Inoue, *J. Am. Chem. Soc.,* **118** (1996) 6311.

218. S. Takagi, T. Okamoto, T. Shiragami and H. Inoue, *J. Org. Chem.,* **59** (1994) 7373.

219. P.E. Esser, B. Drieben-Holscher and W. Keim, *J. Mol. Cat. A: Chem.,* **140** (1999) 13.

220. A. Maldotti, L. Andreotti, A. Molinari, S. Borisov and V. Vasil'ev, *Chem. Eur. J.,* **7** (2001) 3564.

221. J. Obirai and T. Nyokong, *Electrochim. Acta,* **50** (2005) 5427.

222. J. Obirai and T. Nyokong, *Electrochim. Acta,* **50** (2005) 3296.

223. R. D. Mair and A. J. Graupner, *Anal. Chem.,* **36** (1964) 194.

224. J. Premkumar and R. Ramaraj, *J. Mol. Catal A: Chem.,* **142** (1999) 153.

225. J. Mertz, O. Scheider and M. Hanack, *Inorg. Chem.*, **23** (1984) 1065.

226. H. Tomoda, S. Saito and S. Shiraishi, *Chem. Lett.*, (1983) 313.

227. N. Trobach, O. Hild, D. Schettwein and D. Wöhrle, *J. Mat. Chem.,* **12** (2002) 879.

228. D. Wöhrle, M. Eskes, K. Shigehara, A. Yamada, Synthesis (1993) 194.

229. S. Griveau, M. Gulppi, F. Bedioui and J. Zagal, *Solid State Ionics,* **169** (2004) 59.

230. J.H. Zagal, M.A. Gulppi, C.A. Caro, and G.I. Cardenas-Jiron, *Electrochem Comm.,* **1** (1999) 389.

231. R.O. Lezna, S. Juanto, and J.H. Zagal, *J. Electroanal. Chem.,* **452** (1998) 221.

232. D. Martel, N. Sojic and A. Kuhn, *J. Chem. Educ.*, **79** (2002) 349.

233. G. Kalyuzhny, A. Vaskevich, G. Ashkenasy, A. Shanzer and I. Rubinstein, *J. Phys. Chem.*, **B 104** (2000) 8238.

234. D.J. Revell, I. Chambrier, M.J. Cook, and D.A. Russell, *J. Mater. Chem.*, **10** (2000) 31.

235. S.S. Khaloo, M.K. Amini, S. Tangestaninejad, S. Shahrokhian and R. Kia, *J. Iranian Chemical Society,* **1** (2004) 128.

236. S.M. Golabi, H.R. Zare, and M. Hamzehloo, *Microchem. J.*, **69** (2001) 111.

237. A. Salimi and K. Abdi, *Talanta*, **63** (2004) 475.

238. M.E.G. Lyons, C.A. Fitzgerald, and M.R. Smyth, *Analyst,* **119** (1994) 855.

239. M.K. Halbert and R.P. Baldwin, *Anal. Chem.*, **57** (1985) 591.

240. S. Griveau, M. Gulppi, J. Pavez, J.H. Zagal, and F. Bedioui, *Electroanalysis*, **15** (2003) 779.

241. J. Vitecek, J. Petrlova, J. Petrek, V. Adam, D. Potesil, L. Havel, R. Mikelova, L. Tronkova and R. Kizek, *Electrochim. Acta,* **51** (2006) 5087.

242. A.C. Gorren, A. Schrammel, K. Schmidt and B. Mayer, *Arch. Biochem. Biophys.,* **330** (1996) 219.

243. E. Ford, M.N. Hughes and P. Wardman, *Free Radic. Biol. Med.,* **32** (2002) 1314.

244. E. Bald, G. Chwatko, R. Glowacki and K. Kusmierek, *J. Chromatogr. A,* **1032** (2004) 109.

245. E. Bramanti, C. Vecoli, D. Neglia, M.P. Pellegrini, G. Raspi, and R. Barsacchi, *Clin. Chem.,* **51** (2005) 1007.

246. K. Ozoemena, T. Nyokong and P. Westbroek, *Electroanalysis*, **15** (2003) 1762.

247. M. Ebadi, C. Alexiou and A.B.P. Lever, *Can. J. Chem.*, **79** (2001) 992.

248. J. Zhang and F. C. Anson, *J. Electroanal. Chem.*, **341** (1992) 323.

249. D. Schlettwein, J.P. Meyer and N.I. Jaeger, *J. Porphyrins Phthalocyanines*, **4** (2000) 23.

250. B.E. Williamson, T.C. VanCott, M.E. Boyle, G.C. Misener, M.J. Stillman and P.N. Schatz, *J. Am. Chem. Soc.*, **114** (1992) 2412.

251. A.B.P. Lever, J.P. Wilshire and S.K. Quan, *J. Am. Chem. Soc.*, **101** (1979) 3668.

252. A.B.P. Lever, J.P. Wilshire and S.K. Quan, *Inorg.Chem.*, **20** (1981) 761.

253. C. Coutanceau, A. Rakotondrainibe, P. Crouigneau, J.M. Leger, and C. Lamy, *J. Electroanal. Chem.*, **386** (1995) 173.

254. W. Nam, M.H. Lim, S.-Y. Oh, J.H. Lee, H.J. Lee, S.K. Woo, C. Kim, W. Shin, Angew *Chem. Int. Ed.*, **39** (2000) 3646.

255. W. Nam, H.J. Lee, S-Y. Oh, C. Kim and H.G. Jang, *J. Inorg. Biochem.*, **80** (2000) 219.

256. Y. Watanabe, *J. Biol. Inorg. Chem.*, **6** (2001) 846.

257. A. Hadasch, A. Sorokin, A. Rabion, L. Fraisse and B. Meunier, *New J. Chem.*, (1998) 45.

258. G. Ferraudi, in *Phthalocyanines: Properties and Applications,* C.C. Leznoff and A.B.P. Lever (Eds.), Vol. 1, VCH Publishers, New York,1989.

259. I.V. Renge, V.A. Kuz'min, A.F. Mironov and Y.E. Borisevich, *Doklady Akademii Nauk SSSR.*, **263** (1982) 143.

260. Z. Gasyna, W.R. Browett and M.J. Stillman, *Inorg. Chim. Acta*, **92** (1984) 37.

261. K. Kasuga, H. Morimoto and M. Ando, *Inorg. Chem.,* **25** (1986) 2478.

262. B.M. Monroe, *J. Am. Chem. Soc.*, **82** (1978) 15.

263. P.D. Bartlett and A.P. Schaap, *J. Am. Chem. Soc.*, **92** (1970) 3223.

264. C.S. Foote and J.W. Peters, *J. Am. Chem. Soc.*, **93** (1971) 3795.

265. P.R. Ogilby and C.S. Foote, *J. Am. Chem. Soc.*, **103** (1981) 1220.

266. L.E. Manring and C.S. Foote, *J. Am. Chem. Soc.*, **105** (1983) 4710.

[1] M.J. Stillman, in *Phthalocyanines: Properties and applications,* C.C. Leznoff and A.B.P. Lever (Ed.s), Vol. 3, VCH Publishers, New York, 1993.

[2] P. Erk and H. Hengelsberg, in *The Porphyrin Handbook,* K.M. Radish, K.M. Smith and R. Guilard (Ed.s), Vol. 19, Academic Press, San Diego, 2003.

[3] J. Simon and T. Toupance, in *Comprehensive supra-molecular chemistry,* D.N. Reinhoudt (Ed.), Vol. 10, Pergamon, London, 1996.

[4] N.B. McKeown, in *The Porphyrin Handbook,* K.M. Radish, K.M. Smith and R. Guilard (Ed.s), Vol. 15, Academic Press, San Diego, 2003.

[5] I. Rosenthal, *Photochem. Photobiol.,* **6** (1991) 859.

[6] E. Luk'yanets, *J. Porphyrins Phthalocyanines,* **3** (1999) 424.

[7] S.R. Flom, in *The Porphyrin Handbook,* K.M. Radish, K.M. Smith and R. Guilard (Ed.s), Vol. 19, Academic Press, San Diego, 2003.

[8] N.S. Nalwa and J.S. Shirk, in *Phthalocyanines: Properties and applications,* Ed. C.C. Leznoff and A.B.P. Lever, Vol. 4, VCH Publishers, New York, 1996.

[9] S. Griveau, J. Pavez, J. Zagal and F. Bedioui, *J. Electroanal. Chem.,* **497** (2001) 75.

[10] C.A. Caro, J.H. Zagal and F. Bedioui, *J. Electrochem. Soc.,* **150** (2003) E95.

[11] M. Kimura and H. Shirai, in *The Porphyrin Handbook,* K.M. Radish, K.M. Smith and R. Guilard (Ed.s), Vol. 19, Academic Press, San Diego, 2003.

[12] K. Kasuga, K. Mori, T. Sugimori and M. Handa, *Bull. Chem. Soc. Jpn.,* **73** (2000) 939.

[13] J.D. Spikes, *Photochem. Photobiol. B: Biol.,* **6** (1990) 259.

[14] R. Hagen and T. Bieringer, *Adv. Mater.,* **13** (2001)1805.

[15] F.H. Moser and A.L. Thomas, in *Phthalocyanine Compounds,* Reinhold: New York, Chapman and Hall, London, 1963.

[16] F.H. Moser and A.L. Thomas, in *The Phthalocyanines,* Vol.s 1&2, CRC, Boca Raton, 1983.

[17] M. Hanack and M. Lang, *Adv. Mat.,* **6** (1994) 819.

[18] D. Wohrle, G. Schnurpfeil and G. Knothe, *Dyes and Pigments*, **18** (1992) 91.

[19] P. Yiru, H. Fenghua, L. Zhipeng, C. Naisheng and H. Jinling, *Inorg. Chem. Commun.,* **7** (2004) 967.

[20] A. Lützen, S.D. Starnes, D.M. Rudkevich and J. Rebeck Jr., *Tet. Lett.,* **41** (2000) 3777.

[21] F. Yilmaz, D. Atilla and V. Ahsen, *Polyhedron*, **23** (2004) 1931.

[22] N.B. Mckeown, in *Phthalocyanine Materials: Synthesis, Structure and Function*, Cambridge University Press, London, 1998.

[23] J. Mack and M.J. Stillman, *J. Am. Chem. Soc.,* **116** (1994) 1292.

[24] K. Walzer and M. Hietschold, *Surf. Sci.,* **471** (2001) 1.

[25] M.J. Stillman and T. Nyokong, in *Phthalocyanines: Properties and applications,* C.C. Leznoff and A.B.P. Lever (Ed.s), Vol. 1, VCH Publishers, New York, 1989.

[26] I. Seotsanyana-Mokhosi, N. Kuznetsova and T. Nyokong, *Photochem. Photobiol. A: Chem.,* **140** (2001) 215.

[27] G. de la Torre, M.V. Martinez-Diaz and T. Torres, *J. Porphyrins Phthalocyanines,* **3** (1999) 560.

[28] S. Maree, D. Phillips and T. Nyokong, *J. Porphyrins Phthalocyanines,* **6** (2002) 17.

[29] Z. Zhao, K. Ozoemena, M.D. Maree and T. Nyokong, *Dalton Trans.*, (2005) 1241.

[30] V.N. Nemykin, V.Y. Chernii, S.V. Volkov, N.I. Bundina, O.L. Kaliya, V.D. Li and E.A. Luk'yanets, *J. Porphyrins Phthalocyanines,* **3** (1999) 87.

[31] J. Jiang, W. Liu and D.P. Arnold, *J. Porphyrins Phthalocyanines,* **7** (2003) 459.

[32] K. Durr and M. Hanack, *J. Porphyrins Phthalocyanines,* **3** (1999) 224.

[33] N. Kobayashi, A. Muranaka, and V.N. Nemykin, *Tet. Lett*., **42** (2001) 913.

[34] P. Matlaba and T. Nyokong, *Polyhedron*, **21** (2002) 2463.

[35] P.N. Day, Z. Wang and R. Pachter, *J. Mol. Struc. (THEO-Chem),* **455** (1998) 33.

[36] T. Nyokong, Z. Gasyna and M.J. Stillman, *Inorg. Chem.,* **26** (1987) 548.

[37] T. Nyokong, Z. Gasyna, and M.J. Stillman, *Inorg. Chem.,* **26** (1987) 1087.

[38] E.A. Ough, T. Nyokong, K.A. Creber and M.J. Stillman, *Inorg. Chem.,* **27** (1988) 2724.

[39] E.A. Ough, Z. Gasyna and M.J. Stillman, *Inorg. Chem.,* **30** (1991) 2301.

[40] E.A. Ough and M.J. Stillman, *Inorg. Chem.,* **33** (1994) 573.

[41] M. Gouterman, in *The Porphyrins,* D. Dolphin (Ed.), Physical Chemistry, Part A, Vol. 3, Academic Press: New York, 1978.

[42] F.R. Fan and L.R. Faulkner, *J. Am. Chem. Soc*., **101** (1979) 4779.

[43] K. Kasuga, N. Matsura, K. Inoue, M. Handa, T. Sugimori, K. Isa and M. Nakata, *Chem. Lett.,* (2002) 352.

[44] G.A. Kumar, J. Thomas, N.V. Unnikrishnan, V.P.N. Nampouri and C.P.G. Vallabhan, *J. Porphyrins Phthalocyanines*, **5** (2001) 456.

[45] M. Stillman, J. Mack and N. Kobayashi, *J. Porphyrins Phthalocyanines,* **6** (2002) 296.

[46] M. Gouterman, *J. Mol. Spectrosc.,* **6** (1961) 138.

[47] A. Ogunsipe, J.-Y. Chen and T. Nyokong, *New J. Chem.,* **28** (2004) 822.

[48] Z. Zhao, A. Ogunsipe, M.D. Maree and T. Nyokong, *J. Porphyrins Phthalocyanines,* **9** (2005) 186.

[49]M.D. Maree, N. Kuznetsova and T. Nyokong, *Photochem. Photobiol. A: Chem.,* **140** (2001) 117.

[50] M.J. Cook, *Chem. Rec.,* **4** (2002) 225.

[51]A. Ogunsipe and T. Nyokong, *J. Mol. Struc.,* **689** (2004) 89.

[52]A. Beeby, S. FitzGerald and C.F. Stanley, *J. Chem. Soc. Perkin Trans.,* **2** (2001) 1978.

[53] W.–F. Law, R.C.W. Liu, J. Jiang and D.K.P. Ng., *Inorg. Chim. Acta.,* **256** (1997) 6349.

[54] N. Kobayashi and H. Konami, in *Phthalocyanines: Properties and applications,* C.C. Leznoff and A.B.P. Lever (Ed.s), Vol. 4, VCH Publishers, New York, 1999.

[55]F.R. Fronczek, R.J. Johnson and R.M. Strongin, *Acta Cryst.,* **E57** (2001) 447.

[56] J.G. Calvert and J.N. Pitts, in *Photochemistry,* John Wiley & Sons, Inc., New York, 1966.

[57] A. Ogunsipe, D. Maree and T. Nyokong, *J. Mol. Struc.,* **650** (2003) 131.

[58] A.B.P. Lever, E.R. Milaeva and G. Speier, in *Phthalocyanines: Properties and applications,* C.C. Leznoff and A.B.P. Lever (Ed.s), Vol. 3, VCH Publishers, New York, 1989.

[59] A.B.P. Lever, M.R. Hempstead, C.C. Leznoff, W. Liu, M. Melnik, W.A. Nevin and P. Seymour, *Pure Appl. Chem.,* **58** (1986) 1467.

[60] M. L'Her and A. Pondaven. in *The Porphyrin Handbook,* K.M. Kadish, K.M. Smith and R. Guilard (Ed.s), Vol. 16, Academic Press, San Diego, 2003.

[61] A.B.P. Lever, S. Licoccia, K. Magnell, R.C. Minor and B.S. Ramaswamy, *ACS Symp. Ser.,* **201** (1982) 237.

[62] T. Nyokong, *S.A. J. Chem.,* **48** (1995) 23.

[63] M.N. Golovin, P. Seymour, K. Jayaraj, Y.S. Fu and A.B.P. Lever, *Inorg. Chem.,* **29** (1990) 1719.

[64] T. Nyokong, *Polyhedron,* **12** (1993) 375.

[65] T. Kuwana, R.K. Darlington and D.W. Leedy, *Anal. Chem.*, **36** (1964) 2023.

[66]J. Obirai and T. Nyokong, *J. Electroanal. Chem.*, **573** (2004) 77.

[67] D.B. Hibbert, in *Introduction to Electrochemistry*, Macmillan, London, 1993.

[68] L. Gaffo, M.J.S.P. Brasil, F. Cerdeira, C. Giles and W.C. Moreira, *J. Porphyrins Phthalocyanines,* **9** (2005) 89.

[69] J.W. Dodd and N.S. Hush, *J. Chem. Soc.*, (1964) 4607.

[70] L.D. Rollman and R.T. Iwamoto, *J. Am. Chem. Soc.,* **90** (1968) 1455.

[71] D.W. Clack and J.R. Yandle, *Inorg. Chem.*, **11** (1972) 1738.

[72] G. Inzelt, in *Electroanalytical methods: Guide to experiments and applications,* F. Scholz (Ed.), Springer 2002.

[73] H. Kahlert, in *Electroanalytical methods: Guide to experiments and applications*, F. Scholz (Ed.), Springer 2002.

[74] W.R. Heineman and P.T. Kissinger, in *Laboratory Techniques in Electroanalytical-chemistry*, 2nd ed, P.T. Kissinger and W.R. Heineman (Ed.s), Marcel Deccer Inc., New York, 1996.

[75]A.J. Bard and L.R. Faulkner, in *Electrochemical Methods: Fundamentals and Applications,* John Willey & Sons, Toronto, 1996.

[76]J. O'M. Bockris and S.U.M. Khan, in *Surface electrochemistry: A molecular level approach*, Plenum Press, New York, 1993.

[77]V.G. Levich, in *Physicochemical hydrodynamics* (English translation), Prentice Hall, New Jersey, 1962.

[78]C.M.A. Brett and A.-M.O. Brett, in *Electrochemistry, principles, methods and applications,* Oxford University Press, 1993.

[79]M.J. Aguirre, M. Isaacs, F. Armijo, L. Basaez and J.H. Zagal, *Electroanalysis,* **14** (2002) 356.

[80] B. Wermeckers and F. Beck, *Electrochim. Acta,* **30** (1985) 1491.

[81] J.H. Zagal, *Coord. Chem. Rev.,* **119** (1992) 89 and references cited therein.

[82] J.H. Zagal and C. Paez, *Electrochim. Acta,* **34** (1989) 243.

[83]J.-M. Zen, A.S. Kumar and M.-R. Chang, *Electrochim. Acta,* **45** (2000)1691.

[84] J. Zagal, R.K. Sen and E. Yeager, *J. Electroanal. Chem.*, **83** (1977) 207.

[85]M. Gulppi, F. Bedioui and J.H. Zagal, *Electroanalysis,* **13** (2001) 1136.

[86] N.B. McKeown, *Chem. Ind.*, (1999) 92.

[87] J. Oni and T. Nyokong, *Anal. Chim. Acta,* **434** (2001) 9.

[88] J. Zagal, P. Bindra and E. Yeager, *J. Electrochem. Soc.*, **127** (1980) 1506.

[89]S. Maree and T. Nyokong, *J. Electroanal. Chem.*, **492** (2000) 120.

[90]M. Sekota and T. Nyokong, *Polyhedron*, **16** (1997) 3279.

[91]S. Ledru, N. Ruillé and M. Boujtita, *Biosens. Bioelectron.*, **21** (2006) 1591.

[92]C.D. Kuhnline, M.G. Gangel, M.K. Hulvey and R.S. Martin, *Analyst*, **131** (2006) 202.

[93]A. Napier and J.P. Hart, *Electroanalysis*, **8** (1996) 1006.

[94] T.J. Mafatle and T. Nyokong, *J. Electroanal. Chem.*, **408** (1996) 213.

[95] M.J. Cook, *Pure Appl. Chem.*, **71** (2002) 2145.

[96]X. Lu, K.W. Hipps, X.D. Wang and U. Mazur, *J. Am. Chem. Soc.*, **118** (1996) 7197.

[97] M.J. Cook, *J. Mater. Chem.*, **6** (1996) 677.

[98] C.A. Caro, F. Bedioui and J.H. Zagal, *Electrochim. Acta*, **47** (2002) 1489.

[99]K.I. Ozoemena, P. Westbroek and T. Nyokong, *Electrochem. Commun.*, **3** (2001) 529.

[100] B.J. Hwang, R. Santhanam and Y.W. Chang, *Electroanalysis*, **14** (2002) 363.

[101] J. Obirai, N. Pereira-Rodrigues, F. Bedioui and T. Nyokong, *J. Porphyrins Phthalocyanines*, **7** (2003) 508.

[102] S. Griveau and F. Bedioui, *Electroanalysis*, **13** (2001) 253.

[103] M.J. Cook and A. JafariFini, *J. Mater. Chem.*, **7** (1997) 5.

[104] Z. Li and M.Lieberman, *Langmuir*, **17** (2001) 4887.

[105] X. Li, W. Xu, X. Wang, H. Jia, B. Zhao, B. Li and Y. Ozaki, *Thin Solid Films*, **457** (2004) 372.

[106] K.I. Ozoemena and T. Nyokong, *J. Electroanal. Chem.*, **579** (2005) 283.

[107]Z. Li and M. Lieberman in *Fundamental and applied aspects of chemically modified surfaces*, J.P. Blitz and C.B. Little (Eds), Royal society of chemistry. Lettchworth, UK, 1999.

[108]K.I. Ozoemena and T. Nyokong, *Talanta*, **67** (2005) 162.

[109] B. Liedberg and P. Tengvall, *Langmuir*, **11** (1995) 3821.

[110] M.P. Somashekarappa, J. Keshavayya and S. Sampath, *Pure Appl. Chem.*, **74** (2002) 1609.

[111] M. Thamae and T. Nyokong, *J. Electroanal. Chem.*, **579** (1999) 126.

[112]J. Obirai and T. Nyokong, *Electrochim. Acta*, **49** (2004) 1417.

[113]S. Griveau, V. Albin, T. Pauporte, J.H. Zagal and F. Bedioui, *J. Mater. Chem.*,**12** (2002) 225.

[114] J. Obirai, F. Bedioui and T. Nyokong, *J. Electroanal. Chem.,* **576** (2005) 323.

[115]E. Crouch, D.C. Cowell, S. Hoskins, R.W. Pittson and J.P. Hart, *Anal. Biochem.,* **347** (2005) 17.

[116]J. Wang and P.V.A. Pamidi, *Talanta,* **42** (1995) 463.

[117]S. Miserere, S. Ledru, N. Ruillé, S. Griveau, M. Boujtita and F. Bedioui, *Electrochem. Comm.,* **8** (2006) 238.

[118]J.R. de Sousa, A.A. Batista, I.C.N. Diogenes, G.F.S. Andrade, M.L.A. Temperini, L.G.F. Lopes and I. D.-S. Moreira, *J. Electroanal. Chem.,* **543** (2003) 93.

[119]J. Chen, J. Su, W. Wang and M.A. Reed, *Physica E,* **16** (2003) 17.

[120]Y. Naitoh, T. Matsumoto, K.-I. Sugiura, Y. Sakata and T. Kawai, *Surf. Sci.,* **487** (2001) L534.

[121]M.S. El-Deab and T. Ahsaka, *Electrochem. Commun.,* **5** (2003) 214.

[122]X. Huang, Y. Liu, S. Wang, S. Zhou and D. Zhu, *Chem. Eur. J.*, **8** (2002) 4179.

[123]F. Bedioui, J. Devynck and C. Bied-Charreton, *Acc. Chem. Res.,* **28** (1995) 30 and references cited therein.

[124]K. Nishiyama, S.I. Tahara, Y. Uchida, S. Tanoue and I. Taniguchi, *J. Electroanal. Chem*., **478** (1999) 83.

[125]K.V. Gothelf, *J. Electroanal. Chem*., **494** (2000) 147.

[126]H.O. Finklea in Electroanalytical Chemistry, A.J. Bard, I. Rubenstein (Eds), Vol 19 (and references therein), Marcel Dekker, New York, 1996.

[127]E. Sabatani and I. Rubinstein, *J. Phys. Chem.,* **91** (1987) 6663.

[128]M.D. Porter, T.B. Bright, D. Allara and C.E.D. Chidsey, *J. Am. Chem. Soc*., **109** (1987) 3559.

[129]D. Losic, J.G. Shapter and J.J. Gooding, *Langmuir*, **17** (2001) 3307.

[130]J. Wang, J.L.P. Paz and M. Jiang, *Langmuir*, **15** (1999) 1884.

[131]D.L. Pilloud, X. Chen, P.L. Dutton and C.C. Moser, *J. Phys. Chem. B,* **104** (2000) 2868.

[132]K.I. Ozoemena and T. Nyokong, *Electrochim. Acta,* **47** (2002) 4035.

[133]H. Ohmori and I. Yamamoto, *J. Exp. Med.,* **155** (1982) 1277.

[134]W.A. Kleinman and J.P. Richie, *Biochem. Pharmacol.,* **60** (2000) 19.

[135]A. Meister, *J. Biol. Chem.,* **263** (1988) 17205.

[136]I. Chatti, A. Ghorbel, P. Grange and J.M. Colin, *Catal. Today,* **75** (2002) 113.

[137]P.M. Schweizer-Berberich, S. Vaihinger and W.Gopel, *Sens. Actuators,* **B18-19** (1994) 282.

[138]D.L.H. Williams, *Chem. Soc. Rev.*, **14** (1985) 171.

[139]C.M. Venturini, R.M. Palmer and S. Moncada, *J. Pharmacol. Exp. Ther.,* **266** (1993) 1497.

[140]M.W. Radomski, D.D. Rees, A. Dutra and S. Moncada, *Br. J. Pharmacol.,* **107** (1992) 745.

[141]E.J. Langford, A.S. Brown, A.J. de Belber, R.E.A. Smith, J.F. Martin, R.J. Wainwright, M.R. Thomas, M.W. Radomski and S. Moncada, *Lancet,* **344** (1994) 1458.

[142]A.D. Belber, C. Lees, J. Martin, S. Moncada and S. Campbell, *Lancet*, **345** (1995) 124.

[143]S. Modi, S.S. Deodhar, D.V. Behere and S. Mitra, *Biochemistry*, **30** (1991) 118.

[144]D. Gao, J.-Z. Li, and R.-Q. Yu, *Anal. Chem.*, **66** (1994) 2245.

[145]M.K. Amini, S. Shahrokhian and S. Tangestaninejad, *Anal. Chim. Acta*, **402** (1999) 137.

[146]N. Phougat and P. Vasudevan, *J. Power Sources,* **69** (1997) 161.

[147]E. Itabashi, *Inorg. Chem*., **24** (1985) 4024.

[148]S. Adak, A. Mazumdar and R.K. Banerjees, *J. Biol. Chem.,* **272** (1997) 11049.

[149]T.M. Aune and E.L. Thomas, *Eur. J. Biochem.,* **80** (1977) 209.

[150]E.L. Thomas, *Biochemistry,* **20** (1981) 3273.

[151]S. Modi, D.V. Behere and S. Mitra, *Biochemistry,* **28** (1989) 4689.

[152]S. Modi, D.V. Behere and S. Mitra, *J. Biol. Chem.,* **264** (1989) 19677.

[153]V.K. Sharma, D.B. O'Connor and D. Cabelli, *Inorg. Chimica Acta,* **357** (2004) 4587.

[154]T. Ohta, T. Kamachi, Y. Shiota and K. Yoshizawa, *J. Org. Chem.,* **6** (2001) 4122.

[155]T. Nyokong in *N_4-macrocyclic metal complexes,* J.H. Zagal, F. Bedioui and J-P. Dodelet (Ed.s), Springer, New York, 2006.

[156]K.I. Ozoemena, T. Nyokong and P. Westbroek, *Electroanalysis,* **14** (2003) 1.

[157]G.I. Cardenas-Jiron, M.A. Gulppi, C.A. Caro, R. del Rio, M. Paez and J.H. Zagal, *Electrochim. Acta,* **46** (2001) 3227.

[158]D. Mimica, F. Bedioui and J.H. Zagal, *Electrochim. Acta*, **48** (2002) 323.

[159]X. Qi and R.P. Baldwin, *J. Electrochem. Soc.,* **143** (1996) 1283.

[160]M.A. Gulppi, M.A. Paez, J.A. Costamagna, G.I. Cardenas-Jiron, F. Bedioui and J.H. Zagal, *J. Electroanal. Chem.*, **580** (2005) 50.

[161]N. Pereira-Rodrigues, R. Cofré, J.H. Zagal and F. Bedioui, *Bioelectrochem.*, 2006, in press.

[162]D. Giustarini, A. Milzani, R. Colombo, I. Dalle-Donne and R. Rossi, *Clin. Chim. Acta,* **330** (2003) 85.

[163]M.P. Gordge, J.S. Hothersall, G.H. Neild and A.A.N. Dutra, *Br. J. Pharmacol.*, **119** (1996) 533.

[164]P.D. Wood, B. Mutus and R.W. Redmond, *Photochem. Photobiol*., **64** (1996) 518.

[165]R.J. Singh, N. Hogg, J. Joseph and B. Kalyanaraman, *J. Biol. Chem.*, **271** (1996) 18596.

[166]M. David-Dufihlo, A. Brunet and F. Bedioui, *Electroanalysis*, **18** (2006) 1827.

[167]Y. Hou, J. Wang, F. Arias, L. Echegoyen and P. G. Wang, *Bioorg. Med. Chem. Lett.*, **8** (1998) 3065.

[168]S. Pfeiffer, A. Schrammel, K. Schmidt and B. Mayer, *Anal. Biochem.*, **258** (1998) 68.

[169]H. Ikezawa, E. Miki, K. Mizumachi, T. Ishimori, T. Nagai and M. Tanaka, *Bull. Chem. Soc. Jpn.*, **66** (1993) 89.

[170]J.H. Zagal, M.A. Gulppi and G. Cardenas-Jiron, *Polyhedron*, **19** (2000) 2255.

[171]J.A.R. van Veen and C. Visser, *Electrochim. Acta,* **24** (1979) 921.

[172]G. Lalande, G. Faubert, R. Cote, D. Guay, J.P. Dodelet, L.T. Weng and P. Bertrand, *J. Power Sources,* **61** (1996) 227.

[173]S. Baranton, C. Coutanceau, C. Roux, F. Hahn and J.M. Leger, *J. Electroanal. Chem.,* **577** (2005) 223.

[174]F. Beck, *J. Appl. Electrochem.*, **7** (1977) 239.

[175]G. Lalande, R. Cote, G. Tamizhmani, D. Guay, J.P. Dodelet, L. Dignard-Bailey, L.T. Weng and P. Bertrand, *Electrochim. Acta,* **40** (1995) 2635.

[176]K. Kinoshita, in *Electrochemical oxygen technology*, 1992, Wiley, New York.

[177]S. Popovici, W. Leyffer and R. Holze, *J. Porphyrins Phthalocyanines,* **2** (1998) 249.

[178]Y. Tse, P. Janda, H. Lam, J. Zhang, W.J. Pietro and A.B.P. Lever, *J. Porphyrins Phthalocyanines,* **1** (1997) 3.

[179]C. Coutanceau, P. Crouigneau, J.M. Leger and C. Lamy, *J. Electroanal. Chem.,* **379** (1994) 389.

[180]J.H. Zagal, R.K. Sen and E. Yeager, *J. Electroanal. Chem.,* **83** (1977) 207.

[181]K. Oyaizu, A. Haryono, J. Natori and E. Tsuchida, *J. Chem. Soc., Faraday Trans.,* **94** (1998) 3737.

[182]J.H. Zagal, M. Paez, A.A. Tanaka, J.R. dos Santos and C.A. Linkous, *J. Electroanal. Chem.,* **339** (1992) 13.

[183]J.H. Zagal, M.J. Aguirre, L. Basaez and J. Pavez, in *Oxygen Electrochemistry*, *The Electrochem. Soc. Symposium Series*, R.R. Adzic, F.C. Anson and K. Kinoshita (Ed.s), Vol. 95(26), 1995.

[184]J.H. Zagal and G.I. Cardenas-Jiron, *J. Electroanal. Chem.*, **489** (2000) 96.

[185]J.H. Zagal, M.A. Paez and J.F. Silva, in *N_4-macrocyclic metal complexes*, J.H. Zagal, F. Bedioui and J.-P. Dodelet (Ed.s), Springer, New York, 2006.

[186]N. Kobayashi, P. Janda and A.B.P. Lever, *Inorg. Chem.,* **31** (1992) 5172.

[187]P. Janda, N. Kobayashi, P.R. Auburn, H. Lam, C.C. Leznoff and A.B.P. Lever, *Can. J. Chem.,* **67** (1989) 1109.

[188]J. Pavez, M. Paez, A. Ringuede, F. Bedioui and J.H. Zagal, *J. Solid State Electrochem.,* **9** (2005) 21.

[189]J.H. Zagal, M. Gulppi, M. Isaacs, G. Cardenas-Jiron and M.J. Aguirre, *Electrochim. Acta,* **44** (1998) 1349.

[190]X.-B. Zhang, C.-C. Guo, J.-B. Xu and R.-Q. Yu, *J. Mol. Cat. A: Chem.,* **154** (2000) 31.

[191]K.T. Moore, I.T. Horváth and M.J. Therien, *Inorg. Chem.,* **39** (2000) 3125.

[192]F.G. Doro, J.R.L. Smith, A.G. Ferreira and M.D. Assis, *J. Mol. Cat. A: Chem.*, **164** (2000) 97.

[193]H.C. Sacvo, Y. Iamamoto and J.R.L. Smith, *J. Chem. Soc. Perkin Trans*., **2** (2001) 181.

[194]Y.-W. Chan and R.B. Wilson Jr., *ACS Natl. Meeting*, **33** (1988) 453.

[195]S. Seelan, M.S. Agashe, D. Srinivas and S. Sivasanker, *J. Mol. Catal. A: Chem.,* **168** (2001) 61.

[196]N. Grootboom and T. Nyokong, *J. Mol. Catal. A: Chem.,* **179** (2002) 113.

[197]K.E. Simmons and D.E. van Sickle, *J. Am. Chem. Soc.*, **95** (1973) 7759.

[198]R.R. Diaz, K. Selby and D.J. Waddington, *J. Chem. Soc. Perkin. Trans.*, **2** (1975) 758.

[199]W. Nam, Y.M. Goh, Y.J. Lee, M.H. Lim and C. Kim, *Inorg. Chem.*, **38** (1999) 3238.

[200]M. Salavati-Niasari, F. Farzaneh and M. Ghandi, *J. Mol. Catal. A: Chem.*, **186** (2002) 101.

[201]M.E. Nino, S.A. Giraldo and E.A. Paez-Mozo, *J. Mol. Cat. A: Chem.*, **175** (2001) 139.

[202]J.-W. Huang, W-Z. Huang, W-J. Mei, J. Liu, S-G. Hu and L-N. Ji, *J. Mol. Catal. A: Chem.*, **156** (2000) 275.

[203]N.A. Kuznetsova, N.S. Gretsova, V.M. Derkachera, O.L. Kaliya and E.A. Luk'yanets, *J. Porphyrins Phthalocyanines*, **7** (2003) 147.

[204]M.A. Schiavon, Y. Iamamoto, O.R. Nascimento and M. D. Assis, *J. Mol. Cat. A: Chem.*, **174** (2001) 213.

[205] A.N. de Sousa, M.E.M.D. de Carvalho and Y.M. Idemori, *J. Mol. Cat. A: Chem.*, **169** (2001) 1.

[206]N. Safari and F. Bahadoran, *J. Mol. Cat. A: Chem.*, **171** (2001) 115.

[207]K. Kasuga, K. Tsuboi, M. Handa, T. Sugimori and K. Sogabe, *Inorg. Chem. Comm.*, **2** (1999) 507.

[208]A. Jablonski, *Nature*, **131** (1933) 839.

[209]A. Jablonski, *Z. Phys.*, **73** (1931) 460.

[210]R. Bonnett, *Chem. Soc. Rev.*, **24** (1995) 19.

[211]R. Bonnett, in *Chemical Aspects of Photodynamic Therapy: Advanced Chemistry Texts*, D. Phillips, P. O'Brein and S. Roberts (Ed.s), Vol. 1, Gordon & Breach, Germany, 2000.

[212]A.K.Sobbi, D. Wohrle and D. Schlettwein, *J. Chem. Soc. Perkin Trans.*, **2** (1993) 481.

[213] I. Rosenthal and E. Ben-Hur, *Int. J. Radiat. Biol.*, **67** (1995) 85.

[214] J.A.S. Cavaleiro, M.G.P.S. Neves, M.J.E. Hewlis and A.H. Jackson, *J. Chem. Soc. Perkin Trans.*, **1** (1990) 1937.

[215]W. Spiller, H. Kliesch, D. Wohrle, S. Hackbarth, B. Roder and G. Schnurpfeil, *J. Porphyrins Phthalocyanines,* **1** (1997) 159.

[216]N.A. Kuznetsova, E. Makarova, S. Dashkevich, N. Gretsova, V. Negrimovsky, O. Kaliya and E. Luk'yanets, *Zh. Obshch. Khim.,* **70** (2000) 140.

[217]T. Shiragami, K. Kubomura, D. Ishibashi and H. Inoue, *J. Am. Chem. Soc.,* **118** (1996) 6311.

[218]S. Takagi, T. Okamoto, T. Shiragami and H. Inoue, *J. Org. Chem.,* **59** (1994) 7373.

[219]P.E. Esser, B. Drieben-Holscher and W. Keim, *J. Mol. Cat. A: Chem.,* **140** (1999) 13.

[220]A. Maldotti, L. Andreotti, A. Molinari, S. Borisov and V. Vasil'ev, *Chem. Eur. J.,* **7** (2001) 3564.

[221]J. Obirai and T. Nyokong, *Electrochim. Acta,* **50** (2005) 5427.

[222]J. Obirai and T. Nyokong, *Electrochim. Acta,* **50** (2005) 3296.

[223]R. D. Mair and A. J. Graupner, *Anal. Chem.,* **36** (1964) 194.

[224]J. Premkumar and R. Ramaraj, *J. Mol. Catal A: Chem.,* **142** (1999) 153.

[225]J. Mertz, O. Scheider and M. Hanack, *Inorg. Chem.,* **23** (1984) 1065.

[226]H. Tomoda, S. Saito and S. Shiraishi, *Chem. Lett.*, (1983) 313.

[227]N. Trobach, O. Hild, D. Schettwein and D. Wöhrle, *J. Mat. Chem.,* **12** (2002) 879.

[228] D. Wöhrle, M. Eskes, K. Shigehara, A. Yamada, Synthesis (1993) 194.

[229]S. Griveau, M. Gulppi, F. Bedioui and J. Zagal, *Solid State Ionics,* **169** (2004) 59.

[230]J. H. Zagal, M. A.Gulppi, C. A. Caro, and G. I. Cardenas-Jiron, *Electrochem Comm.*, **1** (1999) 389.

[231]R. O. Lezna, S. Juanto, and J. H. Zagal, *J. Electroanal. Chem.,* **452** (1998) 221.

[232]D. Martel, N. Sojic and A. Kuhn, *J. Chem. Educ.,* **79** (2002) 349.

[233]G. Kalyuzhny, A. Vaskevich, G. Ashkenasy, A. Shanzer and I. Rubinstein, *J. Phys. Chem.,* **B 104** (2000) 8238.

[234]D. J. Revell, I. Chambrier, M. J. Cook, and D. A. Russell, *J. Mater. Chem.,* **10** (2000) 31.

[235]S. S. Khaloo, M. K. Amini, S. Tangestaninejad, S. Shahrokhian and R. Kia, *J. Iranian Chemical Society,* **1** (2004) 128.

[236]S.M. Golabi, H.R. Zare, and M. Hamzehloo, *Microchem. J.*, **69** (2001) 111.

[237]A. Salimi and K. Abdi, *Talanta,* **63** (2004) 475.

[238]M.E.G. Lyons, C.A. Fitzgerald, and M.R. Smyth, *Analyst,* **119** (1994) 855.

[239]M.K. Halbert and R.P. Baldwin, *Anal. Chem.*, **57** (1985) 591.

[240]S. Griveau, M. Gulppi, J. Pavez, J. H. Zagal, and F. Bedioui, *Electroanalysis*, **15** (2003) 779.

[241]J. Vitecek, J. Petrlova, J. Petrek, V. Adam, D. Potesil, L. Havel, R. Mikelova, L. Trnkova and R. Kizek, *Electrochim. Acta*, **51** (2006) 5087.

[242]A. C. Gorren, A. Schrammel, K. Schmidt and B. Mayer, *Arch. Biochem. Biophys.*, **330** (1996) 219.

[243]E. Ford, M. N. Hughes and P. Wardman, *Free Radic. Biol. Med.*, **32** (2002) 1314.

[244]E. Bald, G. Chwatko, R. Glowacki and K. Kusmierek, *J. Chromatogr. A*, **1032** (2004) 109.

[245]E. Bramanti, C. Vecoli, D. Neglia, M. P. Pellegrini, G. Raspi, and R. Barsacchi, *Clin. Chem.*, **51** (2005) 1007.

[246]K. Ozoemena, T. Nyokong and P. Westbroek, *Electroanalysis*, **15** (2003) 1762.

[247]M. Ebadi, C. Alexiou and A.B.P. Lever, *Can. J. Chem.*, **79** (2001) 992.

[248]J. Zhang and F. C. Anson, *J. Electroanal. Chem.*, **341** (1992) 323.

[249]D. Schlettwein, J.P. Meyer and N.I. Jaeger, *J. Porphyrins Phthalocyanines*, **4** (2000) 23.

[250]B.E. Williamson, T.C. VanCott, M.E. Boyle, G.C. Misener, M.J. Stillman and P. N. Schatz, *J. Am. Chem. Soc.*, **114** (1992) 2412.

[251]A. B. P. Lever, J. P. Wilshire and S. K. Quan, *J. Am. Chem. Soc.*, **101** (1979) 3668.

[252]A.B.P. Lever, J.P. Wilshire and S.K. Quan, *Inorg.Chem.*, **20** (1981) 761.

[253]C. Coutanceau, A. Rakotondrainibe, P. Crouigneau, J.M. Leger, and C. Lamy, *J. Electroanal. Chem.*, **386** (1995) 173.

[254]W. Nam, M.H. Lim, S.-Y. Oh, J.H. Lee, H.J. Lee, S.K. Woo, C. Kim, W. Shin, Angew *Chem. Int. Ed.*, **39** (2000) 3646.

[255]W. Nam, H.J. Lee, S-Y. Oh, C. Kim and H.G. Jang, *J. Inorg. Biochem.*, **80** (2000) 219.

[256]Y. Watanabe, *J. Biol. Inorg. Chem.*, **6** (2001) 846.

[257]A. Hadasch, A. Sorokin, A. Rabion, L. Fraisse and B. Meunier, *New J. Chem.*, (1998) 45.

[258]G. Ferraudi, in *Phthalocyanines: Properties and Applications,* C.C. Leznoff and A.B.P. Lever (Eds.), Vol. 1, VCH Publishers, New York,1989.

[259]I.V. Renge, V.A. Kuz'min, A.F. Mironov and Y.E. Borisevich, *Doklady Akademii Nauk SSSR.*, **263** (1982) 143.

[260]Z. Gasyna, W.R. Browett and M.J. Stillman, *Inorg. Chim. Acta*, **92** (1984) 37.

[261]K. Kasuga, H. Morimoto and M. Ando, *Inorg. Chem.*, **25** (1986) 2478.

[262]B.M. Monroe, *J. Am. Chem. Soc.*, **82** (1978) 15.

[263]P.D. Bartlett and A.P. Schaap, *J. Am. Chem. Soc.*, **92** (1970) 3223.

[264]C.S. Foote and J.W. Peters, *J. Am. Chem. Soc.*, **93** (1971) 3795.

[265]P.R. Ogilby and C.S. Foote, *J. Am. Chem. Soc.*, **103** (1981) 1220.

[266]L.E. Manring and C.S. Foote, *J. Am. Chem. Soc.*, **105** (1983) 4710.